

REPORT DOCUMENTATION PAGE				Form Approved OMB No. 0704-0188	
The public reporting burden for this collection of information is estimated to average 1 hour per response, including the time for reviewing instructions, searching existing data sources, gathering and maintaining the data needed, and completing and reviewing the collection of information. Send comments regarding this burden estimate or any other aspect of this collection of information, including suggestions for reducing the burden, to Department of Defense, Washington Headquarters Services, Directorate for Information Operations and Reports (0704-0188), 1215 Jefferson Davis Highway, Suite 1204, Arlington, VA 22202-4302. Respondents should be aware that notwithstanding any other provision of law, no person shall be subject to any penalty for failing to comply with a collection of information if it does not display a currently valid OMB control number.					
1. REPORT DATE (DD-MM-YYYY) 19/Feb/2002		2. REPORT TYPE THESIS		3. DATES COVERED (From - To)	
4. TITLE AND SUBTITLE THE SLEF INDUCTION THEORY OF VORTEX BREAKDOWN				5a. CONTRACT NUMBER	
				5b. GRANT NUMBER	
				5c. PROGRAM ELEMENT NUMBER	
				5d. PROJECT NUMBER	
6. AUTHOR(S) 1ST LT CAIN CHARLES B				5e. TASK NUMBER	
				5f. WORK UNIT NUMBER	
7. PERFORMING ORGANIZATION NAME(S) AND ADDRESS(ES) UNIVERSITY OF WASHINGTON				8. PERFORMING ORGANIZATION REPORT NUMBER CI02-17	
9. SPONSORING/MONITORING AGENCY NAME(S) AND ADDRESS(ES) THE DEPARTMENT OF THE AIR FORCE AFIT/CIA, BLDG 125 2950 P STREET WPAFB OH 45433				10. SPONSOR/MONITOR'S ACRONYM(S)	
				11. SPONSOR/MONITOR'S REPORT NUMBER(S)	
12. DISTRIBUTION/AVAILABILITY STATEMENT Unlimited distribution In Accordance With AFI 35-205/AFIT Sup 1					
13. SUPPLEMENTARY NOTES					
14. ABSTRACT					
<div style="display: flex; justify-content: space-between; align-items: center;"> <div style="text-align: left;"> DISTRIBUTION STATEMENT A Approved for Public Release Distribution Unlimited </div> <div style="font-size: 2em; font-weight: bold;">20020305 163</div> </div>					
15. SUBJECT TERMS					
16. SECURITY CLASSIFICATION OF:			17. LIMITATION OF ABSTRACT	18. NUMBER OF PAGES 228	19a. NAME OF RESPONSIBLE PERSON
a. REPORT	b. ABSTRACT	c. THIS PAGE			19b. TELEPHONE NUMBER (Include area code)

The Self-Induction Theory of Vortex Breakdown

by

Charles Bourmorck Cain

A thesis submitted in partial fulfillment of the
requirements for the degree of

Master of Science in Aeronautics and Astronautics

University of Washington

2001

Program Authorized to Offer Degree:

University of Washington Department of Aeronautics and Astronautics

University of Washington
Graduate School

This is to certify that I have examined this copy of a master's thesis by

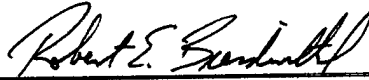
Charles B. Cain

and have found that it is complete and satisfactory in all respects,
and that any and all revisions required by the final
examining committee have been made.

Committee Members:



Mitsuru Kurosaka



Robert E. Breidenthal

Date: May 23, 2001

Master's Thesis

In presenting this thesis in partial fulfillment of the requirements for a Master's degree at the University of Washington, I agree that the Library shall make its copies freely available for inspection. I further agree that extensive copying of this thesis is allowable only for scholarly purposes, consistent with "fair use" as prescribed in the U.S. Copyright Law. Any other reproduction for any purposes or by any means shall not be allowed without my written permission.

Signature 

Date 23 MAY, 2001

University of Washington

Abstract

The Self-Induction Theory of Vortex Breakdown

by Charles B. Cain

Chairperson of the Supervisory Committee

Professor Mitsuru Kurosaka
Department of Aeronautics and Astronautics

A new study of the transient stages leading to the formation of vortex breakdown shows that vortex breakdown is initiated by a negative vorticity gradient that causes an inviscid self-induction feedback mechanism resulting in steady state vortex breakdown. We call this the self-induction theory of vortex breakdown. The vortex filament method captures the evolution of this transient formation of vortex breakdown. An axial vorticity gradient is introduced into the vortex tube by changing the circulation along the tube. Thereafter, the self-induction process starts on its own as the axial vorticity induces azimuthal velocity, which in turn tilts the vorticity vector in the azimuthal direction. Due to the gradient in azimuthal vorticity caused by the increase in circulation, the vortex tube radially expands and the vortex filaments contract in an action we call pile-up. This is followed by a sign switch in the azimuthal vorticity caused by the region downstream of the vorticity gradient rotating slower than the upstream region. These actions proceed together until they form what we call the turning point where the vortex filaments turn inward on themselves causing a sign switch in the axial vorticity. Vorticity and velocity data produced from this simulation compare well to experimental data. In conjunction with the computer simulation, we have verified these results experimentally with a delta wing model in a water tunnel using dye flow visualization, laser-induced fluorescence, and particle image velocimetry. These results, combined with comparisons with previous experiments agree with one another and support the self-induction theory of vortex breakdown.

TABLE OF CONTENTS

LIST OF FIGURES.....	iii
LIST OF TABLES	viii
1. Introduction to Vortex Flows.....	1
1.1 Vortex flow in a pipe	4
1.2 Vortex flow over a delta wing.....	6
1.3 Equations of motion.....	8
1.3.1 Vorticity equation	15
1.3.2 Derivation of Biot-Savart law.....	17
1.3.3 Physical interpretation of equation of the Biot-Savart law	23
2. Vortex filament method.....	26
2.1 Vortex tube interacts with itself	26
2.2 Discretizing the vortex tube	27
2.3 Model setup.....	29
2.3.1 Ideal case	30
2.3.2 Numerical case.....	35
2.4 Algorithm	37
2.4.1 Initialize simulation	38
2.4.2 Calculating induced velocities.....	50
2.4.3 Update vortex filament node location.....	54
2.4.4 Update Vortex Filament Segment Core Radius.....	55
2.4.5 Repeat main program loop	55
2.5 Previous vortex filament method work.....	55
3. Vortex Filament Method Results	59
3.1 Model Output	59
3.1.1 Streaklines and pathlines.....	59
3.1.2 Vortex filament method flow visualization.....	61
3.1.3 Vorticity and Velocity Data.....	69
3.2 Application to vortex breakdown	72
3.3 Vorticity gradient in the discretized vortex tube	73
3.4 Primary Case	74
3.4.1 Vortex filament plots	75
3.4.2 Velocity and Vorticity plots on meridional plane.....	84
3.4.3 Streamline plot.....	96
3.4.4 Case 1 pathlines, rendered.....	97
3.5 Other Cases, Vary C_{final}	101
3.6 Model Optimization.....	102
4. Self-induction theory of vortex breakdown	110
4.1 Difference from previous theories.....	110
4.2 Assumptions	111
4.3 Initial cause of breakdown	111

4.3.1 Circulation gradient	112
4.3.2 Velocity gradient.....	112
4.4 Self-induced feedback mechanism	115
4.4.1 Radial expansion.....	116
4.4.2 Pile-up	122
4.4.3 Vorticity sign switch	129
4.4.4 Turning point	137
4.5 Implications of self-induction mechanism on vortex breakdown	141
5. Experimental and Computational Evidence.....	145
5.1 Case 1, vortex breakdown over delta wing with vorticity gradient.....	145
5.1.1 Experiment setup	146
5.1.2 Dye flow visualization	147
5.1.3 Laser induced fluorescence (LIF) flow visualization	150
5.1.4 Particle image velocimetry (PIV)	151
5.2 Case 2, vortex breakdown due to vorticity gradient in vortex tube with fixed circulation	159
5.3 Case 3, vortex breakdown in cylinder with rotating end wall.....	161
5.4 Case 4, Navier-Stokes solution to case 2	164
5.5 Other experimental and computation evidence	170
5.6 Vortex breakdown control experiments and the self-induction theory	174
5.6.1 Vorticity gradient.....	174
5.6.2 Radial Expansion	177
5.6.3 Pile-up	179
5.6.4 Vorticity sign switching	180
6. Suggested future work	183
7. Conclusions.....	184
8. APPENDIX A—Vortex Filament Simulation Source Code	189
8.1 vlinec.cpp - Main simulation code.....	189
8.2 init_incase.cpp - Vortex filament initialization code.....	202
8.3 init_incase.cpp - Vortex filament input file	207
9. Appendix B—Additional Vortex filament simulation results	208
9.1 Vortex filament, $r = 0.12$, side view	208
9.2 Vortex filament, $r = 0.12$, rendered perspective view	210
9.3 Vortex filament, $r = 0.12$, closer rendered perspective view	215
9.4 Color contour azimuthal velocity plots.....	217
9.5 Color contour axial velocity plots	219
9.6 Color contour radial velocity plots	221
9.7 Color contour azimuthal vorticity plots	223
9.8 Color contour axial vorticity plots.....	225
9.9 Color contour radial vorticity plots	227

LIST OF FIGURES

<i>Number</i>	<i>Page</i>
Figure 1-1, Vortex flows in nature (<i>ref. 1</i>)	1
Figure 1-2, Vortex flow over F/A-18 (<i>ref. 2</i>)	2
Figure 1-3, Vortex breakdown over a delta wing	3
Figure 1-4, Swirl vane vortex generator in a pipe (<i>ref. 7</i>)	4
Figure 1-5, Numerical model of swirl vane vortex generator in a pipe (<i>ref. 7</i>)	5
Figure 1-6, Vortex breakdown in a pipe (<i>ref. 8</i>)	5
Figure 1-7, Horizontally mounted delta wing in water tunnel	6
Figure 1-8, Vortex flow over a delta wing (<i>ref. 9</i>)	7
Figure 1-9, Diagram of vortex flow	9
Figure 1-10, Vortex line	10
Figure 1-11, Vortex Tube	10
Figure 1-12 Real vortex velocity and vorticity distribution (<i>ref. 1.10</i>)	12
Figure 1-13 Rankine vortex velocity and vorticity distribution (<i>ref. 10</i>)	12
Figure 1-14, Wingtip vortex interactions (<i>ref. 13</i>)	18
Figure 1-15 Source and observation points	20
Figure 2-1, Vortex Tube	27
Figure 2-2 Real vortex velocity and vorticity distribution (<i>ref. 10</i>)	27
Figure 2-3 Vortex Tube Discretization	28
Figure 2-4 Vortex Filament Segments	29
Figure 2-5 Axial Vorticity Source	30
Figure 2-6 Closed Loop Vortex Lines	32
Figure 2-7 Changing Circulation	34
Figure 2-8 Creating Azimuthal Vorticity	35
Figure 2-9 Numerical construction of axial vorticity source	37
Figure 2-10 Simulation Algorithm	38
Figure 2-11 Vortex node location	39
Figure 2-12 Initial location of vortex lines, perspective view one	41

Figure 2-13 Initial location of vortex lines, perspective view two	42
Figure 2-14 Initial location of vortex lines, side view	43
Figure 2-15 Initial location of vortex lines, end view	44
Figure 2-16 Ideal vs. actual initial axial vorticity profile	47
Figure 2-17 Circulation sum	48
Figure 2-18 Circulation in a ring of vortex filaments	49
Figure 2-19 Induced velocity from P on Q	51
Figure 2-20 Points P and Q on vortex filament segments	52
Figure 3-1 Streaklines in a vortex flow	59
Figure 3-2. Pathlines vs. streaklines	60
Figure 3-3 Example of model output, all vortex filaments, side view	62
Figure 3-4 Example of model output, all vortex filaments, perspective view	62
Figure 3-5 Example of model output, with radial spokes, perspective view	63
Figure 3-6 Example of model output, $r = 0.42$, $r = 0.12$, side view	64
Figure 3-7 Example of model output, $r = 0.42$, $r = 0.12$, perspective view	64
Figure 3-8 Example of model output, $r = 0.12$, side view	65
Figure 3-9 Example of model output, $r = 0.12$, perspective view	65
Figure 3-10 Example of model output, $r = 0.12$, rendered side view	66
Figure 3-11 Example of model output, $r = 0.12$, rendered perspective view	67
Figure 3-12 Closer view, $r = 0.12$, rendered perspective view	68
Figure 3-13 Simulation results, with (bottom) and without (top) vortex filaments, $T = 1.8$	69
Figure 3-14 Example of azimuthal velocity, meridional plane, perspective view	70
Figure 3-15 Example of axial velocity, meridional plane	71
Figure 3-16 Circulation of vortex tube at vorticity source	73
Figure 3-17 Streamlines, $T = 2.4$, meridional plane	96
Figure 3-18 Simulation optimization, centerline, axial velocity, vary dz , $T = 1.8$	104
Figure 3-19 Vortex filament simulation results, vary vortex filament segment length, dz	105

Figure 3-20 Simulation optimization, centerline axial velocity, vary dt, $T = 1.8$	106
Figure 3-21 Vortex filament simulation results, vary simulation time step, dt	108
Figure 3-22 Simulation optimization, vortex tube end location, $T = 1.8$	109
Figure 4-1 Creating Azimuthal Vorticity	111
Figure 4-2 Pressure distribution over NACA 0012 airfoil (<i>ref. 3</i>).....	113
Figure 4-3 Vortex tube in negative velocity gradient	114
Figure 4-4 Self-Induced, inviscid feedback mechanism of vortex breakdown	116
Figure 4-5 Radial expansion.....	117
Figure 4-6 Azimuthal vorticity in meridional plane.....	117
Figure 4-7 Induced radial velocities.....	119
Figure 4-8 Radial expansion, rendered vortex filaments, $r = 0.12$ (L), $r = 0.42$ (R), $T = 0.9$	120
Figure 4-9 Induced radial velocity in vorticity gradient region.....	121
Figure 4-10 Vorticity gradient leading to pile-up	122
Figure 4-11 Pile-up with radial expansion.....	123
Figure 4-12 Pile-up along vortex tube centerline.....	124
Figure 4-13 Pile-up along vortex tube, centerline and $r = 0.12$	125
Figure 4-14 Pile-up along vortex tube, rendered $r = 0.12$	126
Figure 4-15 Pile-up, axial velocity, $T = 1.2$	127
Figure 4-16 Pile-up, axial vorticity, $T = 1.2$	128
Figure 4-17 Induced azimuthal velocity, $T = 1.2$	130
Figure 4-18 Vortex tube, rotating and different velocities	131
Figure 4-19 Azimuthal vorticity sign switch	132
Figure 4-20 Vortex filaments, azimuthal vorticity sign switch	133
Figure 4-21 Azimuthal vorticity sign switch, meridional plane	134
Figure 4-22 Backflow.....	135
Figure 4-23 Beginning of backflow, axial velocity, $T = 1.2$	135
Figure 4-24 Radial vorticity sign switch	136
Figure 4-25 Turning point formation	137

Figure 4-26 Turning point established	138
Figure 4-27 Vortex filaments projected on meridional plane, $T = 1.5$	138
Figure 4-28 Axial vorticity sign switch.....	139
Figure 4-29 Axial vorticity sign switch, meridional plane, $T = 1.5$	140
Figure 4-30 Steady state vortex breakdown location	142
Figure 4-31 Vortex breakdown location change with AOA increase	143
Figure 4-32 Vortex breakdown location change with freestream velocity increase	144
Figure 5-1 Generating a vorticity gradient over a delta wing.....	146
Figure 5-2 Vortex breakdown, dye visualization.....	147
Figure 5-3 Dye flow visualization, turning point.....	148
Figure 5-4 Vortex filament simulation, features of self-induction mechanism, $T = 1.5$.	149
Figure 5-5 Turning in vortex breakdown experiments (<i>ref. 8</i>).....	150
Figure 5-6 Laser induced fluorescence, delta wing vortex breakdown.....	151
Figure 5-7 PIV experimental setup	152
Figure 5-8 PIV results, vorticity gradient enters capture area, $t = t_0$	153
Figure 5-9 PIV results, azimuthal vorticity sign switch, $t = t_0 + 45 \text{ ms}$	154
Figure 5-10 PIV results, vortex breakdown established, $t = t_0 + 60 \text{ ms}$	155
Figure 5-11 Azimuthal vorticity, simulation (top) and experiment (bottom).....	156
Figure 5-12 Axial velocity profile, experiment (top, middle) and simulation (bottom) .	157
Figure 5-13 Azimuthal vorticity sign switch and velocity profile	158
Figure 5-14 Vorticity gradient caused by vortex tube perturbation.....	159
Figure 5-15 Vortex perturbing periodic jet.....	160
Figure 5-16 Vortex breakdown in perturbed vortex tube	161
Figure 5-17 Vortex breakdown in cylinder, experiment setup	162
Figure 5-18 Vortex breakdown in cylinder, $H/R = 2$, $Re = 1854$	163
Figure 5-19 Azimuthal vorticity and secondary vortex breakdown, $T = 2.4$	164
Figure 5-20 Instantaneous streamlines, vortex filament simulation, $T = 2.4$	164
Figure 5-21 Streamlines, Navier-Stokes Simulation (L) and Experiment (R)	166
Figure 5-22 Meridional Plane Data, Navier-Stokes Simulation, ω_θ (L), ω_z (C), ω_r (R) .	167

Figure 5-23 Rendered vortex tube, numerical solution to Escudier's experiment.....	168
Figure 5-24 Rendered vortex filament simulation results, $T = 0.9$	168
Figure 5-25 Axial vorticity at various radial location along vortex tube, Navier-Stokes Simulation (L) and vortex filament simulation (R).....	170
Figure 5-26 Shock wave/vortex interactions (<i>ref. 29</i>).....	171
Figure 5-27 Azimuthal vorticity sign switch (<i>ref. 30</i>)	172
Figure 5-28 Axial vorticity sign switch, meridional (top) and cross flow (bottom) plane (<i>ref. 30</i>)	173
Figure 5-29 F/A-18 Leading edge strake modification (<i>ref. 4</i>)	176
Figure 5-30 Delay in vortex breakdown location with rounded strake LE (<i>ref. 4</i>).....	177
Figure 5-31 Vortex flow over a delta wing (<i>ref. 9</i>).....	178
Figure 5-32 Tangential blowing setup (<i>ref. 35</i>).....	181
Figure 5-33 Delaying vortex breakdown with tangential jet (<i>ref. 35</i>)	182

LIST OF TABLES

<i>Number</i>	<i>Page</i>
Table 2-1 Vortex filament circulation distribution	50
Table 3-1 Primary case parameters	74
Table 4-1 Induced radial velocities	118

ACKNOWLEDGEMENTS

I would like to express sincere thanks to the many people who helped bring this thesis research into being. Special thanks goes to my advisor, Prof. Mitsuru Kurosaka, for his help, advice, and guidance in this work. I thank him for giving me the opportunity to come to the University of Washington and pursue this line of study. I would also like to thank Suttiiphong Srigrarom, the hardest working student I have ever met, for his extensive help in the lab, his constant availability for discussing these new ideas, and for his contribution to the experimental work cited in this paper. I also need to thank Dennis Peterson for his expertise in the machine shop, both in building various apparatus for me and for teaching me to use the machinery myself. Let me also thank Wanda Frederick and the UW AA department staff for their unwavering support for me and for this research.

I am especially thankful to the Gordon C. Oates Memorial Endowed Fellowship and the Donald C. Whitworth Endowed Scholarship for their generous support for my studies. Their financial support made it possible for me to attend the University of Washington and pursue this research. I also want to thank the U.S. Air Force for allowing me to accept this support and attend the University of Washington. I also extend thanks to my USAF Program Manager, Capt. Melissa Flattery, for her help and assistance in meeting program requirements and in making it possible for me to present this work at several conferences.

Most of all, I would like to thank my wife and my family for their support and encouragement throughout the course of this work. Special thanks go to my Grandfather for inspiring me to join the U.S. Air Force and to study engineering. Finally, I thank God for my blessings, my talents, and the inspiration to do this work. With God all things are possible.

DISCLAIMER

The views expressed in this thesis are those of the author and do not reflect the official policy or position of the United States Air Force, Department of Defense, or the US Government.

1. Introduction to Vortex Flows

Vortex flows are regions of rotating flow in air, water, or any fluid. Vortex flows are common in nature. We see them in weather phenomena like tornadoes and hurricanes. We might also notice a vortex that develops when we drain a sink or a tub. Figure 1-1 shows a vortex flow in an image of Hurricane Fran taken by *NASA-GSFC*, using the NOAA GOES-8 imaging satellite.

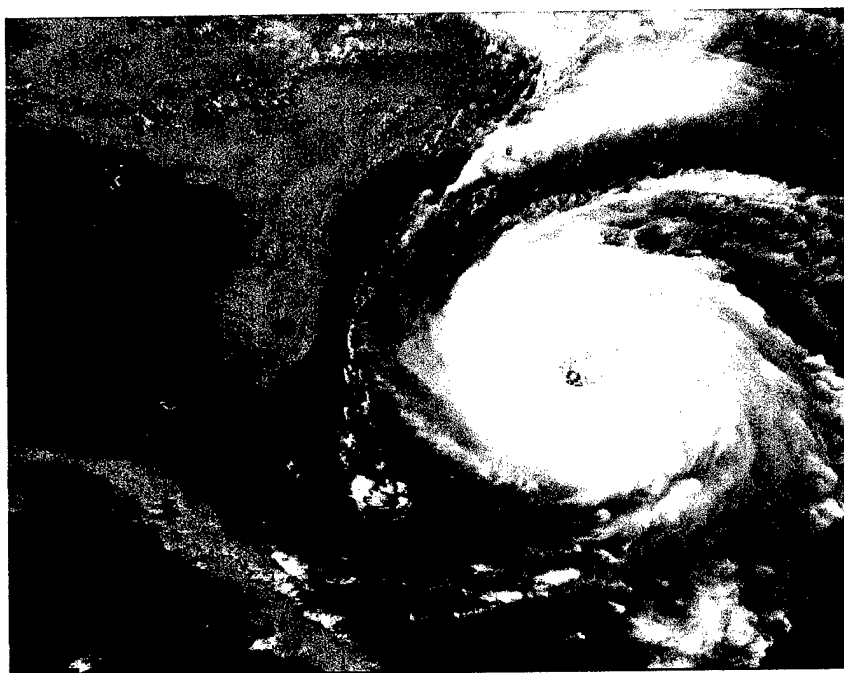


Figure 1-1, Vortex flows in nature (*ref. 1*)

Vortex flows are also commonly found around aircraft, especially aircraft with significant leading edge sweep or leading edge strakes. Figure 1-2 displays two images of an F/A-18 fighter aircraft with a vortex generated at the root of its leading edge strake.

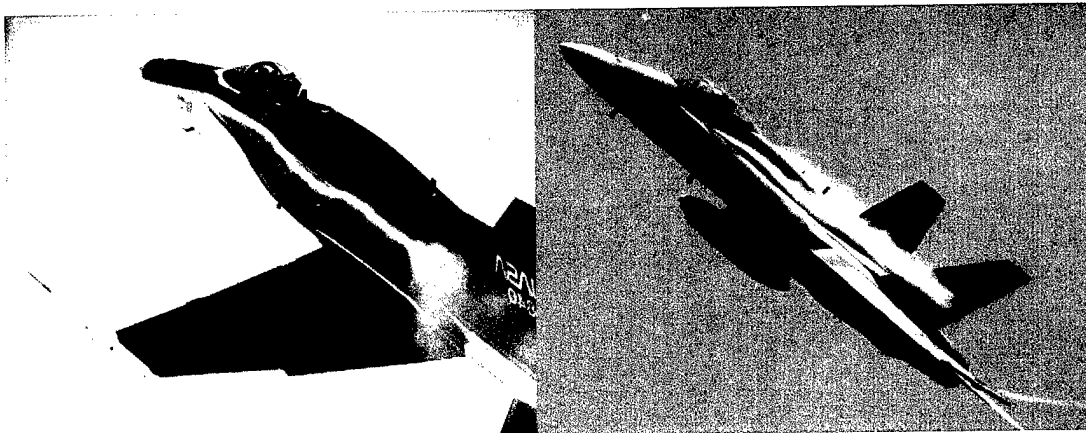


Figure 1-2, Vortex flow over F/A-18 (*ref. 2*)

At these high angles of attack, the leading edge strakes generate two strong vortices on the suction surface of the wing. In the first pictures, the vortices are made visible by injecting smoke into the flow. In the second picture, water vapor condenses to make the vortices visible.

A vortex flow, like that on the suction surface of an F/A-18 wing generates a strong component of axial velocity along the centerline of the vortex. This is beneficial to the aircraft's performance at high angles of attack because the higher velocities decrease pressure, thereby increasing lift. The kinetic energy of the vortex also energizes the flow in the boundary layer to help delay separation. The overall result of the leading edge strake and its associated vortex is an increase in the aircraft's maximum angle of attack and its maximum lift coefficient (*ref. 3*). Certainly, there is a penalty to be paid for this increased lift in terms of increased drag, but most modern fighter aircraft have sufficient thrust to overcome this.

At large angles of attack, this vortex can undergo a rapid change in flow properties called vortex breakdown. Figure 1-3 shows an example of vortex breakdown over a Plexiglas delta wing in a water tunnel (*ref. 4*).

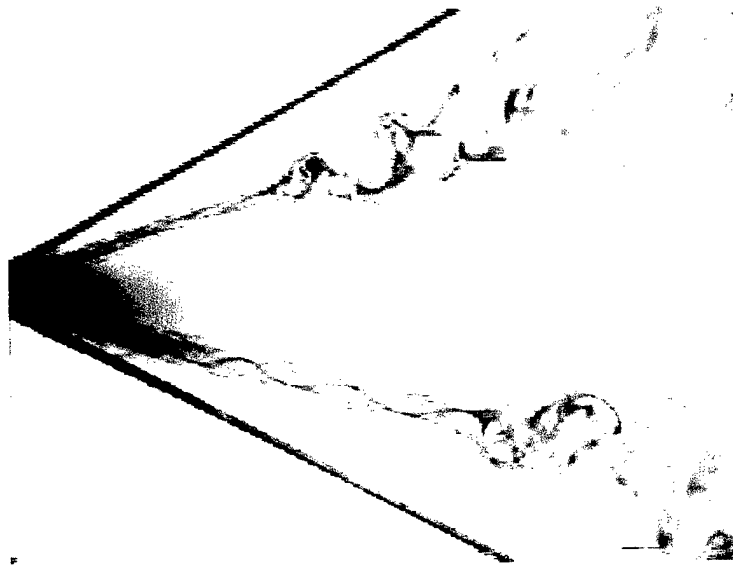


Figure 1-3, Vortex breakdown over a delta wing

Vortex breakdown is usually characterized by a rapid radial expansion of the vortex, downstream turbulence, and backflow. This rapid change in flow properties can affect the stability of the aircraft and the downstream turbulence can cause structural damage through high-cycle fatigue. This structural damage is especially prevalent on twin-tailed aircraft like the F/A-18, where the vertical tail is immediately downstream of the vortex. This is clear in the pictures of the F/A-18 in Figure 1-2.

The purpose of this research is to understand how we can preserve the positive effects of the vortex, while suppressing the negative effects of vortex breakdown. We do this by trying to understand the cause of vortex breakdown. Many others have approached this same problem and yet, as stated recently, "a comprehensive theory of vortex breakdown still does not exist" (*ref. 5*). Similar comments were made in 1977 when another person said, "the embarrassing number of different theoretical notions has not, it must be admitted, led to satisfactory understanding of the flows observed" (*ref. 6*). So there is work yet to be done.

It is often easier to study vortices and vortex breakdown in controlled laboratory settings. In a laboratory, vortices are often generated in pipes, or in water and wind tunnels with a simple delta wing model.

1.1 Vortex flow in a pipe

You need two things to generate a vortex in a pipe—something to introduce rotation into the flow, and something to send that rotating flow downstream. Usually, experimenters use swirl vanes, a swirl manifold, or angled jets do this. Swirl vanes are nothing more than small wing sections, arranged around the circumference of the pipe. Usually, you can change their angle of attack to change the amount of swirl in the flow. The downwash generated by the wing sections deflects the flow to make it swirl. A swirling manifold has spiraling ducts that introduce rotation into the flow. Angled jets send fluid into the pipe at an angle to the walls of the pipe to cause the flow to rotate.

The velocity component that sends the flow downstream can be created any number of ways. One way is to use gravity. The pipe is setup vertically with a tank of water about it. The swirl generators are place at the junction between the pipe and the tank, with some type of flow control valve in between the tank and the pipe. The valve is opened, and the flow moves into the pipe, through the swirl generators, and down to a test section where the vortex can be observed.

Figure 1-5 shows the geometry of a swirl vane vortex generator. Other ways to generate the downstream velocity component involve using pumps, fans, or exploiting flow mechanisms like Ekman layer pumping where a rotating bottom in a closed cylinder causes flow to circulate.

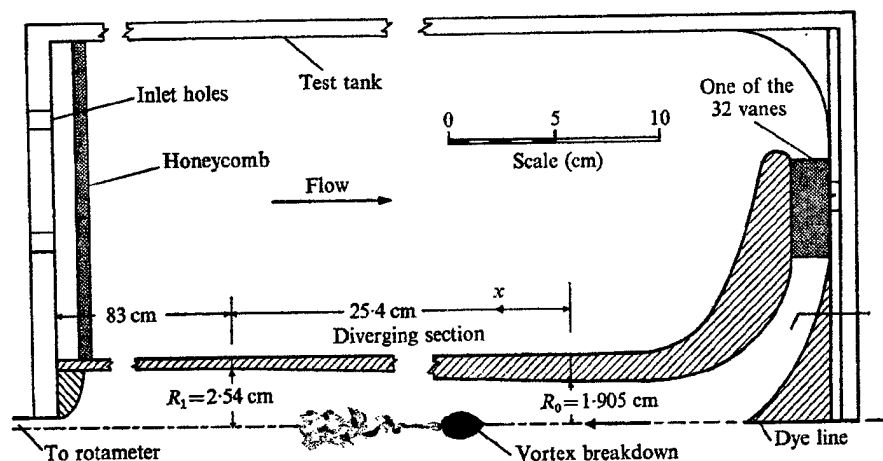


Figure 1-4, Swirl vane vortex generator in a pipe (ref. 7)

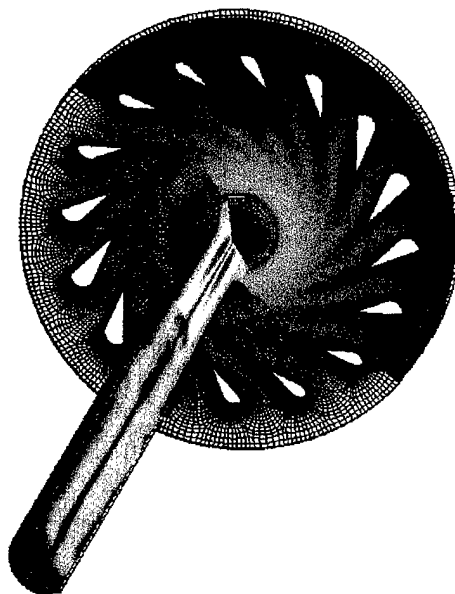


Figure 1-5, Numerical model of swirl vane vortex generator in a pipe (*ref. 7*)

Vortex flows in pipes are very useful for study because the vortices can be made very symmetric. This allows the researcher to clearly see the rotating flow without the asymmetries and turbulence that can be present in flow over wings in a wind or water tunnel. This is especially important when studying vortex breakdown, where one would like to separate the turbulence and potential asymmetries of the breakdown from the turbulence and asymmetries of the surrounding flow. Figure 1-6 presents an example of a vortex and its breakdown in a pipe. The apparatus used to generate this vortex is the one shown in Figure 1-4. The symmetry possible with this type of apparatus is clear.

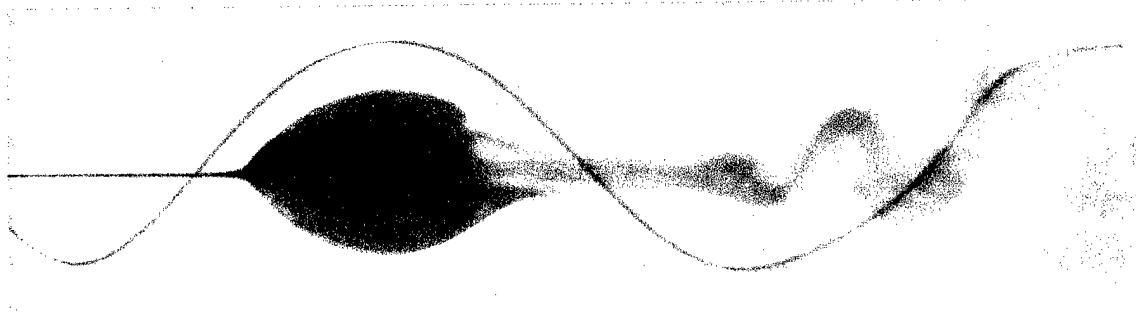


Figure 1-6, Vortex breakdown in a pipe (*ref. 8*)

1.2 Vortex flow over a delta wing

Vortex flows in a pipe can be very useful to the researcher. However, the apparatus used is very specialized. Also, the vortex that forms over real aircraft will not be as symmetrical as the one in the pipe. Furthermore, it can be difficult to collect data from pipe flows, due to the confined nature of the pipe. For that reason, we also study vortex flows in regular wind and water tunnels. A simple flat plate delta wing like those in Figure 1-7, can be used to generate vortices.

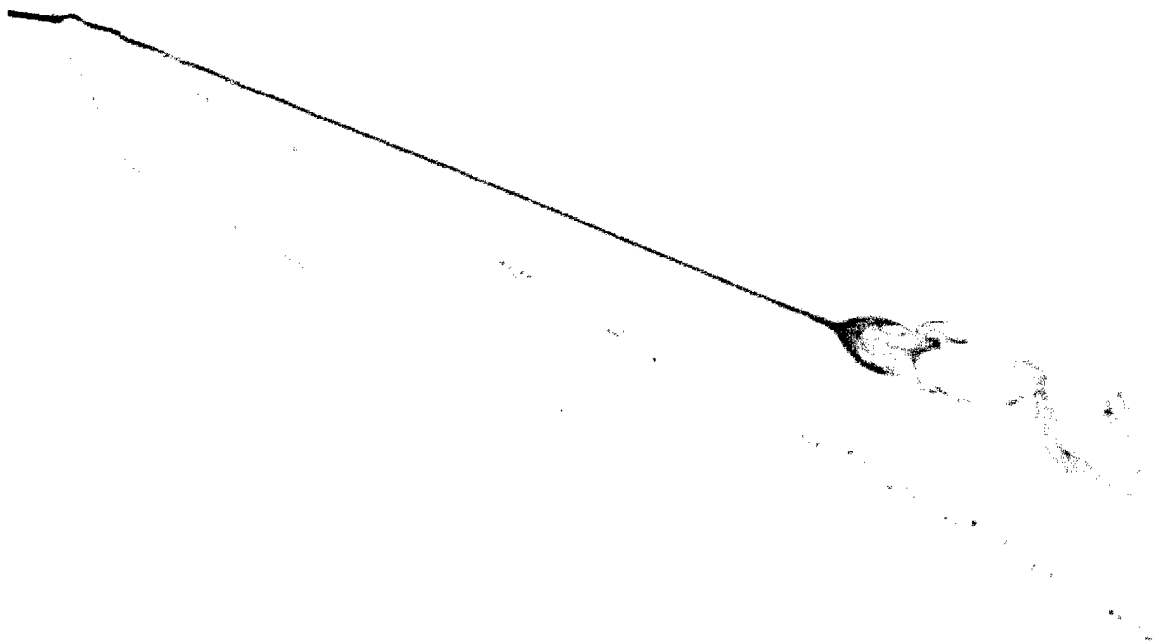


Figure 1-7, Horizontally mounted delta wing in water tunnel

Flow over a triangular shaped delta wing is characterized by two counter-rotating vortices. The vortices form as the flow separates from the sharp, swept-back leading edge of the delta wing as it tries to move from the high-pressure lower surface of the wing to the low-pressure upper surface of the wing, as seen in Figure 1-8. This separation line is called S_1 in the figure. Once separated, the low pressure on the top surface of the wing reattaches the flow at line A_1 . However, the flow separates again,

along line S_2 , drawn off the surface of the wing by the even lower pressures accompanying the fast moving flow that separated from S_1 .

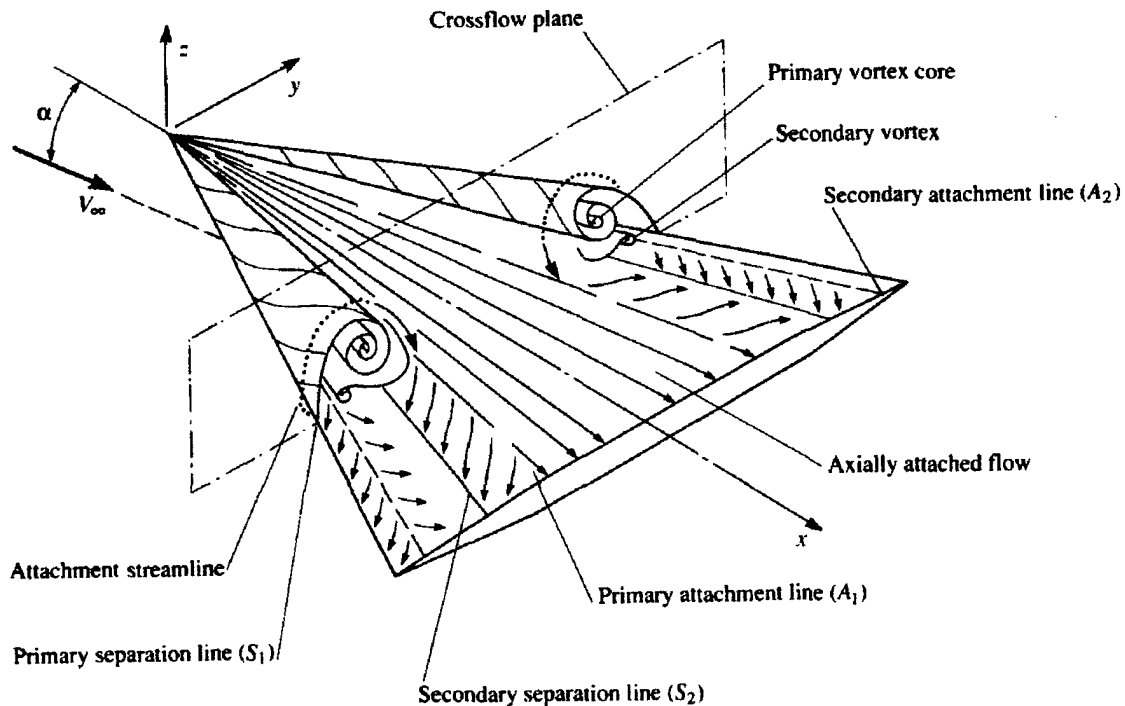


Figure 1-8, Vortex flow over a delta wing (ref. 9)

After the secondary separation, the flow turns in on itself and wraps up into the primary vortex. The flow turning inward on itself is self-similar, in that as it turns inward, the surrounding flow that previously turned inward will sustain the flow in its inward turning direction. It continues to spiral inward at a smaller and smaller radius, thus forming the vortex. This second separation causes a secondary rotating flow that reattaches along the attachment line A_2 . The secondary flow then separates again, turning back inward to form a secondary vortex. While the flow is rotating, there is an axial (chordwise) velocity component. That component is undisturbed by the vortices near the centerline of the wing.

As we will describe in more detail in the next section, very low pressures characterize the center of these vortices. It is this strong low pressure that produces the aircraft performance benefits of a vortex flows. However, these benefits do not last

forever. As the delta wing is brought to larger angles of attack (angles of attack greater than 10 degrees or so, depending on leading edge sweep among other factors), these strong, previously stable vortices will breakdown. They will transit from a state of organized rotation, to a state of spiraling turbulence, characterized by rapid radial expansion and backflow. Look again at Figure 1-6 on page 5 to see how dramatic the transition is. If we can prevent, delay, or weaken this transition, we can use the positive benefits of the vortex at higher angles of attack for increased aircraft performance.

The key is to understand why the vortex breaks down. Then, we can devise ways to prevent that breakdown. We will introduce new ideas as to why vortices breakdown occurs in later sections. First, we should describe the vortex flow more precisely. With a more precise understanding, we can think of ways to model the flow. If we can produce a model of the vortex that over time seems to develop the properties of vortex breakdown, we can look at the model for clues as to the mechanism for that breakdown and see if it applies to real flows. If it does, we will know where to intercede to stop or weaken the vortex breakdown in real flows.

1.3 Equations of motion

As with many flows in fluid dynamics, we can describe the motion of vortex flows with several equations. First, let us look at vortex flows in a broader sense. Let us define vortex flows as flows with large velocity components rotating in a circular path. This fits the examples of vortex flows previously presented. There may be other velocity components in the flow, but that velocity around centerline characterizes it. That velocity will be called the azimuthal velocity and will be given the symbol u_θ to signify that the direction of the velocity is in the theta direction of a cylindrical coordinate system. Another often mentioned term is vorticity. Vorticity ($\vec{\omega}$) is a measure of rotation in a flow. It is defined as the curl of the velocity. So vorticity is vector that measures rotating motion in a flow. It has units of $(time)^{-1}$. Equations (1-1) through (1-4) show the components of vorticity in cylindrical coordinates

$$\vec{\omega} \equiv \text{curl}(\vec{u}) \equiv \nabla \times \vec{u} \quad (1-1)$$

$$\omega_r = \frac{1}{r} \frac{\partial u_x}{\partial \theta} - \frac{\partial u_\theta}{\partial x} \quad (1-2)$$

$$\omega_\theta = \frac{\partial u_\theta}{\partial x} - \frac{\partial u_x}{\partial r} \quad (1-3)$$

$$\omega_z = \frac{1}{r} \frac{\partial(r u_\theta)}{\partial r} - \frac{1}{r} \frac{\partial u_r}{\partial \theta} \quad (1-4)$$

Using the right hand rule, you can see the sense of rotation. If you align the thumb of your right hand with the vorticity vector and curl your fingers, the flow will be rotating in the same direction you are curling your fingers. Figure 1-9 presents a diagram of a rotating fluid element.

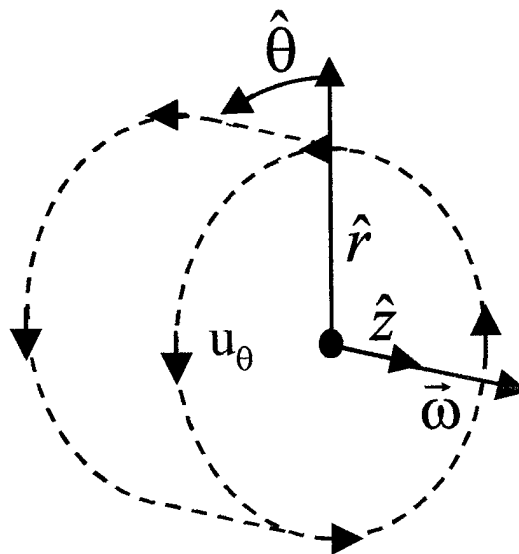


Figure 1-9, Diagram of vortex flow

Now, let's take this element of rotating flow and extend it along a line, as in Figure 1-10. The local vorticity vector will be aligned with this line and the flow will rotate tangentially about this line at every point. We can call this a vortex line. The vorticity vector is always aligned with a vortex line, so the velocity associated with that vorticity is always known. A formula, called the Biot-Savart Law, describes the velocity vector associated with a given vorticity vector. This law will be described in detail later, as it

allows us to calculate how vortices interact with each other and how they interact with themselves.

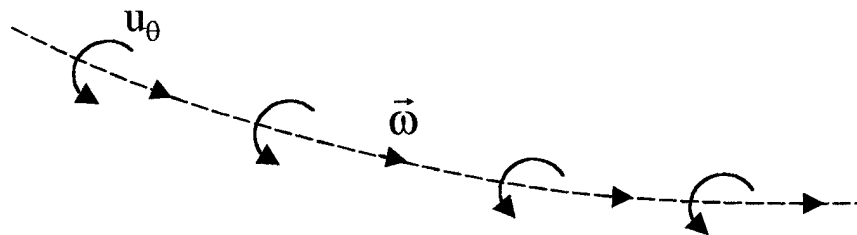


Figure 1-10, Vortex line

Next, let's collect several vortex lines together in a group. If they are oriented in the same direction, we can call this group of vortex lines a vortex tube.

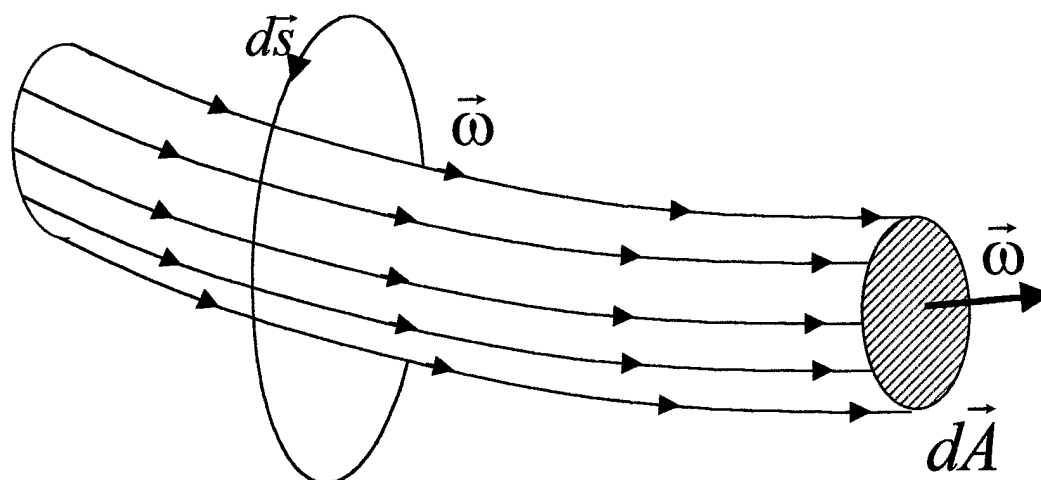


Figure 1-11, Vortex Tube

It might be important to measure the strength of this vortex tube. One way would be to add up vorticity in the vortex tube, multiplying each vorticity vector by the cross-sectional area of the vortex tube that it occupies. This is essentially what is done. We call the measure of vortex strength circulation. It is given the symbol Γ , though at later points we may refer to circulation as C . Later, we will distinguish between the circulation of the entire vortex tube and the circulation in an individual vortex line.

This measurement of vortex strength, Γ , is an important measure of vortex flows. We can further describe this term in several ways. One useful way to think of circulation is to consider it in terms of vorticity flux. It can be defined in terms of velocity or vorticity. In terms of velocity, circulation is the line integral of velocity around a closed contour, C , as Equation (1-5) describes. Equation (1-6) shows how this expression can be put in terms of vorticity using Stokes' theorem. This expression of circulation in terms of vorticity shows that vorticity can be thought of as circulation per unit area (*ref. 10*).

$$\Gamma = \oint_C \vec{u} \cdot d\vec{s} \quad (1-5)$$

$$\Gamma = \int_A \text{curl}(\vec{u}) \cdot d\vec{A} = \int_A \vec{\omega} \cdot d\vec{A} \quad (1-6)$$

Let us look in more detail at the way a real vortex, like the examples presented earlier, actually behave. Real vortex flows typically have distinct regions of rotation. Each region rotates with its own types of azimuthal velocity profiles. Figure 1-12 shows the velocity and vorticity distribution of a real vortex. A real vortex is often idealized by making the vorticity profile a uniform step function in the vortex core. Figure 1-13 shows this idealization. This idealized vortex is called a Rankine vortex.

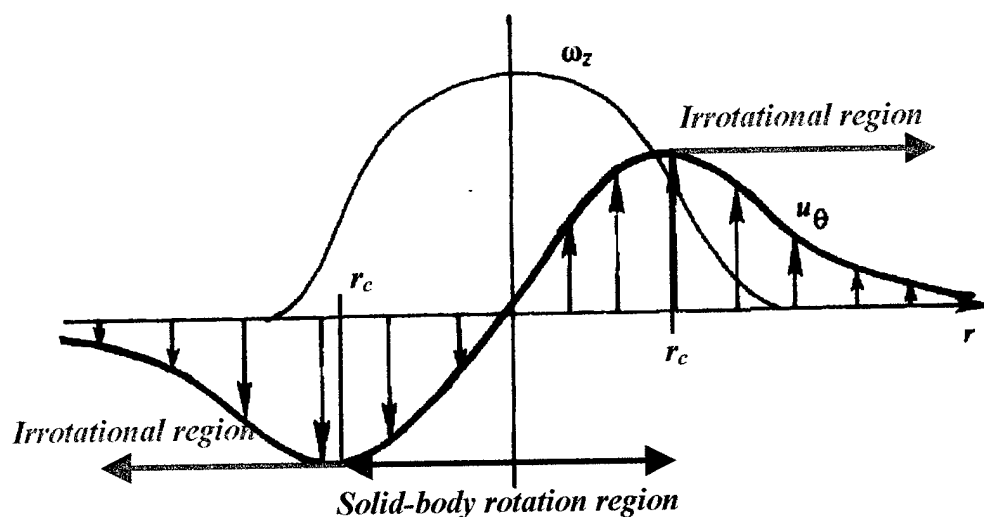


Figure 1-12 Real vortex velocity and vorticity distribution (ref 1.10)

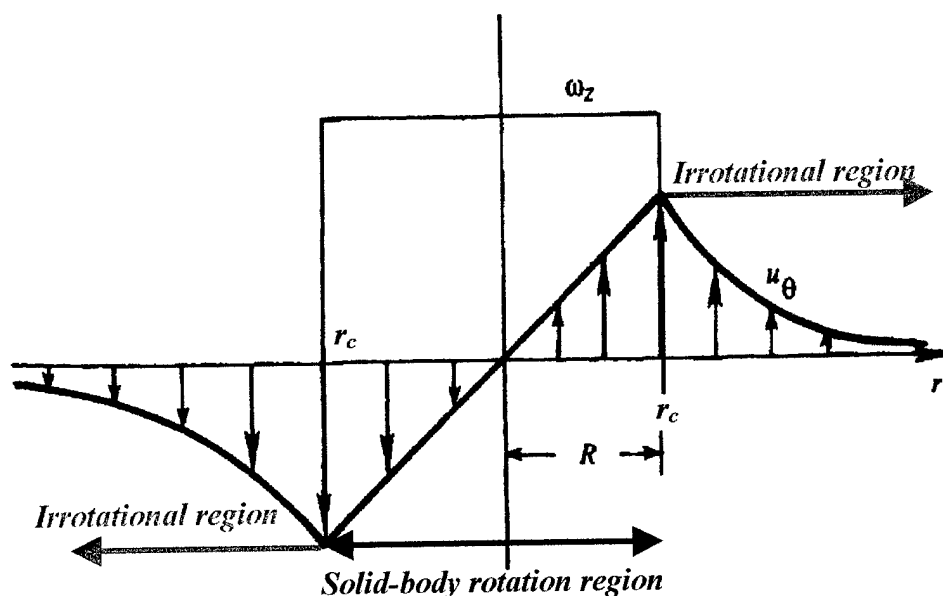


Figure 1-13 Rankine vortex velocity and vorticity distribution (ref. 10)

In this section we will be speaking mostly about the Rankine vortex, though the concepts also apply to the real vortex. The only change is the vorticity distribution. We will also be assuming that the flow is incompressible and inviscid. Let us look more closely at the two regions of rotation. The first is the solid-body rotation region. This

region is often called the vortex core. This region starts at the core of the vortex and extends out to the radius, r_c . As its name implies, this region of the vortex rotates like a solid body, with an azimuthal velocity that is proportional to the radial distance to the center of the vortex. Equation (1-7) shows the azimuthal velocity distribution, where ω_0 is the angular velocity of the solid body rotation region. If the only velocity component is that in the azimuthal direction, we can see that the vorticity in this region only in the z -component, as Figure 1-9 suggests. Circulation in this region is defined in terms of Equation (1-5) and described in Equation (1-9). Because the circulation is non-zero, this region of the vortex is rotational. In rotational flow, the vorticity, $\vec{\omega} \equiv \text{curl}(\vec{u}) \equiv \nabla \times \vec{u}$, is non-zero.

$$u_\theta = \omega_0 r \quad (1-7)$$

$$\omega_z = \frac{1}{r} \frac{\partial(ru_\theta)}{\partial r} - \frac{1}{r} \frac{\partial u_r}{\partial \theta} = 2\omega_0 \quad (1-8)$$

$$\Gamma = \oint_C \vec{u} \cdot d\vec{s} = \int_0^{2\pi} u_\theta r d\theta = 2\pi r u_\theta = 2\pi r^2 \omega_0 \quad (1-9)$$

The second region of rotation is the irrotational region. As its name implies, this region is not rotational. Hence, the vorticity is zero and the circulation is constant in this region. Figure 1-12 and Figure 1-13 show the rotational and irrotational vorticity profile. In the irrotational region, the azimuthal velocity is proportional to the inverse of the radial distance from the center of the vortex, as described in Equation (1-10) where c is some constant.

$$u_\theta = \frac{c}{2\pi r} \quad (1-10)$$

$$\omega_z = \frac{1}{r} \frac{\partial(ru_\theta)}{\partial r} - \frac{1}{r} \frac{\partial u_r}{\partial \theta} = 0 \quad (1-11)$$

$$\Gamma = \oint_C \vec{u} \cdot d\vec{s} = \int_0^{2\pi} u_\theta r d\theta = 2\pi r u_\theta = c \quad (1-12)$$

$$u_\theta = \frac{\Gamma}{2\pi r} \quad (1-13)$$

If the only velocity component is the azimuthal velocity, then the vorticity is zero and the circulation is constant, as Equations (1-11) and (1-12) show. As a result of Equation (1-12) we can now find the proportionality constant in Equation (1-10). As Equation (1-13) describes, that constant is the circulation, Γ . These results indicate, that, outside of the vortex core, the circulation is constant and independent of radial distance from the vortex center. Another outcome of this, implied by the definition of circulation in Equation (1-5), is that in close loop regions that do not contain the vortex core, the circulation is zero. For closed loop regions that do contain the vortex core and are outside of that core, the circulation is equal to the expression in Equation (1-14), where r_c is the radius of the vortex core, which is a constant for inviscid vortex flows.

$$\Gamma = \oint_C \vec{u} \cdot d\vec{s} = \int_0^{2\pi} u_\theta r_c d\theta = 2\pi r_c u_\theta = 2\pi r_c^2 \omega_0 \quad (1-14)$$

The outcome that circulation is constant for all time along a closed path for inviscid, incompressible, barotropic flow is known as Kelvin's circulation theorem.

Mathematically, this is expressed as $\frac{D\Gamma}{Dt} = 0$. Thus, irrotational flow (the flow outside of the vortex core) will remain irrotational for all time, under the stated assumptions.

Another important theorem to vortex flows is the Helmholtz vortex theorem. This theorem applies directly to the vortex lines that were mentioned previously. Again, assuming inviscid, incompressible, barotropic flow, Helmholtz shows that (1) vortex lines move with the fluid elements, (2) circulation is constant along vortex line, (3) a vortex

line or vortex tube must end at a boundary or form a loop (it cannot end in a fluid), and (4) the strength of a vortex line in a vortex tube remains constant for all time (*ref. 10*).

We have defined how rotating flow acts and how we can define that rotating flow by vorticity and vortex lines. The next question is, how does this vortex line interact with its environment? How does it interact with itself? To answer this question, we need to look at the governing equations that show how vorticity can change in the fluid. This is succinctly defined with the so-called vorticity equation. Next, we want to know exactly what velocity field is associated with a given vorticity field. The Biot-Savart law defines this velocity. With these principles in mind, we can look at models for the vortex flow.

1.3.1 Vorticity equation

The vorticity equation is essentially an angular form of the momentum equation. It is derived from that momentum equation (1-15), using the continuity equation (1-16), and a vorticity solenoidality condition (1-17).

$$\text{div}(\vec{u}) = 0 \quad (1-15)$$

$$\frac{D\vec{u}}{Dt} = \frac{\partial \vec{u}}{\partial t} + (\vec{u} \cdot \vec{\nabla})\vec{u} = -\frac{1}{\rho} \nabla(p) + \nu \nabla^2 \vec{u} \quad (1-16)$$

$$\text{div}(\vec{\omega}) = \text{div}(\nabla \times \vec{u}) = 0 \quad (1-17)$$

Assuming incompressible flow and no body force, we can find the vorticity equation by taking the curl of the momentum (1-21) equation and using the vector identities in Equations (1-18), (1-19), and (1-20) (*ref. 11*). What results is the vorticity equation, which is shown in Equation (1-22).

$$\text{curl}(\nabla \vec{A}) \equiv 0 \quad (1-18)$$

$$\text{div}(\text{curl}(\vec{A})) \equiv \nabla \cdot (\nabla \times \vec{A}) \equiv 0 \quad (1-19)$$

$$\text{curl}(\vec{A} \times \vec{B}) \equiv \vec{A} \text{div}(\vec{B}) - \vec{B} \text{div}(\vec{A}) + (\vec{B} \cdot \nabla) \vec{A} - (\vec{A} \cdot \nabla) \vec{B} \equiv 0 \quad (1-20)$$

$$\text{curl} \left(\frac{D\vec{u}}{Dt} = \frac{\partial \vec{u}}{\partial t} + (\vec{u} \cdot \nabla) \vec{u} = \frac{-1}{\rho} \nabla(p) + \nu \nabla^2 \vec{u} \right) \quad (1-21)$$

$$\frac{D\vec{\omega}}{Dt} = \frac{\partial \vec{\omega}}{\partial t} + (\vec{u} \cdot \nabla) \vec{\omega} = (\vec{\omega} \cdot \nabla) \vec{u} + \nu \nabla^2 \vec{\omega} \quad (1-22)$$

There are several interesting things in Equation (1-22). First, there is no pressure term. It drops out because the curl of the pressure gradient is zero, by the vector identity (1-18). If the fluid is barotropic, then the center of pressure always acts through the center of mass in a fluid element. Thus, pressure can generate no torque and no vorticity. If we had included conservative body forces like gravity, they would have dropped out of the equation for the same reason.

For this incompressible, barotropic flow, vorticity can only change in two ways corresponding to the two terms on the right hand side of (1-22). Let us look at each of these terms. First, look at the term $\nu \nabla^2 \vec{\omega}$. The ν term is the kinematic viscosity. The solution to $\frac{D\vec{\omega}}{Dt} = \nu \nabla^2 \vec{\omega}$ is like the solution to the heat equation. Thus, vorticity diffuses like heat. By solving this differential equation for a two-dimensional vortex with the vorticity initially concentrated at the origin, that is with the initial condition

$$\omega(r, t) = \frac{\Gamma_0 \delta(r)}{2\pi r}, \text{ it can be shown that the core radius of the vortex diffuses according to}$$

$$r_c = \sqrt{1.256 \cdot (4\nu t)}. \text{ In air, } \nu = 1.45 \times 10^{-5} \frac{m^2}{s}, \text{ and in water, } \nu = 1.12 \times 10^{-6} \frac{m^2}{s}. \text{ For}$$

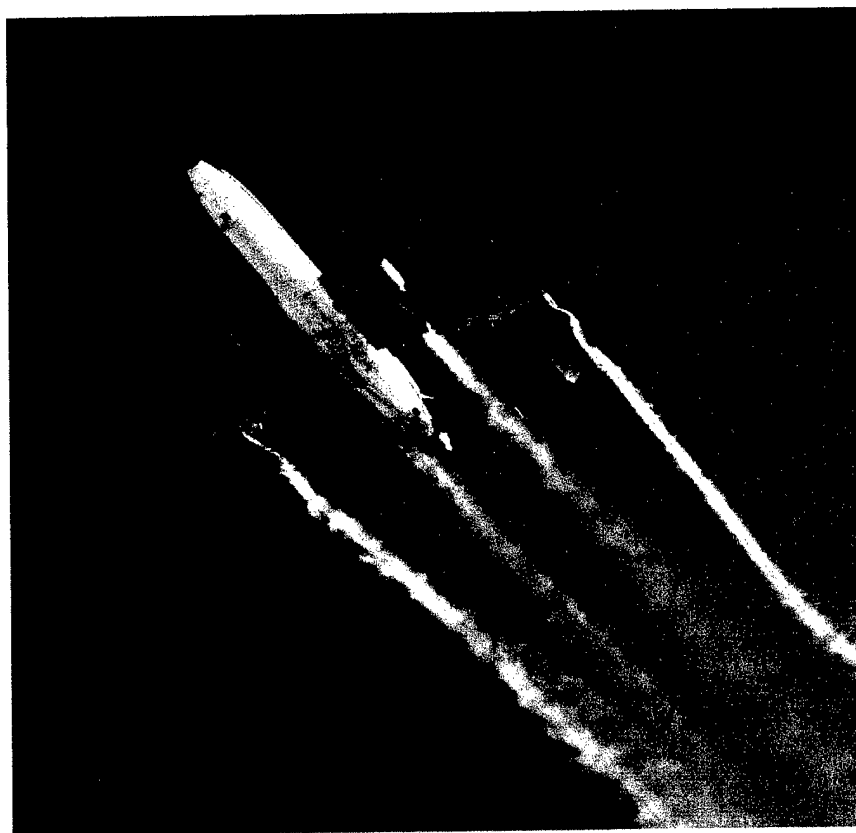
these values, it would take that initially concentrated vortex 3.8 hrs to diffuse to a core radius of 1 meter in air. In water it would take 49.4 hours to diffuse to that radius. If the time scale of the motion of interest are considerably shorter than time scales of the vortex diffusion, it is acceptable to say that diffusion is small and its effects are negligible.

The second term in this vorticity equation is $(\vec{\omega} \cdot \vec{\nabla})\vec{u}$. This is called the stretching and tilting term, and it describes how angular momentum is conserved when a vortex undergoes these processes. Essentially, if a vortex tube is stretched out, its radius will decrease. To conserve angular momentum, it will have to rotate faster, since the moment of inertia of the fluid elements decreases as it is stretched out to conserve mass. This is equivalent to the familiar example of ice skaters spinning slowly with their arms stretched out and spinning faster when they draw their arms to their bodies. Likewise, if a vortex is tilted, components of that vorticity will translate into the direction the vortex is tilted. This means that the vorticity vector is at all times proportional to the fluid line vector, $d\vec{r}$. Thus, at $t = t_0$, $\vec{\omega} = \text{const.} \cdot d\vec{r}$, with this same proportionality constant holding for any t .

Now we have determined that, under the assumed conditions, once introduced to a flow field, vorticity only can change by tilting, stretching, and diffusion. Even more, we have determined that, over short periods, the effects of diffusion are small. Now that we have vorticity present, and know how it can change, let us find out the velocities that are associated with that vorticity field. To find this, we turn to the Biot-Savart Law.

1.3.2 Derivation of Biot-Savart law

The Biot-Savart law gets its name from a magnetic field equation that describes the magnetic field that is associated with electric current as it flows through a wire (*ref. 12*). In one of those wonderful parallels in nature, this law also describes the velocity associated with a given vorticity profile. For example, if we specified a vortex line that formed a loop with a given radius and a given circulation, we could find that velocity that the vortex line induces at the center of that loop, or at any point around that loop. In a more practical sense, the Biot-Savart law would describe how the wingtip vortices of an aircraft interact with each other, as in Figure 1-14.



Dryden Flight Research Center ECN 7848 1977 Photo
L-1011 Wing Vortex Study. NASA photo



Figure 1-14, Wingtip vortex interactions (*ref. 13*)

The Biot-Savart law is very important. It uniquely describes the velocity field associated with a given vorticity field. If this field acts linearly, the associated velocity fields of several different vortex lines and their vorticity fields can be linearly added to each. This will produce an overall velocity field that, while in sum is very complicated, is simply the linear addition of many smaller parts and straightforward calculations.

Let us assume that vorticity, $\bar{\omega}(x', y', z')$, is given and that the flow is incompressible. We are trying to find the relationship between the given $\bar{\omega}$ at point (x', y', z') and the velocity, \bar{u} , at a different point, (x, y, z) . Since the flow is incompressible, we know (1-23) is true.

$$\text{div}(\vec{u}) = 0 \quad (1-23)$$

$$\vec{u} = \text{curl}(\vec{A}) \quad (1-24)$$

$$\text{div}(\text{curl}(\vec{A})) = 0 \quad (1-25)$$

Then vector potential, \vec{A} , satisfying (1-23) exist. Furthermore, we know (1-25) by the vector identity (1-19). It should be noted that \vec{A} is not unique. If we add to \vec{A} any arbitrary vector $\vec{A}_0 = \text{grad}(\phi)$, (1-28) will result by the vector identity (1-27) (ref. 11). Therefore \vec{A} is indeterminate. As a result, we can choose \vec{A} as we like. For later convenience, we will choose \vec{A} such that (1-29) is true.

$$\vec{A} + \vec{A}_0 = \vec{A} + \text{grad}(\phi) \quad (1-26)$$

$$\text{curl}(\text{grad}(\phi)) \equiv 0 \quad (1-27)$$

$$\vec{u} = \text{curl}(\vec{A} + \text{grad}(\phi)) = \text{curl}(\vec{A}) + \text{curl}(\text{grad}(\phi)) = \text{curl}(\vec{A}) \quad (1-28)$$

$$\text{div}(\vec{A}) = 0 \quad (1-29)$$

Now, we can substitute (1-24) into the definition of vorticity, as in (1-30). Using the vector identity (1-31) (ref. 11), we find (1-32). Because we have chosen \vec{A} such that it satisfies (1-29), (1-32) reduces to (1-33).

$$\vec{\omega} = \text{curl}(\text{curl}(\vec{A})) \quad (1-30)$$

$$\text{curl}(\text{curl}(\vec{F})) = \text{grad}(\text{div}(\vec{F})) - \nabla^2 \vec{F} \quad (1-31)$$

$$\vec{\omega} = \text{grad}(\text{div}(\vec{A})) - \nabla^2 \vec{A} \quad (1-32)$$

$$\vec{\omega} = -\nabla^2 \vec{A} \quad (1-33)$$

If we split (1-33) into its vector components, we get the expressions in (1-34), (1-35), and (1-36).

$$-\omega_x = \nabla^2 A_x \quad (1-34)$$

$$-\omega_y = \nabla^2 A_y \quad (1-35)$$

$$-\omega_z = \nabla^2 A_z \quad (1-36)$$

These expressions are in the form of Poisson's equation (1-37). The solution of Poisson's equation is well known (1-38).

$$\nabla^2 \phi(x, y, z) = f(x, y, z) \quad (1-37)$$

$$\phi(x, y, z) = \frac{-1}{4\pi} \iiint \frac{f(x', y', z')}{[(x-x')^2 + (y-y')^2 + (z-z')^2]^{3/2}} dx' dy' dz' \quad (1-38)$$

The integral in (1-38) is evaluated over the entire space. Now, let us define two points in space, as in Figure 1-15. We will call point P the source point and point Q the observation point. Thus, we are going to observe something at point Q whose source is at point P. Let us also define the vector between them as \vec{R} .

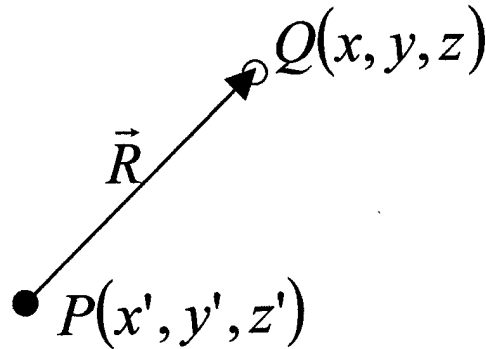


Figure 1-15 Source and observation points

If we apply the solution to Poisson's equation to the expressions in (1-34), (1-35), and (1-36) we will find (1-39), (1-40), and (1-41). Note that the denominator of (1-38) is simply the magnitude of \vec{R} as defined in Figure 1-15. Also, note that $dV' = dx' dy' dz'$.

$$A_x(x, y, z) = \frac{1}{4\pi} \iiint \frac{\omega_x(x', y', z')}{\|\vec{R}\|} dV' \quad (1-39)$$

$$A_y(x, y, z) = \frac{1}{4\pi} \iiint \frac{\omega_y(x', y', z')}{\|\vec{R}\|} dV' \quad (1-40)$$

$$A_z(x, y, z) = \frac{1}{4\pi} \iiint \frac{\omega_z(x', y', z')}{\|\vec{R}\|} dV' \quad (1-41)$$

Remembering how we defined \vec{A} in (1-24), we can break that up into its vector components, as in (1-42), (1-43), and (1-44).

$$u_x = \text{curl}(\vec{A})_x = \frac{\partial A_z}{\partial y} - \frac{\partial A_y}{\partial z} \quad (1-42)$$

$$u_y = \text{curl}(\vec{A})_y = \frac{\partial A_x}{\partial z} - \frac{\partial A_z}{\partial x} \quad (1-43)$$

$$u_z = \text{curl}(\vec{A})_z = \frac{\partial A_y}{\partial x} - \frac{\partial A_x}{\partial y} \quad (1-44)$$

Now, if we take the partial derivatives of the components of \vec{A} , as defined in (1-39) through (1-41), and substitute those partial derivatives, as shown below in (1-45) through (1-50), into the expressions for \vec{u} in (1-42) through (1-44), we will get an expression for velocity as a function of vorticity and distance.

$$\frac{\partial A_z}{\partial y} = \frac{1}{4\pi} \iiint \omega_z(x', y', z') \frac{\partial}{\partial z} \left(\frac{1}{\|\vec{R}\|} \right) dV' = \frac{-1}{4\pi} \iiint \omega_z(x', y', z') \cdot (y - y') \|\vec{R}\|^{-3} dV' \quad (1-45)$$

$$\frac{\partial A_x}{\partial y} = \frac{-1}{4\pi} \iiint \omega_x(x', y', z') \cdot (y - y') \|\vec{R}\|^{-3} dV' \quad (1-46)$$

$$\frac{\partial A_y}{\partial z} = \frac{-1}{4\pi} \iiint \omega_y(x', y', z') \cdot (z - z') \|\vec{R}\|^{-3} dV' \quad (1-47)$$

$$\frac{\partial A_x}{\partial z} = \frac{-1}{4\pi} \iiint \omega_x(x', y', z') \cdot (z - z') \|\vec{R}\|^{-3} dV' \quad (1-48)$$

$$\frac{\partial A_z}{\partial x} = \frac{-1}{4\pi} \iiint \omega_z(x', y', z') \cdot (x - x') \|\vec{R}\|^{-3} dV' \quad (1-49)$$

$$\frac{\partial A_y}{\partial x} = \frac{-1}{4\pi} \iiint \omega_y(x', y', z') \cdot (x - x') \|\vec{R}\|^{-3} dV' \quad (1-50)$$

Collecting all these expressions together, and recognizing the vector components of $\vec{\omega} \times \vec{R}$ we get the following expressions, (1-51) to (1-53), for \vec{u} as a function of $\vec{\omega}$ and \vec{R} .

$$u_x = \frac{-1}{4\pi} \iiint \frac{[\omega_z(x', y', z') \cdot (y - y') - \omega_y(x', y', z') \cdot (z - z')]}{\|\vec{R}\|^3} dV' = \frac{1}{4\pi} \iiint \frac{(\vec{\omega} \times \vec{R})_x}{\|\vec{R}\|^3} dV' \quad (1-51)$$

$$u_y = \frac{1}{4\pi} \iiint \frac{(\vec{\omega} \times \vec{R})_y}{\|\vec{R}\|^3} dV' \quad (1-52)$$

$$u_z = \frac{1}{4\pi} \iiint \frac{(\vec{\omega} \times \vec{R})_z}{\|\vec{R}\|^3} dV' \quad (1-53)$$

If we put these components back into vector form, we get (1-54), which is the expression for the well know Biot-Savart law.

$$\vec{u}(x, y, z) = \frac{1}{4\pi} \iiint \frac{(\vec{\omega}(x', y', z') \times \vec{R})}{\|\vec{R}\|^3} dV' \quad (1-54)$$

However, there is an obvious problem with this equation: it is singular when $\vec{R} = 0$. That is because the Biot-Savart law only models the irrotational region of a

vortex. If we are interested in the velocity associated at point Q from the vorticity at point P, as in Figure 1-12, and point Q is far enough away from point P, this does not present a problem. However, if we need to find the velocity close to the vorticity at point P, we need to modify (1-54).

Another factor that (1-54) does not take into account is vortex stretching. If we define the vortex core radius as $\sigma = r_c$, and designate a constant vortex core volume, based on an initial distribution of vorticity, we can account for stretching by changing σ as required to keep the core volume constant. To account for the effects of the vortex core and stretching, we modify the Biot-Savart law by a function, s , that is dependent on \bar{R} and the vortex core diameter (*ref. 14*). Since we are going to be calculating the velocities induced by one vortex at point P on another vortex at point Q, we need to account for the diameter of both vortices. For that reason, the s -function is dependent on the diameter of both vortex tubes. The results of these modifications are in (1-55) and (1-56). In (1-56) the α -term sets the distribution of vorticity within the core. Setting $\alpha = 0.413$ gives a Gaussian distribution of vorticity for the vortex core (*ref. 14*).

$$\bar{u}(x, y, z) = \frac{1}{4\pi} \iiint \frac{(\bar{\omega}(x', y', z') \times \bar{r}) \cdot s(\|\bar{R}\|, \sigma(x', y', z'), \sigma(x, y, z))}{\|\bar{R}\|^3} dV' \quad (1-55)$$

$$s(\|\bar{R}\|, \sigma_P, \sigma_Q) = \frac{1}{\left[1 + \alpha(\sigma_P^2 + \sigma_Q^2) / 2\|\bar{R}\|^2 \right]^{\frac{3}{2}}} \quad (1-56)$$

1.3.3 Physical interpretation of equation of the Biot-Savart law

With the expression in Equation (1-55) and (1-56), we can now find the velocity at the observation point Q that is associated with the given vorticity at the source point P, taking into account the solid-body rotation vortex core and the effects of stretching. This is clear mathematically, but what does it mean physically? How can we describe motion in various type of fluids without any viscous or pressure terms?

To answer these questions, we should describe just what the Biot-Savart equation is. The Biot-Savart law is not prescriptive in that it does not define what the velocity field *will be*. Rather, it is descriptive. It describes what *is*. It simply describes what velocity field is associated with a given vorticity field at a given time. We could equally describe what vorticity is associated with a given velocity by taking the curl of the velocity field ($\vec{\omega} \equiv \text{curl}(\vec{u})$). So in that way, the Biot-Savart law is a translation tool. We can describe fluid motion in the language of velocity or in the language of vorticity. The Biot-Savart law simply tells us how to switch between the two languages.

But should not the translation depend on the fluid the motion is in? Do we not need pressure terms to move fluid? The key is that the Biot-Savart law does not describe transient conditions. It assumes the flow is steady. When steady, the viscosity of the fluid mediums and the pressures have done their job by bringing the fluid into a steady state.

However, we want to use the Biot-Savart law to calculate unsteady time-evolution of vortex flows. That is, we want to take a given vorticity field and use it to find the associated induced velocities at points around it (including points that contain vorticity). Then, we take those induced velocities, multiply them by a time step, and calculate how far those points will move. We then move them by that amount and recalculate the velocity associated with the new distribution of vorticity. We should be able to use the Biot-Savart law in this way as long as we assume that the associated steady induced velocity field is formed at a time scale smaller than the time step used to move the flow solution forward in time. At distances on the order of the diameter of most vortex tubes, this should be true in most fluid, except perhaps fluids with extremely low viscosity, like super-cooled liquid helium or the like.

Another thing we should assume to be able to use the Biot-Savart law in this way is infinite (or at least sufficiently large) signal speed. If this is the case, there time lag due to signal propagation will be sufficiently small that it occurs at time scales much smaller than the time scale used to advance the solution in time. Again, if the fluid is incompressible (or nearly so, as is the case in most vortex flows) this is not a concern.

The bottom line is that an equation is only as good as its assumption. However, within the limits of those assumptions, an equation can be very good at describing physical effects, even in very simple terms. The Biot-Savart law is one such equation. As long as we meet the necessary assumptions, we can use the Biot-Savart law to describe how an element of vorticity interacts with the fluid surrounding it, to include other elements of vorticity. We will use this property to break a vortex tube into many vortex elements and then describe, using the Biot-Savart law, how those vortex elements interact with each other. This is known as the vortex filament method. If we can use this method, with an appropriate set of initial conditions, to model vortex breakdown, perhaps we can better understand the mechanism that causes that vortex breakdown. From this understanding of the mechanism that causes the breakdown, we should be able to gain some insight as to how we can interrupt that mechanism to delay, prevent, or weaken vortex breakdown and its detrimental effects.

2. Vortex filament method

The vortex filament method allows us to look at vortex flows using the Biot-Savart law, as was previously developed, to calculate the motion of those flows. If the vortex filament method captures the important physics of the flow, it will yield accurate results. Conversely, if the vortex filament method yields accurate results, we can know with a reasonable degree of certainty, that the important physics in the flow are limited to those present in the vortex filament method.

The Biot-Savart law describes the induced velocities associated with a given distribution of vorticity. If we modify that law to include the induced velocity profile inside a vortex core and the effects of vortex stretching, we can limit our discussion of vortex motions that are calculated using the vortex filament method to those things associated with induced velocities, the vortex core velocity profile, and vortex stretching. With this in mind, let us now turn to how we can use the vortex filament method to model a vortex tube.

2.1 Vortex tube interacts with itself

As we discussed previously, a vortex tube is composed of many vortex lines. A vortex line is the same thing as a vortex filament. So what we call the vortex filament method could just as easily be called the vortex line method. These vortex lines are aligned with the vorticity vector associated with the fluid motion, as in

Figure 2-1.

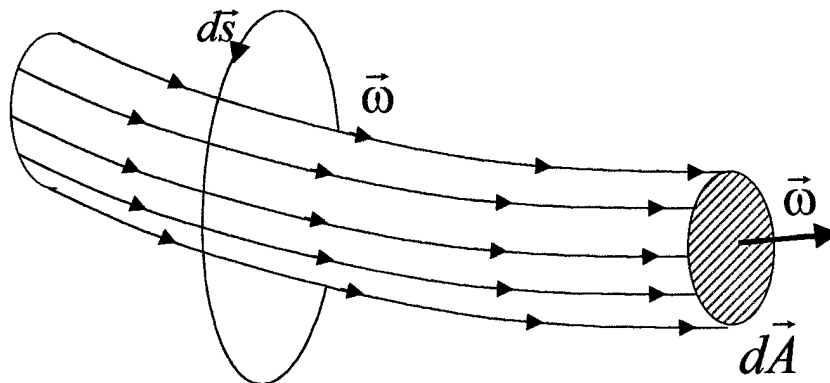


Figure 2-1, Vortex Tube

With the Biot-Savart law, we should be able to calculate the velocity induced by the vorticity of one vortex line on another vortex line. With this, we can find how that other vortex line will move as a result of this induced velocity. By the Helmholtz vortex theorem, we know that vorticity will move with the motion of a material fluid line. This means that as induced velocities cause motion to fluid elements, they in turn move the vorticity associated with those fluid elements. For this reason, we can calculate the induced velocities associated with the vortex lines of a vortex tube, multiply those velocities by a small time step, and then calculate how far the vortex lines will move in that small time step. We do this again and again, and observe the vortex tube moving forward in time. In this way, the vortex lines that compose a vortex tube interact with themselves such that this interaction can affect the shape of that vortex tube. If a real vortex tube can be described with a series of vortex lines, with a given distribution of vorticity, then the vortex filament method can be used to model real vortex motion.

2.2 Discretizing the vortex tube

To use the vortex filament method, we need to discretized a vortex tube into an adequate number of vortex filaments.

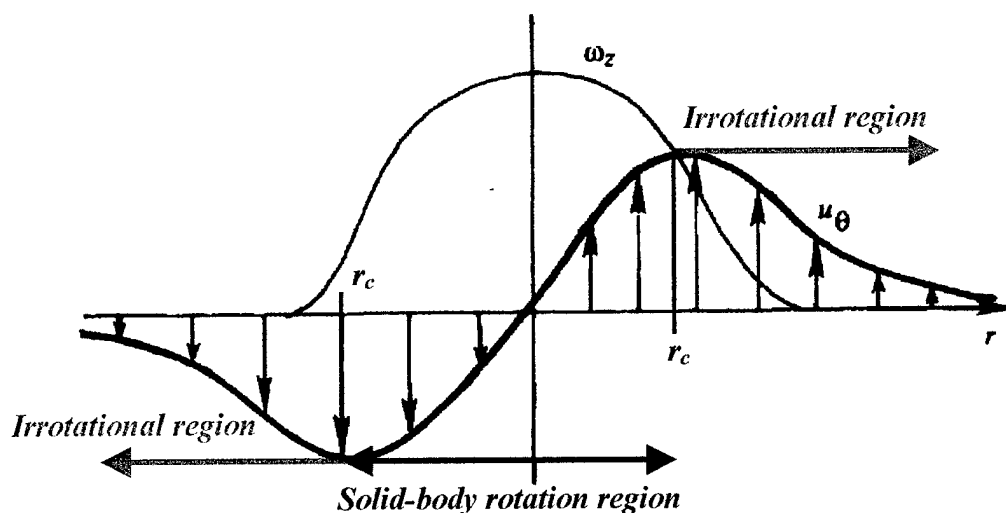


Figure 2-2 Real vortex velocity and vorticity distribution (ref. 10)

A vortex tube has a certain cross-sectional area, defined by the vortex tube core radius, and a certain distribution of vorticity within that area. Figure 2-2 shows that distribution for a real vortex. We only need to model the vortex core because we know that almost all of the vorticity is contained in this core. Outside of the core, the flow is nearly irrotational, and thus contains a negligible amount of vorticity. A vortex line with very little vorticity will not induce significant velocities and, for purposes of discretization, it can be neglected.

To adequately discretize that vortex tube, the vortex lines, should, in total, occupy the same cross sectional area as the vortex tube. To do this, each vortex line is given its own cross sectional area and its own vortex core radius. Each vortex line has the same Gaussian distribution of vorticity as the overall vortex tube. It is the vorticity magnitude and the vortex line core radius of each vortex line that is set, as required, so that in sum, the overall vortex tube core radius and vorticity distribution of the now discretized vortex tube matches that of the original vortex tube. These vortex lines are then packed densely enough that there is no empty space inside the vortex tube. This overlap allows the discretized vortex tube to maintain its original smooth distribution of vorticity within the original vortex tube. Figure 2-3 shows an illustration of a discretized vortex tube.

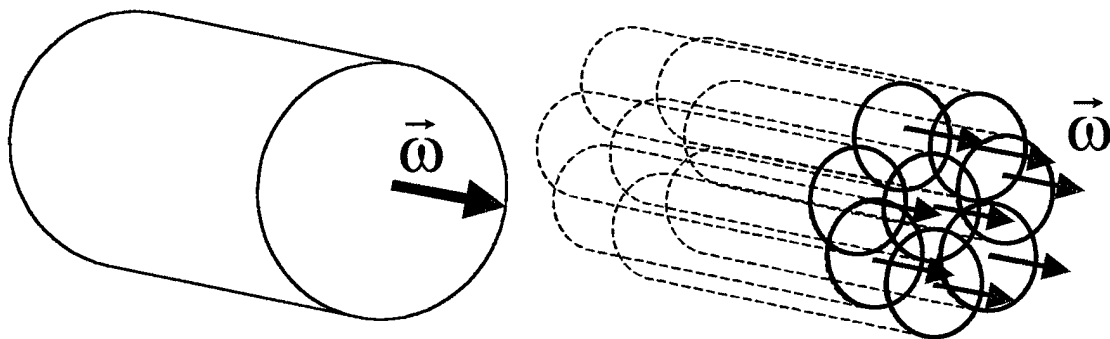


Figure 2-3 Vortex Tube Discretization

After the vortex tube is discretized into many overlapping axial vortex lines, it is further discretized along those lines. The vortex lines are broken up into many smaller vortex filaments segments. This allows portions of the vortex line to be moved by induced velocities in different directions along its axis. The character of the original

vortex lines is maintained by enforcing the condition that each vortex filament segment is connected to the one initially upstream and downstream of itself. This preserves the material line. We will refer to the endpoints of each vortex filament segment as a nodes. The induced velocity associated with all other vortex filament segments is calculated at these nodes. This total induced velocity is multiplied by the time step so that the location of each endpoint node of the vortex filament segment can move in time. Figure 2-4 shows a diagram of this.

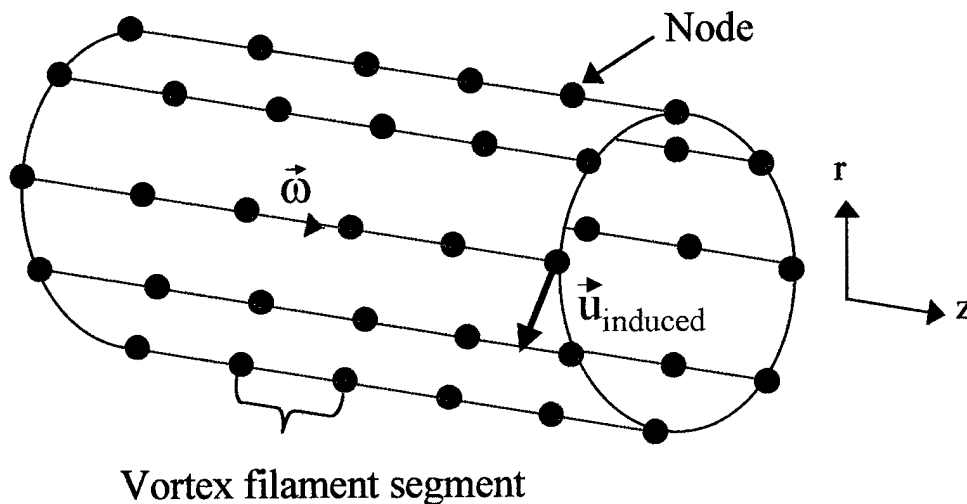


Figure 2-4 Vortex Filament Segments

This, in essence, is how the vortex filament method works. How these vortex lines are initially setup and what boundary conditions or external flow conditions are imposed on them are specific to each individual model. Next we will describe the how the model is specifically setup for this research.

2.3 Model setup

As with many numerical model, our vortex filament model can be discussed in terms of what it ideally represents, and by what reasonable compromises we make to make it computationally more efficient. The explicit calculation of induced velocities of one vortex filament segment on every other vortex filament requires $O(n^2)$ operations (*ref. 15*), so we hope to minimize the required operations whenever possible. We shall

present the ideal case first, and then discuss what changes we made to this ideal representation to turn the ideal representation into an efficient numerical code.

2.3.1 Ideal case

We model an unconstrained vortex tube that is being fed downstream ($z > 0$) from a vorticity source, located at $z = 0$, at a steady rate that we will call $U_\infty(z)$. The vortex tube convects downstream at that rate, $U_\infty(z)$. All vorticity in the vortex tube is initially aligned in the axial direction (which we will call z). As it is initially fed out of the vorticity source, the circulation in the vortex lines is set such that there is overall a Gaussian distribution of this axial vorticity in the vortex tube. Figure 2-5 shows a diagram of this vorticity source. The circulation in the vortex tube is described as it was previously, $C = \int_A \text{curl}(\vec{u}) \cdot d\vec{A} = \int_A \vec{\omega} \cdot d\vec{A}$. If we are speaking of the circulation of the entire vortex tube, we will call that circulation C . If we are speaking of the circulation in a particular vortex line, we will call the circulation Γ .

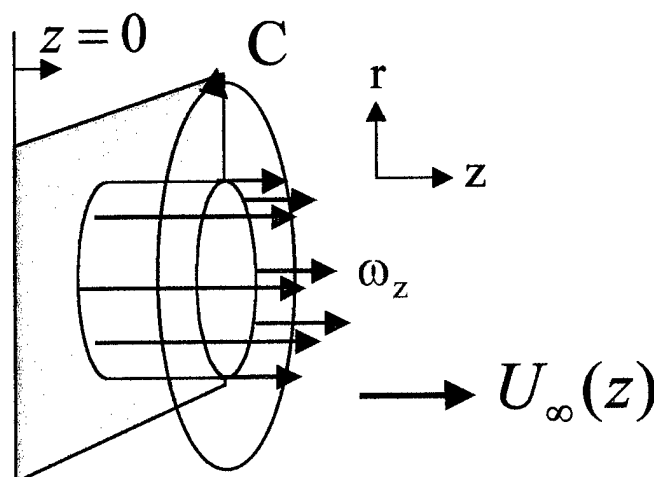


Figure 2-5 Axial Vorticity Source

We will allow the circulation of the vortex tube, as it comes from the vorticity source to change in time. Thus at one time, the vorticity source may produce a vortex tube with circulation $C = C_1$, while at another time it may produce a vortex tube with a

different circulation $C = C_2$. At this point, we must be careful not to violate any of the Helmholtz vortex theorems.

Let us restate the Helmholtz vortex theorem. Assuming inviscid, incompressible, barotropic flow, Helmholtz shows that (1) vortex lines move with the fluid elements, (2) circulation is constant along a vortex line, (3) a vortex line or vortex tube must end at a boundary or form a loop, it cannot end in a fluid, and (4) the strength of a vortex line in a vortex tube remains constant for all time (*ref. 10*).

The model meets the first part by moving the vortex filament segments according to the velocity induced on the segment endpoints and the downstream convection velocity, $U_\infty(z)$. The second part is met until we change the circulation that is produced by the vortex source. At this point, since we cannot change the vorticity in the vortex lines coming from the vortex source, the only way we can increase the circulation is to add vortex lines to the vortex tube. We can place these vortex lines coincident to the existing vortex lines, but we must do so keeping the third part of the Helmholtz vortex theorem in mind.

Vortex lines and vortex tubes cannot end in a fluid. They must have a boundary, as they do at the vorticity source, they must form closed loops, or they must exist downstream to $z = \infty$. What our model will do is insure that all the vortex lines that make up the vortex tube form closed loops. In this way, the vortex tube will not end in a fluid, but will, itself, form a closed loop by way of its vortex lines. Let us make this clear with the illustration in Figure 2-6.

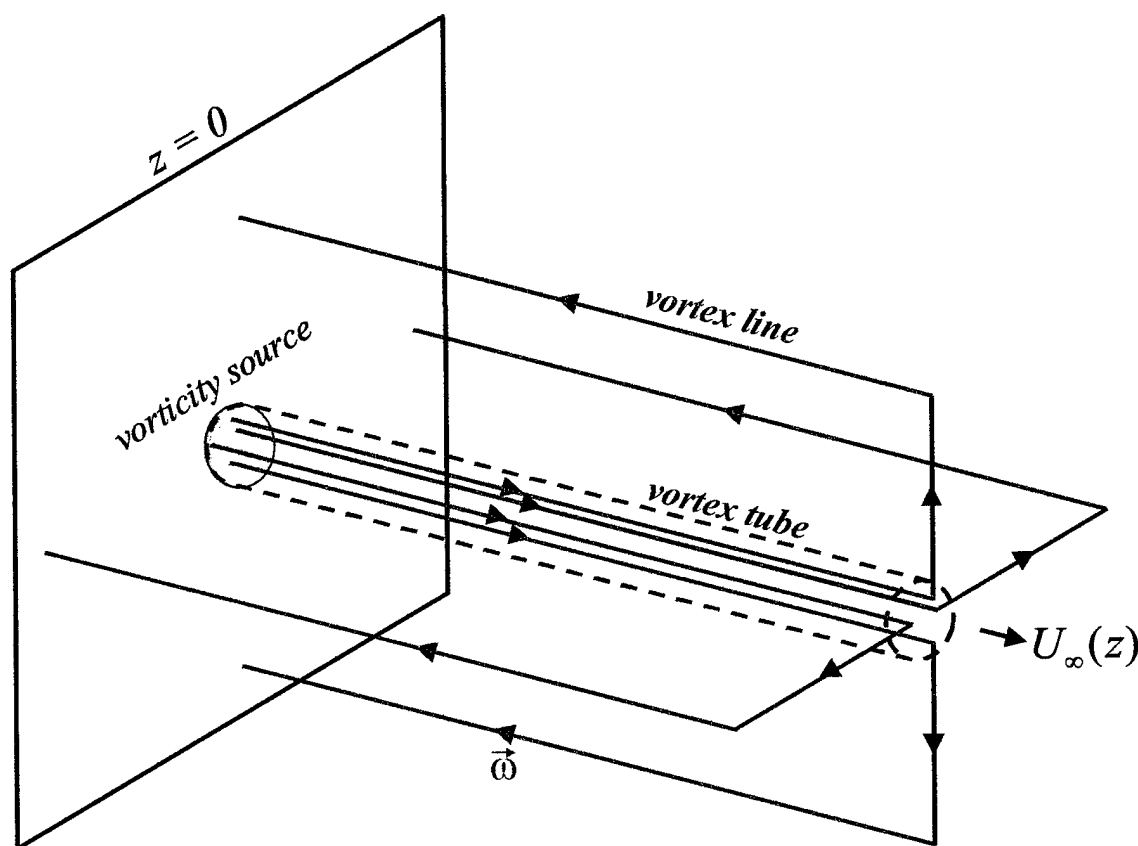


Figure 2-6 Closed Loop Vortex Lines

In this example, we discretized a vortex tube into four vortex lines. Please note that at this time, we are not considering the time evolution of the vortex tube. If it were evolving in time, it would convect to the right, with the vortex lines that are aligned in the axial (z -direction) direction growing longer. There would also be self-induction among all the lines. For now, we are showing the basic setup and ignoring the motion of the lines.

These vortex lines are aligned with the vortex tube in the axial direction. They emanate from the vorticity source. However at the end of the vortex tube, they branch off radially and then turn back upstream where they end at the $z = 0$ boundary that defines the location of the vorticity source. It can be helpful to think of these radial “spokes” of vorticity as something similar to the starting vortex of a wing’s bound vortex system. They exist to insure that the vortex lines do not end in the fluid. In our simulation, we

will allow this vortex tube end and these radial spokes to convect far enough downstream that they will have a negligible effect on the region where the vortex breakdown will take place. Also, we will assume that the radial spokes extend far enough radially, that the vortex lines that have turned upstream will have negligible effect on our region of interest.

However, it will turn out that a gradient in vorticity, brought about by a gradient in the z -direction of the vortex tube circulation, C , will be important to our study of vortex breakdown. In fact, we will find that a vorticity gradient will initiate the vortex breakdown. Thus, we must create this circulation gradient without violating any of the Helmholtz vortex theorems.

We will do this by making use of two principles. Figure 2-7 helps to describe these ideas. The first principle is the superposition of vortex lines. We can linearly add vorticity fields together, just as we add induced velocities together to get the overall induced velocity on each vortex filament node. Thus, the vorticity source will feed out additional vortex lines at $z = 0$ at the times we specify to increase the circulation in the vortex tube. To achieve a circulation gradient these additional vortex lines extend downstream to the point where the circulation gradient is to exist and then branch radially outward in radial spokes of vorticity. Just as we used the radial vorticity spokes to bring the vortex lines back to a boundary where they met the end of the vortex tube, we will do the same thing to insure that there is a vorticity gradient in the z -direction.

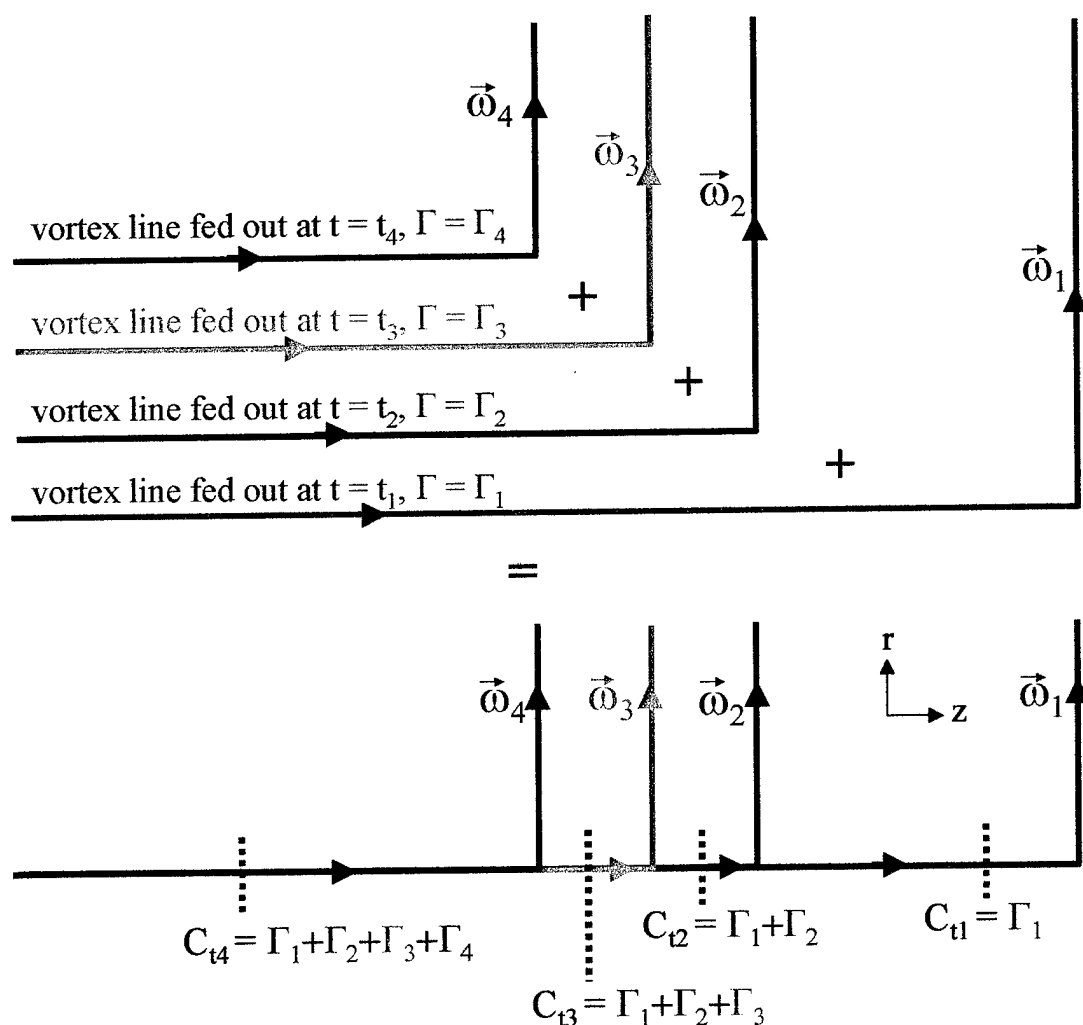


Figure 2-7 Changing Circulation

2.3.1.1 Boundary Conditions

The location of the circulation gradient will be a time-dependent boundary condition, which we will explicitly define in the model. Thus, we will have an upstream boundary condition specified at the vorticity source. There will be no boundary condition downstream. However, we will allow the end of the vortex tube to convect far enough downstream that it will have a negligible effect on the vorticity source when the circulation gradient is introduced into the flow. Thus, while it is not explicitly specified, the downstream boundary condition is a vortex tube going to infinity. This is inherently different than a previous study of vortex breakdown using the vortex filament method by

Nakamura et al (*ref. 14*), where they specified both upstream and downstream boundary conditions for the vortex tube.

Another aspect of the upstream boundary condition is that we will only introduce axial vorticity. However, all real vortex flows typically have both axial and azimuthal vorticity. One could explicitly specify an initial azimuthal vorticity, as do Nakamura, Leonard, and Spalart in their work (*ref. 14*). In doing so they specify an initial helical angle. However, we wanted to allow the vortex tube to assume whatever helical angle it naturally would (that is, whatever helical angle the induced velocities will create). Thus, we specify only axial vorticity, and allow the helical angle to develop on its own, based on the azimuthal velocity induced by the vortex filaments at each radial location in the vortex tube. This is another difference from the Nakamura et al study where they specified the helical angle of the vortex tube. Figure 2-8 illustrates how the helical angle can develop on its own. Please note that any radial vortex lines have been omitted for clarity.

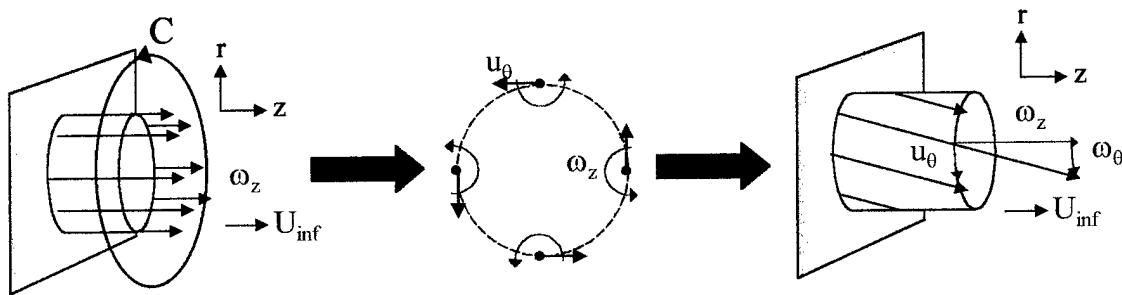


Figure 2-8 Creating Azimuthal Vorticity

The filaments are in a fixed azimuthal and radial location as they come out of the vorticity source. The specified distribution of axial vorticity, ω_z , induces an azimuthal velocity, u_θ . This azimuthal velocity twists the vortex lines, creating azimuthal vorticity, ω_θ , by means of vortex lines tilting.

2.3.2 Numerical case

The primary numerical simplification is to not include vortex filaments that are far enough away that their induced velocity is small as compared with the induced

velocities near the area of interest. How far is far enough? There are two ways to determine this. The first way is to look at two cases. One case will have the far away vortex filaments present and the other will have the vortex filaments absent. If there is little or no change between the two cases, we can be sure that vortex filaments in question can be safely ignored.

The second way is to look at the far away vortex filaments in question and see if they are affected by the vortex filaments in the region of interest. If they are clearly not, then one can also say that these vortex filaments are far enough away to safely ignore them. In all cases, we are conservative in ignoring vortex filaments. The only time this comes into use is with the vortex filaments is (a) at the end of the vortex tube, and (b) the vortex filaments in the radial spokes that are far away from the centerline of the vortex tube. For (a), in our numerical model, we track the vortex filaments to the end of the vortex tube, which we have allowed to travel far downstream. However, because it is far downstream, we do not track the radial spokes and upstream traveling vortex lines from the end of the vortex tube. For (b), we track the radial spokes in the region of the vorticity gradient out to a radius of approximately ten times the vortex tube radius. At this point, we track them no further. Nor do we track their upstream traveling components of vorticity.

These are good simplification because the vortex filaments at the end of the vortex tube or at the end of the radial spokes from the circulation increase have little influence in the main vortex tube. Hence, we can infer that the main vortex tube is unaffected by them. Since it would make no difference to the outcome of the simulation whether we track these far away nodes or not, for numerical efficiency, we choose not to track them.

Another numerical issue is that of how we model the vorticity source at $z = 0$. It is helpful to think of it as a plane where vortex filaments with a specified amount of axial vorticity materialize. Numerically, we treat it slightly differently, but to the same effect. In the numerical model, we initially prescribe all vortex filaments in the vortex tube. However we locate that tube entirely upstream of the $z = 0$ plane. The $z = 0$ plane

denotes a boundary where, to the left ($z \leq 0$), which is upstream, vortex filaments are only moved by the convection of the freestream velocity, U_∞ . Vortex filaments located at $z \leq 0$ are not allowed to induce motion to each other. However, as soon as they are convected downstream to the right of the $z = 0$ plane, they are allowed to induce mutually, in addition to being convected downstream by the free stream velocity. This is summarized in equations (1-55) and (1-56) and illustrated in Figure 2-9.

$$z \leq 0 \quad \vec{u}_{total} = U_\infty \vec{e}_z \quad (2-1)$$

$$z > 0 \quad \vec{u}_{total} = \vec{u}_{induced} + U_\infty \vec{e}_z \quad (2-2)$$

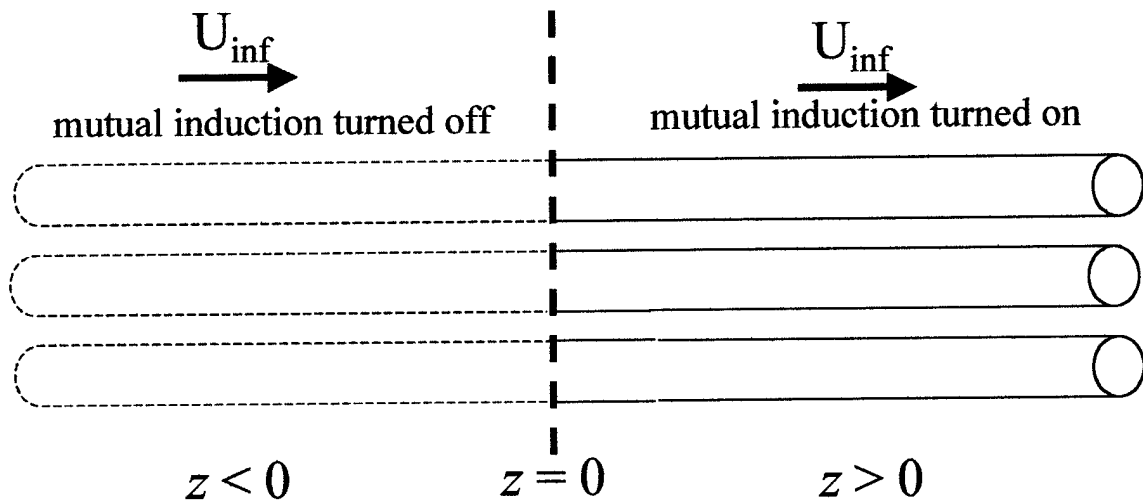


Figure 2-9 Numerical construction of axial vorticity source

A further numerical simplification we make is to exploit symmetry whenever it is present. We do not assume the flow to be axisymmetric, but once we discover that it is, we can employ an algorithm that allows use to take advantage of this symmetry to reduce the number of operations and decrease model run time.

2.4 Algorithm

Now let us look at the general algorithm of our model.

Figure 2-10 shows an outline of this. We will look at each part specifically. The complete simulation code, written in C++ is in the appendix.

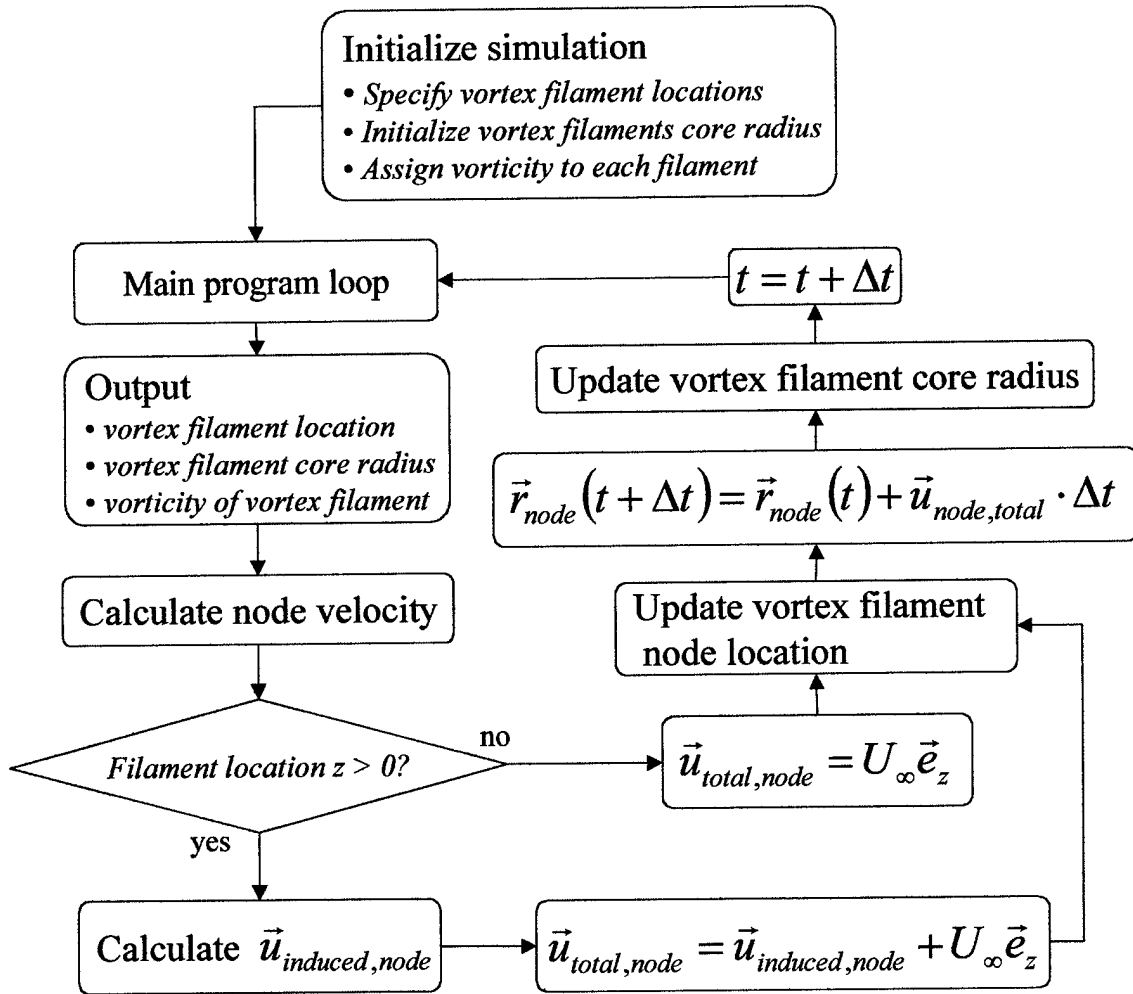


Figure 2-10 Simulation Algorithm

2.4.1 Initialize simulation

The first step is to initialize the simulation. We specify the initial location of all vortex filament segments. We assign a specified amount of circulation to each vortex filament. Finally, each vortex filament segment is given an initial radius so that a fixed vortex filament volume can be calculated.

2.4.1.1 Specify vortex filament location

To specify the location of the vortex filament segments, we specify the location of their endpoint nodes. Each node is the endpoint of the vortex filament segment, so

specifying the node location defines the vortex filament segment location. In the model we discretize the vortex tube into nine (9) concentric cylinders. These cylinders have radii of 0.42, 0.36, 0.3, 0.24, 0.18, 0.12, 0.08, 0.06, and 0.03. Each cylinder is further discretized into sixteen (16) vortex filaments, which are evenly distributed around the circumference of the cylinder. A tracking filament is also specified at the centerline, $r = 0$. These centerline vortex filament segments contains no vorticity, as it has been distributed to the surrounding vortex filaments. Thus, not counting the radial spoke vortex filaments, there are $9 \cdot 16 + 1 = 145$ vortex filaments.

Each vortex filament is then discretized axially with the nodes of each vortex filament segment initially set at a distance, dz , equal to 0.1. Specific units are not described, but they are units of length. Enough filaments are created to insure that there will always be some filaments located at $z \leq 0$ for the entire length of the simulation. Thus, if the simulation were to go for a time equal to 1.0 s with $U_\infty = 5 \text{ m/s}$, the vortex filaments would have to extend back to at least $z = -5$. This would require at least $\frac{5}{dz} = 50$ vortex filament segments and 51 nodes for $dz = 0.1$. We arrive at this value through an optimization process that will be discussed in a later chapter. Thus, each vortex filament node has its own location, defined by $\vec{r}_{m,n}(x, y, z)$, where $m = 1$ to the maximum number of axial nodes (M) and $n = 1$ to the maximum number of vortex filaments (N). Figure 2-11 shows how $\vec{r}_{m,n}(x, y, z)$ is defined.

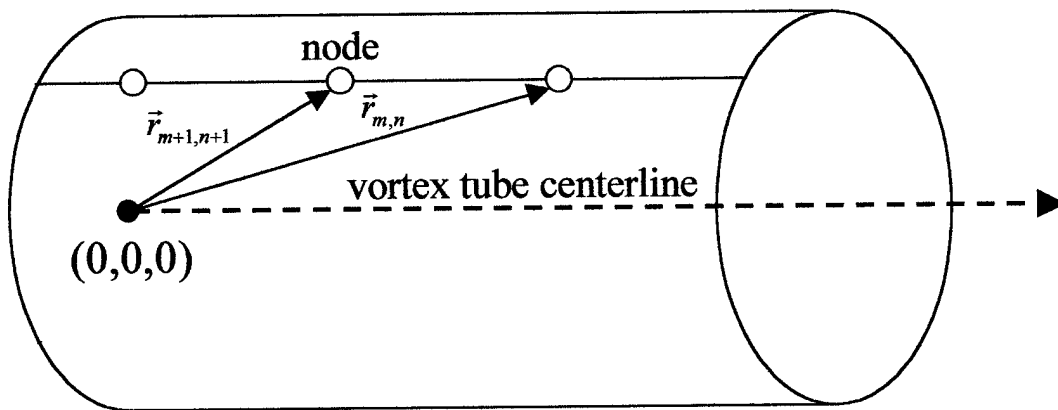


Figure 2-11 Vortex node location

The locations are initialized according to equations (2-3) to (2-6). Though we often describe things in cylindrical coordinates, Cartesian coordinates are used throughout the actual simulation.

$$x_{m,n} = r_j \cdot \cos\left(\frac{2\pi \cdot (n-1)}{16}\right) \quad (2-3)$$

for $n = j$ to $N = 16 \cdot j$, for $j = 1$ to 9, for $m = 1$ to M

$$y_{m,n} = r_j \cdot \sin\left(\frac{2\pi \cdot (n-1)}{16}\right) \quad (2-4)$$

for $n = j$ to $N = 16 \cdot j$, for $j = 1$ to 9, for $m = 1$ to M

$$z_{m,n} = z_{init_j} - dz \cdot m \quad (2-5)$$

for $n = j$ to $N = 16 \cdot j$, for $j = 1$ to 9, for $m = 1$ to M

$$\vec{r}_{m,n}(x, y, z) = (x_{m,n}, y_{m,n}, z_{m,n}) \quad (2-6)$$

In these equations, r_j is the initial radial location of the particular concentric of vortex filaments, and z_{init_j} is the initial location of the end of the vortex tube. When required, radial spoke vortex filament segments are also defined. In that case, the nodes of the radial spokes are given the z -location where the circulation increase is to occur based on a Galilean transformation, depending on what time the circulation increase is to come out of the vorticity source. Then, they are assigned radial and circumferential locations to coincide with the existing vortex filaments that are in the vortex tube. The radial spoke nodes that are outside of the vortex tube are spaced a distance dz apart, with whatever number of vortex filament segments required to place the ends of the radial spoke filaments at least ten times the radius of the initial vortex tube. In this case, the vortex tube radius is 0.42 and the radial spoke filaments end at $r = 4.6$. The following figures (Figure 2-12 to Figure 2-15) show location of all the vortex filament segments. For clarity, only the filaments at the outermost radius and the radial spoke filaments are shown.

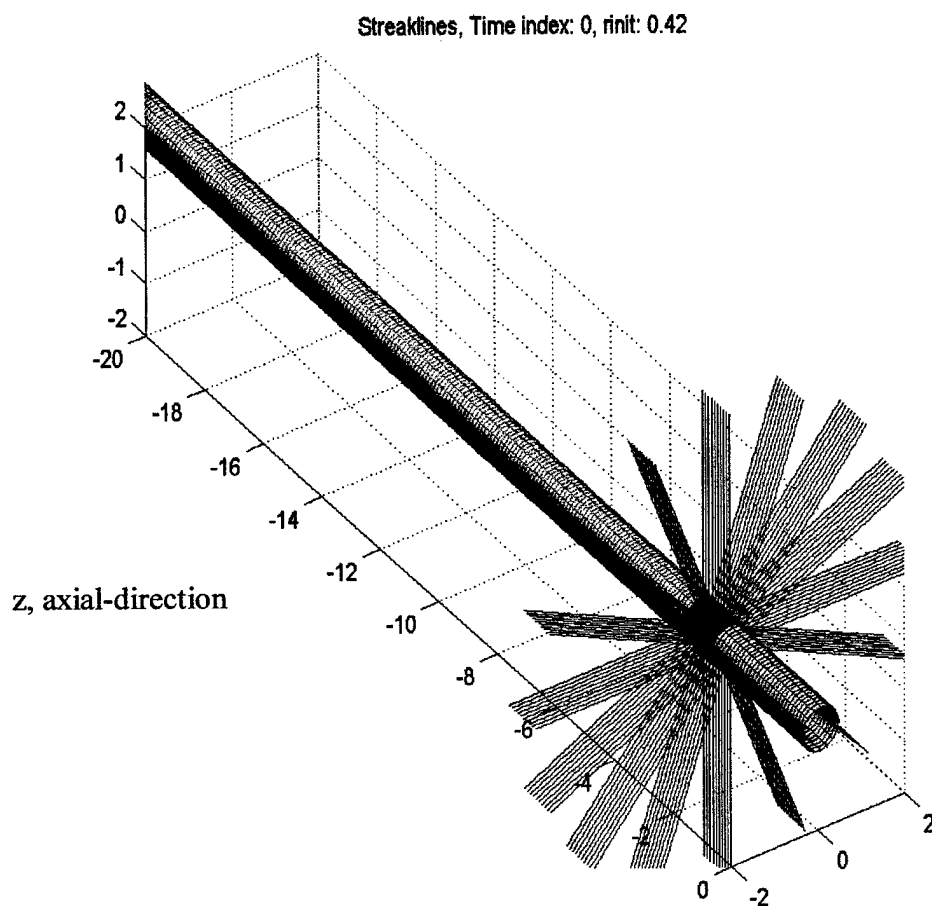


Figure 2-12 Initial location of vortex lines, perspective view one

The filaments at the outermost radius of vortex filaments in the vortex tube are shaded to look like a solid surface. The green shaded filaments indicate regions of the high, final value of circulation. The blue regions indicate the area of low circulation. The red region indicates the area that circulation is increasing. Hence, this is the region where the radial spokes of vorticity exist to insure solenoidality of the vorticity field.

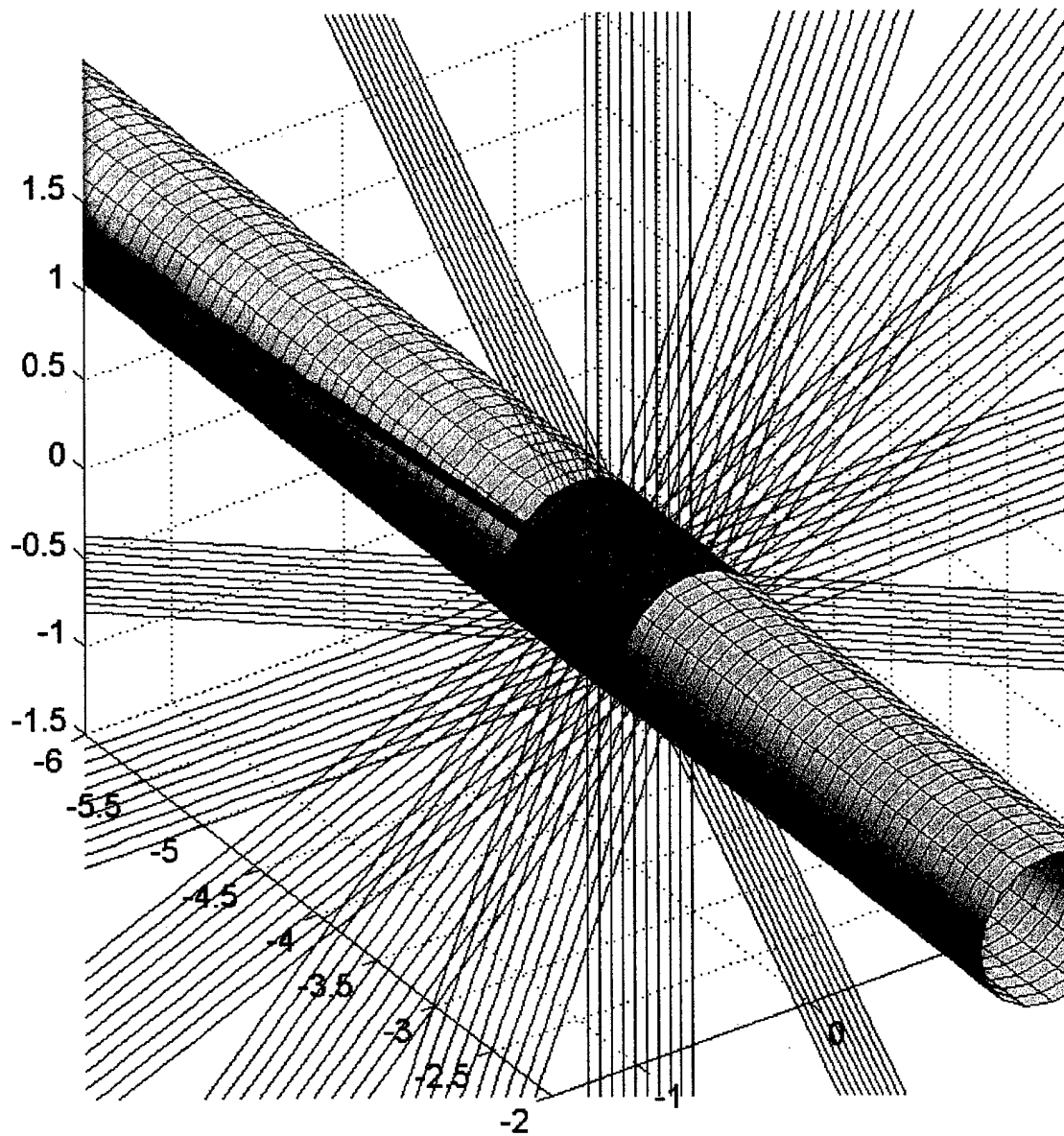


Figure 2-13 Initial location of vortex lines, perspective view two

The lines that run along the length of the vortex tube (in the axial direction) are the actual vortex lines. The circumferential lines are merely tracking lines connecting nodes of vortex segments and they do not represent vorticity vectors. In this initial configuration, all vortex filaments are located at $z \leq 0$. Thus, they are not allowed to induce each other. It is not until the individual filaments are convected downstream ($+z$) that self-induction will be allowed. Figure 2-13 shows a closer view of the circulation

increase region, where the radial spokes extend outward. Once the radial spokes cross the $z = 0$ plane, they do not remain purely in the radial direction to do mutual induction. This region is sufficiently upstream of the end of the vortex tube that the presence of that vortex tube end has no bearing on the induced motion in the circulation increase region.

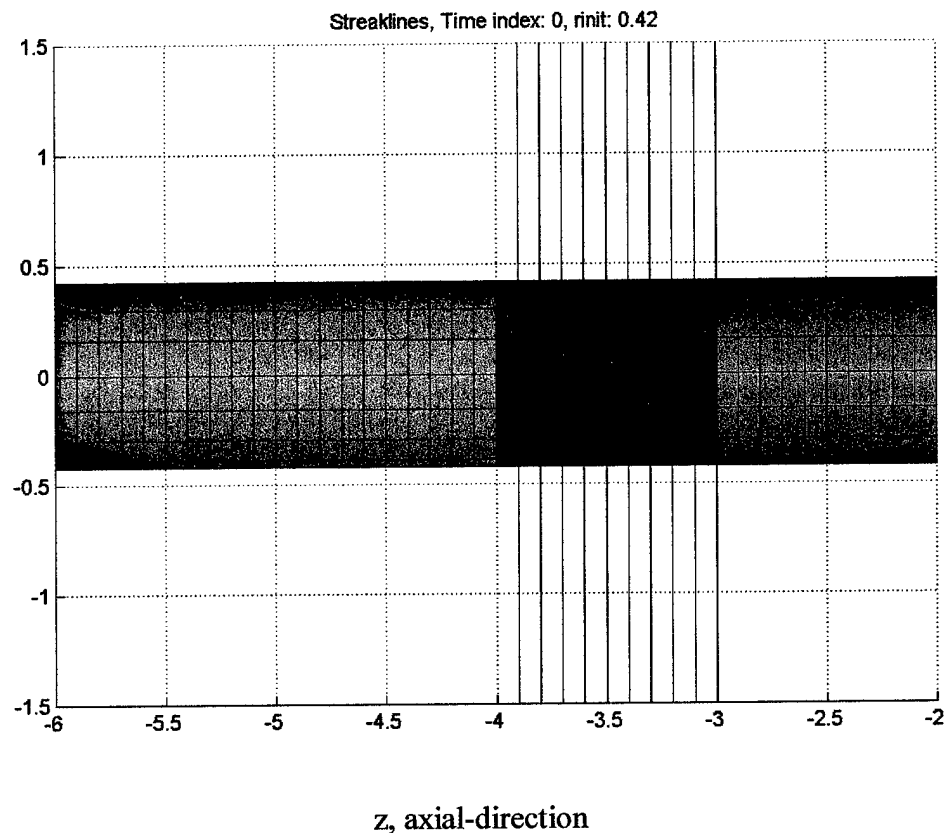


Figure 2-14 Initial location of vortex lines, side view

Figure 2-14 shows the side view of the initial vortex filament configuration. In this view the vortex lines run from left to right. Interior to the surface visible in this figure are nine (9) more similar cylinders, each composed of sixteen (16) axially aligned vortex filaments. The concentric rings are clearly visible in Figure 2-15, which shows the initial configuration of the vortex filaments from an end view. Here we see the radial spokes extending outward. We also see nine concentric rings of vortex filaments.

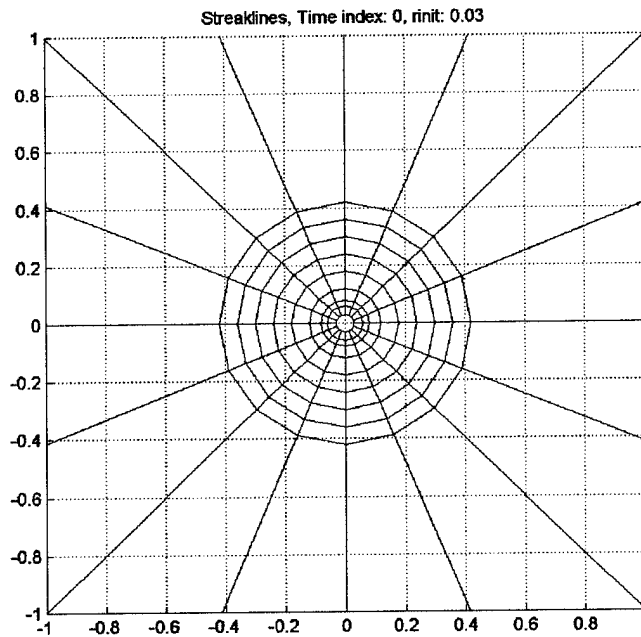


Figure 2-15 Initial location of vortex lines, end view

2.4.1.2 Initialize vortex filament core radius

Each vortex filament has the cross sectional properties of a real vortex tube. Each vortex filament has its own Gaussian distribution of vorticity and its own core radius. However, because, in sum, we want to vortex filaments to model a larger vortex tube, we must assign each vortex filament a core radius that creates an overlap of the circulation in each vortex filament. This overlap will give the entire vortex tube a smooth vorticity distribution, as we will see in the next section. Another reason we assign each vortex tube its own radius is that it allows us to give each vortex filament segment a fixed volume. By continuity, this volume will remain constant throughout the simulation. However, as the vortex filament segment endpoints are stretched apart or pushed closer together during the simulation, the core radius of the vortex filament segment will have to change to maintain the constant volume. This is how the model deals with the stretching (or contraction) in the vortex filaments. If the nodes are stretched apart, the core radius of the vortex filament segment will have to decrease to maintain the constant volume.

The effect in the simulation is that the velocity induced by that local vortex filament segment increases as the vorticity increases. The circulation remains the same, but it is contained in a smaller cross sectional area. Equation (2-7) shows this constraint.

$$\sigma_{m,n}^2 \|\vec{r}_{m+1,n} - \vec{r}_{m,n}\| = V = \text{const.} \quad (2-7)$$

$$\sigma_{m,n} = \sqrt{\frac{V}{\|\vec{r}_{m+1,n} - \vec{r}_{m,n}\|}} \quad (2-8)$$

The core radius of the m^{th} vortex filament segment on the n^{th} vortex filament is $\sigma_{m,n}$. The vortex filament nodes are defined by $\vec{r}_{m+1,n}$ and $\vec{r}_{m,n}$. The value of $\sigma_{m,n}$ is updated at each time step according to Equation (2-8). In our model, we initially set $\sigma_{m,n} = 0.12$ for all vortex filaments. This radius provides sufficient overlap to give the overall vortex tube a very smooth distribution of vorticity. Next, we will assign circulation to each of these vortex filament segments.

2.4.1.3 Assign vorticity to each filament

After the location of the vortex filaments has been specified and they have all been given a core radius, vorticity is assigned to each vortex filament segment. The filament segments are all initially aligned in the axial direction, which means that all the vorticity is initially aligned in the axial direction. We specify vorticity for each vortex filament segment by giving each vortex filament segment an amount of circulation, $\Gamma_{i,j}$. If we were to add up all the $\Gamma_{i,j}$ at a particular axial location, we would get the total circulation, C , at that location.

Vorticity will remain constant along a vortex line. In those regions where the circulation increases, vortex lines of constant vorticity are superimposed on each other, with the superimposed vortex lines turning radially outward at the appropriate axial location to give the desired total circulation profile in the axial direction. However, vortex filaments at different radii will have different amounts of vorticity, with the vorticity being set to make the vorticity distribution interior to the vortex tube match that

of an ideal vortex tube. Thus, we have an ideal vorticity distribution that we want to match. In this case, we will use the ideal case of unbounded swirling flow. For this case, the circumferential velocity and the axial vorticity are defined by Equations (2-9) and (2-10) respectively.

$$u_{\theta} = \frac{C(1 - e^{-br^2})}{2\pi r} \quad (2-9)$$

$$\omega_z = \frac{1}{r} \frac{d}{dr} (r \cdot u_{\theta}) = \frac{C \cdot b \cdot e^{-br^2}}{\pi} \quad (2-10)$$

To match experimental data, we choose $b = 10.9$ (*ref. 14*). C is specified, as it is the total circulation at a given axial location. We cannot exactly match a continuous vorticity distribution in a discretized vortex tube, but we can do it in a way that minimizes the error. This is done following Nakamura, Leonard, and Spalart's technique using the Lagrange multiplier method to minimize the error while satisfying the constraint of total circulation fixed (*ref. 14*). Using this method, we achieve the initial axial vorticity profile that is shown in Figure 2-16.

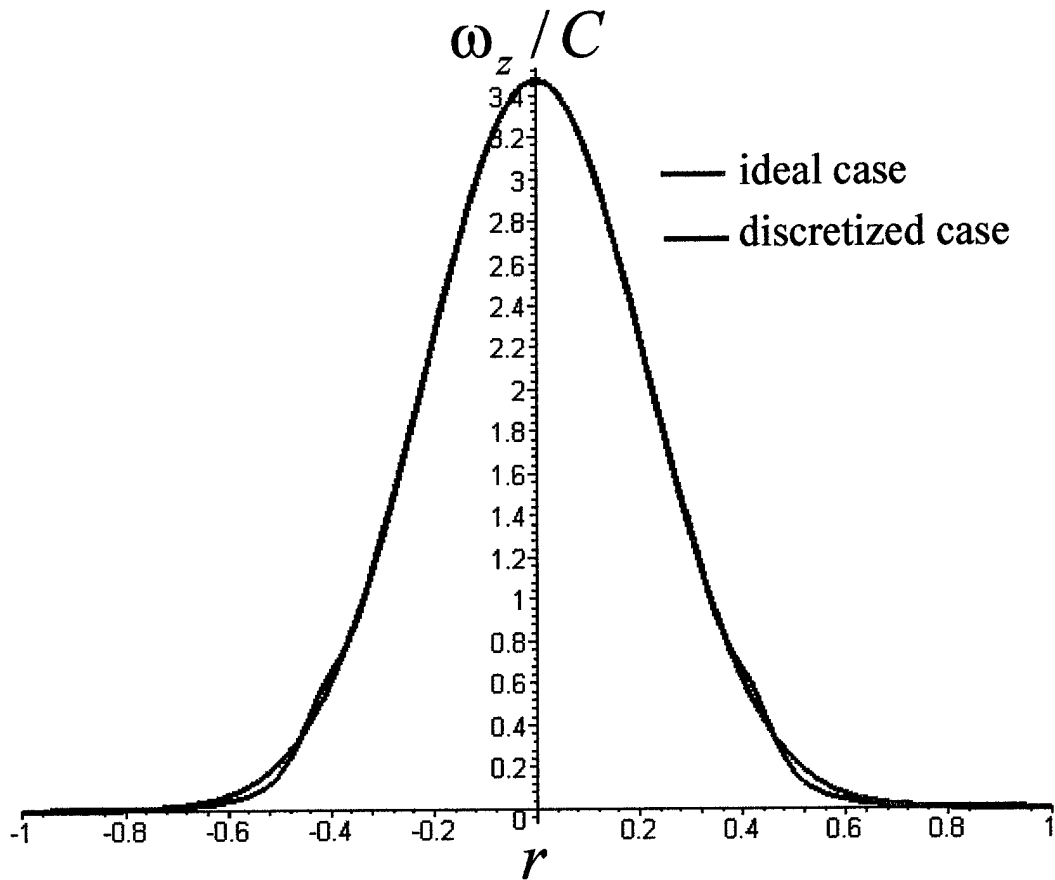


Figure 2-16 Ideal vs. actual initial axial vorticity profile

As was stated before, this total circulation, C , at a given axial location is simply the sum of the circulation, $\Gamma_{j,k}$.

Figure 2-17 shows the total circulation, as well as the circulation in each concentric ring of vortex filaments. To say it another way, every non-black line represents the sum of the circulation from the sixteen vortex filaments in each of the nine rings of vortex filaments. The sum of the circulation represented by these non-black lines in the total circulation. Thus, we see peaks of circulation near the radial location of each ring of vortex lines.

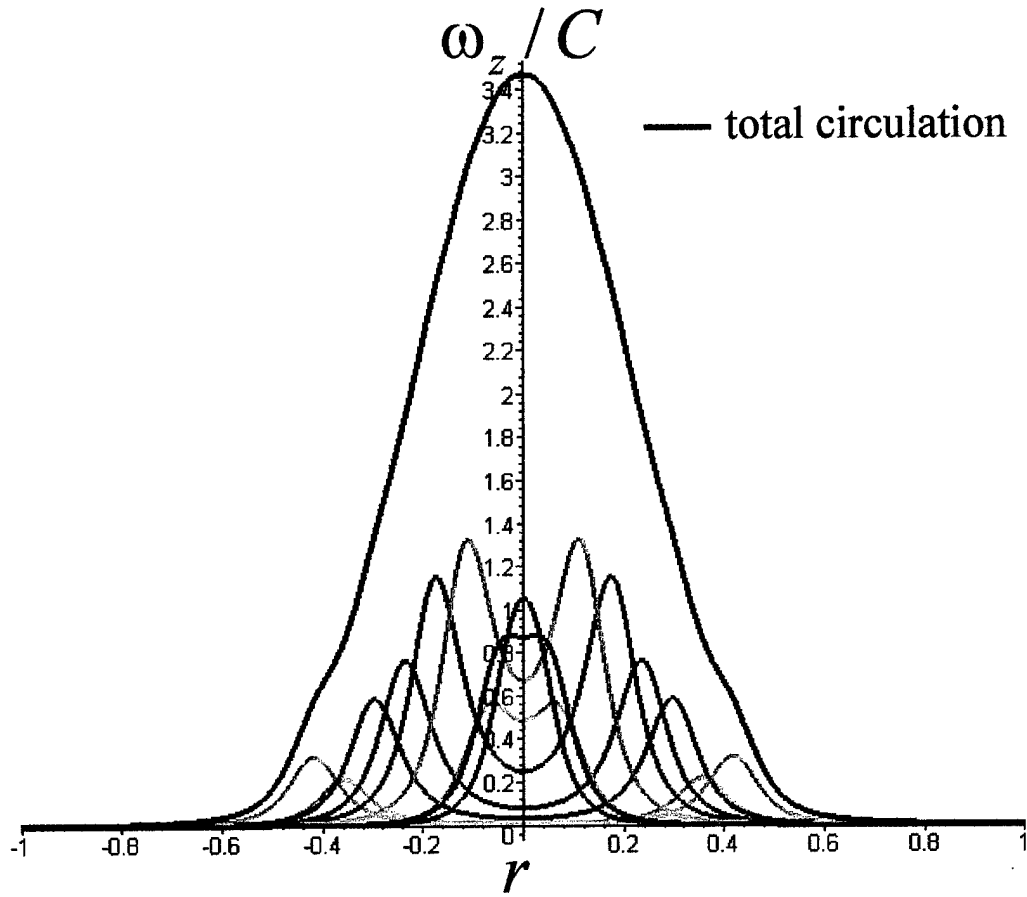


Figure 2-17 Circulation sum

The axial vorticity in each concentric ring of vortex filaments (this is the vorticity plotted in each non-black line in

Figure 2-17) is given by equation (2-11) (*ref. 14*). This approximates the distribution of axial vorticity in each vortex filament core with a Gaussian distribution.

$$\omega_{z,j} = C \cdot \bar{\Gamma}_j \frac{2\alpha\sigma_j^2 r_j (r_j^2 + r^2 + \alpha\sigma_j^2)}{\left\{ (r_j + r)^2 + \alpha\sigma_j^2 \right\} \left\{ (r_j - r)^2 + \alpha\sigma_j^2 \right\}^{3/2}}, \text{ for } j = 1 \text{ to } 9 \quad (2-11)$$

In equation (2-11), the j -subscripted values refer to the value of those quantities in an entire concentric ring. As we said before, the vortex tube is discretized into nine (9) concentric rings, so j goes from one (1) to nine (9). C is the circulation of the entire

vortex tube. $C \cdot \bar{\Gamma}_j$ is the circulation per unit circumference of the j^{th} ring of vortex filaments. Thus, C has units of circulation, and $\bar{\Gamma}_j$ has units of [1/length]. We choose $\alpha = 0.413$ to achieve a Gaussian distribution of vorticity. The circulation in an individual filament in that ring is $\frac{2\pi \cdot r_j \cdot C \cdot \bar{\Gamma}_j}{16}$, since each concentric ring is made up of sixteen (16) individual filaments. Figure 2-18 shows how circulation is defined for a single concentric ring of vortex filaments. It should be noted that the filaments overlap both in the radial and in circumferential direction. This provides the continuous vorticity distribution that is seen in the previous figures.

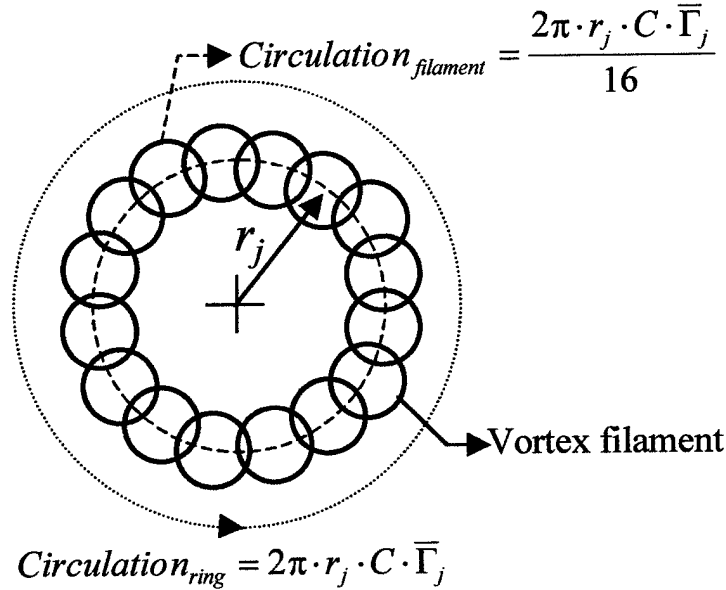


Figure 2-18 Circulation in a ring of vortex filaments

Nine (9) rings of vortex filaments with sixteen (16) filaments in each ring are chosen as a compromise between the required resolution of the discretized vortex tube to adequately model the Gaussian distribution of vorticity in the vortex core and numerical simulation run time. The following table shows the optimized values of that

$\frac{2\pi \cdot r_j \cdot C \cdot \bar{\Gamma}_j}{16}$ that are used to achieve the vorticity distributions in the preceding figures.

Each vortex filament at radius r_j is given the initial circulation, $\frac{2\pi \cdot r_j \cdot C \cdot \bar{\Gamma}_j}{16}$, as shown in this table.

Table 2-1 Vortex filament circulation distribution

$r_1 = 0.03$	$\Gamma_{j,k(r_1)} = \frac{2\pi \cdot r_1 \cdot C \cdot \bar{\Gamma}_1}{16} = 0.001640452531 \cdot C$
$r_2 = 0.06$	$\Gamma_{j,k(r_2)} = \frac{2\pi \cdot r_2 \cdot C \cdot \bar{\Gamma}_2}{16} = 0.002628594294 \cdot C$
$r_3 = 0.08$	$\Gamma_{j,k(r_3)} = \frac{2\pi \cdot r_3 \cdot C \cdot \bar{\Gamma}_3}{16} = 0.002429657471 \cdot C$
$r_4 = 0.12$	$\Gamma_{j,k(r_4)} = \frac{2\pi \cdot r_4 \cdot C \cdot \bar{\Gamma}_4}{16} = 0.009090954102 \cdot C$
$r_5 = 0.18$	$\Gamma_{j,k(r_5)} = \frac{2\pi \cdot r_5 \cdot C \cdot \bar{\Gamma}_5}{16} = 0.01223904142 \cdot C$
$r_6 = 0.24$	$\Gamma_{j,k(r_6)} = \frac{2\pi \cdot r_6 \cdot C \cdot \bar{\Gamma}_6}{16} = 0.01097097189 \cdot C$
$r_7 = 0.30$	$\Gamma_{j,k(r_7)} = \frac{2\pi \cdot r_7 \cdot C \cdot \bar{\Gamma}_7}{16} = 0.01061059381 \cdot C$
$r_8 = 0.36$	$\Gamma_{j,k(r_8)} = \frac{2\pi \cdot r_8 \cdot C \cdot \bar{\Gamma}_8}{16} = 0.004780605093 \cdot C$
$r_9 = 0.42$	$\Gamma_{j,k(r_9)} = \frac{2\pi \cdot r_9 \cdot C \cdot \bar{\Gamma}_9}{16} = 0.008114549976 \cdot C$

2.4.2 Calculating induced velocities

Now that the vorticity has been assigned to each vortex filament segment, we can calculate the velocity that they induce on each other. This involves a decision, though, because, as we already stated, to model an axial vorticity source, we will only allow vortex filament segment endpoint nodes located at $\vec{r}_{m,n}(t) = (x_{m,n}(t), y_{m,n}(t), z_{m,n}(t))$ to induce velocities or to receive induced velocities if they are located at $z_{m,n} > 0$. We re-list the following equations to show the distinction.

$$z_{m,n} \leq 0 \quad \vec{u}_{m,n} = U_{\infty} \vec{e}_z \quad (2-12)$$

$$z_{m,n} > 0 \quad \vec{u}_{m,n} = \vec{u}_{induced,m,n} + U_{\infty} \vec{e}_z \quad (2-13)$$

If the nodes are located at $z \leq 0$, then they only receive the freestream velocity, U_{∞} . Likewise, we will ignore the induced velocities of any vortex filament segment whose endpoint nodes are not both located at $z > 0$. If a node receives only U_{∞} , it has all the velocity that it will get during the time step.

Assuming that all nodes involved in the following equations are located at $z > 0$, we will proceed. Recalling the discussion of the Biot-Savart law in the previous chapter, we know that vorticity at point P will induce a velocity at point Q according to equations (2-14) and (2-15). Recall that the s function allows for the vortex core and vortex stretching.

$$\vec{u}(x, y, z) = \frac{1}{4\pi} \iiint \frac{(\vec{\omega}(x', y', z') \times \vec{r}) \cdot s(\|\vec{r}\|, \sigma_P, \sigma_Q)}{\|\vec{R}\|^3} dV' \quad (2-14)$$

$$s(\|\vec{r}\|, \sigma_P, \sigma_Q) = \frac{1}{\left[1 + \alpha(\sigma_P^2 + \sigma_Q^2) / 2\|\vec{R}\|^2\right]^{\frac{3}{2}}} \quad (2-15)$$

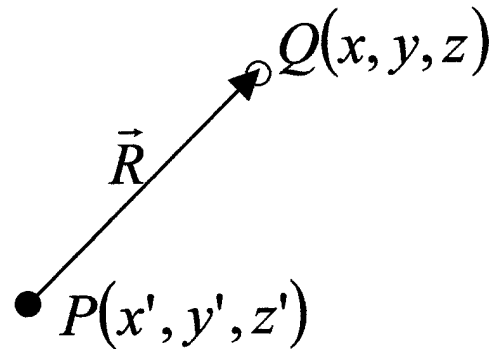


Figure 2-19 Induced velocity from P on Q

In our model, we will define point P as the centroid of the inducing vortex filament segment. Point Q is the endpoint node of a vortex filament segment that is receiving the induced velocity. The vortex filament core radii, σ_P and σ_Q , are the

vortex filament radii associated with the inducing vortex filament segment at point P and the induced vortex filament node at point Q, respectively. Figure 2-20 shows how we apply points P and Q to vortex filament segments.

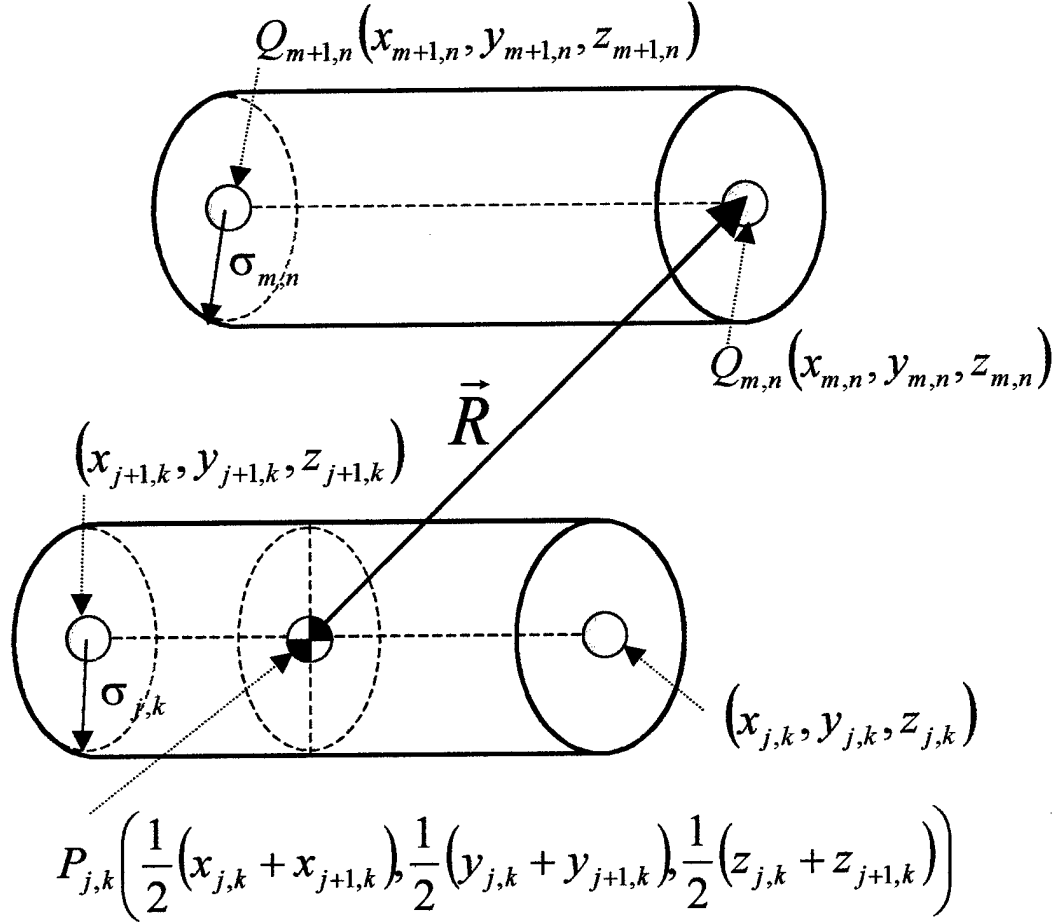


Figure 2-20 Points P and Q on vortex filament segments

With these locations defined, we can calculate the induced velocity at a point Q due to all other vortex filaments. We do this according to equation (2-16) and (2-17) which is simply a discretized integration of the Biot-Savart law from equation (2-14).

$$\bar{u}_{m,n}(t) = \frac{1}{4\pi} \sum_{j=1}^{J-1} \sum_{k=1}^K \Gamma_{j,k} \frac{(\bar{r}(t) \times \Delta l(t)) \cdot s(\|\bar{r}(t)\|, \sigma_{m,n}(t), \sigma_{j,k}(t))}{\|\bar{R}(t)\|^3} \quad (2-16)$$

for $m = 1$ to J for $n = 1$ to K

$$s(\|\vec{R}(t)\|, \sigma_{m,n}(t), \sigma_{j,k}(t)) = \frac{1}{\left[1 + \alpha(\sigma_{j,k}^2(t) + \sigma_{m,n}^2(t)) / 2\|\vec{R}(t)\|^2\right]^{\frac{3}{2}}} \quad (2-17)$$

In these equations, $\vec{u}_{m,n}(t)$ is the velocity induced on the node located at $\vec{r}_{m,n} = (x_{m,n}(t), y_{m,n}(t), z_{m,n}(t))$ by all other vortex filaments at time, t . The limits of summation J and K are the maximum number of nodes located at positions $z > 0$ and the total number of filaments, respectively. The limit is $J-1$ because there are J nodes and $J-1$ vortex filament segments. The circulation, $\Gamma_{j,k}$, is the circulation of an individual vortex filament. The rest of the terms are defined in equations (2-18) through (2-27).

$$\Delta l_x(t) = x(t)_{j+1,k} - x(t)_{j+1,k} \quad (2-18)$$

$$\Delta l_y(t) = y(t)_{j+1,k} - y(t)_{j+1,k} \quad (2-19)$$

$$\Delta l_z(t) = z(t)_{j+1,k} - z(t)_{j+1,k} \quad (2-20)$$

$$R_x(t) = \left(x_{j+1,k}(t) + \frac{1}{2} (x_{j+1,k}(t) - x_{j+1,k}(t)) \right) - x_{m,n}(t) \quad (2-21)$$

$$R_y(t) = \left(y_{j+1,k}(t) + \frac{1}{2} (y_{j+1,k}(t) - y_{j+1,k}(t)) \right) - y_{m,n}(t) \quad (2-22)$$

$$R_z(t) = \left(z_{j+1,k}(t) + \frac{1}{2} (z_{j+1,k}(t) - z_{j+1,k}(t)) \right) - z_{m,n}(t) \quad (2-23)$$

$$\vec{R}(t) = (R_x(t), R_y(t), R_z(t)) \quad (2-24)$$

$$(\vec{R}(t) \times \Delta l(t))_x = R_y(t) \cdot \Delta l_z - R_z(t) \cdot \Delta l_y \quad (2-25)$$

$$(\vec{R}(t) \times \Delta l(t))_y = R_z(t) \cdot \Delta l_x - R_x(t) \cdot \Delta l_z \quad (2-26)$$

$$(\vec{R}(t) \times \Delta l(t))_z = R_x(t) \cdot \Delta l_y - R_y(t) \cdot \Delta l_x \quad (2-27)$$

2.4.3 Update vortex filament node location

With the induced velocities and freestream velocity calculated and assigned to each node, we will update the location of the nodes according to a first order Euler integration, as in equations (2-28) through (2-30), depending on the location of $z_{m,n}$. In our model, we choose $\Delta t = 0.01$. We arrive at this value through an optimization process that will be discussed in section 3.6

$$\vec{r}_{m,n}(t) = (x_{m,n}(t), y_{m,n}(t), z_{m,n}(t)) \quad (2-28)$$

for $z_{m,n} \leq 0$:

$$\vec{r}_{m,n}(t + \Delta t) = \vec{r}_{m,n}(t) + \int (U_{\infty} \vec{e}_z) dt \cong \vec{r}_{m,n}(t) + (U_{\infty} \vec{e}_z) \cdot \Delta t \quad (2-29)$$

for $z_{m,n} > 0$:

$$\vec{r}_{m,n}(t + \Delta t) = \vec{r}_{m,n}(t) + \int (\vec{u}_{ind,m,n}(t) + U_{\infty} \vec{e}_z) dt \cong \vec{r}_{m,n}(t) + (\vec{u}_{ind,m,n}(t) + U_{\infty} \vec{e}_z) \cdot \Delta t \quad (2-30)$$

2.4.4 Update Vortex Filament Segment Core Radius

At each time step, the core radius of a vortex filament segment is updated to preserve continuity and to account for the effects of stretching. Recalling that we initialized the vortex filament segment core radius according to the following equations, we see how to update it.

$$\sigma_{m,n}^2(t_0) \|\vec{r}_{m+1,n}(t_0) - \vec{r}_{m,n}(t_0)\| = V = const. \quad (2-31)$$

$$\sigma_{m,n}(t + \Delta t) = \sqrt{\frac{V}{\|\vec{r}_{m+1,n}(t + \Delta t) - \vec{r}_{m,n}(t + \Delta t)\|}} \quad (2-32)$$

2.4.5 Repeat main program loop

With the new node position and the updated vortex filament segment core radii, we can update the time step, $t = t + \Delta t$, and repeat the main program loop. In the main program loop, we output the current vortex node location, core radii, and vorticity. We then calculate the velocity on each vortex node from every vortex filament segment. Next, we update the position and core radii of all the nodes and vortex filament segments. This continues until $t = t_{final}$.

2.5 Previous vortex filament method work

Several other researchers have used the vortex filament method to study vortex flows. In fact, the vortex filament method is really just an extension of the well know vortex lattice method for calculating aerodynamic properties over three dimensional

wings. The vortex filament method takes the framework of the vortex lattice method, adds in the effects of a viscous vortex core and vortex stretching and tilting, and then removes the condition that the vortex must remain bound to the wing. In the vortex filament method, as has been previously described, the vortex filaments are arranged in a vortex tube, allowed to induce themselves, and then advance in time with a small but finite time step.

Two previous works deserve special note as they relate to this research. The first is Nakamura, Leonard, and Spalart's, "Numerical Simulation of Vortex Breakdown by the Vortex-Filament Method" (*ref. 14*). The computational method for our present study is largely based on their work. Specifically, we use their approximation for the viscous core and their method of taking into the account of stretching. Furthermore we base the method for calculating and applying the initial distribution of vorticity to match the cross-sectional Gaussian vorticity distribution.

Our work differs in model resolution and the boundary conditions. As a result, the outcome of our simulation is significantly different. In terms of model distribution, due to increases in computer capabilities, our vortex tube is discretized into many more vortex filament segments. In terms of the boundary conditions, Nakamura, Leonard, and Spalart fix both the upstream and downstream ends of the vortex tube. Additionally, they specify an initial helical angle. Furthermore, they give the vortex tube a vorticity distribution that is constant along the length of the vortex tube. Our research models an axial vorticity source where the vortex tube is fed downstream by a freestream velocity. The amount of vorticity created at the vorticity source can change in time using radial spokes of vorticity. Figure 2-21 shows the results of the Nakamura, Leonard, and Spalart simulation as compared to the present results.

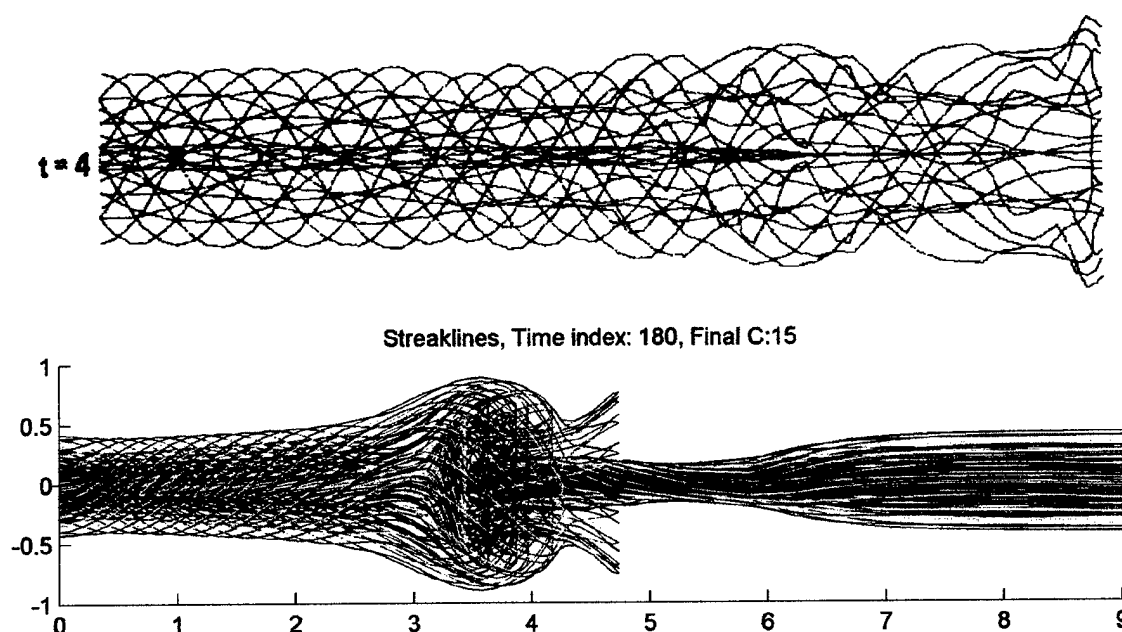


Figure 2-21 Nakamura, Leonard, and Spalart results (top), new results (bottom)

The second work we should note is that of Saghbini and Ghoniem in their paper "Numerical Simulation of the Dynamics and Mixing in a Swirling Flow" (*ref. 15*). As we were formulating our ideas we came across their work. They use a similar vortex filament method to study vortex breakdown. Much like our model, they simulate a vorticity source that convects downstream, without an explicit downstream boundary condition. However, several things are not clear. The first is how they can account for the effects of diffusion while still using a vortex line method without violating the Helmholtz vortex theorem that vorticity follows the fluid element. Others have said that this limitation is "one of the biggest obstacles toward extending it [the vortex filament method] to viscous flows" (*ref. 16*). Furthermore, they apparently use the finite length of the vortex tube as the source of a vorticity gradient that leads to vortex breakdown. They state that "[a]t time zero, a negative axial vorticity gradient is established due to the finite length of the vortex lines" (*ref. 15*). While this vorticity gradient does seem to be a necessary condition for vortex breakdown, it seems improper to model it in a way that violates another one of Helmholtz's vortex theorems, namely that a vortex line cannot end in a fluid. Numerically, one can say that the end of a finite length vortex line is far

enough away from the region of interest that one can say that, for all practical purposes, the vortex line may as well extend downstream to infinity. It is not clear that this is the case here. Furthermore, several asymmetries appear to develop in their solution that are not specifically accounted for. In a vortex filament model, if everything is initially symmetric in the flow, and the algorithm is applied properly, it should always remain symmetric. Whether things were initially symmetric or not in their model is not clear.

Still, Saghbini and Ghoniem bring forward the idea about the importance of the vorticity gradient. They point to the vorticity gradient, coupled with radial expansion as the initiating cause of vortex breakdown. Furthermore, they identify the azimuthal vorticity sign switch, first supposed by Brown and Lopez (*ref. 17*), as being part of a feedback mechanism that leads to a steady state vortex breakdown. We largely agree, and we reach similar conclusions with our model, thus adding to the evidence that supports the validity of these claims. We will attempt to be more rigorous with the Helmholtz vortex theorems.

3. Vortex Filament Method Results

3.1 Model Output

Before we present our test cases, we need to explain exactly what the output of those cases shows. First, we need to discuss the differences and similarities between streaklines, pathlines as they relate to material lines, and vortex lines in unsteady flows. Then we will present an example of the results and show what that output describes.

3.1.1 Streaklines and pathlines

In flow visualization experiments, the researcher will often use tracers, be they smoke or dye, to view the path that the particles take in whatever flow is being studied. The lines that these tracers form are called streaklines. We call them streaklines because the tracers often do not appear as distinct particles, but in a continuous streaking line. If we were to mark the vortex over a delta wing in a water tunnel with dye, we would see the picture that is in Figure 3-1

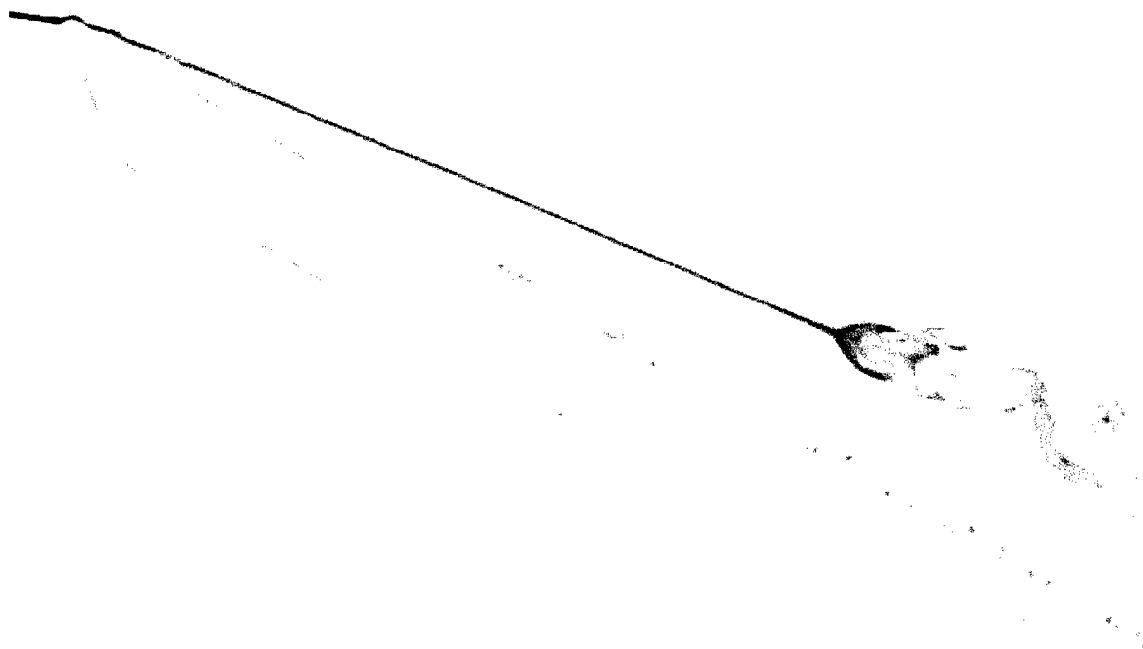


Figure 3-1 Streaklines in a vortex flow

Though we are marking particles, we cannot distinguish the actual movement of a particular particle. In steady flow, this presents no difficulty because the pathline and the streakline are coincident. However, in periodic regions of steady flow, or in all regions of unsteady flow, pathlines and streaklines are not coincident (*ref. 18*). This can be easily illustrated in the following example, illustrated in Figure 3-2.

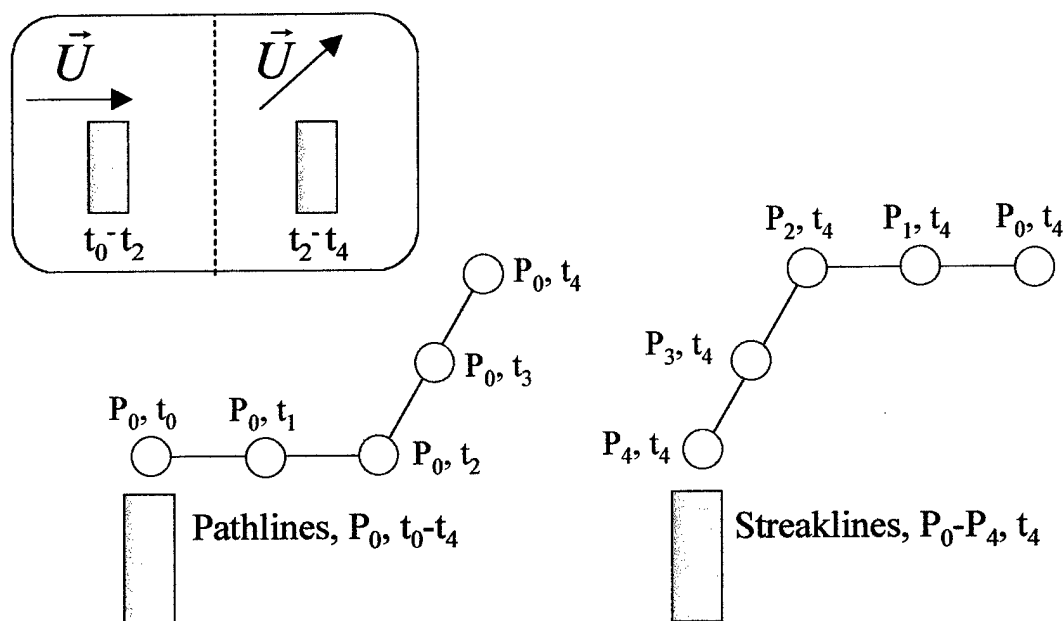


Figure 3-2. Pathlines vs. streaklines

Imagine we have a chimney that sends out smoke. There is breeze that blows the smoke to the right. At time t_2 the wind changes direction. Here we can clearly see the difference between the actual pathlines of the particles and the streaklines. Streaklines show all particles, released successively from a fixed point, at one instant in time: P_0, P_1, P_2, P_3 , at time t_4 . Pathlines shows how one particle travels over time: P_0 at t_0, t_1, t_2, t_3 , and t_4 .

In vortex flows the vortex breakdown is inherently periodic or unsteady, and the fact that the streaklines we see in flow visualization experiments do not reveal the pathlines has caused much difficulty. One thing that can happen is that a region of flow may appear to rotate in the opposite direction of the rest of the flow, when in reality it is

rotating in the same direction, only more slowly. Particles that are actually moving on a very benign path may appear, by looking only at their streaklines, to move violently and in odd directions. This illusion is especially strong in the region downstream of vortex breakdown. Therefore, one must be very careful when looking at streaklines not to draw too many inferences about the actual fluid motion. To do this we need to look at velocity and vorticity fields or we need to track individual particles. With the vortex filament method, velocity and vorticity fields are associated with the location of all the vortex filaments at a given instant in time. These vortex filaments can be regarded as streaklines in that they show the position of many vortex filaments segments or fluid particles, 'released' at a fix position, $z = 0$, at a single instant in time. Thus, we can use their position to discuss induced velocity and associated vorticity, but we can not use their relative positions at any one instant in time to say much of anything about the fluid motion over time.

3.1.2 *Vortex filament method flow visualization*

At this point, we will not discuss what any output tells us about the nature of vortex breakdown. We will only discuss how we will present that output. Remember that, in this model, we discretized the vortex tube into nine (9) concentric rings of vorticity. We further discretized each ring into sixteen (16) vortex filaments plus an additional center tracking line. As we previously discussed, the vortex lines are equivalent to streaklines. Thus, what we see in the model output corresponds to dye streaks in experimental flow visualization, as in Figure 3-1. However, if we show all the vortex filaments segments, we will see a very tangled picture of vortex filaments. Figure 3-3 and Figure 3-4 show a perspective view of the output with all the vortex filaments at $T = 1.8$. Again, we will discuss the conditions the generated this case later. For now we are only concerned with the presentation of the output. The freestream velocity always acts in the positive axial direction. We will indicate this on the next two figures with arrows, and assume it from then on with the arrows omitted.

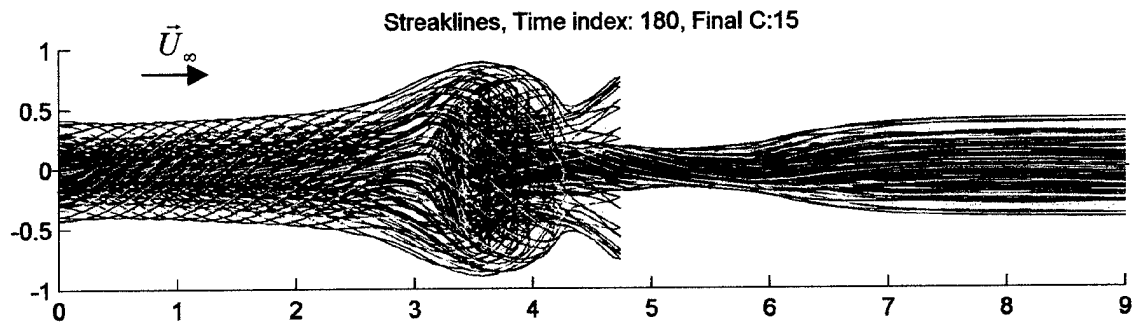


Figure 3-3 Example of model output, all vortex filaments, side view

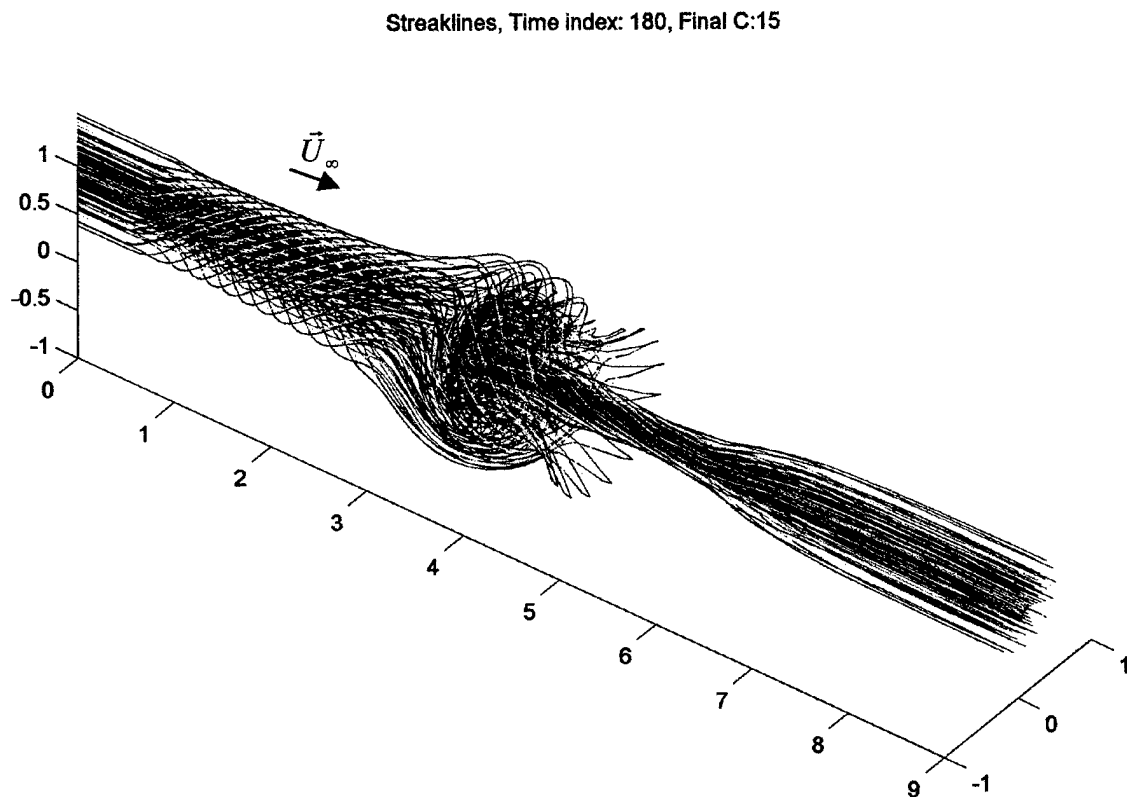


Figure 3-4 Example of model output, all vortex filaments, perspective view

As you can see, it is difficult to see the structure of the vortex tube when it is described by a mass of lines. We have even left out the radial spokes of vorticity (they are present in the simulation in all cases, but we may leave them out of the output for

clarity). Figure 3-5 shows the same perspective view with the radial vortex spokes included. As you can see, the results get even more muddled.

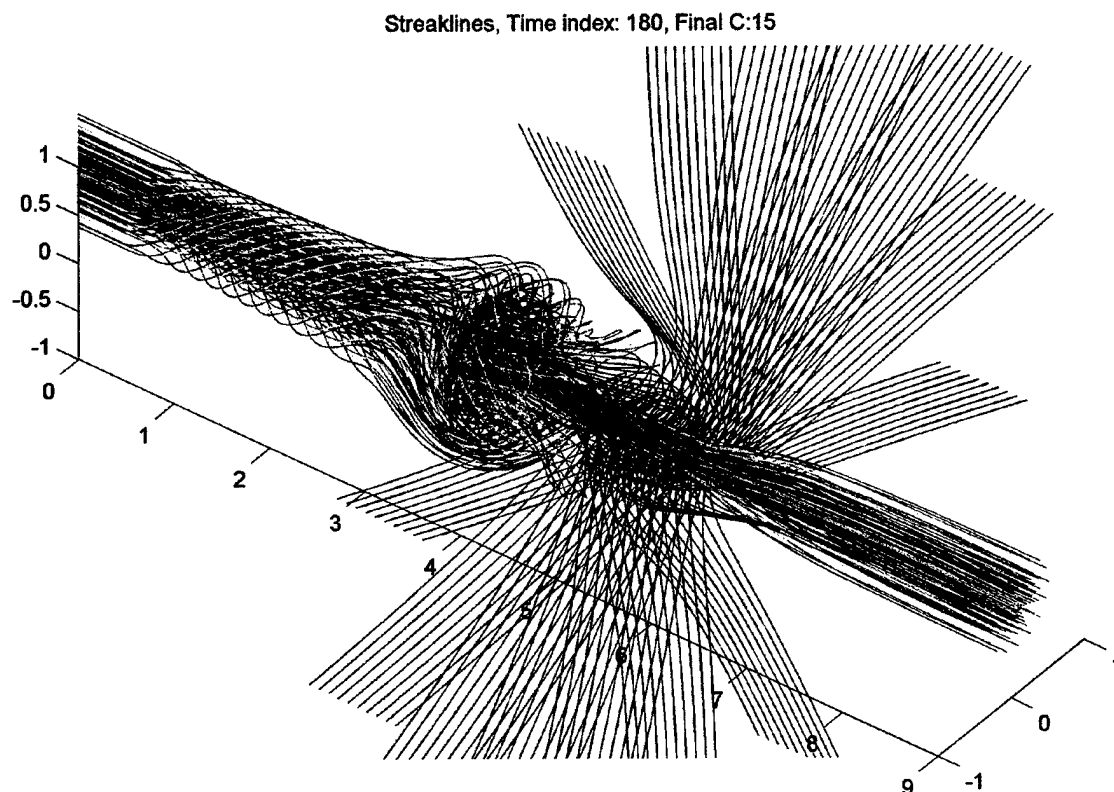


Figure 3-5 Example of model output, with radial spokes, perspective view

To make the output clearer, we will often only show one or two of the discretized vortex tube radii. We will often include the center tracking line because it gives clear picture of the relative flow at the very center of the vortex tube. Thus, in the following figures, we include the $r = 0.42$ and the $r = 0.12$ concentric sleeves of vortex filaments. Figure 3-6 shows the side view and Figure 3-7 shows a perspective view.

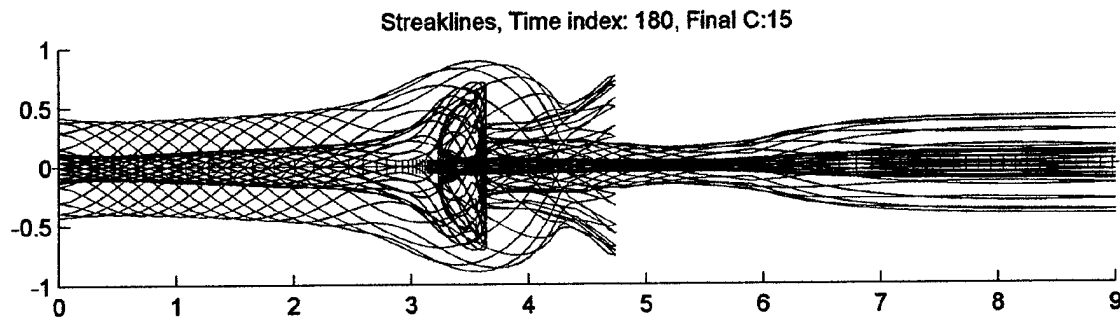


Figure 3-6 Example of model output, $r = 0.42$, $r = 0.12$, side view

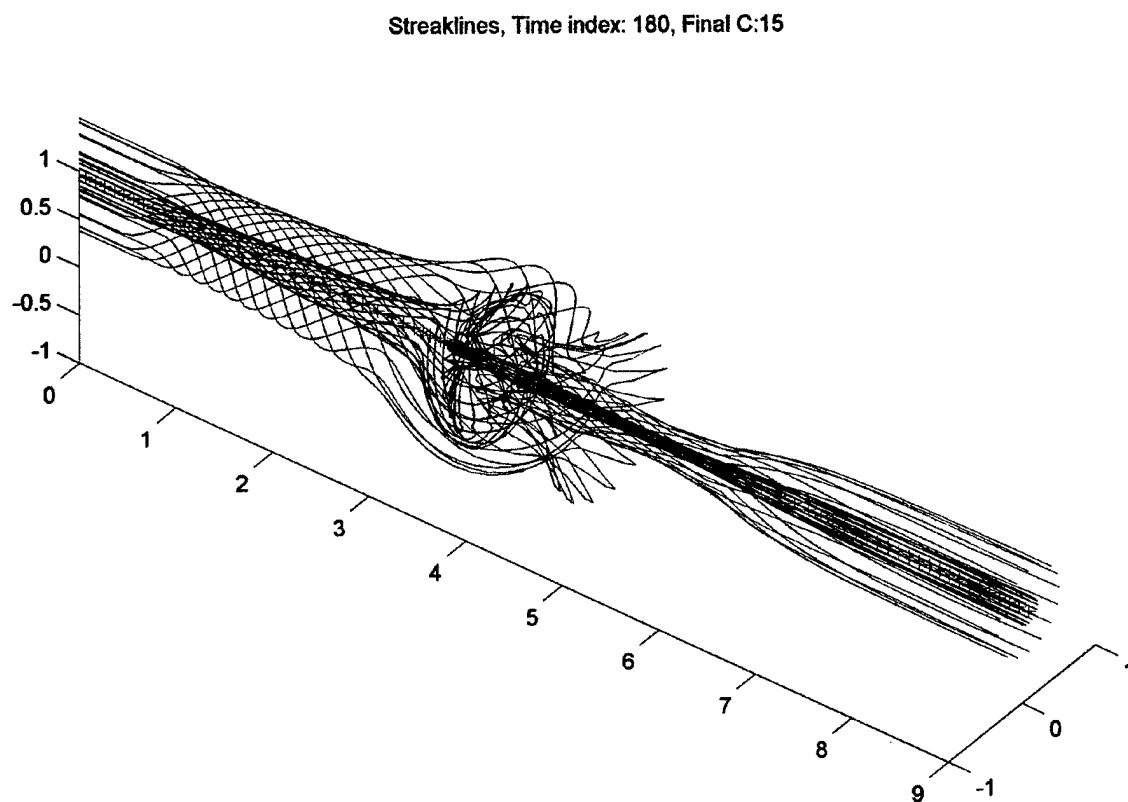


Figure 3-7 Example of model output, $r = 0.42$, $r = 0.12$, perspective view

By just removing all but two radii, the picture becomes much clearer. However, even with two radii it can be difficult to see specific features of the output. So we may want to look at just one radius, as in Figure 3-8 and Figure 3-9.

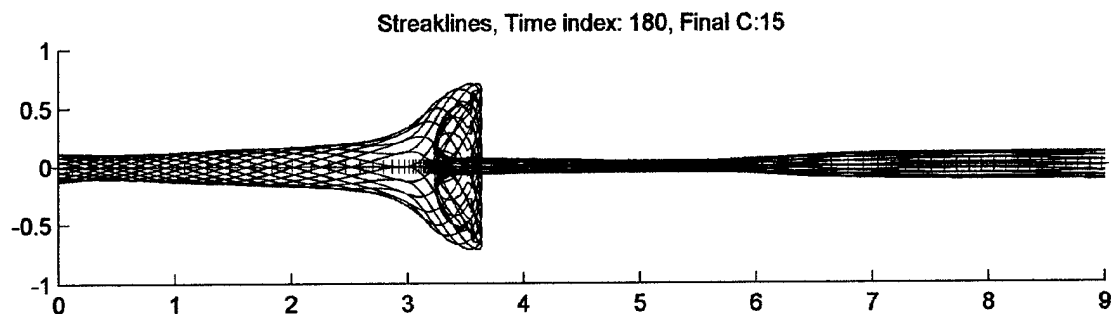


Figure 3-8 Example of model output, $r = 0.12$, side view

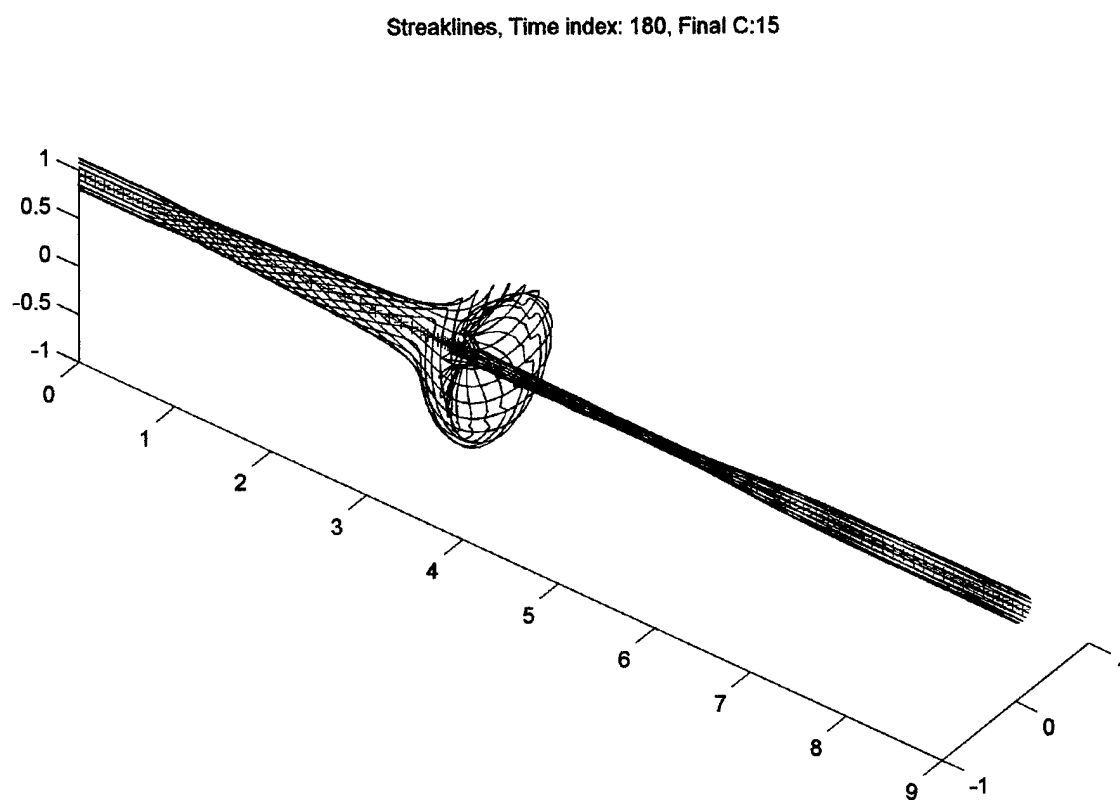


Figure 3-9 Example of model output, $r = 0.12$, perspective view

This is the output that most closely matches what one would see in a dye streak flow visualization experiment. There dye gets entrained into a single interior radial layer of the vortex tube and remains with that layer, marking its vortex lines to form streaklines. Experimentally, you can mark different radial layers of the vortex tube, or

you can just mark one. The previous figures, where we show only one ring of concentric vortex filaments, are equivalent to that. All the other vortex filaments are present in the simulation, just as they are present in a real vortex tube. They affect the movement of the marked radius, but we only see that one marked radius, just as in the one radius of vortex filaments that we are showing.

Even this view, while better than the others, has its difficulties. For instance, in Figure 3-8, the side view, it is not clear which way the vortex filaments are tilting because we seen vortex lines on both sides of the vortex tube. To overcome this, we will render the vortex lines as a surface, with the axial running lines being the vortex filaments and the circumferential lines being simply lines that mark the axial length of a vortex filament segment. Figure 3-10 and Figure 3-11 give a side and perspective view of this rendered case.

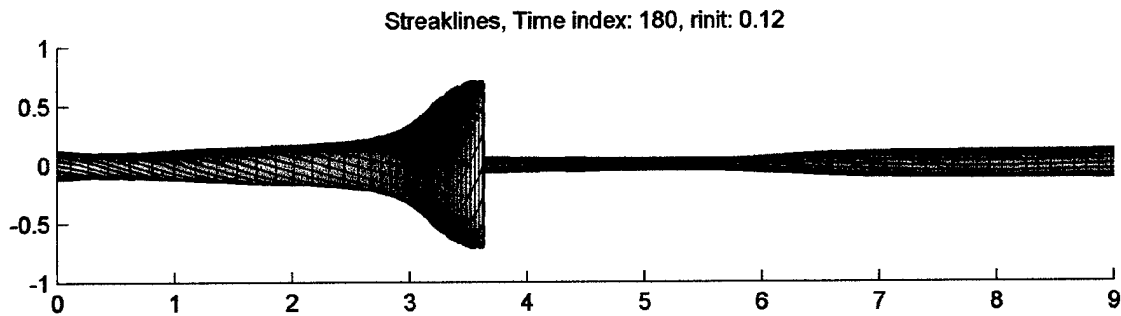


Figure 3-10 Example of model output, $r = 0.12$, rendered side view

Streaklines, Time index: 180, rinit: 0.12

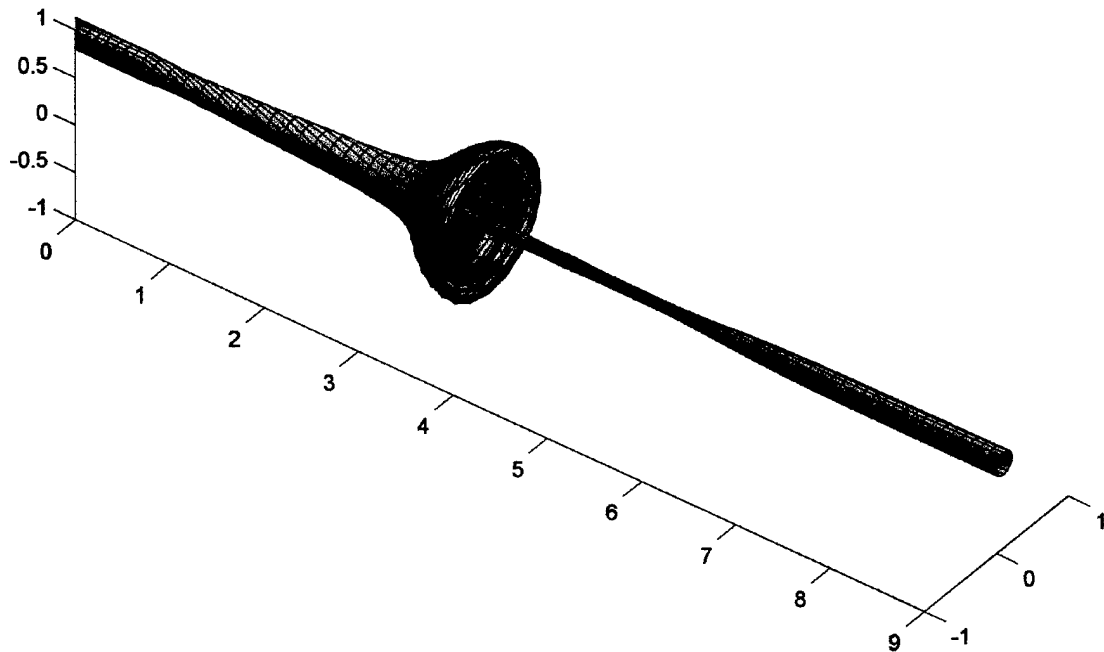


Figure 3-11 Example of model output, $r = 0.12$, rendered perspective view

We can use a closer view to look at the specific features of this rendered view.

Figure 3-12 shows one such image. In this view, the yellow line shows one particular vortex filament. The purple line shows the circumferential spacing line that indicates the length of the vortex filament segments. Each intersection of a vortex filament segment and a circumferential tracking line indicates a vortex filament segment node. The green shaded regions show areas of the vortex tube with a large circulation. The blue shaded regions show areas of the vortex tube with low circulation, and the red shaded regions show areas where the circulation of the vortex tube is changing due to the superposition of vortex lines. We will describe why we change the circulation along the vortex tube in the next section.

Streaklines, Time index: 180, rinit: 0.12

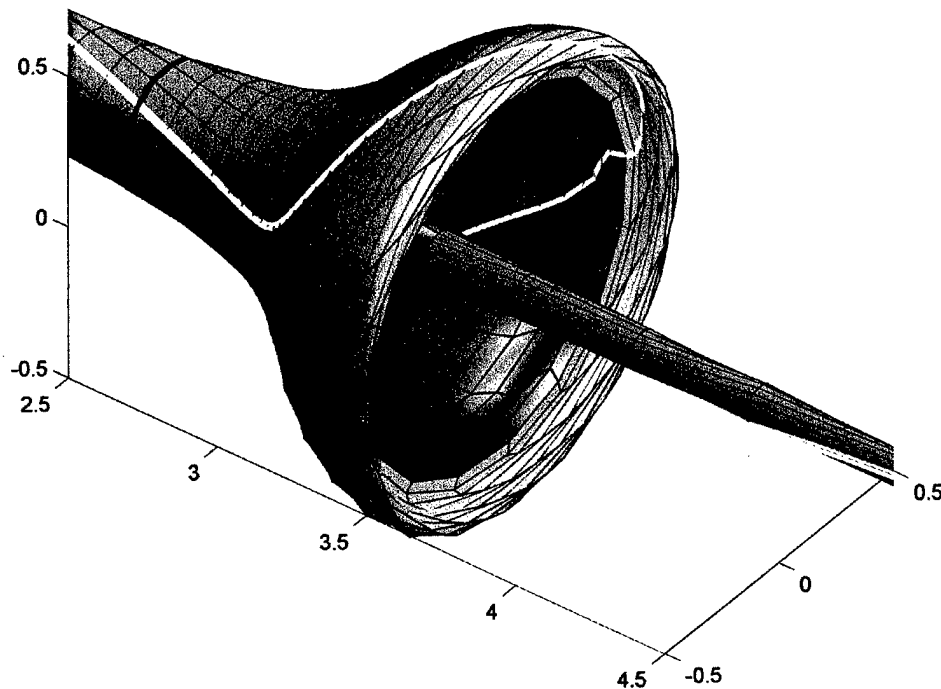


Figure 3-12 Closer view, $r = 0.12$, rendered perspective view

An intrinsic benefit to the vortex filament method is to be able to infer induced velocities by looking at the orientation of the vortex filaments. We know that the vorticity vector is always aligned with the vortex filaments, so simply by using the right hand rule, we can quickly see what the induced velocity should be from any given vortex filament. This provides insight into how vortex breakdown occurs that cannot be found by looking more complicated vortex simulations techniques. These techniques do not intrinsically preserve the vortex line, so often plots of the vortex filaments are not present. To see the loss in information, we can compare the vortex filament simulation results with and without the vortex lines present. Figure 3-13 shows the rendered results at $T = 1.8$. While we can see the vortex breakdown in the top image, we can see the vortex filaments and determine the resulting induced velocities that lead to this

breakdown in the bottom image. The ability to visualizing these vortex filaments is one of the principal benefit of the vortex filament method.

Vortex Filaments, Time: 1.8

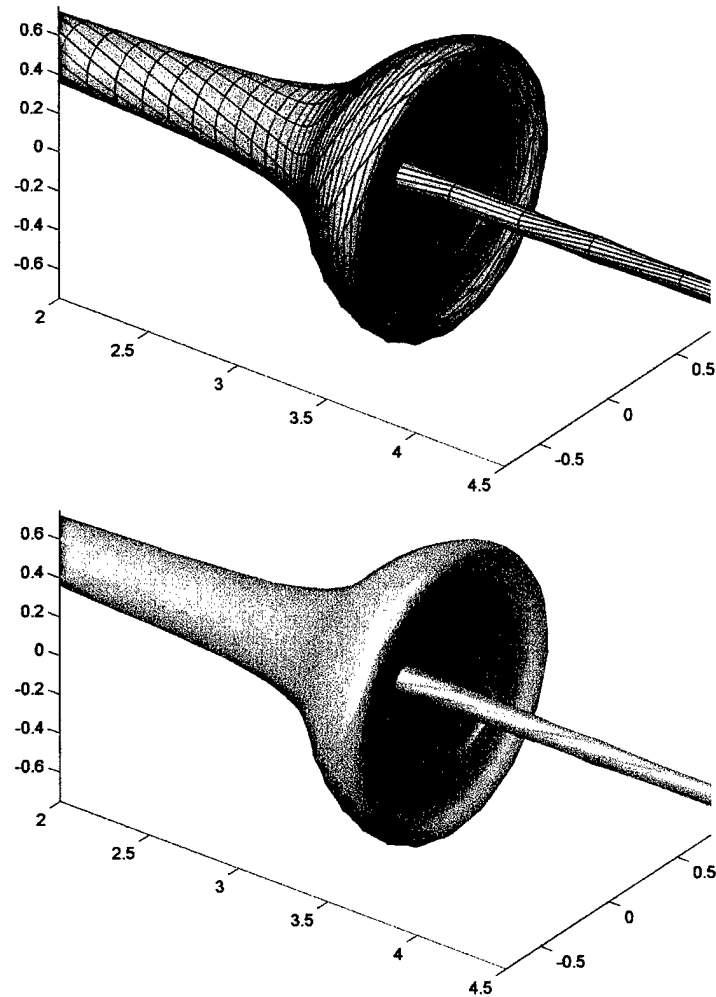


Figure 3-13 Simulation results, with (bottom) and without (top) vortex filaments, $T = 1.8$

3.1.3 Vorticity and Velocity Data

Besides presenting the vortex filament locations at a given instant in time, we have also calculated the velocity and vorticity associated with the vortex tube on the meridional plane passing through the vortex tube. This was done by simply taking the

vortex filaments at a given point in time, with their circulation and vortex core radii known, and calculating their induced velocity on fixed nodes evenly placed on the meridional plane of the vortex tube. Figure 3-14 and Figure 3-15 show illustrations of this. The first shows a perspective view with the induced azimuthal velocity presented on the meridional plane. The second shows a side view of the vortex tube overlaid with the axial velocity (including the freestream velocity) on the meridional plane.

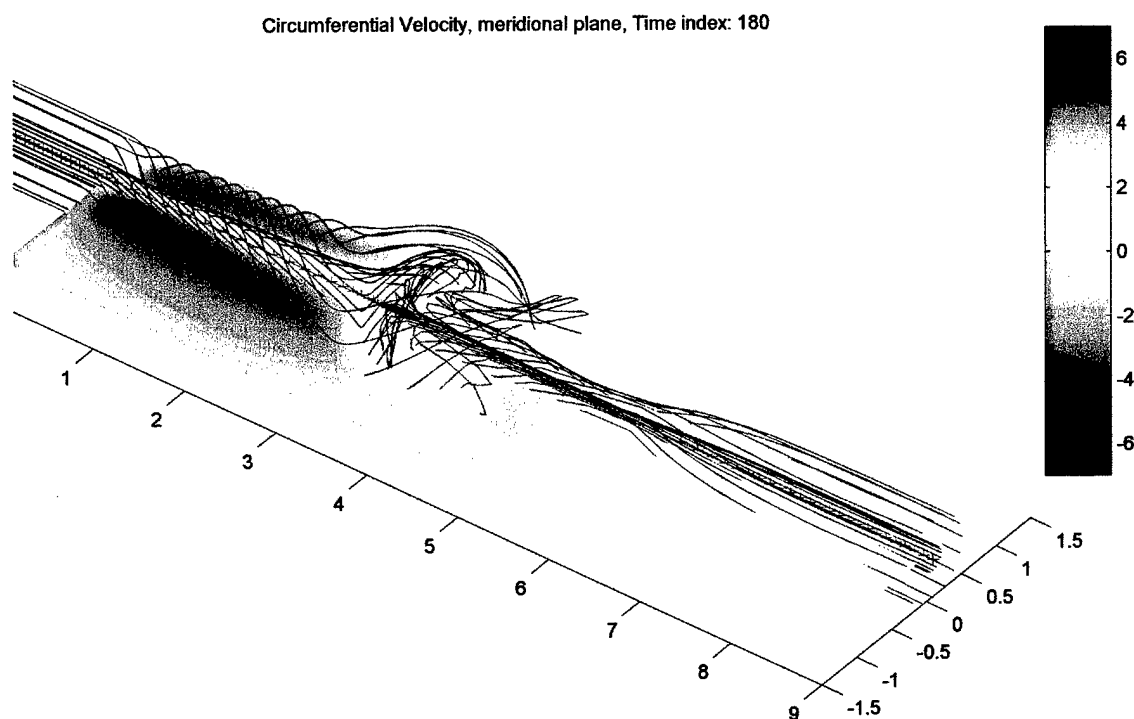


Figure 3-14 Example of azimuthal velocity, meridional plane, perspective view

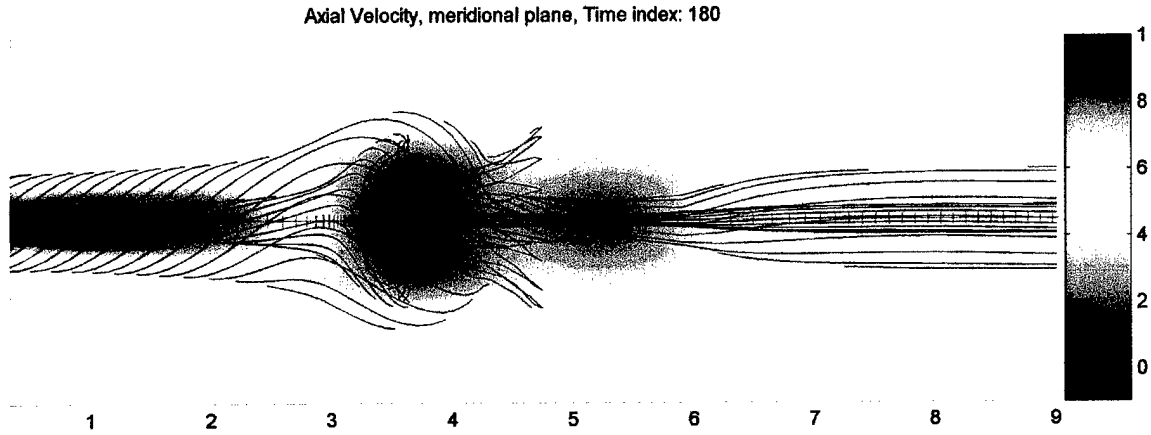


Figure 3-15 Example of axial velocity, meridional plane

The velocity is in units of $[length]/[time]$ and the vorticity is in units of $1/[time]$. Specific units are not used because we are concerned with the differences in values and not their absolute value. From this velocity field, we can calculate the vorticity field. Calculating the axial and radial vorticity requires that we calculate induced velocities slightly away from each side of the meridional plane in addition to the meridional plane velocities. We calculate the vorticity according to the second order scheme in equations (3-1) and (3-2) (*ref. 19*). This equation shows the calculation of ω_z . The calculations for ω_θ and ω_r are equivalent. In the meridional plane, $\omega_\theta = \omega_y$ and $\omega_r = \omega_x$.

$$(\omega_z)_{i,j} \cong \frac{\Gamma_{i,j}}{4\Delta x \cdot \Delta y} \quad (3-1)$$

$$\begin{aligned} \Gamma_{i,j} = & \frac{\Delta x}{2} \left((u_x)_{i-1,j-1} + 2(u_x)_{i,j-1} + (u_x)_{i+1,j-1} \right) \\ & + \frac{\Delta y}{2} \left((u_y)_{i+1,j-1} + 2(u_y)_{i+1,j} + (u_y)_{i+1,j+1} \right) \\ & - \frac{\Delta x}{2} \left((u_x)_{i+1,j+1} + 2(u_x)_{i,j+1} + (u_x)_{i-1,j+1} \right) \\ & - \frac{\Delta y}{2} \left((u_y)_{i-1,j+1} + 2(u_y)_{i-1,j} + (u_y)_{i-1,j-1} \right) \end{aligned} \quad (3-2)$$

The equations are applied to evenly distributed nodes on (or slightly off) the meridional plane where we have calculated the induced velocity.

3.2 *Application to vortex breakdown*

Much of the current theory on vortex breakdown deals with the breakdown in a steady state condition. This theory is very useful. However, it must typically assume an initiating condition in the vortex tube, such as a radially expanded vortex tube (*ref. 17*). Often, a pressure gradient is assumed to initiate the breakdown (*ref. 20*). We want to take a step back from that and look at the unsteady formation of vortex breakdown, starting with a constant radius vortex tube fed from a vorticity source and seeing what input conditions are required to initiate breakdown. Vortex breakdown may not require a pressure gradient, but it may be brought about through a self-induction caused by a vorticity gradient in the vortex core. Initial research into a possible self-induction method that initiates vortex breakdown (*ref. 21 and 22*), supports this conclusion for the importance of a vorticity gradient. We conclude that a vorticity gradient, with axial and azimuthal vorticity in the vortex tube increasing in the upstream direction, is an important initiator of the vortex breakdown mechanism. Others have concluded this as well (*ref. 15*). Therefore, we will use the previously described vortex filament method to test this hypothesis. If a vorticity gradient leads to a configuration of the vortex tube that has the same conditions as a vortex breakdown in a real flow, we can conclude that a vorticity gradient can initiate vortex breakdown. Furthermore, with the vortex filament method, we can observe how the vorticity gradient changes the vortex tube so that we might understand the specific unsteady mechanism that leads to a steady vortex breakdown. With this insight, one can devise specific ways to prevent, weaken, or delay vortex breakdown in real flows.

In our model, we will generate a vorticity gradient by causing a change in circulation in the vortex tube. This is not the only way a vorticity gradient can be created in a vortex tube. It is possible that a pressure gradient causes a vorticity gradient in the vortex tube, which would then initiate vortex breakdown. This may be a fine point, but it shows that the physical mechanism for vortex breakdown is present in the vortex tube itself. After we present the results, we will discuss other possible ways to achieve this vorticity gradient, especially in vortex tube over real wings.

3.3 Vorticity gradient in the discretized vortex tube

In this case, we will cause a vorticity gradient in the vortex tube by specifying a change in circulation in that vortex tube. As was previously described, we change the circulation in the vortex tube by the superposition of vortex filaments that turn outward in radial spokes of vorticity at the required axial location to achieve the prescribed circulation profile while maintaining solenoidality within the vortex tube. For a negative vorticity gradient case (vorticity in the vortex tube increasing upstream), the circulation in the vortex tube coming out of the vorticity source as a function of time is given the profile in Figure 3-16. The circulation has the unspecified units of $[length]^2/[time]$. This is the circulation of the vortex tube as it leaves the vorticity source. Those filaments leaving at that time keep their given circulation for the entire simulation. Therefore, downstream of the vorticity source, there may be vortex filaments with a lower circulation than those leaving the vorticity source at the current instant in time.

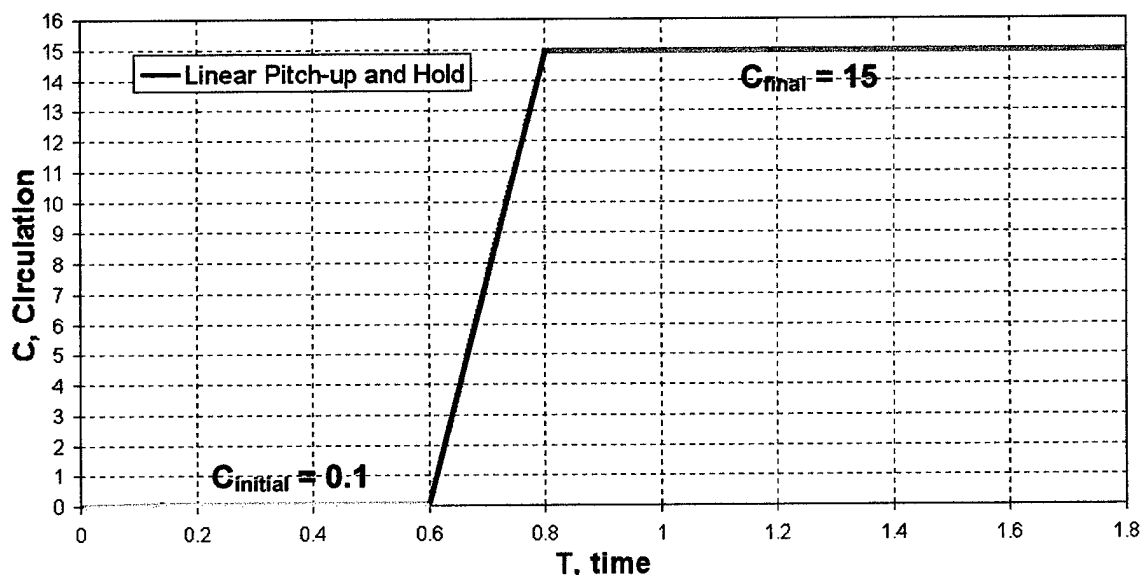


Figure 3-16 Circulation of vortex tube at vorticity source

For the circulation profile in Figure 3-16, the initial circulation of the vortex tube is very low ($C = 0.1 [length]^2/[time]$). It then starts to increase (as it is fed out of the vorticity source) at $T = 0.6 [time]$. The vorticity source continues increasing its

circulation output until $T = 0.8$ [time] when the circulation reaches its final value ($C = 15$ [length]²/[time]). In this case, $U_{\infty} = 5$ [length]/[time]. The end of the vortex tube is far enough downstream not to affect the region of interest.

One should remember that, while we talk about the vorticity source changing its circulation output in time, the vortex tube has, in the actual model algorithm, already been assigned the circulation increase in the region of $z < 0$. However, it is only able to affect the vortex tube when the vortex filaments with the higher circulation convect downstream to a location $z > 0$. Therefore, we can speak either in terms of the vorticity source changing its circulation output in time, or in terms of the vortex filaments pre-assigned in $z < 0$ convecting into the $z > 0$ region. It is more physical to talk about the former case, so that is how we will describe it.

3.4 Primary Case

We will present the case of the simulation responding to the circulation change described in Figure 3-16. We will present the vortex filament plots, as previously described, in a variety of forms to convey the results. We will present velocity and vorticity color contour plots along the meridional plane for the entire vortex tube. The following chart summarizes the case parameters. We will present the results at intervals of $T = 0.3$.

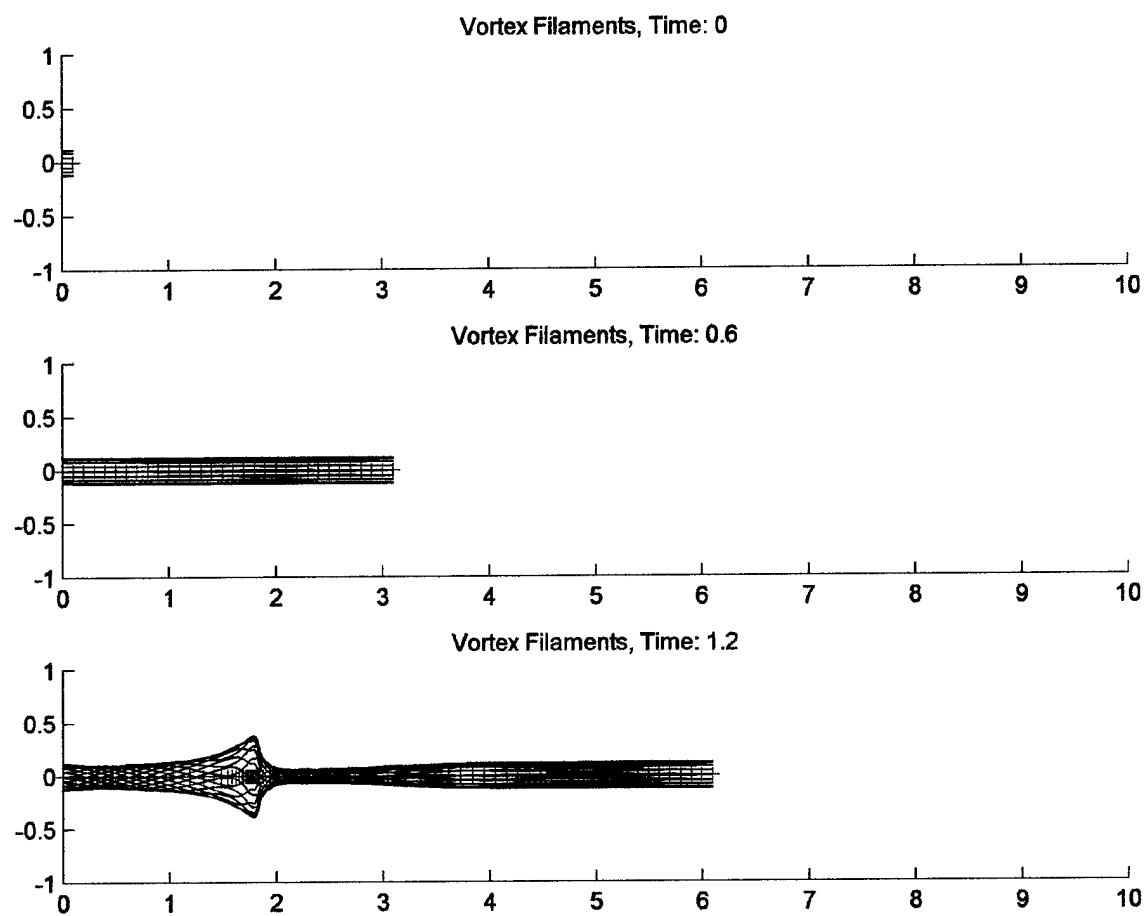
Table 3-1 Primary case parameters

Δz , initial vortex filament segment length	0.1 [length]
Δt , simulation time step	0.01 [time]
$C_{initial}$	0.1 [length] ² /[time]
C_{final}	15 [length] ² /[time]
$T_{C_{initial}}$	0.6 [time]
$T_{C_{final}}$	0.8 [time]

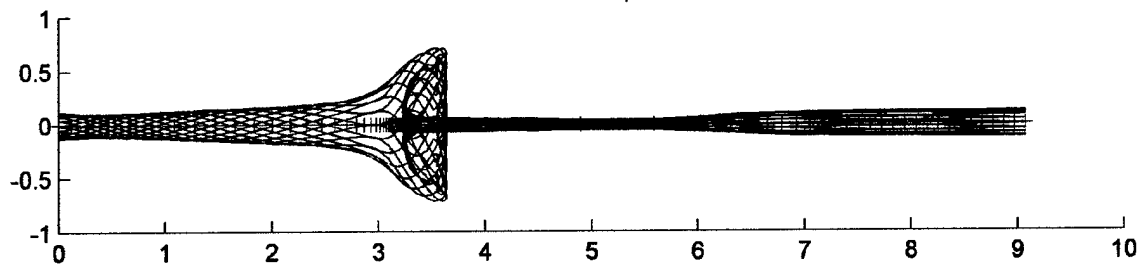
3.4.1 *Vortex filament plots*

We present four different plots of the simulation results. The first shows a side view of the vortex filaments that start at $r = 0.12$. The second set of plots show the same view with both $r = 0.12$ and $r = 0.42$ vortex filaments. The third set includes both $r = 0.12$ and $r = 0.42$ and adds the radial spokes. The last set shows a side rendered view of the $r = 0.12$ vortex filaments.

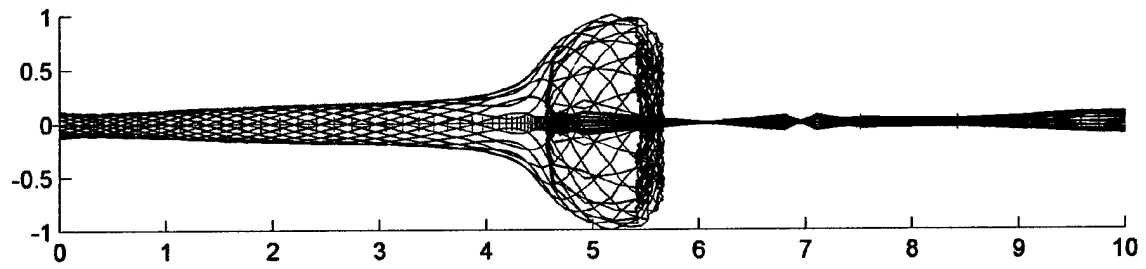
3.4.1.1 Vortex filaments, $r = 0.12$



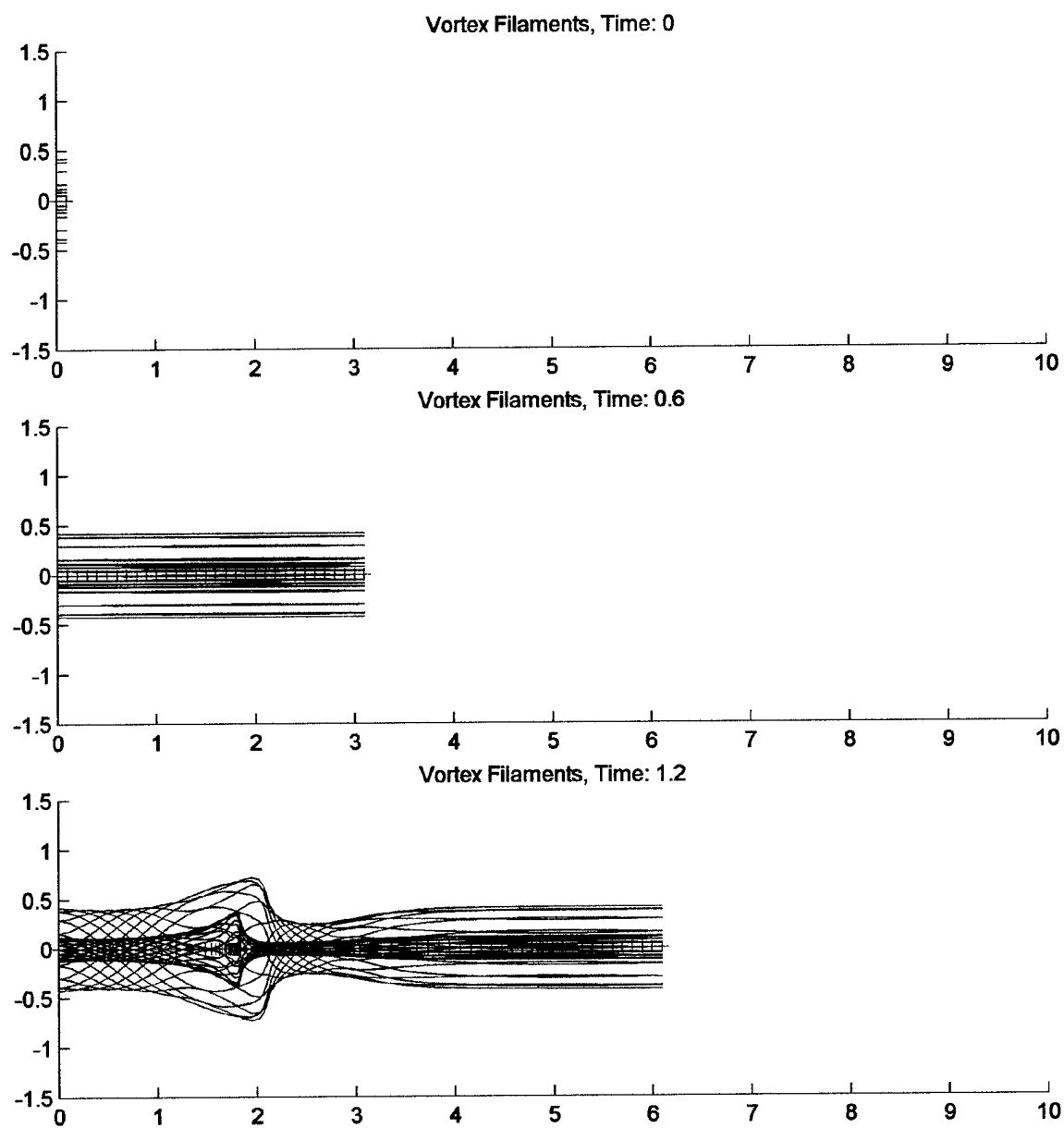
Vortex Filaments, Time: 1.8



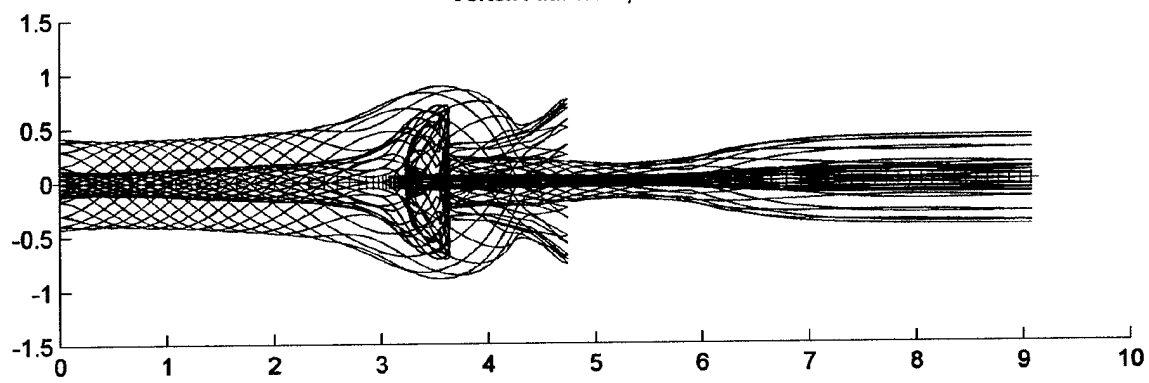
Vortex Filaments, Time: 2.4



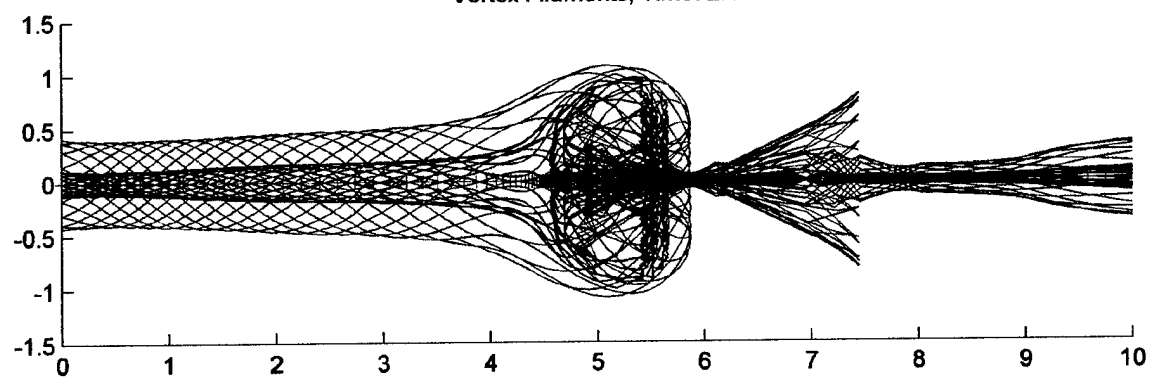
3.4.1.2 Vortex filaments, $r = 0.12$, $r = 0.42$



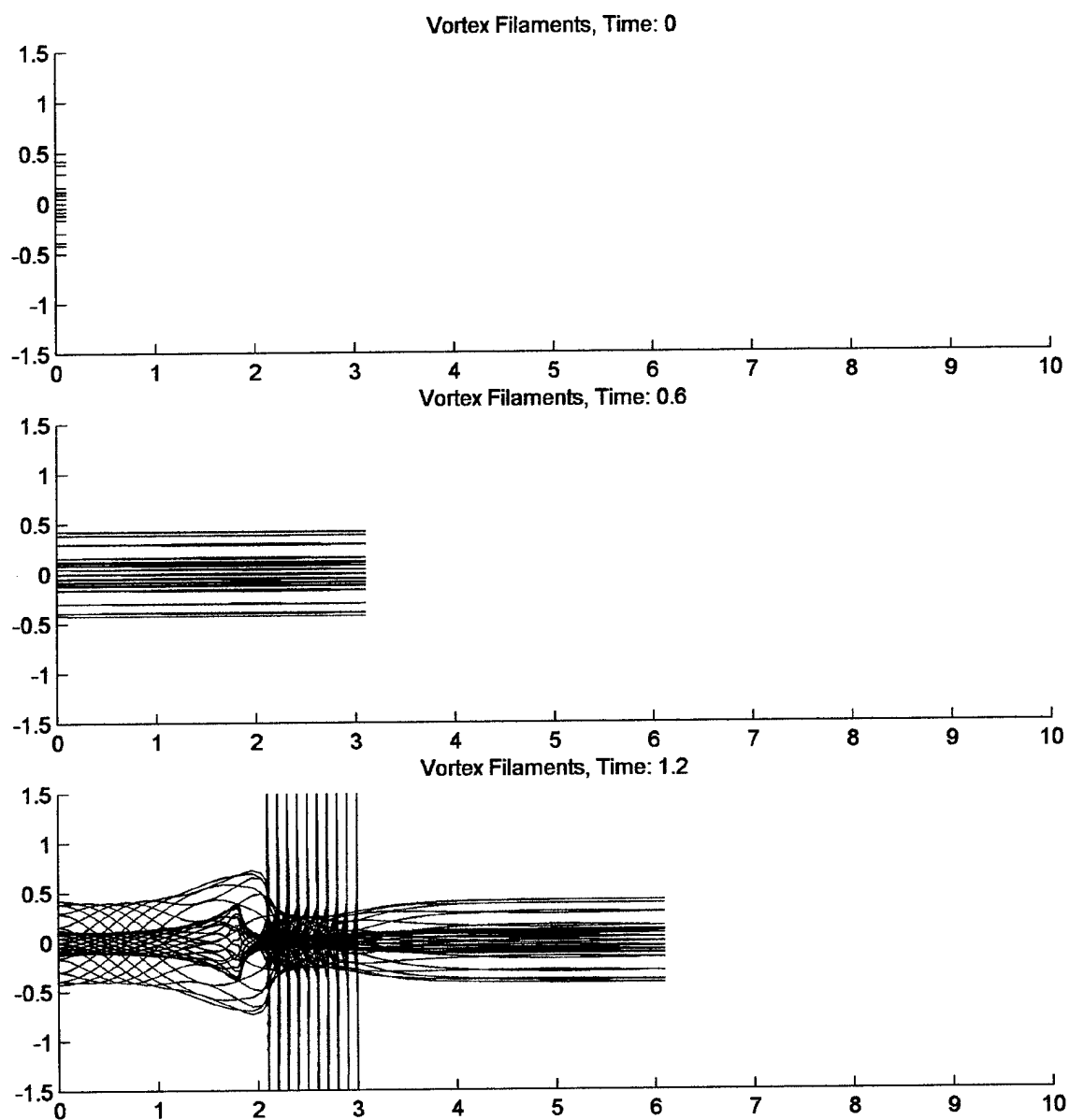
Vortex Filaments, Time: 1.8

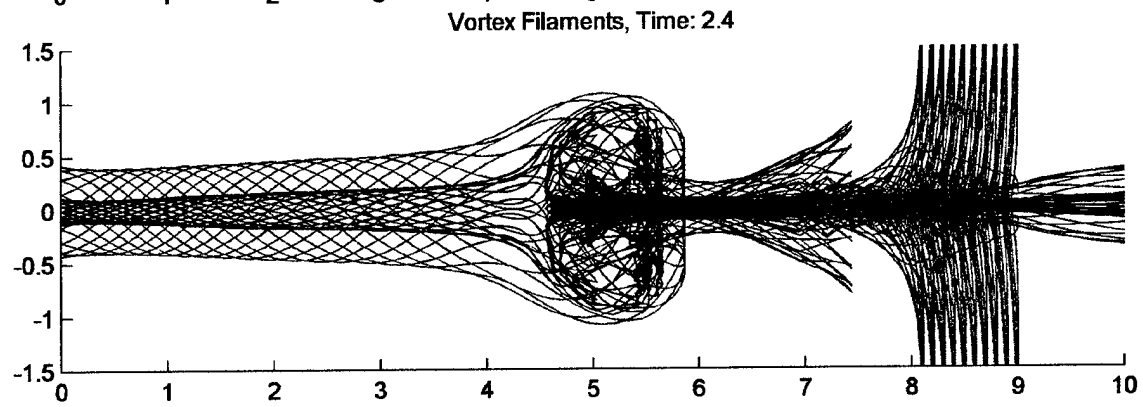
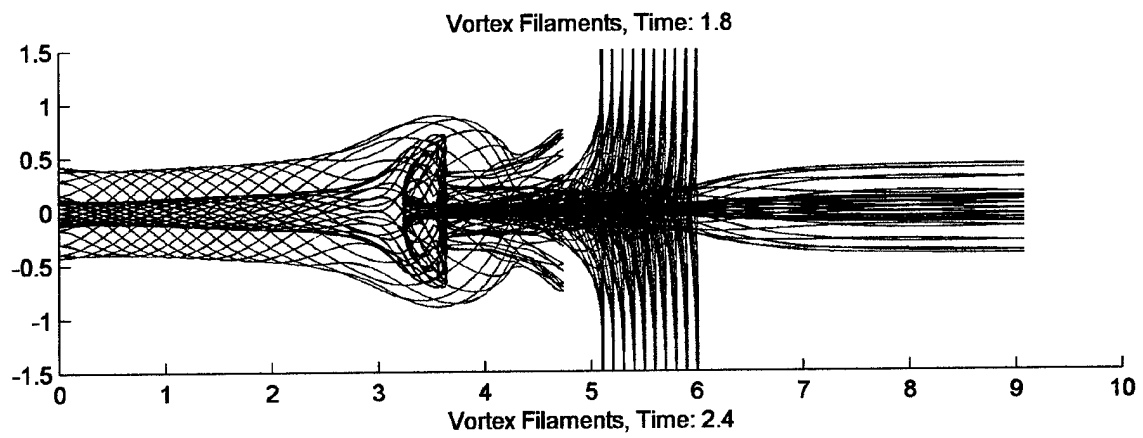


Vortex Filaments, Time: 2.4

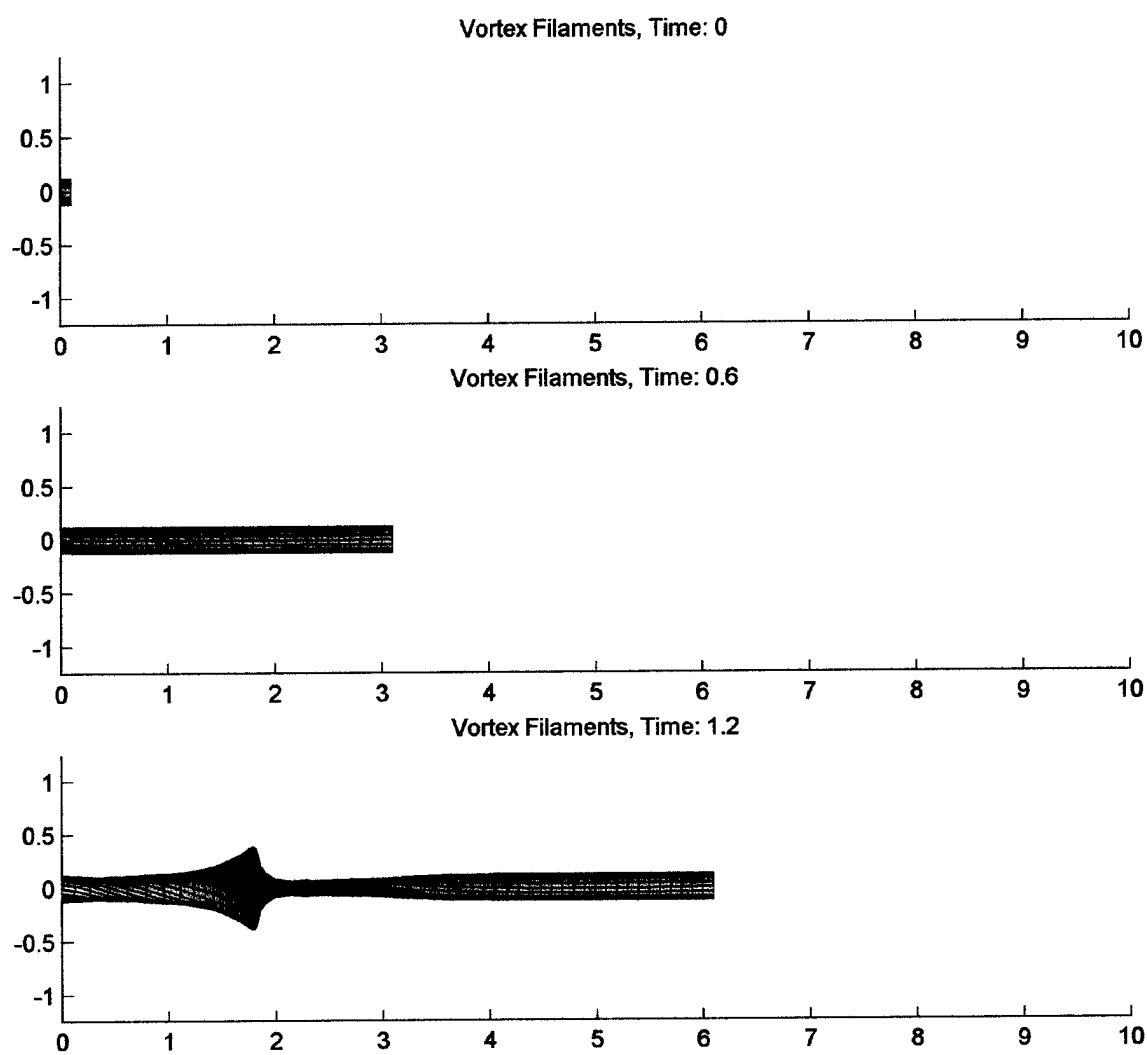


3.4.1.3 Vortex filaments, $r = 0.12$, $r = 0.42$ and radial spokes

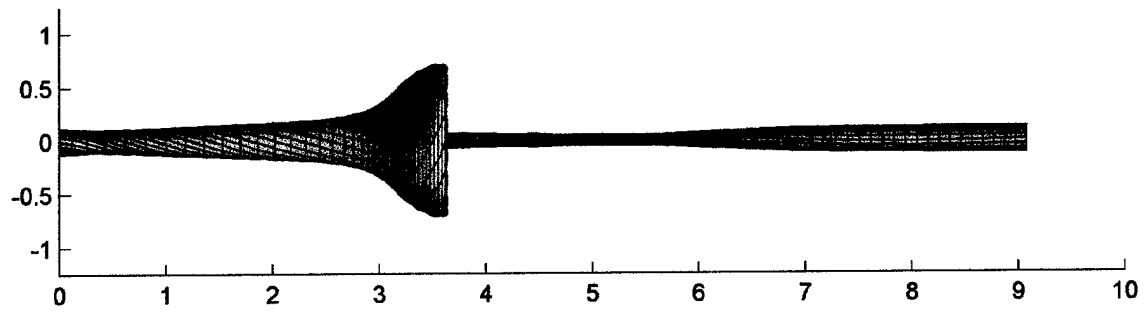




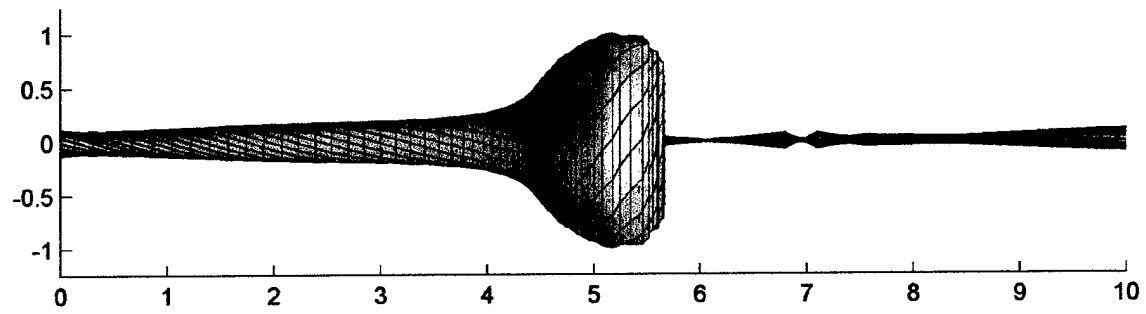
3.4.1.4 *Rendered vortex lines, rendered, $r = 0.12$, side view*



Vortex Filaments, Time: 1.8



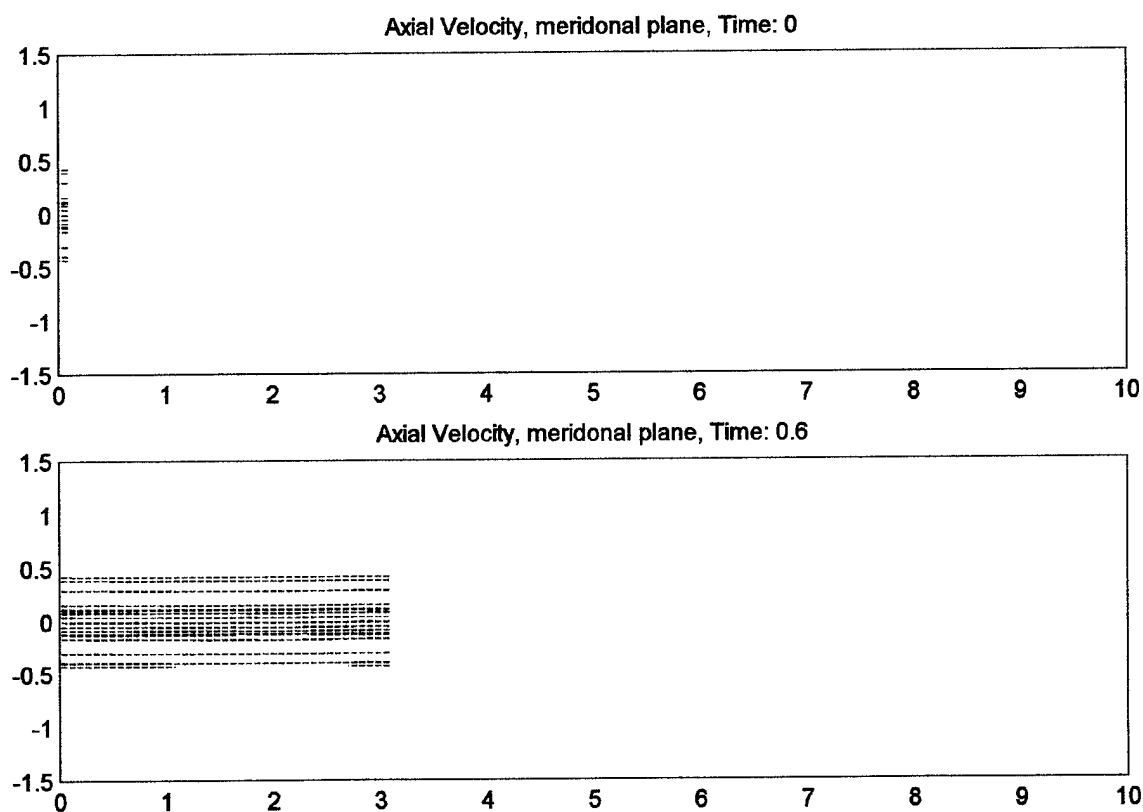
Vortex Filaments, Time: 2.4

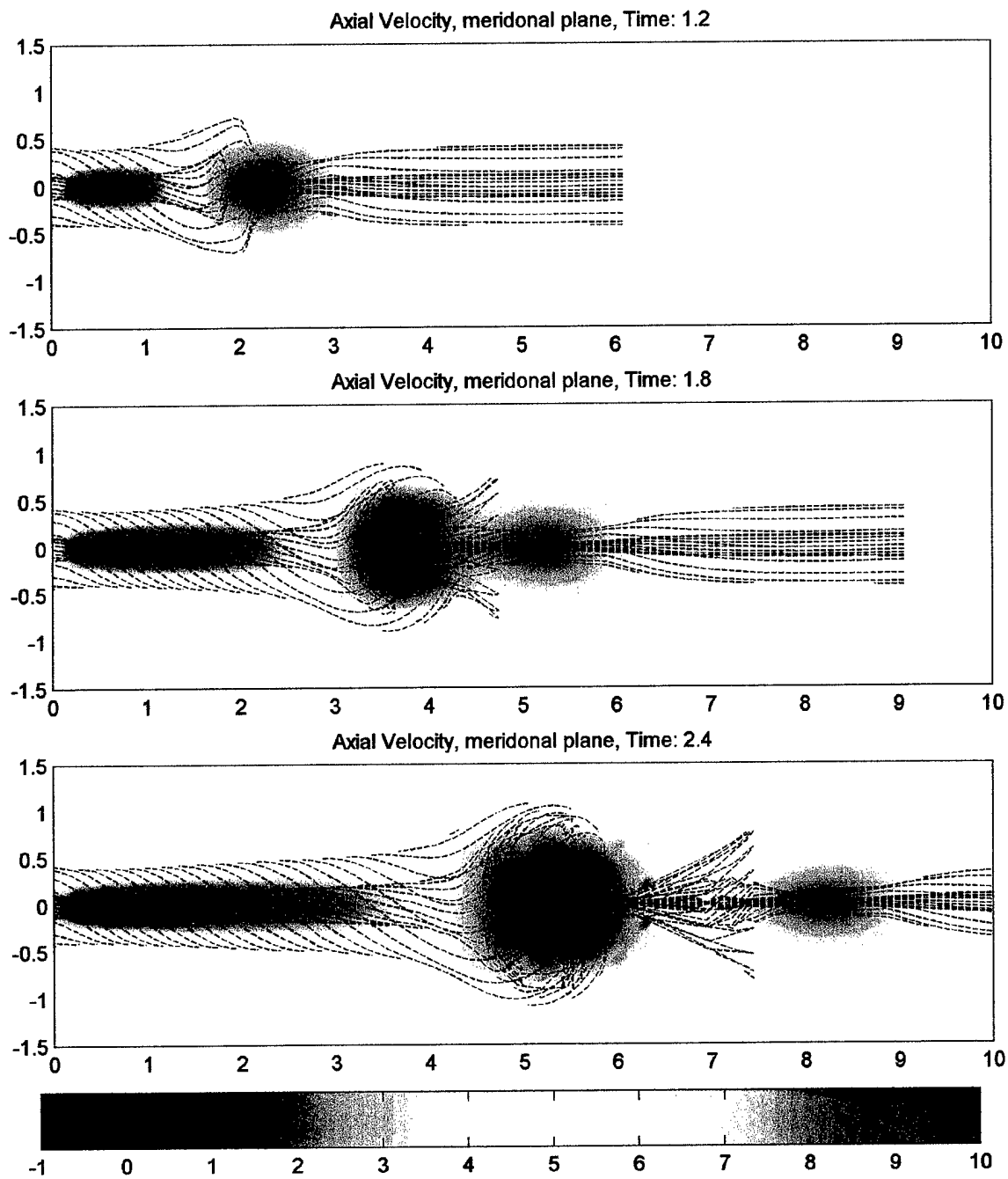


3.4.2 Velocity and Vorticity plots on meridional plane

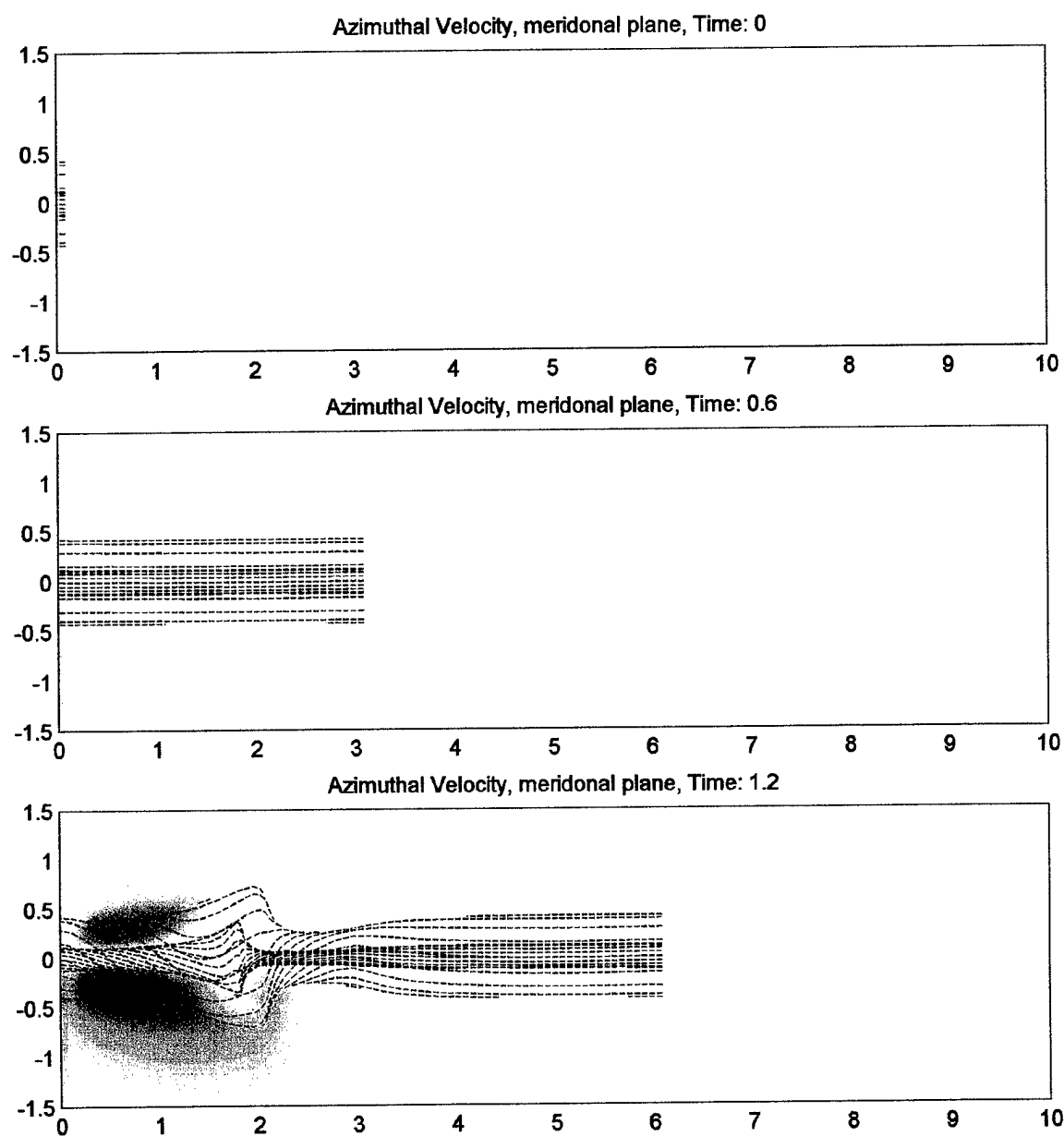
In the following plots, we present the axial and azimuthal velocity and vorticity, as calculated along the meridional plane of the vortex tube. The vortex filaments at $r = 0.12$ and $r = 0.42$ are overlaid to show how their instantaneous location correlates with the vorticity and velocity data. A color bar scale is located at the end of each section.

3.4.2.1 Color contour axial velocity plots

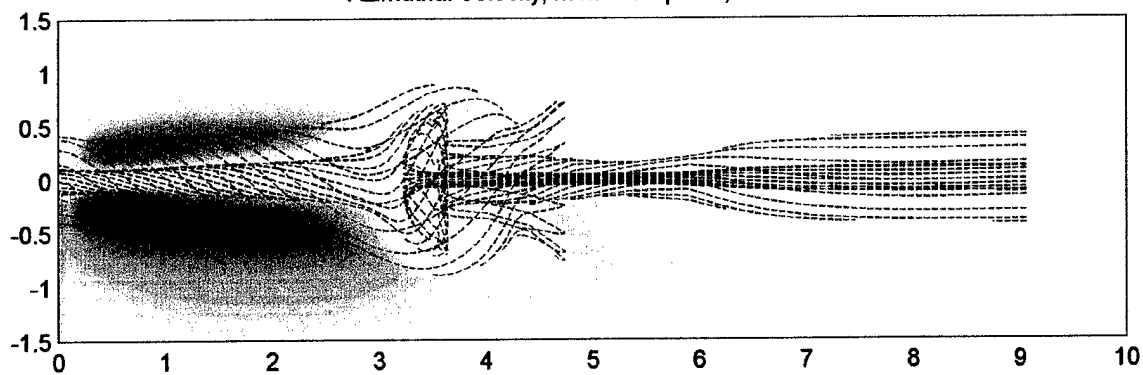




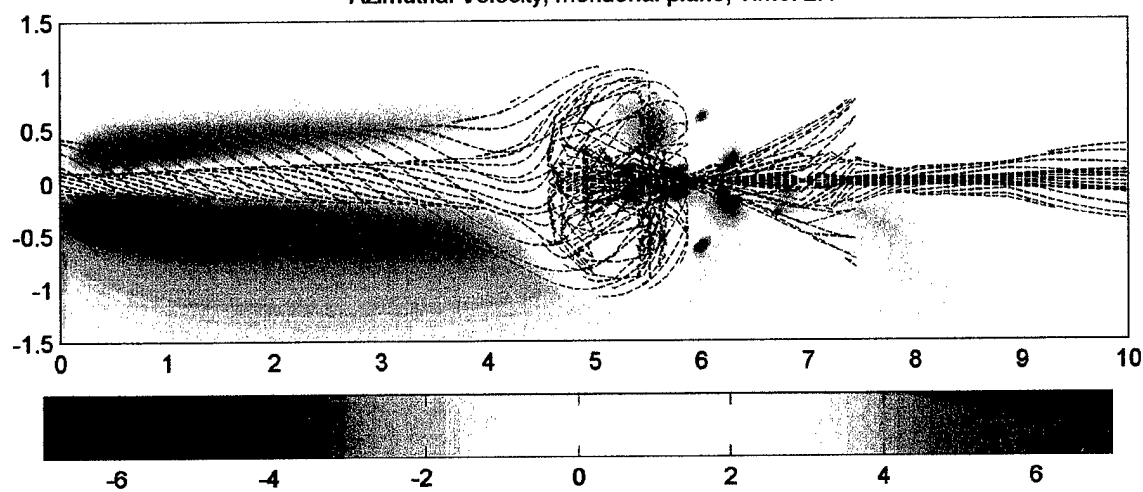
3.4.2.2 Color contour azimuthal velocity plots



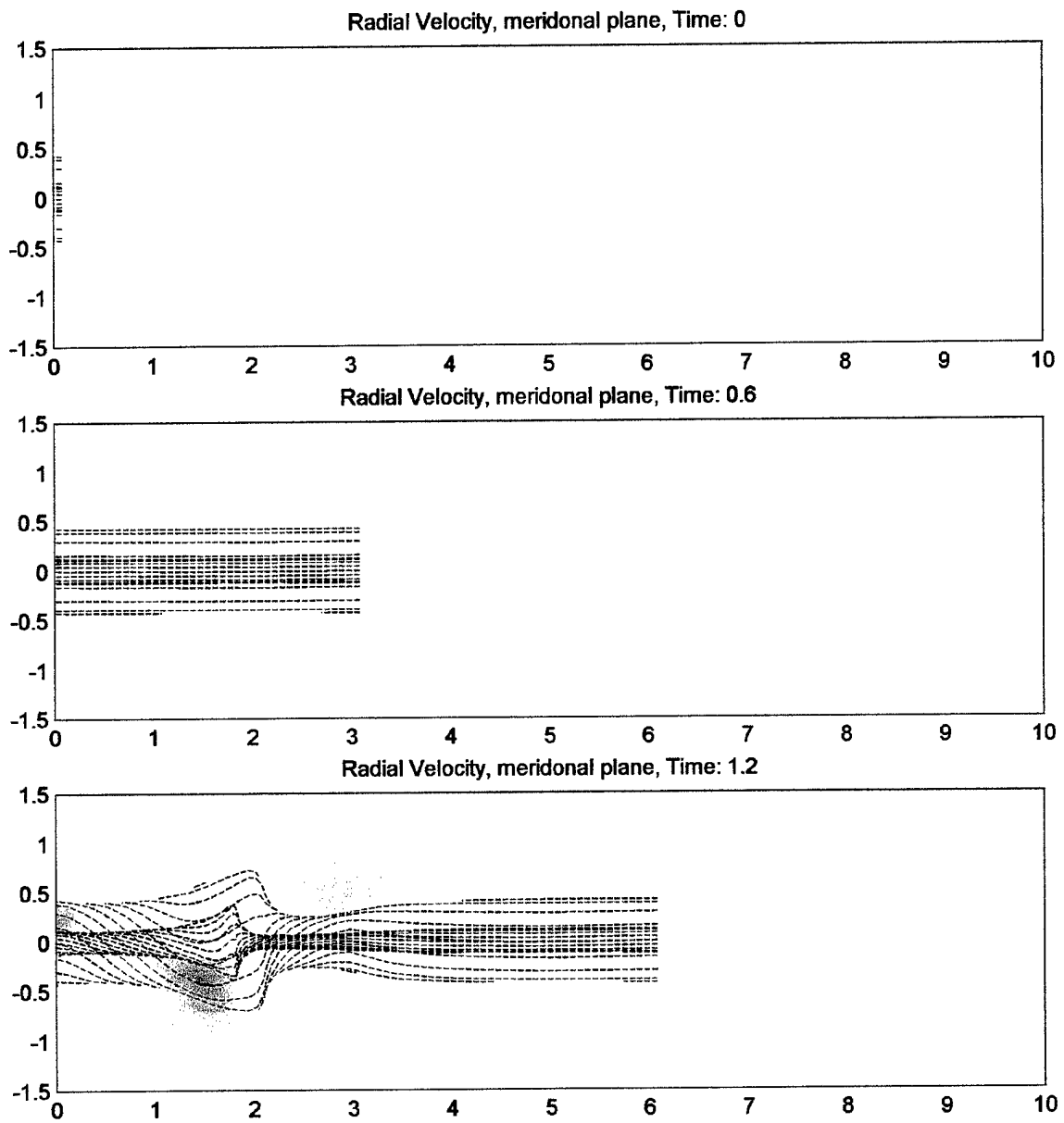
Azimuthal Velocity, meridional plane, Time: 1.8

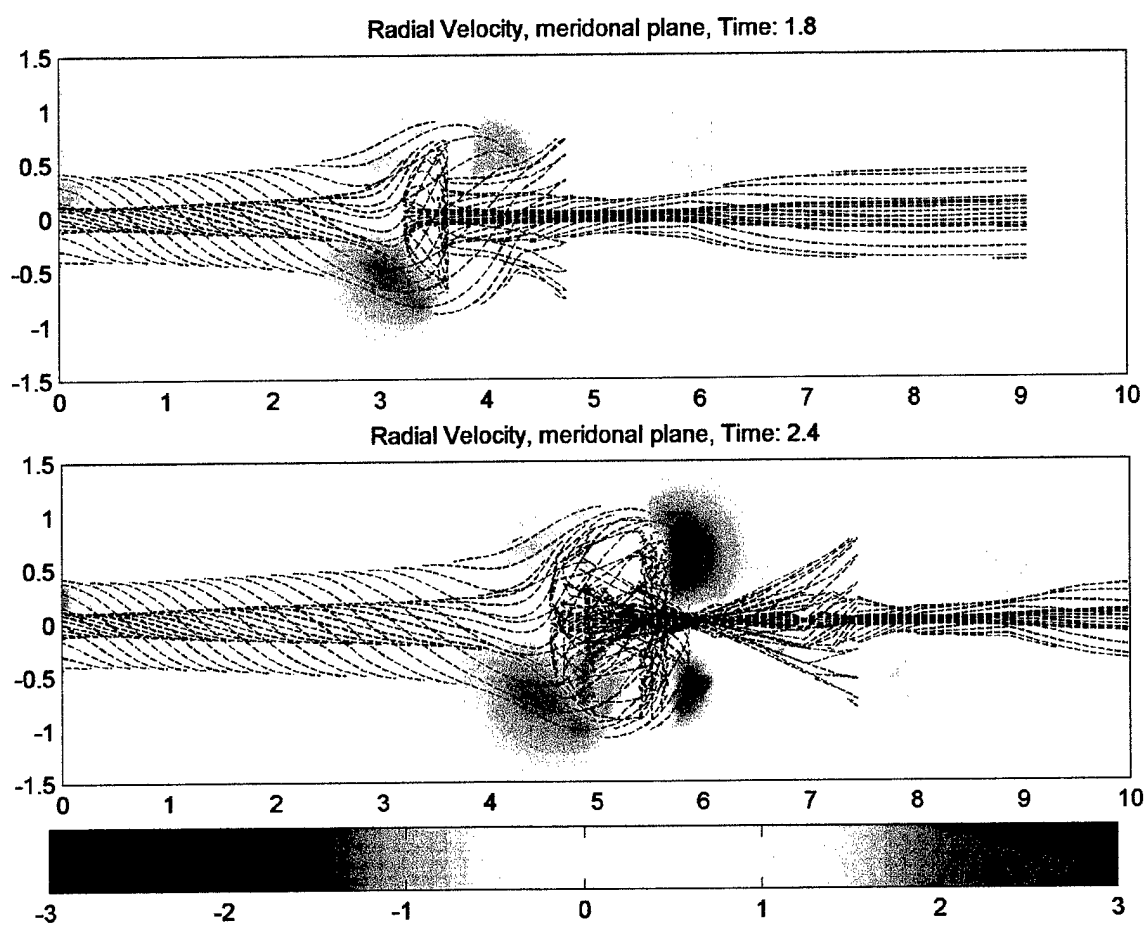


Azimuthal Velocity, meridional plane, Time: 2.4

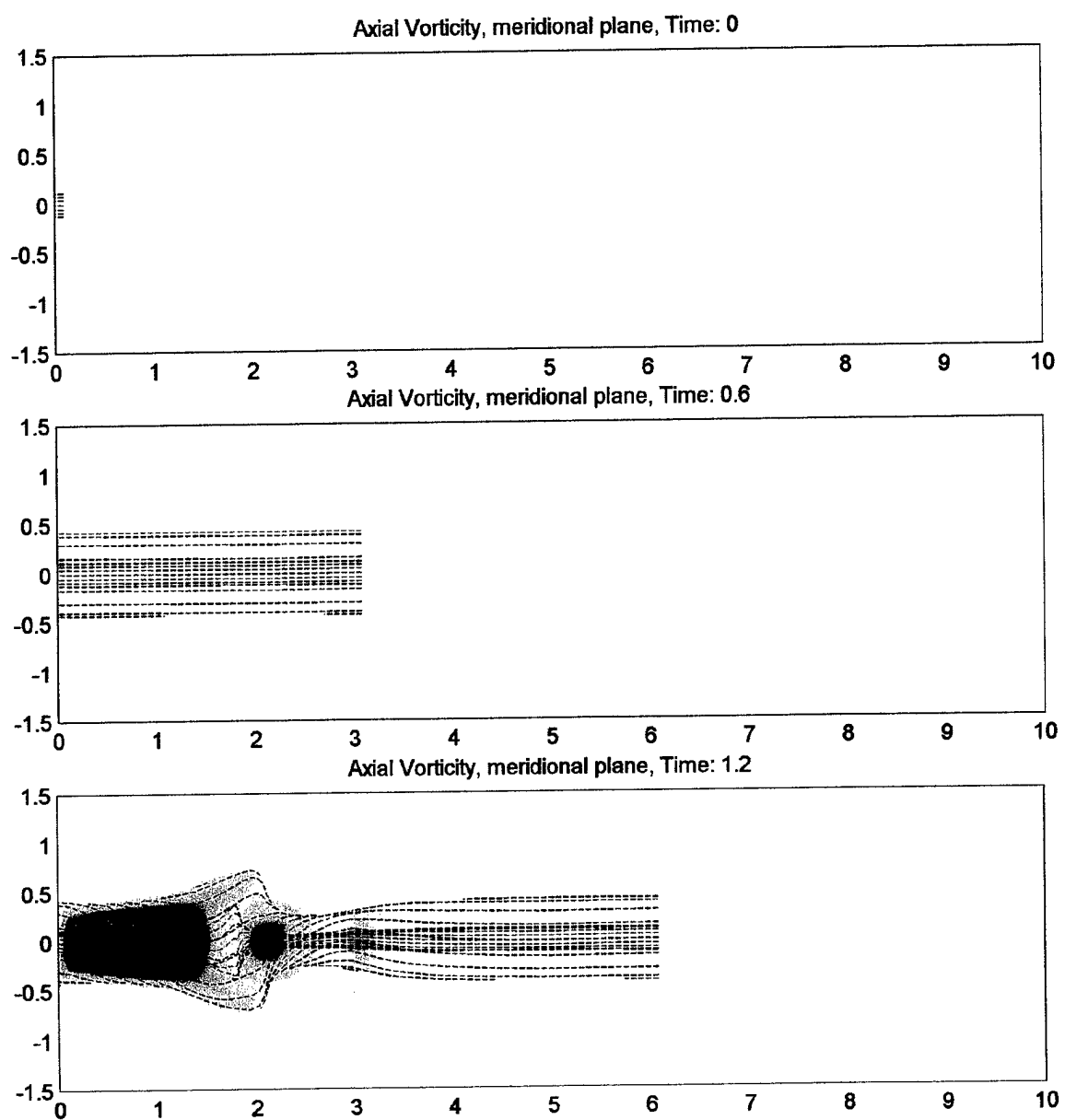


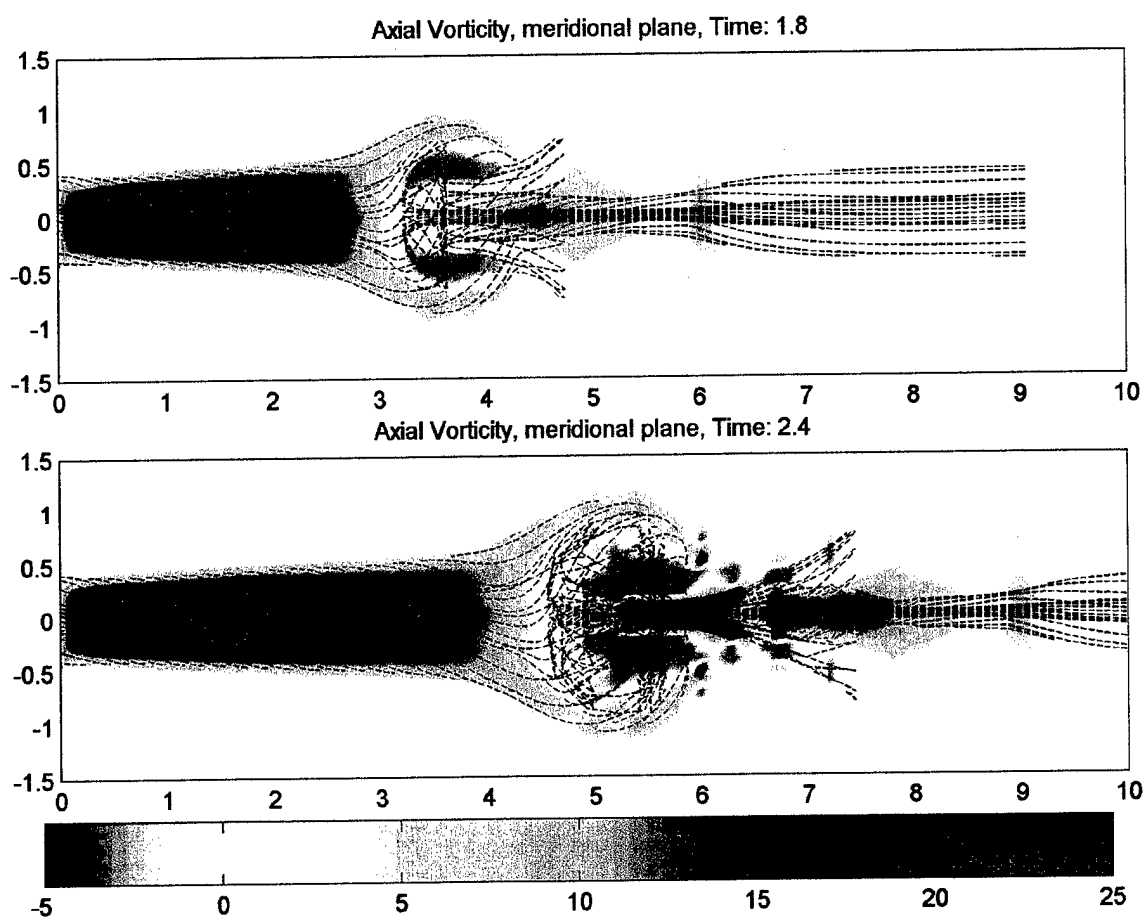
3.4.2.3 Color contour radial velocity plots



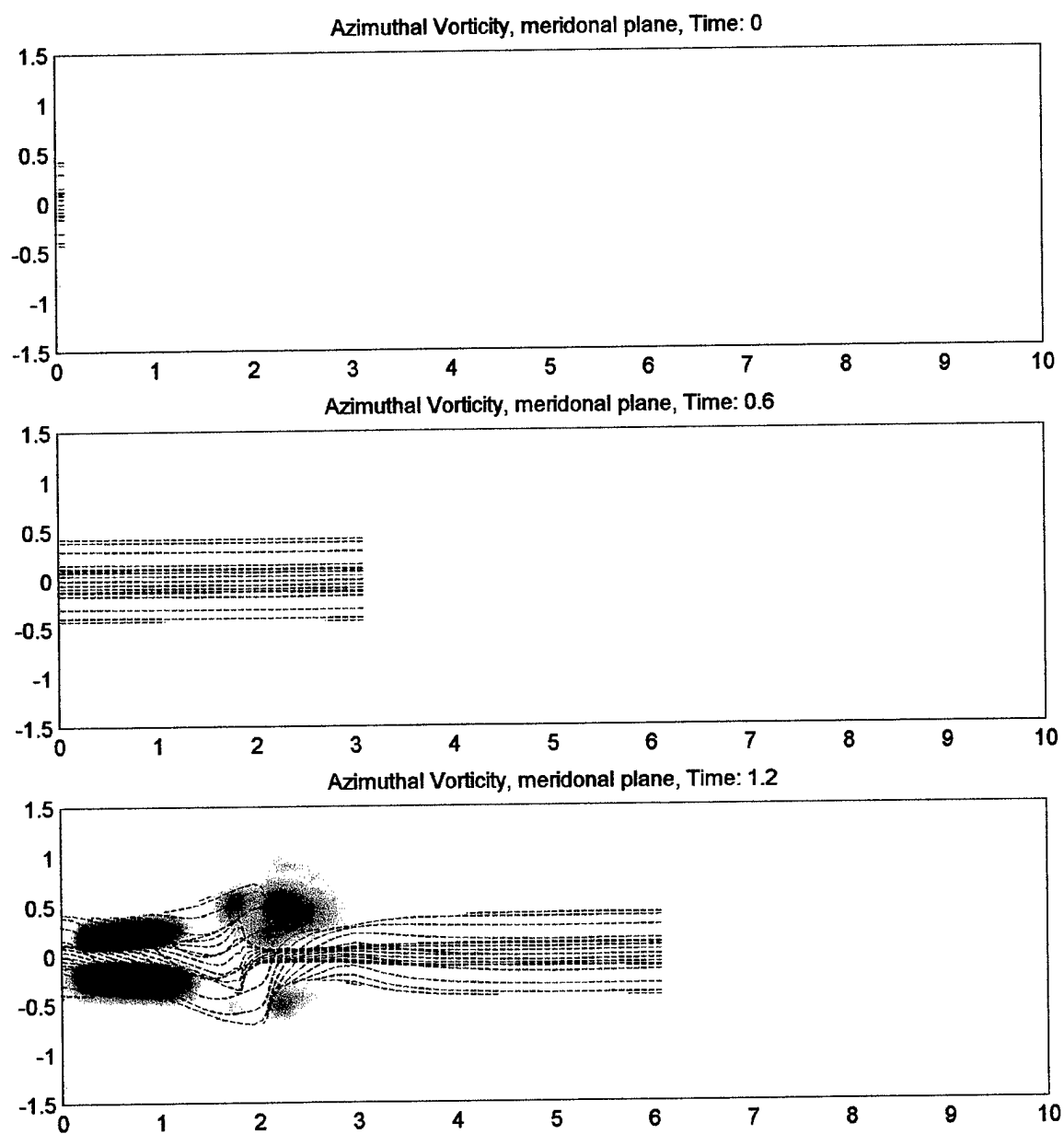


3.4.2.4 Color contour axial vorticity plots

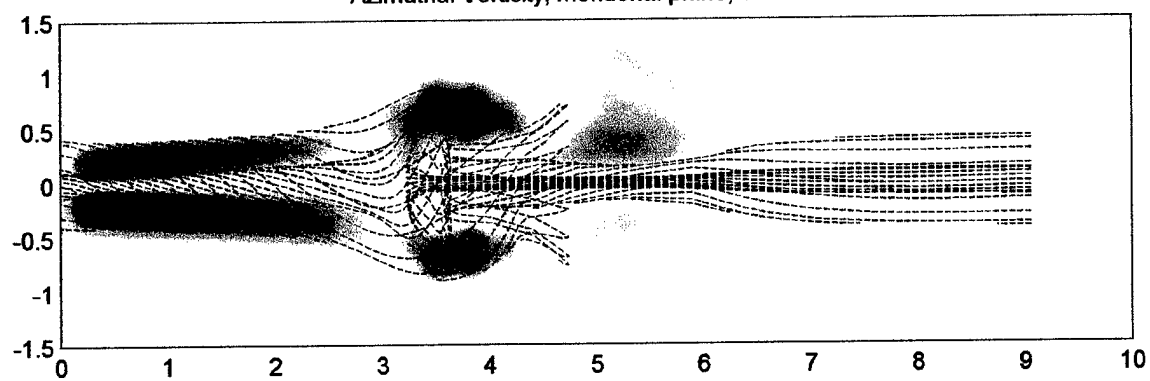




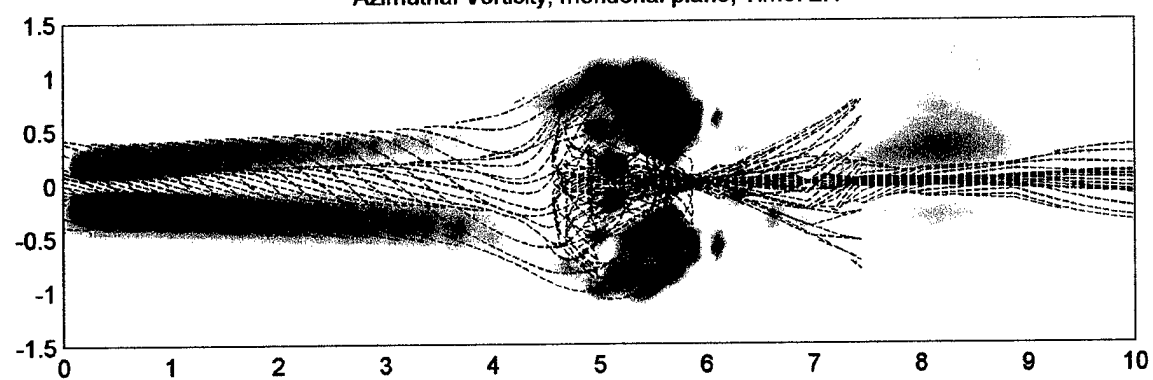
3.4.2.5 Color contour azimuthal vorticity plots



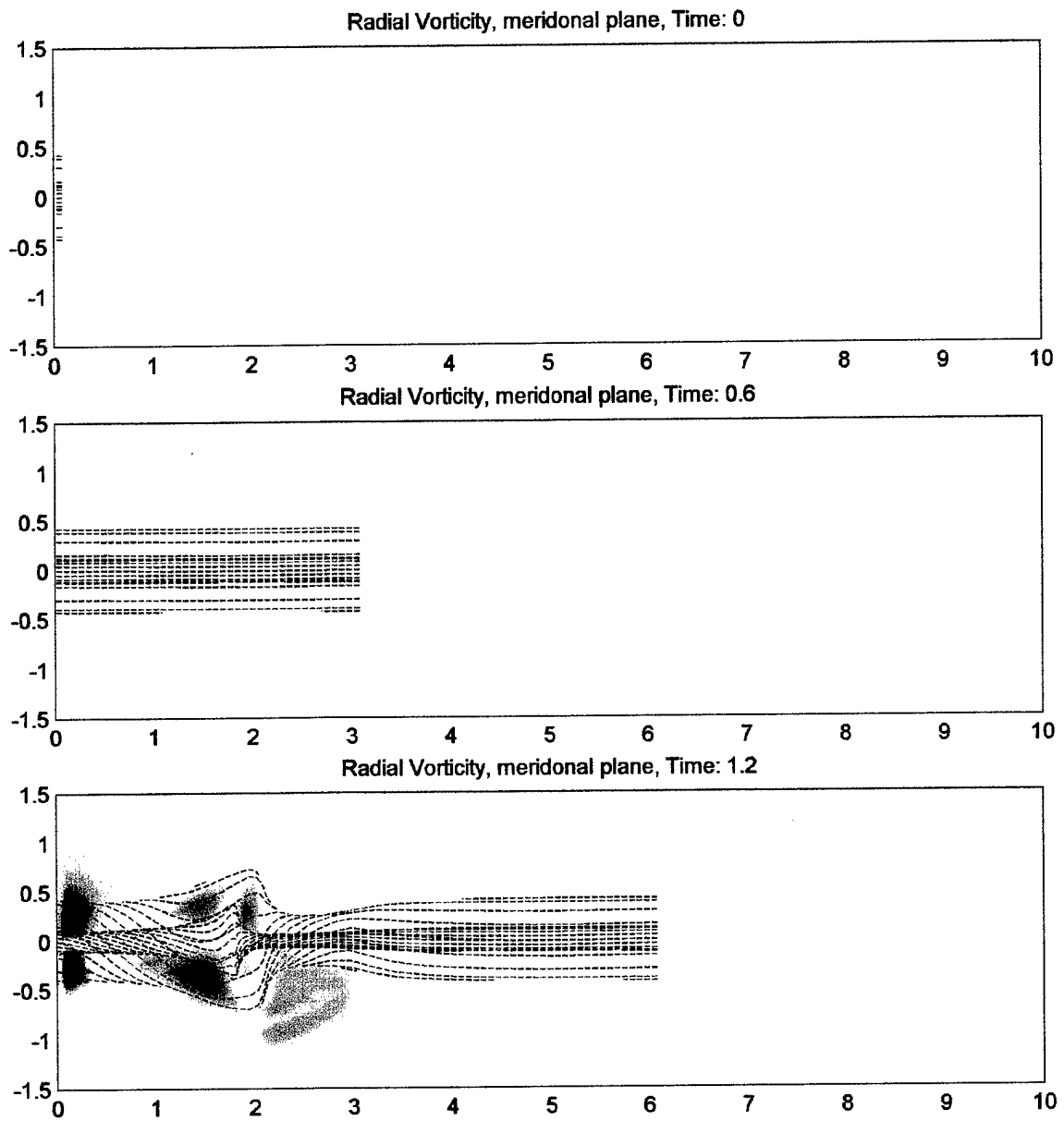
Azimuthal Vorticity, meridonal plane, Time: 1.8

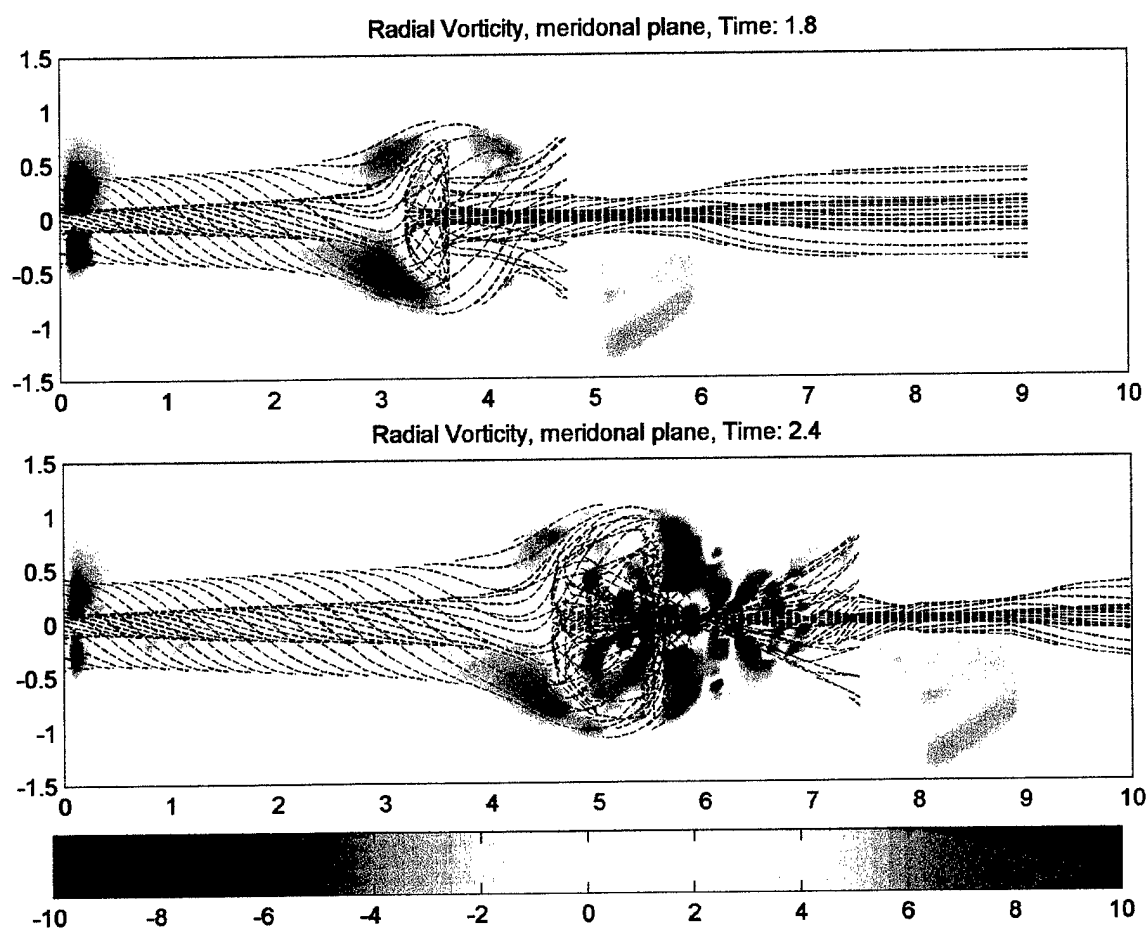


Azimuthal Vorticity, meridonal plane, Time: 2.4



3.4.2.6 Color contour radial vorticity plots





3.4.3 Streamline plot

Based on the meridional velocity data, we can construct a plot of the streamline at the meridional plane. The plot below shows the streamlines at $T = 2.4$. The main recirculation region is clear, but another area of radial expansion is beginning to form downstream of the main breakdown. While not as clear in the vortex filament plots, this secondary breakdown region is very clear in this streamline plot.

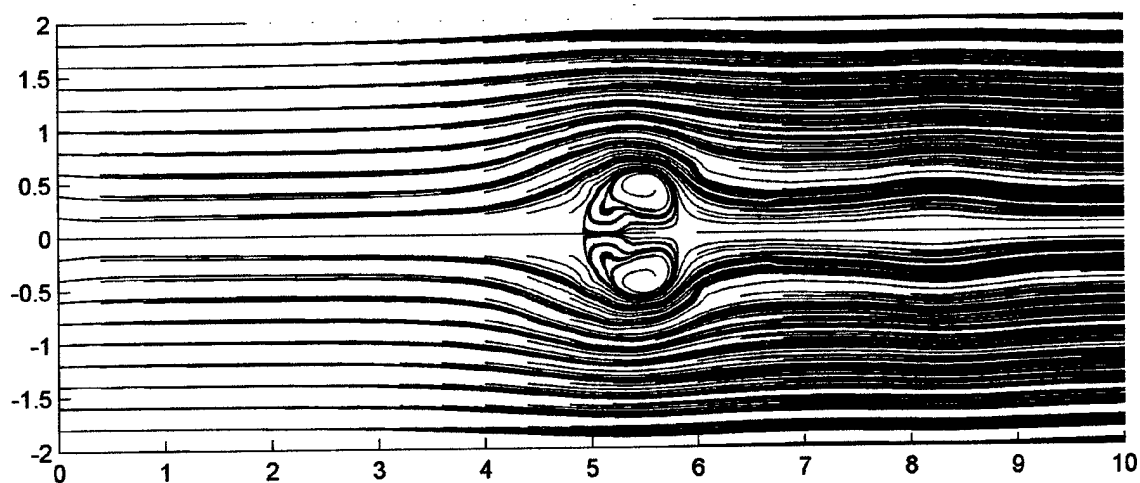
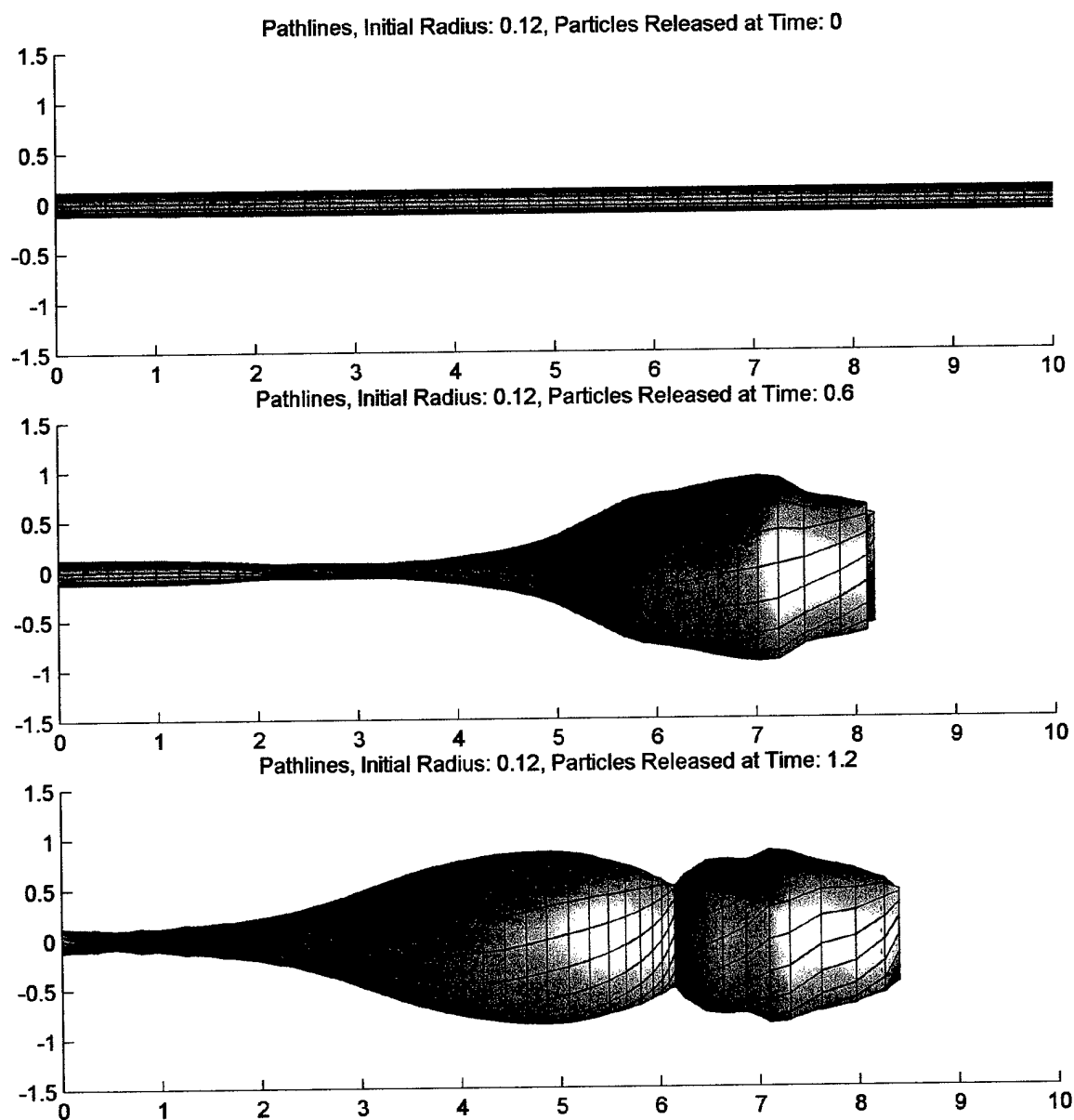


Figure 3-17 Streamlines, $T = 2.4$, meridional plane

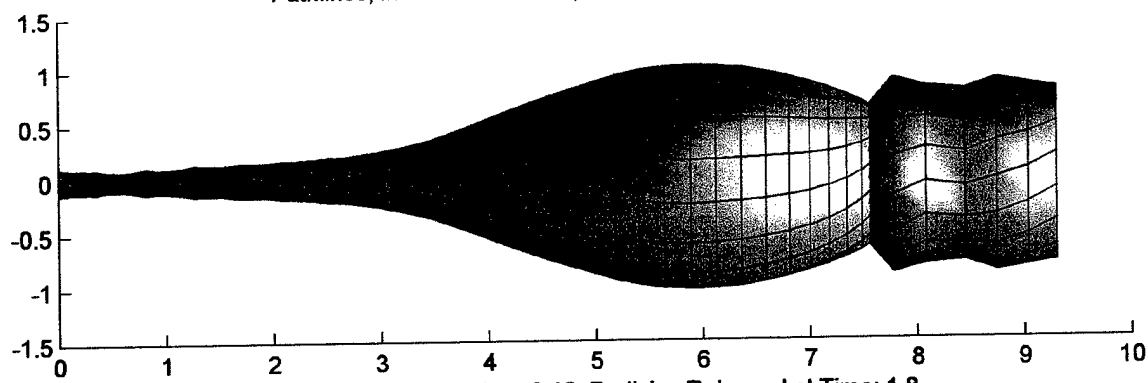
3.4.4 Case 1 pathlines, rendered

As was previously stated, with streaklines, very odd patterns can occur in the flow visualization, while the actual particle pathlines may appear very different. The following plots show the pathlines for Case 1, for particles released at the below stated radii and the stated time. In all cases, the final time is $T = 2.7$.

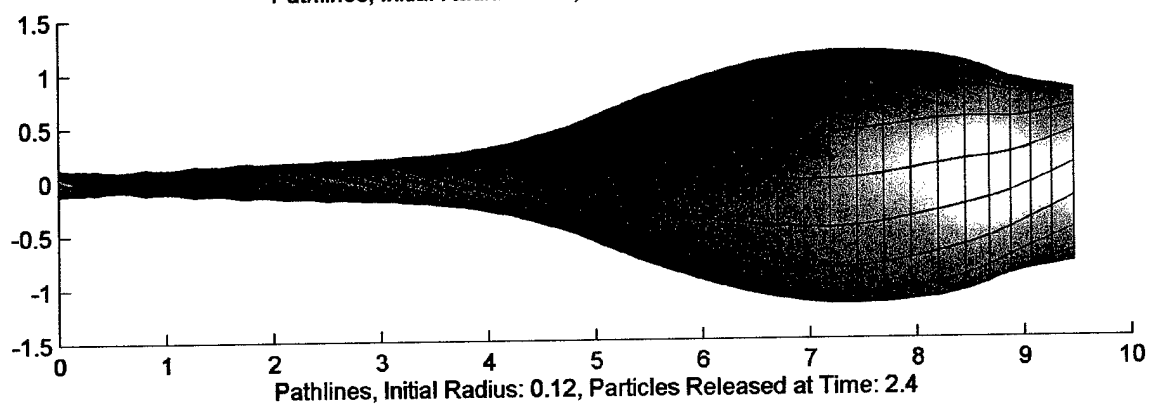
3.4.4.1 Pathlines, $r_{init} = 0.12$



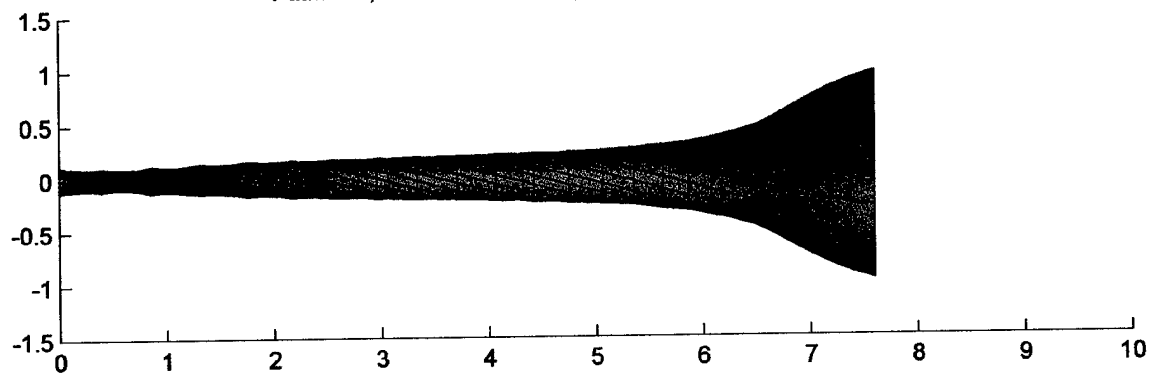
Pathlines, Initial Radius: 0.12, Particles Released at Time: 1.5



Pathlines, Initial Radius: 0.12, Particles Released at Time: 1.8

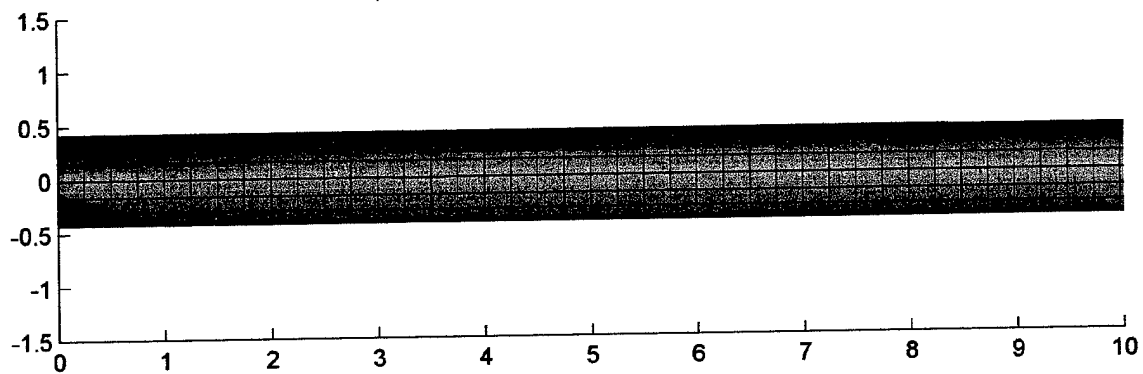


Pathlines, Initial Radius: 0.12, Particles Released at Time: 2.4

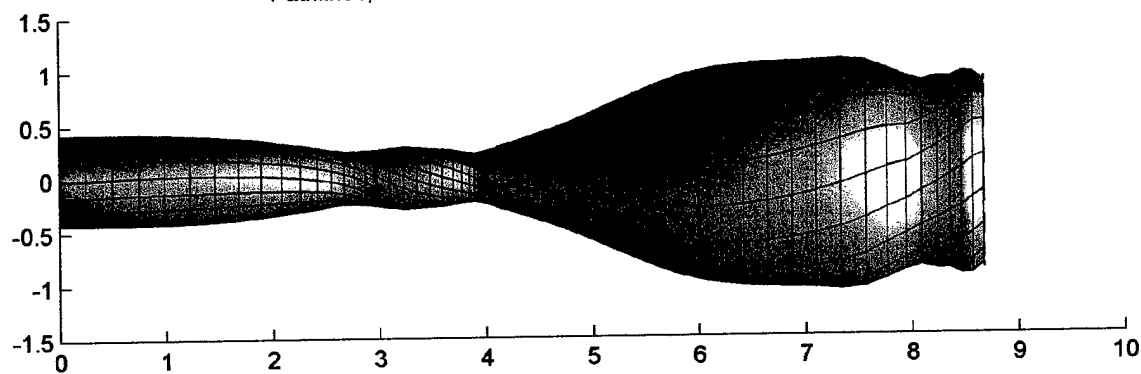


3.4.4.2 Pathlines, $r_{init} = 0.42$

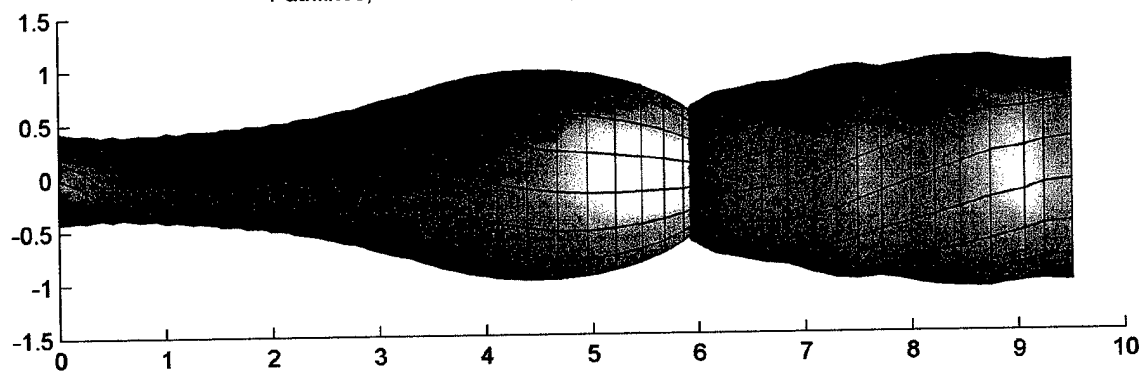
Pathlines, Initial Radius: 0.42, Particles Released at Time: 0



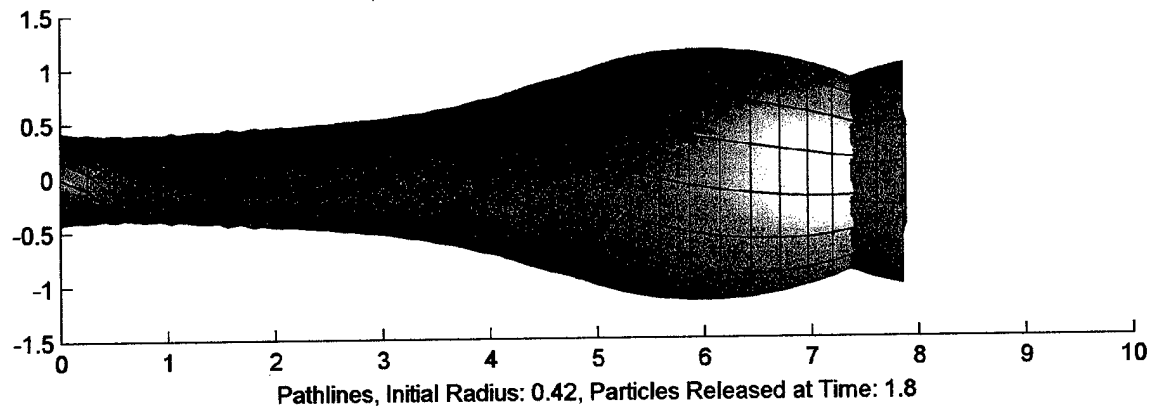
Pathlines, Initial Radius: 0.42, Particles Released at Time: 0.6



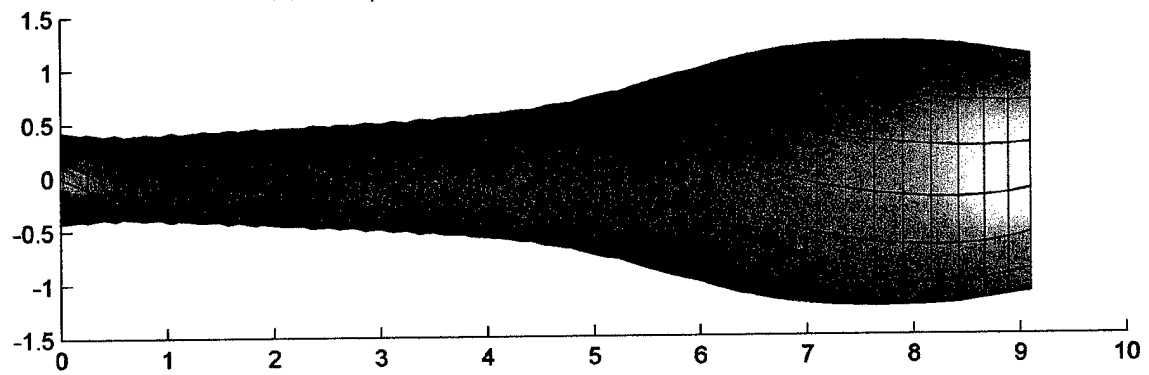
Pathlines, Initial Radius: 0.42, Particles Released at Time: 1.2



Pathlines, Initial Radius: 0.42, Particles Released at Time: 1.5

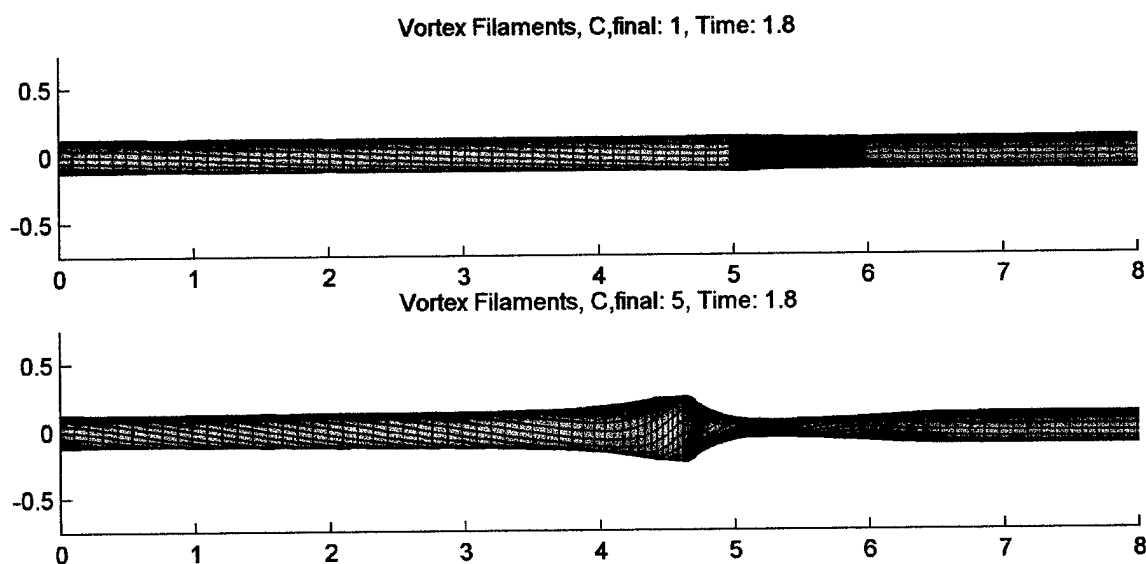


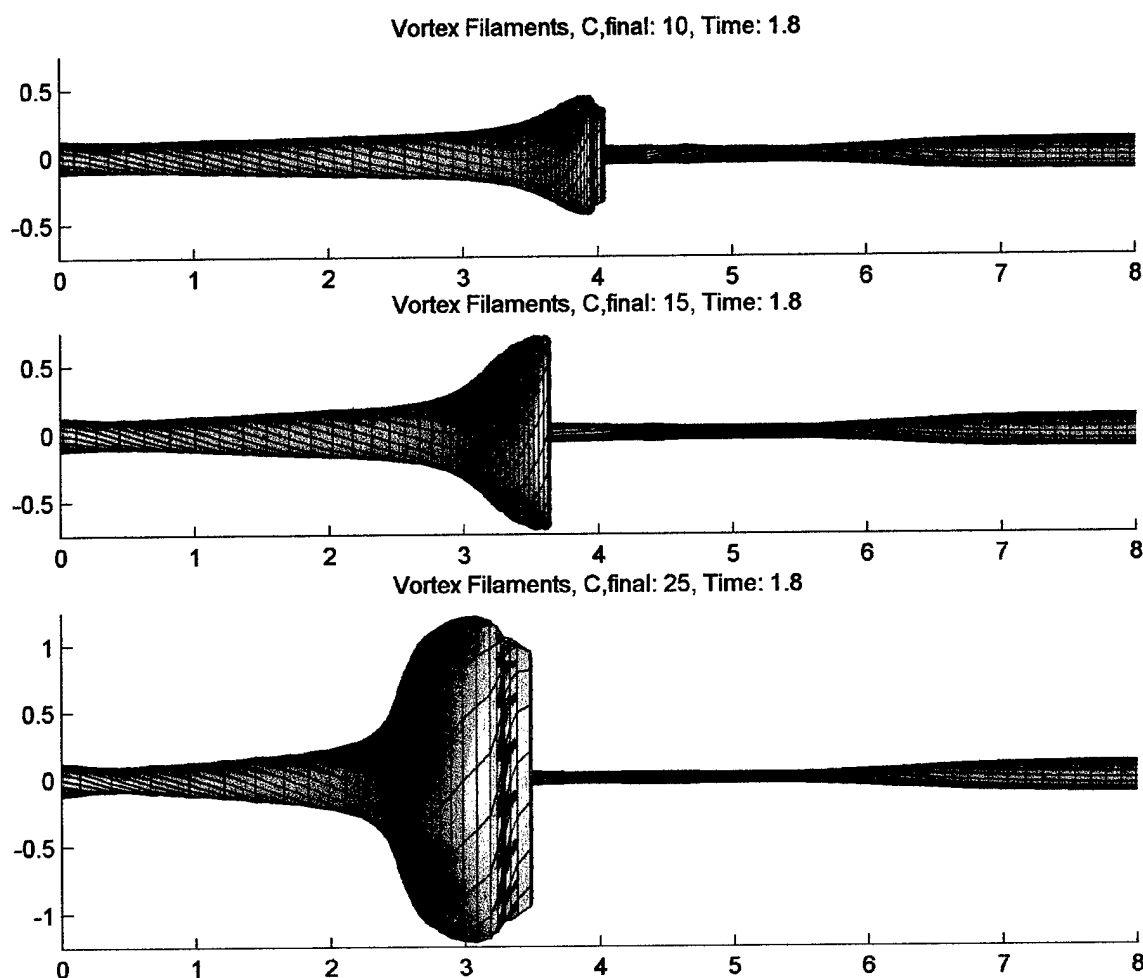
Pathlines, Initial Radius: 0.42, Particles Released at Time: 1.8



3.5 Other Cases, Vary C_{final}

The following results show how the output changes when the final circulation (see Figure 3-16), and hence the strength of the vorticity gradient, varies from $C = 1$ to $C = 25$. The results are presented at $T = 1.8$. The initial circulation remain $C = 0.1$. It is clear from these results, that the higher the final circulation, the sooner the characteristics of vortex breakdown develop. This points to some type of criteria involving the strength of the vorticity gradient whether vortex breakdown will develop over a wing or not. If the critical factor in vortex breakdown is the formation of the turning point (the turning point is where the vortex filaments turn inward on themselves, see section 4.4.4 for details), then we can say the following. If, for a given negative vorticity gradient in a vortex tube, the turning point forms at $T = T_{tp}$, then if T_{tp} is greater than the time for the region of that vorticity gradient to convect downstream over the surface of the wing, then a steady, sustained vortex tube will not develop. Conversely, if T_{tp} is less than the time it takes for the region of the vorticity gradient to convect downstream of the wing surface, there will be a steady, sustained vortex breakdown over that wing. Other factors such as a velocity gradient and the vortex sheet that constrains the vortex core would also need to be taken into account to elaborate fuller on this idea.





3.6 Model Optimization

The simulation is optimized by varying such factors as the number of vortex filaments, the spacing between vortex filament nodes, the time step in the simulation, and the location of the vorticity gradient with respect to the numerical end of the vortex. A balance must be made in terms of resolution of the model and numerical efficiency.

The number of filaments in the simulation are chosen to provide an initial vorticity profile that very nearly matches the ideal Gaussian distribution, while at the same time being practical to implement in terms of computational time. Reference section 2.4.1.3 for a discussion on the distribution of vorticity. In terms of balancing the simulation resolutions with simulation runtime, the optimum value number of filaments is

sixteen (16) vortex filaments evenly distributed about the circumference of nine (9) radial sleeves of vorticity. Thus, in results presented here, the vortex tube is discretized into 144 vortex filaments.

Next the length of the vortex filament segment is optimized. Again, while we would like the segment length to be as small as possible, processing constraints require a trade off between small segment length and simulation run time. Figure 3-18 shows the axial velocity along the vortex tube centerline at $T = 1.8$ for various vortex filament segment lengths, dz . With a vortex segment length of $dz = 0.05$, the simulation run time is objectionable, with current processing power. Therefore, $dz = 0.1$ is used in the results presented in the previous sections. With $dz = 0.1$, the simulation exhibits the characteristics of $dz = 0.05$, while maintaining a practical simulation run-time. For $dz = 0.2$, the results do not compare well with the $dz = 0.05$, so this vortex segment length is not used. Therefore, while the simulation exhibits qualitative convergence, in terms of solution characteristics, it does not exhibit quantitative convergence. That is the main reason why results are discussed and compared in terms of their quality and not the exact numerical quantity.

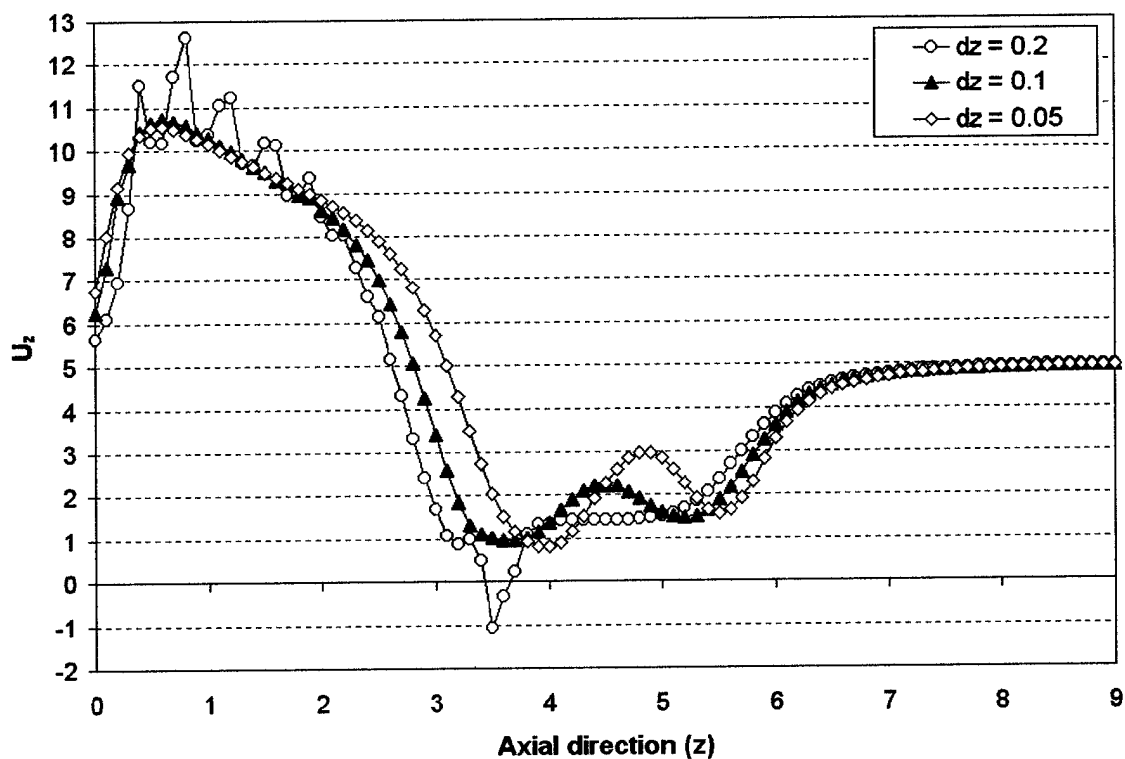


Figure 3-18 Simulation optimization, centerline, axial velocity, vary dz , $T = 1.8$

We can see this qualitative similarity by comparing at the vortex filament plot for these cases. Figure 3-19 shows these results for $dz = 0.2$, 0.1 , and 0.05 .

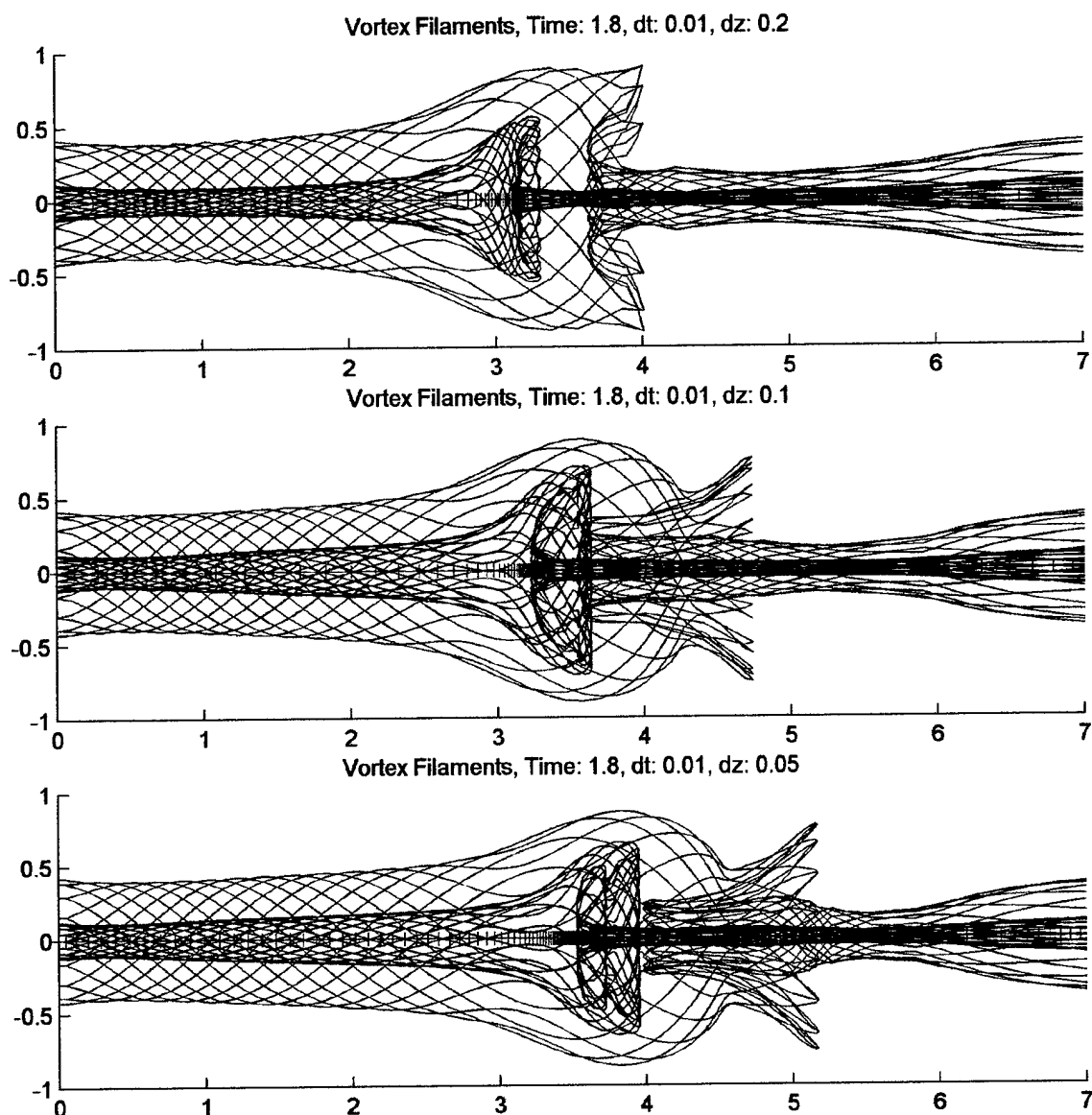


Figure 3-19 Vortex filament simulation results, vary vortex filament segment length, dz

The same optimization process is done with the simulation time step. Figure 3-20 shows the centerline axial velocity with the time step, dt , varying from 0.1 to 0.001 at $T = 1.8$. Again, to achieve a balance between run-time and accuracy, a reasonably small time step is chosen. This reasonable time step is one that has the general characteristics of results at smaller time steps, while being computational efficient. Thus, for this

simulation, we choose $dt = 0.01$. If we compare the vortex filament plots that results for using these various time steps, we can see that $dt = 0.01$ is a reasonable choice.

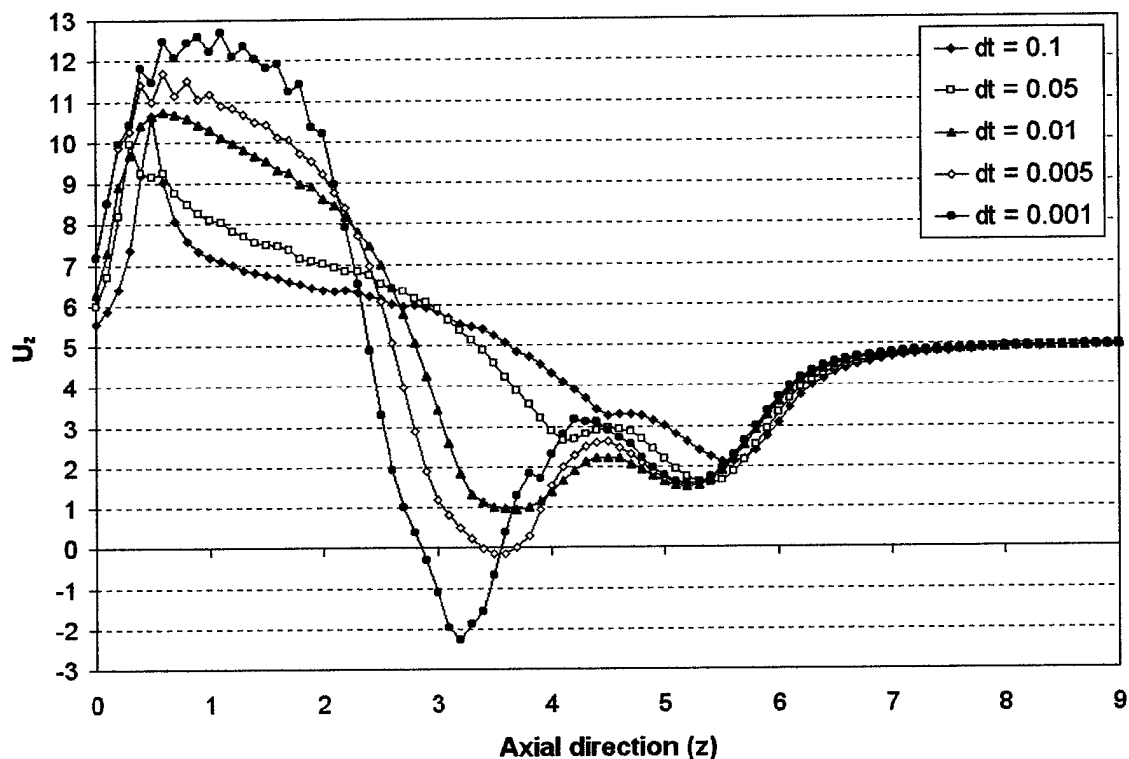
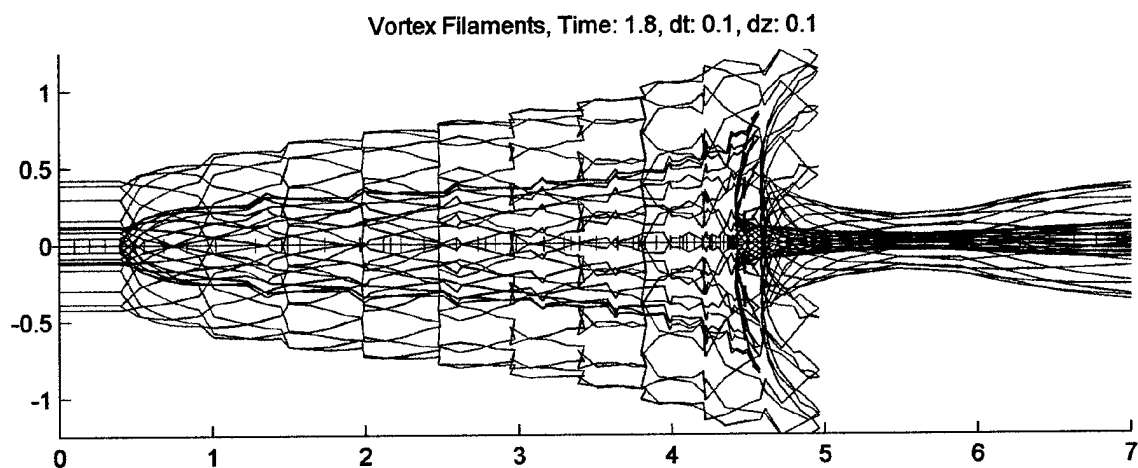
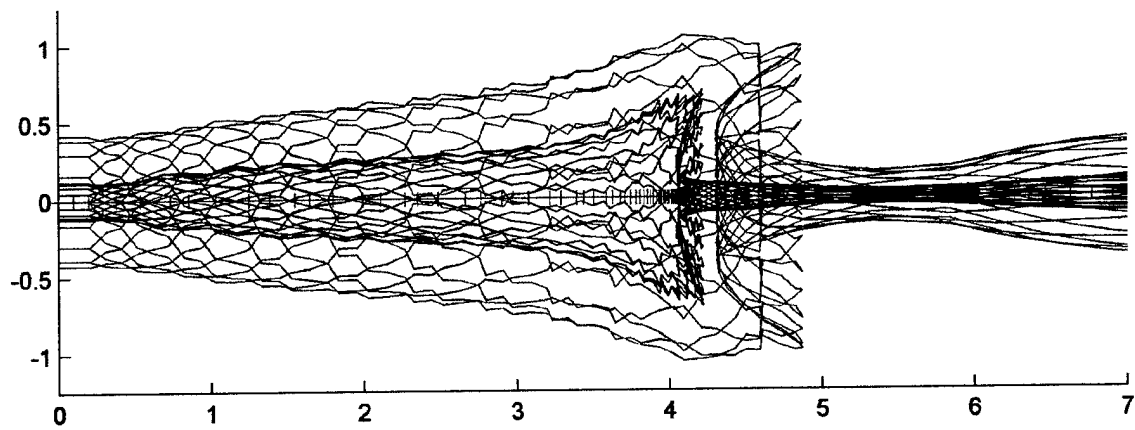


Figure 3-20 Simulation optimization, centerline axial velocity, vary dt , $T = 1.8$

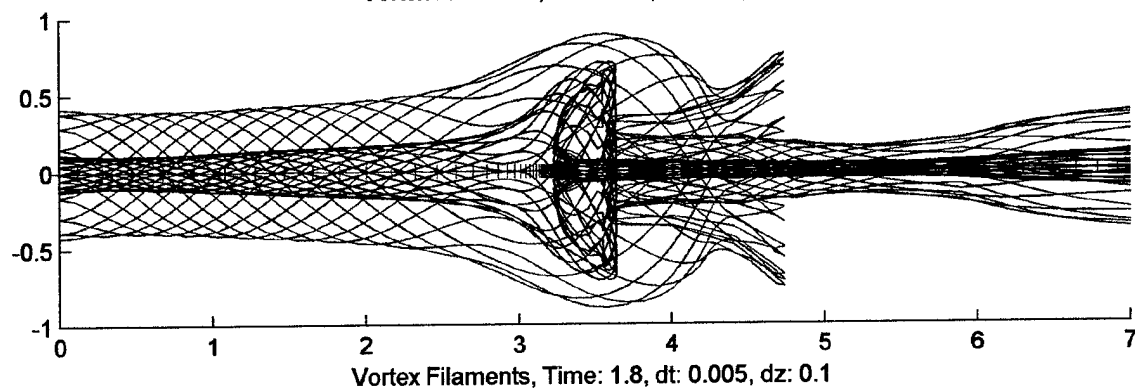
Figure 3-21 shows the vortex filaments at $T = 1.8$ for the various time steps. Clearly, when $dt = 0.01$, the results take on the characteristics of the results with smaller time step.



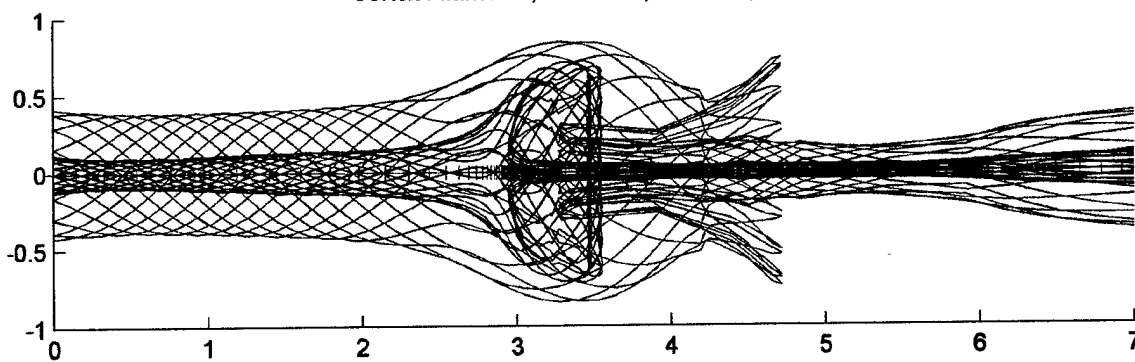
Vortex Filaments, Time: 1.8, dt: 0.05, dz: 0.1



Vortex Filaments, Time: 1.8, dt: 0.01, dz: 0.1



Vortex Filaments, Time: 1.8, dt: 0.005, dz: 0.1



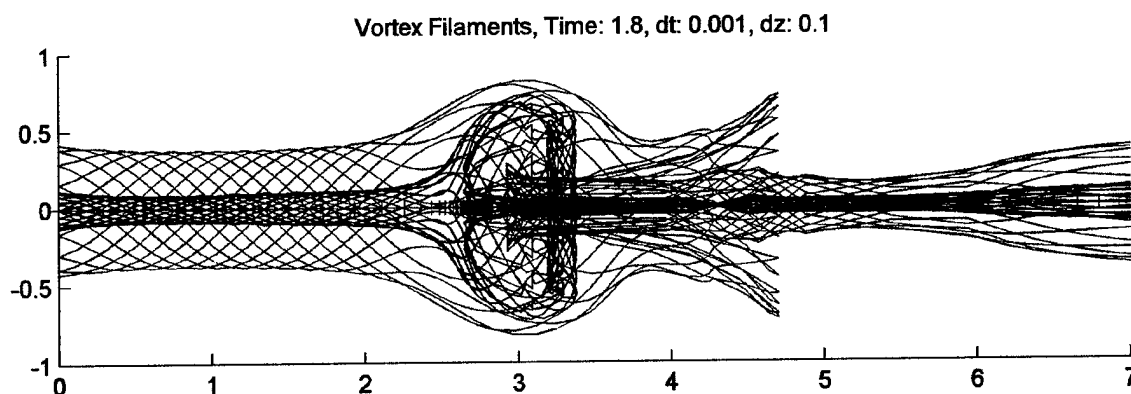


Figure 3-21 Vortex filament simulation results, vary simulation time step, dt

Another thing that is optimized is the location of the end of the vortex tube.

Theoretically, the vortex tube extends downstream to infinity. Numerically, it must have some finite length. However, we want the vortex tube to end far enough downstream that that end has a negligible effect on the results. The area of interest is the vorticity gradient region, thus the end of the vortex tube is measured from the beginning of that region.

Figure 3-22 shows the velocity along the centerline of the vortex tube when the end of the vortex tube is three and six length units from the beginning of the vorticity gradient.

There is virtually no change in the result when the length to the numerical end of the vortex tube is doubled, so it is reasonable to use a length of three. This balances the need to have a virtually infinite tube, with the need for reasonable computational times. Thus, in the results previously presented, the end of the vortex tube is three length units from the beginning of the vorticity gradient region. In temporal terms, with a freestream velocity of five length units/time units, the vorticity gradient does not start until 0.6 time units.

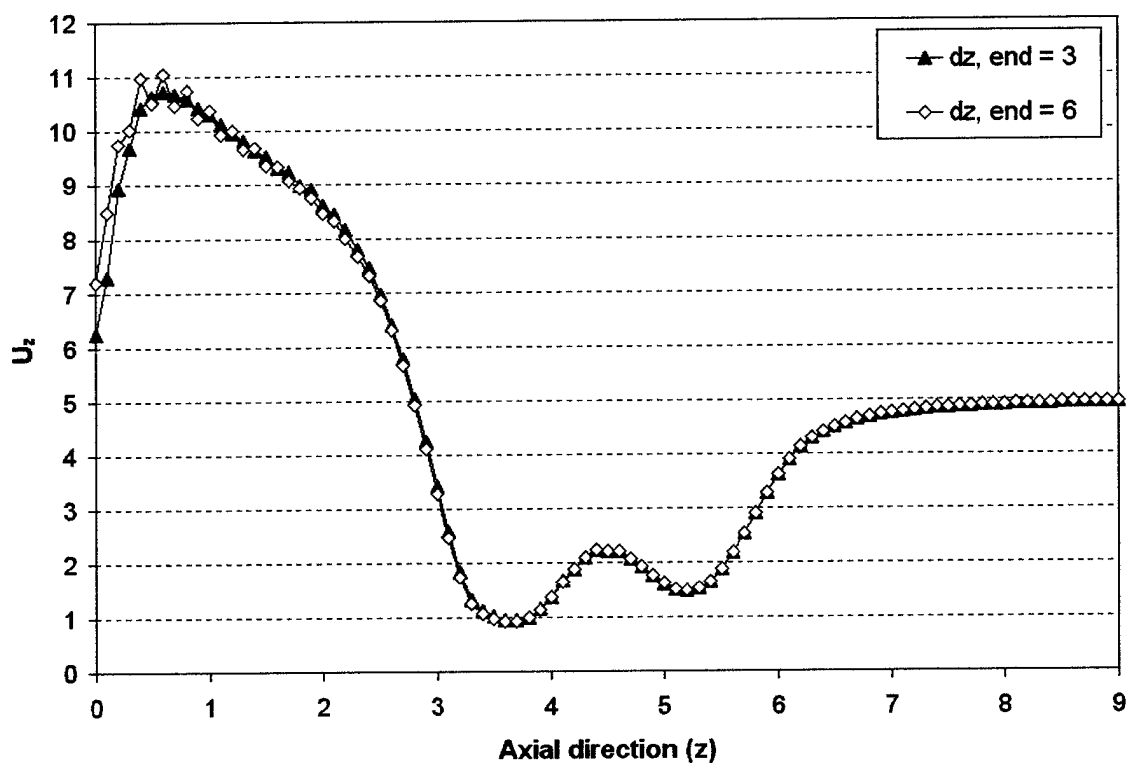


Figure 3-22 Simulation optimization, vortex tube end location, $T = 1.8$

4. Self-induction theory of vortex breakdown

The vortex filament method, as presented in the previous section, indicates vortex breakdown behavior in the vortex tube. The only mechanism involved in that model is the initial vorticity gradient and the ensuing self-induction of the vortex tube. Thus, we can say that, if the vortex filament model captures vortex breakdown, the cause of the vortex breakdown is a vorticity gradient and the mechanism is self-induction. With this self-induction theory, we can look specifically at the steps that lead to vortex breakdown. Once we understand these steps, we can better understand the best ways to prevent, delay, or weaken vortex breakdown.

4.1 Difference from previous theories

Much work has been done on vortex breakdown. Many of these ideas focus on the shock-like nature of vortex breakdown, with many people making the analogy between vortex breakdown and a hydraulic jump. Benjamin, Keller, Escudier, Saffman, and others have done much exceptional work along this line of study. We do not disagree with these theories. In fact, if you look at many of the later time results in the vortex filament simulation, you can see many shock-like behaviors. For example, you will see a sudden change in axial velocity down the centerline of the vortex tube. Also, you can see sudden changes in the sign of the vorticity. However, our model does not model the wave effects necessary to generate shock like behavior. Instead, we are modeling the unsteady initial formation of vortex breakdown. Thus, once a steady state breakdown is achieved, modeling the vortex breakdown as shock or hydraulic jump is likely a very good model. However, that simplification tells you little about the actual formation of that hydraulic jump. For that, we find that the inviscid self-induction theory provides many insights not previously available. Thus, we do not seek to supersede existing vortex breakdown theory; we merely bridge the gap during the time of vortex breakdown formation and the steady state vortex breakdown. This would be analogous to studying a steady shock wave with simple shock relationships versus studying the unsteady, and more complicated transient formation of that shock wave.

4.2 Assumptions

If we still achieve vortex breakdown after excluding certain physical elements from the model, we can say with a reasonable amount of certainty that those physical mechanisms are not necessary for the formation of vortex breakdown. In this case, we are limited by the assumptions implicit in the vortex filament method. Since we still achieve vortex breakdown behavior, we can say that the physical mechanisms present in the vortex filament method are the ones important to the vortex breakdown mechanism. In the vortex filament method, we have assumed unsteady, incompressible, inviscid flow. The motion of the vortex tube is determined by its vorticity distribution and the induction of the vortex tube on itself.

4.3 Initial cause of breakdown

It is clear from the results that the initiator of vortex breakdown is a negative vorticity gradient. That is, the vorticity in a vortex tube is greater upstream than downstream. That vorticity gradient will be in the axial and azimuthal components of vorticity, though any axial vorticity gradient will cause an azimuthal vorticity gradient, as Figure 4-1 shows. In Figure 4-1 we see that the axial vorticity will induce azimuthal velocities in the vortex tube. These azimuthal velocities will twist the vortex filaments. Because the vorticity vector is always aligned with these vortex filaments, the twisting of the vortex filaments results in a component of vorticity in the azimuthal direction. The effect of this is that the vortex tube develops whatever helical angle is most "natural" to the initial distribution of axial vorticity. It does this through self-induction.

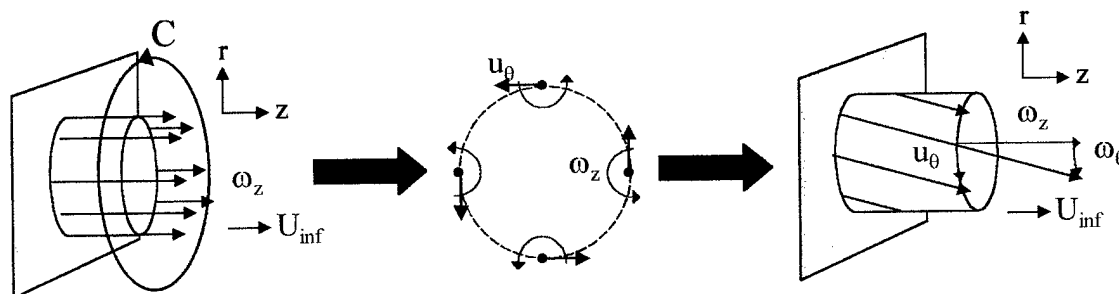


Figure 4-1 Creating Azimuthal Vorticity

It seems clear that the vorticity gradient is the prime factor in initiating the vortex breakdown. However, we can take it a step further and ask, what causes the vorticity gradient? If the cause of vortex breakdown is self-induction of a vortex tube associated with a negative vorticity gradient, then it may be that this negative vorticity gradient can be caused in more than one way. Still, the negative vorticity gradient is the most important initiator of vortex breakdown.

4.3.1 Circulation gradient

In the vortex filament method results we have shown, the vorticity gradient is caused by a circulation gradient. Vortex filaments are linear superimposed, and turn outward at the appropriate axial location to preserve solenoidality. The result is that the upstream region of vortex filaments has more vorticity than the downstream regions. This creates the vorticity gradient that leads to vortex breakdown. In physical situations, this would be equivalent to a pitch up and hold maneuver over a delta wing. It would also be equivalent to an increase in velocity over a delta wing at a fixed angle of attack, since the increased velocity causes increased circulation. In a vortex generated in a tube, this would be equivalent to an increase in pitch of the swirl vanes. This type of vorticity gradient is the most clear and straightforward one to model with the vortex filament method. That is why we limit our test cases to this type vorticity gradient initiator.

4.3.2 Velocity gradient

Over strakes and delta wing aircraft, one can think of another way to achieve this a vorticity gradient without an explicitly defined circulation gradient. This involves the change in vorticity associated with stretching and contraction (the opposite of stretching) in a vortex tube with fixed circulation. Over a two-dimensional wing, there is a peak negative pressure occurring on the upper surface near the leading edge of the airfoil. From this peak, the pressure increases to the trailing edge of the airfoil, with positive pressure occurring at the trailing edge. Figure 4-2 shows an example of this from a classical and numerical solution for the pressure coefficient over a NACA 0012 airfoil at 9 degrees angle of attack. What we have is a positive pressure gradient (in terms of the

absolute value of the pressure coefficient). If we are dealing with incompressible or nearly incompressible flows, we can talk equivalently about velocity, since the pressure coefficient is defined by equation (1-55).

$$C_p = 1 - \left(\frac{U}{U_\infty} \right)^2 \quad (4-1)$$

So if we have a positive pressure gradient, we also have a negative velocity gradient. Thus, if you were to place a vortex tube in the pressure field, it would see a velocity that decreases along the downstream axial direction of the vortex tube. Figure 4-2 shows the velocity that the vortex tube sees downstream of the negative pressure peak.

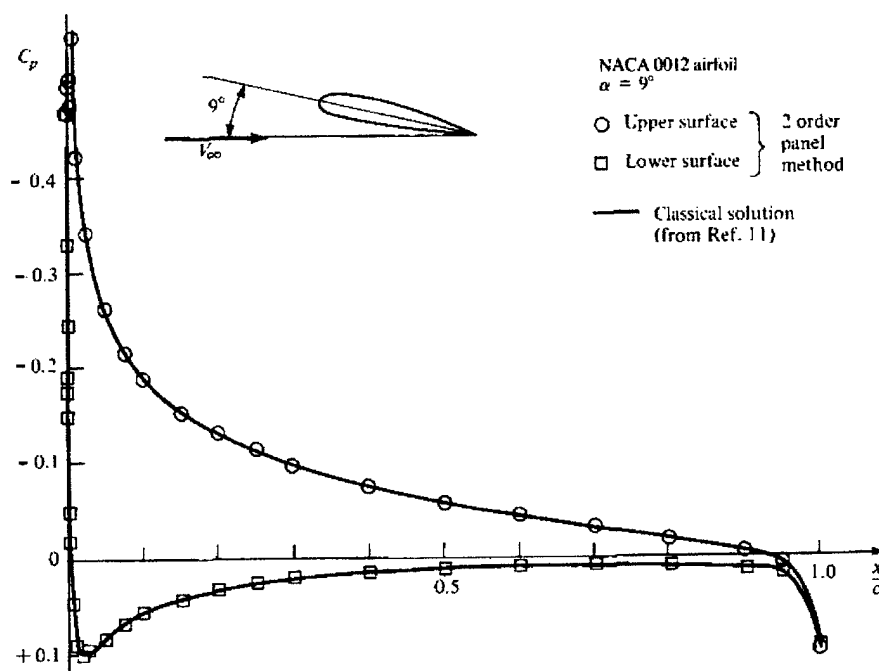


Figure 4-2 Pressure distribution over NACA 0012 airfoil (ref. 3)

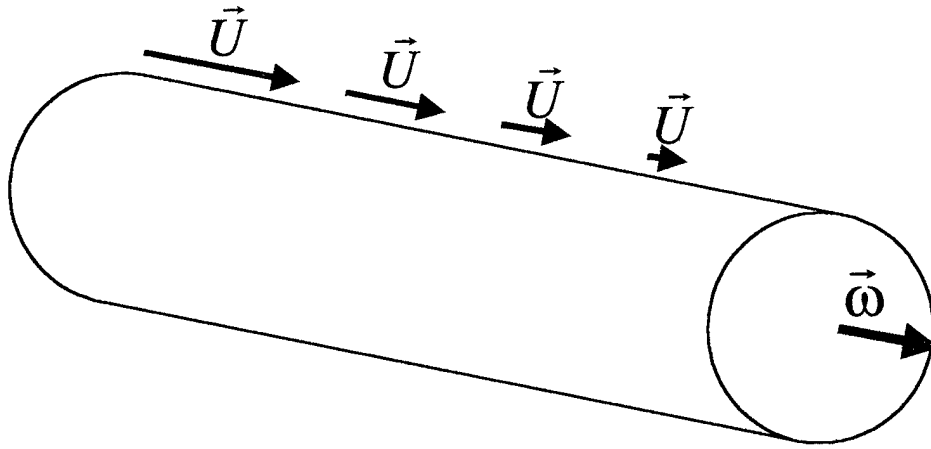


Figure 4-3 Vortex tube in negative velocity gradient

This negative velocity gradient will affect the vorticity in a vortex tube in terms of stretching. The vorticity equation defines this interaction, as in equation (4-2). We will only take the stretching term into account and if we will assume velocity and vorticity only change in the axial direction (z -direction). Also, we will assume that the velocity is constant, while the vorticity can change in time. If we do this we get the expression in equation (4-3).

$$\frac{D\vec{\omega}(t)}{Dt} = (\vec{\omega}(t) \cdot \vec{\nabla})\vec{u} \quad (4-2)$$

$$\frac{\partial \omega_z(t)}{\partial t} + u(z) \frac{\partial \omega_z(t)}{\partial z} = \omega_z(t) \frac{\partial u(z)}{\partial z} \quad (4-3)$$

If we were looking at a steady state case, the time changing term would drop out, and we would have equation (4-4).

$$u(z) \frac{\partial \omega_z}{\partial z} = \omega_z \frac{\partial u(z)}{\partial z} \quad (4-4)$$

If we assume that $u(z)$ and $\omega_z(t)$ remain the same sign (aligned in the axial direction), we can very easily see that the $\frac{\partial \omega_z(t)}{\partial z}$ and $\frac{\partial u(z)}{\partial z}$ terms will have to be the same sign. If the positive z -direction is to the right (downstream), then a negative velocity gradient will cause the vortex tube to have a negative vorticity gradient. This is similar to the

argument that M.J. Lighthill introduces and Whitman derives when they show that vorticity vectors not only move with the fluid elements, but are proportional to the length of the line element, $\delta \vec{l}$ (*ref. 23*). Therefore, $\vec{\omega} = c \cdot \delta \vec{l}$, so if velocity changes along the wing, the length of line element, $\delta \vec{l}$, will change, as will the magnitude of the vorticity vector. Thus, it is clear that the velocity profile above wing associated with an adverse pressure gradient is sufficient to cause a vorticity gradient in a vortex tube. With that vorticity gradient, this vortex tube can cause itself to breakdown through the self-induction mechanism.

4.4 Self-induced feedback mechanism

If a vortex tube causes itself to breakdown, what steps does it take to do so? Others have proposed various feedback mechanisms for vortex breakdown (*ref. 20*), but we will approach it from a self-induction perspective, with the starting point being the vorticity gradient, however it is brought about. With this, we have the following feedback mechanism that causes vortex breakdown. Using the results from the vortex filament simulation, we will explain each part of this diagram in this section.

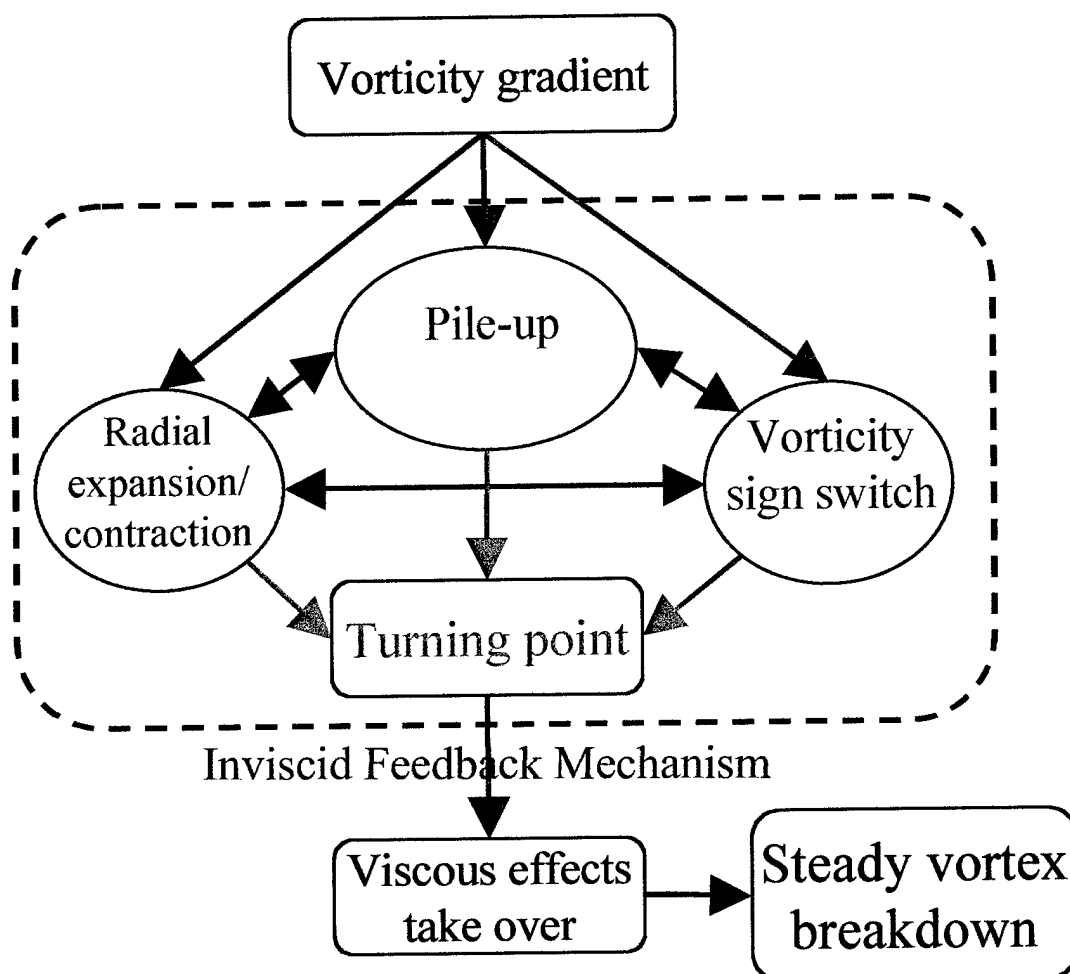


Figure 4-4 Self-Induced, inviscid feedback mechanism of vortex breakdown

4.4.1 Radial expansion

As shown in previous sections, an axial vorticity gradient will lead to an azimuthal vorticity gradient. If we look at a cross section of a vortex tube in the region of an azimuthal vorticity gradient, we will see what is illustrated in Figure 4-5. The red circles indicate azimuthal vorticity, ω_θ , out of the plane. The blue crosses indicate azimuthal vorticity into the plane. Their arced arrows show the individual induced velocities. The black arrows show the net induced radial velocity along the vortex tube. The azimuthal vorticity increases in the upstream direction to the left. In this situation, we can see that the induced radial velocity is greater downstream than upstream.

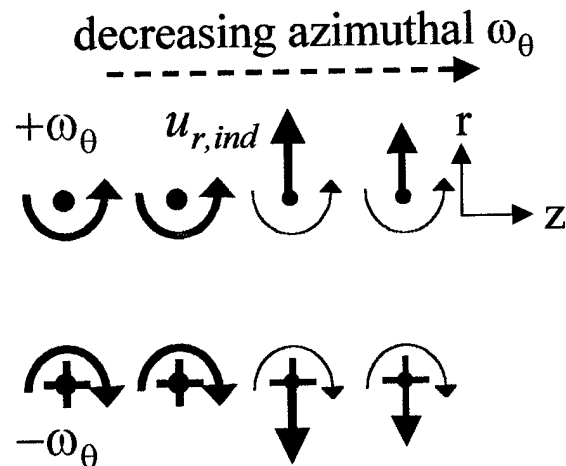


Figure 4-5 Radial expansion

This becomes clearer if we look at the induced radial velocities in more detail. Figure 4-6 shows an expanded diagram of a cross section of the vortex tube in the region of the vorticity gradient. We will represent the azimuthal vorticity component as 2-D potential vortices, with each vortex spaced a distance, d , apart. The strength of the vorticity is Γ_j . In this simplified, 2-D case, the induced velocity from one vortex on

another vortex is $u_j = \frac{\Gamma_k}{2\pi \cdot r}$.

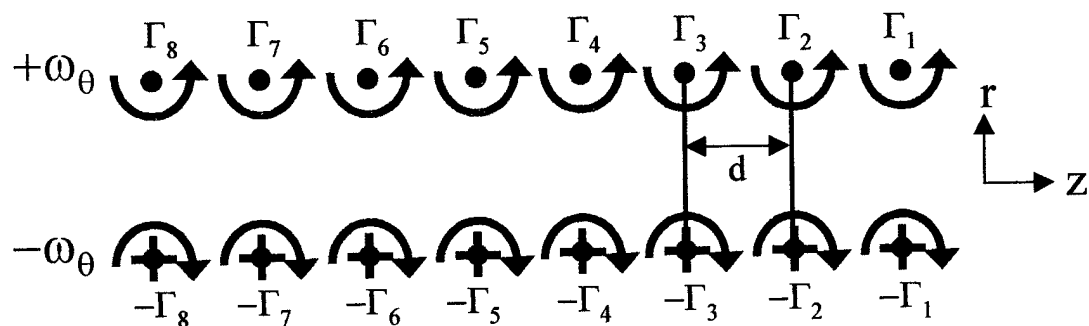


Figure 4-6 Azimuthal vorticity in meridional plane

The vorticity gradient can be represented by increasing Γ to the left. Table 4-1 shows the induced radial velocities associated with this setup.

Table 4-1 Induced radial velocities

Vorticity	Induced Radial Velocity
$\Gamma_1 = \Gamma_1$	$u_{r,1} = \frac{1}{2\pi} \left[\frac{\Gamma_2}{d} + \frac{\Gamma_3}{2d} + \frac{\Gamma_4}{3d} + \frac{\Gamma_5}{4d} + \frac{\Gamma_6}{5d} + \frac{\Gamma_7}{6d} + \frac{\Gamma_8}{7d} \right] = \frac{\Gamma_1}{3.27 \cdot \pi \cdot d}$
$\Gamma_2 = \Gamma_1$	$u_{r,2} = \frac{1}{2\pi} \left[\frac{-\Gamma_1}{d} + \frac{\Gamma_3}{d} + \frac{\Gamma_4}{2d} + \frac{\Gamma_5}{3d} + \frac{\Gamma_6}{4d} + \frac{\Gamma_7}{5d} + \frac{\Gamma_8}{6d} \right] = \frac{\Gamma_1}{3.46 \cdot \pi \cdot d}$
$\Gamma_3 = 2 \cdot \Gamma_1$	$u_{r,3} = \frac{1}{2\pi} \left[\frac{-\Gamma_1}{2d} + \frac{-\Gamma_2}{d} + \frac{\Gamma_4}{d} + \frac{\Gamma_5}{2d} + \frac{\Gamma_6}{3d} + \frac{\Gamma_7}{4d} + \frac{\Gamma_8}{5d} \right] = \frac{\Gamma_1}{3.71 \cdot \pi \cdot d}$
$\Gamma_4 = 3 \cdot \Gamma_1$	$u_{r,4} = \frac{1}{2\pi} \left[\frac{-\Gamma_1}{3d} + \frac{-\Gamma_2}{2d} + \frac{-\Gamma_3}{d} + \frac{\Gamma_5}{d} + \frac{\Gamma_6}{2d} + \frac{\Gamma_7}{3d} + \frac{\Gamma_8}{4d} \right] = \frac{\Gamma_1}{3.29 \cdot \pi \cdot d}$
$\Gamma_5 = 4 \cdot \Gamma_1$	$u_{r,5} = \frac{1}{2\pi} \left[\frac{-\Gamma_1}{4d} + \frac{-\Gamma_2}{3d} + \frac{-\Gamma_3}{2d} + \frac{-\Gamma_4}{d} + \frac{\Gamma_6}{d} + \frac{\Gamma_7}{2d} + \frac{\Gamma_8}{3d} \right] = \frac{\Gamma_1}{2.29 \cdot \pi \cdot d}$
$\Gamma_6 = 5 \cdot \Gamma_1$	$u_{r,6} = \frac{1}{2\pi} \left[\frac{-\Gamma_1}{5d} + \frac{-\Gamma_2}{4d} + \frac{-\Gamma_3}{3d} + \frac{-\Gamma_4}{2d} + \frac{-\Gamma_5}{d} + \frac{\Gamma_7}{d} + \frac{\Gamma_8}{2d} \right] = \frac{\Gamma_1}{0.44 \cdot \pi \cdot d}$
$\Gamma_7 = 5 \cdot \Gamma_1$	$u_{r,7} = \frac{1}{2\pi} \left[\frac{-\Gamma_1}{6d} + \frac{-\Gamma_2}{5d} + \frac{-\Gamma_3}{4d} + \frac{-\Gamma_4}{3d} + \frac{-\Gamma_5}{2d} + \frac{-\Gamma_6}{d} + \frac{\Gamma_8}{d} \right] = \frac{-\Gamma_1}{1.93 \cdot \pi \cdot d}$
$\Gamma_8 = 5 \cdot \Gamma_1$	$u_{r,8} = \frac{1}{2\pi} \left[\frac{-\Gamma_1}{7d} + \frac{-\Gamma_2}{6d} + \frac{-\Gamma_3}{5d} + \frac{-\Gamma_4}{4d} + \frac{-\Gamma_5}{3d} + \frac{-\Gamma_6}{2d} + \frac{-\Gamma_7}{d} \right] = \frac{-\Gamma_1}{5.15 \cdot \pi \cdot d}$

Figure 4-7 plots the induced radial velocities from Table 4-1. Looking at even this simple case, we can see how a vorticity gradient induces radial velocities that will lead to radial expansion. The large negative induced velocity for vortex 8 is largely caused by vortex 7 and the absence of a vortex to the left of vortex 8. In essence, this is similar to the radial expansion and contraction between two vortex rings, as in the case of the so-called “leap-frogging” vortex rings.

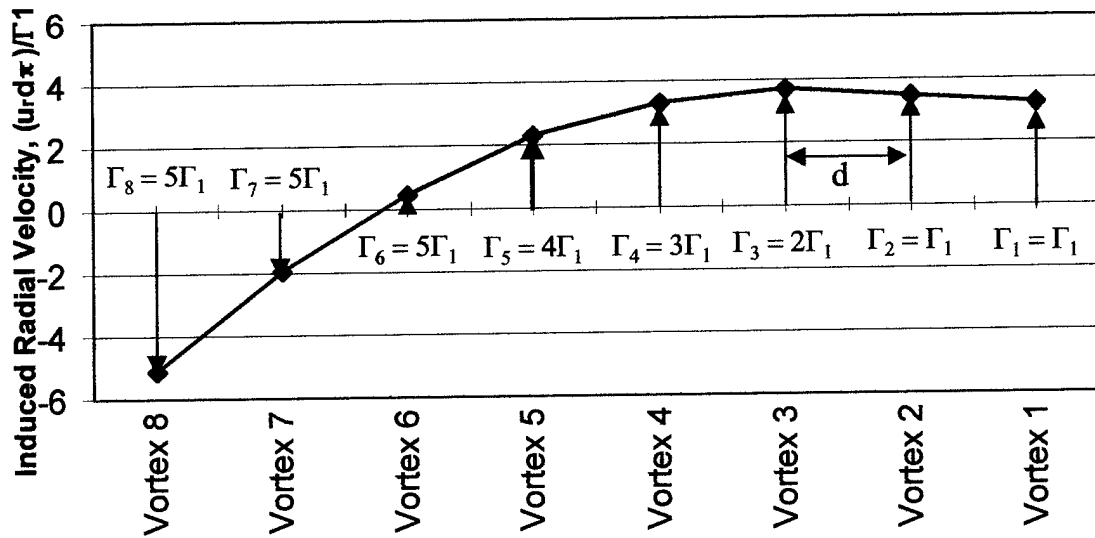


Figure 4-7 Induced radial velocities

Now we can expand this 2-D analogy to the 3-D case. As a result of this induced radial velocity caused by the azimuthal vorticity gradient, the vortex tube expands radially in the vorticity gradient region. This is exactly what happens in the 3-D vortex filament simulation. Figure 4-8 shows the rendered vortex tube for the filaments initially at $r = 0.12$ and $r = 0.42$. In both cases, by $T = 0.9$ (the increase in vorticity started at $T = 0.6$), the vortex tube has started to expand radially. The red shaded region shows the area where the circulation is increasing. The radial spokes of vorticity that maintain solenoidality of the vorticity field are left out of these images for clarity. The radial expansion continues. However, it also leads to several other effects, like pile-up and vorticity sign switching that are visible in this image. We cannot isolate these effects of the feedback mechanism, because they all interact with each other simultaneously to lead to vortex breakdown.

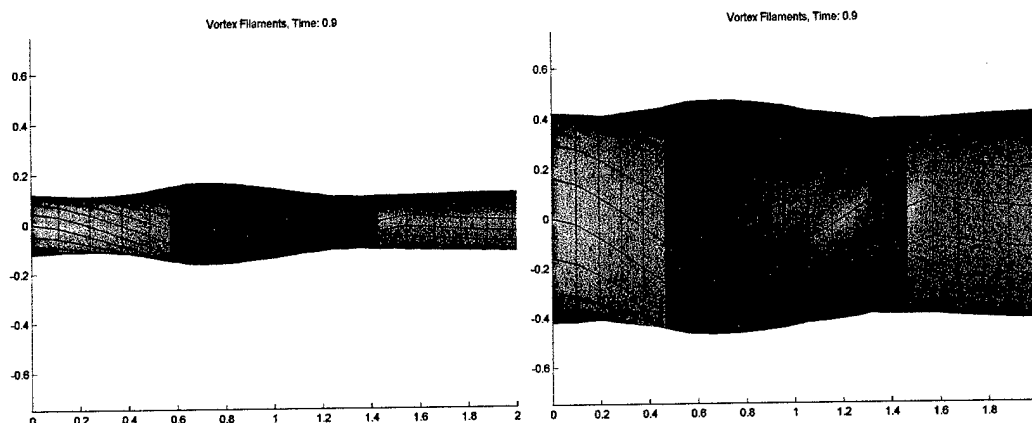


Figure 4-8 Radial expansion, rendered vortex filaments, $r = 0.12$ (L), $r = 0.42$ (R), $T = 0.9$

If we look at the radial velocity component at this time, we should see the velocities that lead to this. Figure 4-9 shows the color contour plot of the induced radial velocity for this area. The induced outward radial velocity is clearly visible in the vorticity gradient region.

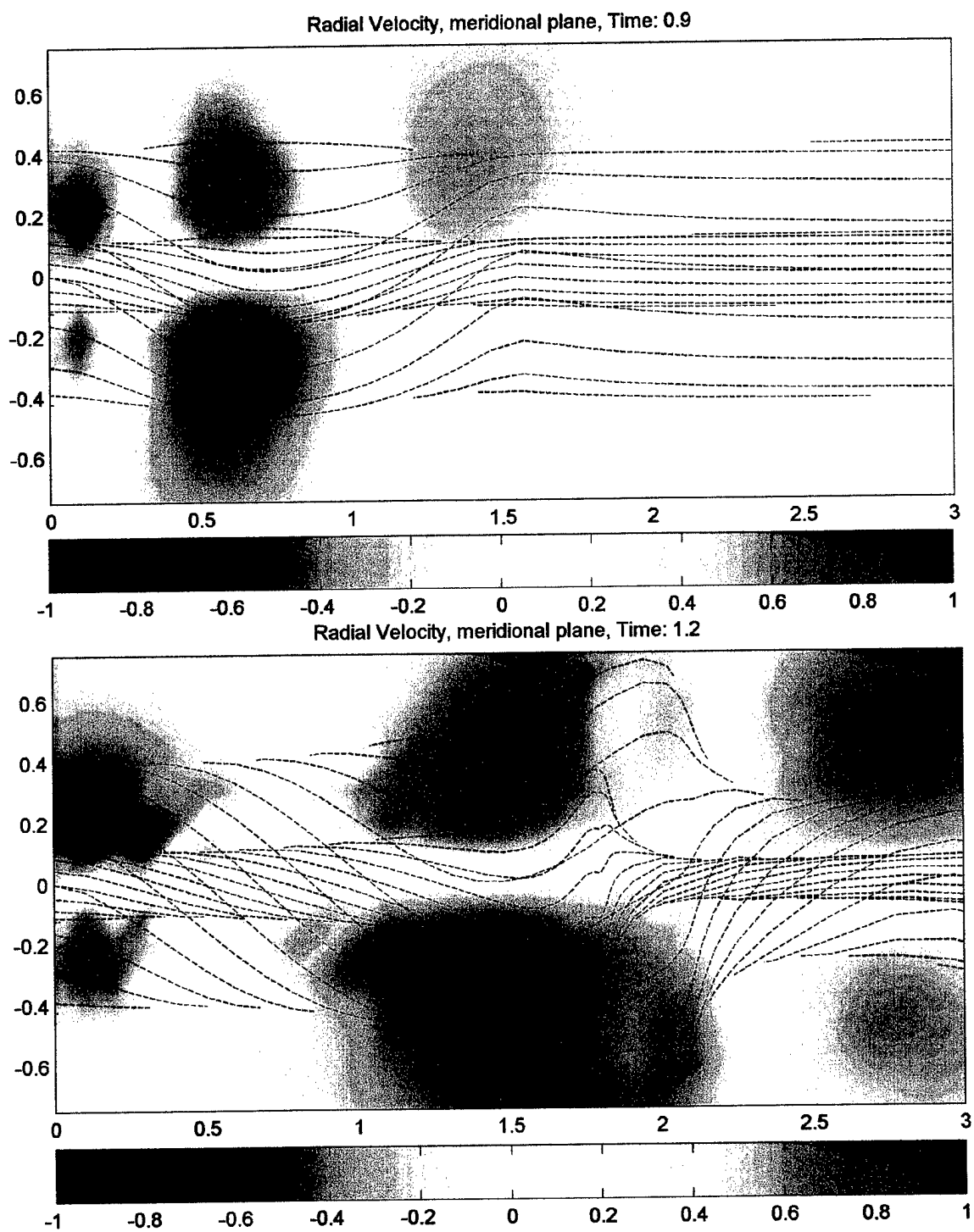


Figure 4-9 Induced radial velocity (top) $T = 0.9$, (bottom) $T = 1.2$

4.4.2 Pile-up

This radial expansion leads to the situation we call pile-up. Pile-up refers to the axial contraction of the vortex tube. However, it should be noted that, even if the radial expansion were suppressed somehow, pile-up would still occur in regions of an azimuthal vorticity gradient. We will first ignore the radial expansion, and then we will take it into account, showing how it increases the effect of pile-up. Pile-up happens as a result of an azimuthal vorticity gradient. The azimuthal vorticity gradient causes an axial velocity gradient, as shown in Figure 4-10. The red circles indicate azimuthal vorticity, ω_θ , out of the plane. The blue crosses indicate azimuthal vorticity into the plane. Their arced arrows show the individual induced velocities. The black arrows show the net induced axial velocity along the centerline of the vortex tube. The azimuthal vorticity increases in the upstream direction to the left. Like a pile-up with automobiles on a highway, the vortex tube upstream is moving slower in the axial direction than the vortex tube upstream.

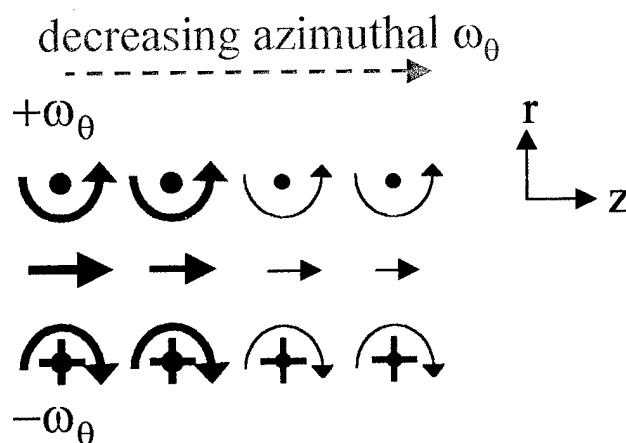


Figure 4-10 Vorticity gradient leading to pile-up

This axial velocity gradient causes the axial components of the vortex filaments to pile-up. When the axial vorticity components pile up, they undergo contraction (the opposite of stretching). This contraction leads to a further decrease in axial vorticity in the pile-up region. Thus, an azimuthal vorticity gradient in the axial direction causes pile-up and a decrease in axial vorticity in that region. The decrease in axial vorticity leads to

a corresponding decrease in azimuthal vorticity, which leads to a stronger azimuthal vorticity gradient and more pile-up. Due to this feedback response, the pile-up effect is magnified over time.

Not only are the two effects of radial expansion and pile-up coupled, they are also accentuated by each other. Figure 4-11 shows a diagram of this.

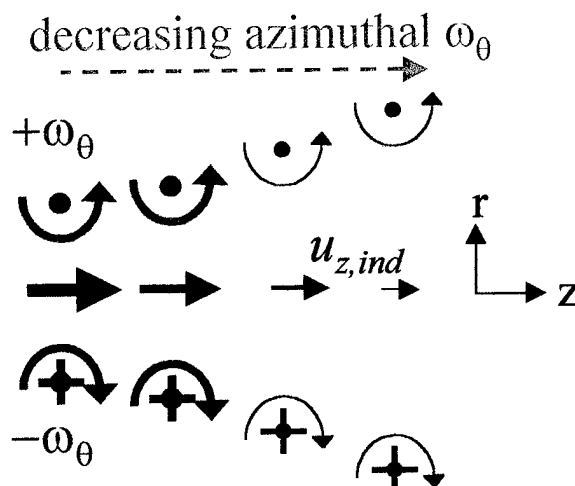


Figure 4-11 Pile-up with radial expansion

The reason a radially expanded vortex tube increases the effect of pile-up is that the azimuthal vorticity components have expanded radially and moved farther away from the vortex tube centerline. As a result, these components induce less axial velocity along the centerline. As a result of radial expansion, induced velocity along the centerline of the vortex tube slows down even more. The upstream axial velocities do not change, so the effects of pile-up increase. This is one way in which the feedback mechanisms are linked.

We can see this effect of the vorticity gradient and the radial expansion in the vortex filament simulation. The first figure, Figure 4-12, shows the vortex tube at $T = 0.9$ and $T = 1.2$. Here, the red line shows tracks particles along the centerline of the vortex tube. The cross marks show distance between the tracking line segment endpoint nodes. They were originally spaced at 0.1 length units apart. The effect of pile-up is clear visible in the $z = 1.5$ to 2.0 region, which is the region of the vorticity gradient.

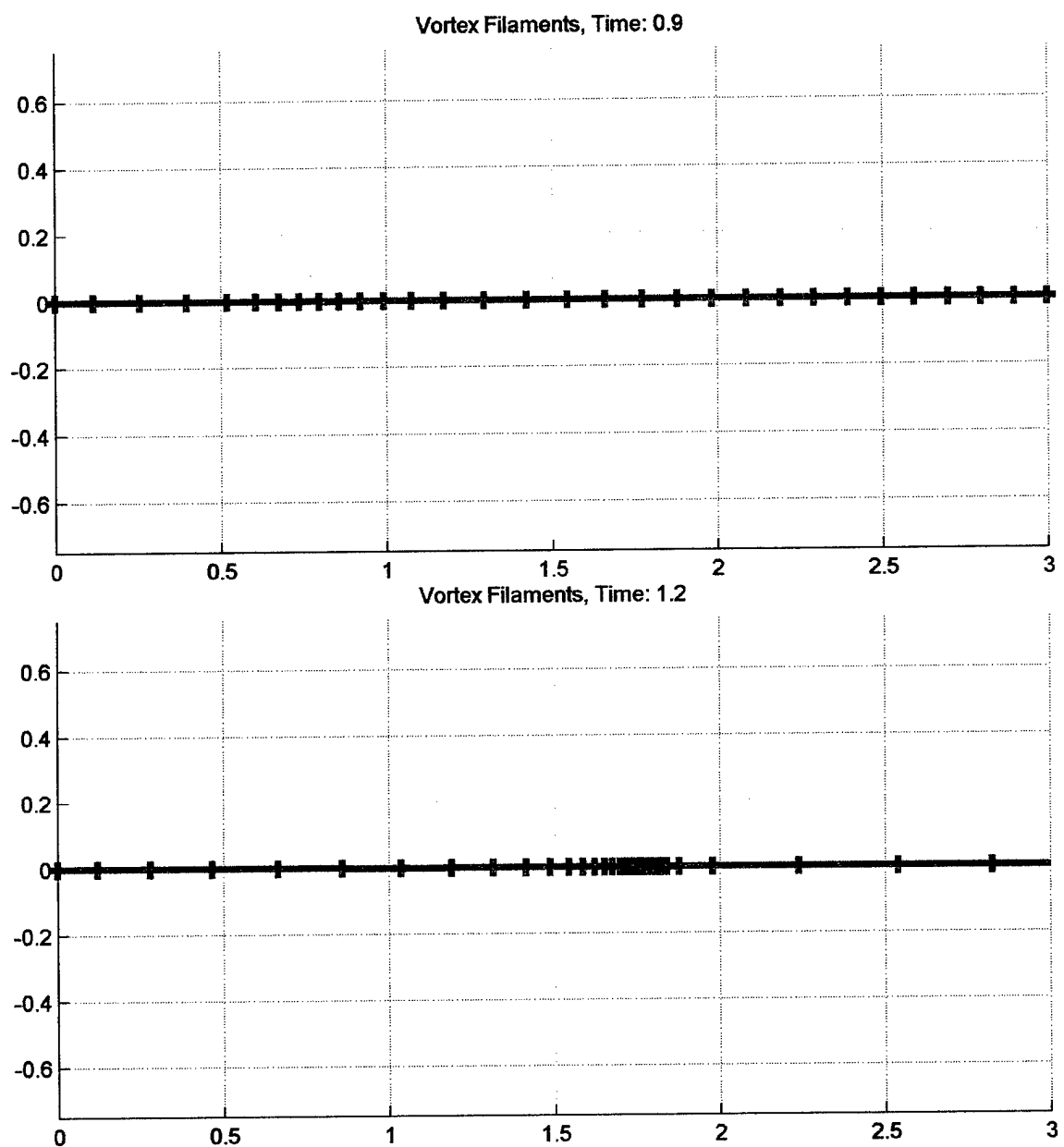


Figure 4-12 Pile-up along vortex tube centerline (top) $T = 0.9$, (bottom) $T = 1.2$

We can see how this fits in to the overall vortex tube by overlaying the $r = 0.12$ filaments on the centerline plot in Figure 4-13. Clearly, the pile-up is strongest in the region of the largest radial expansion.

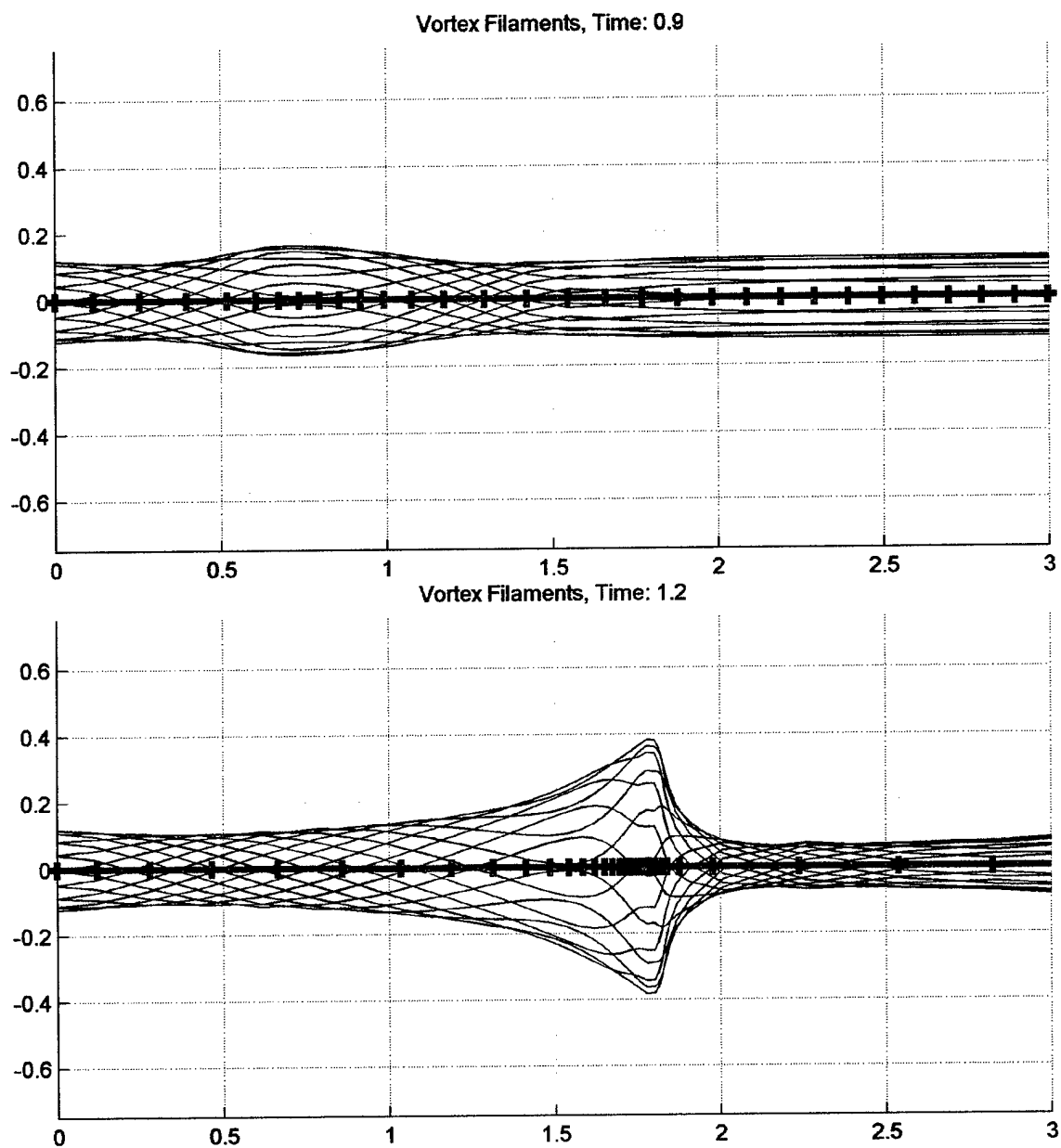


Figure 4-13 Pile-up along vortex tube, center and $r = 0.12$, (top) $T = 0.9$, (bottom) $T = 1.2$

If we look at the rendered view of the same radius, in Figure 4-14, we can see that pile-up occurs throughout the vortex tube and not just at the centerline. Looking at the circumferential tracking lines, we see that the vortex filament segments endpoint nodes get closer and closer together and they get nearer to the vorticity gradient region. This is

a result of pile-up. As a consequence, we should expect the axial component of vorticity to decrease throughout the vortex tube in regions of pile-up.

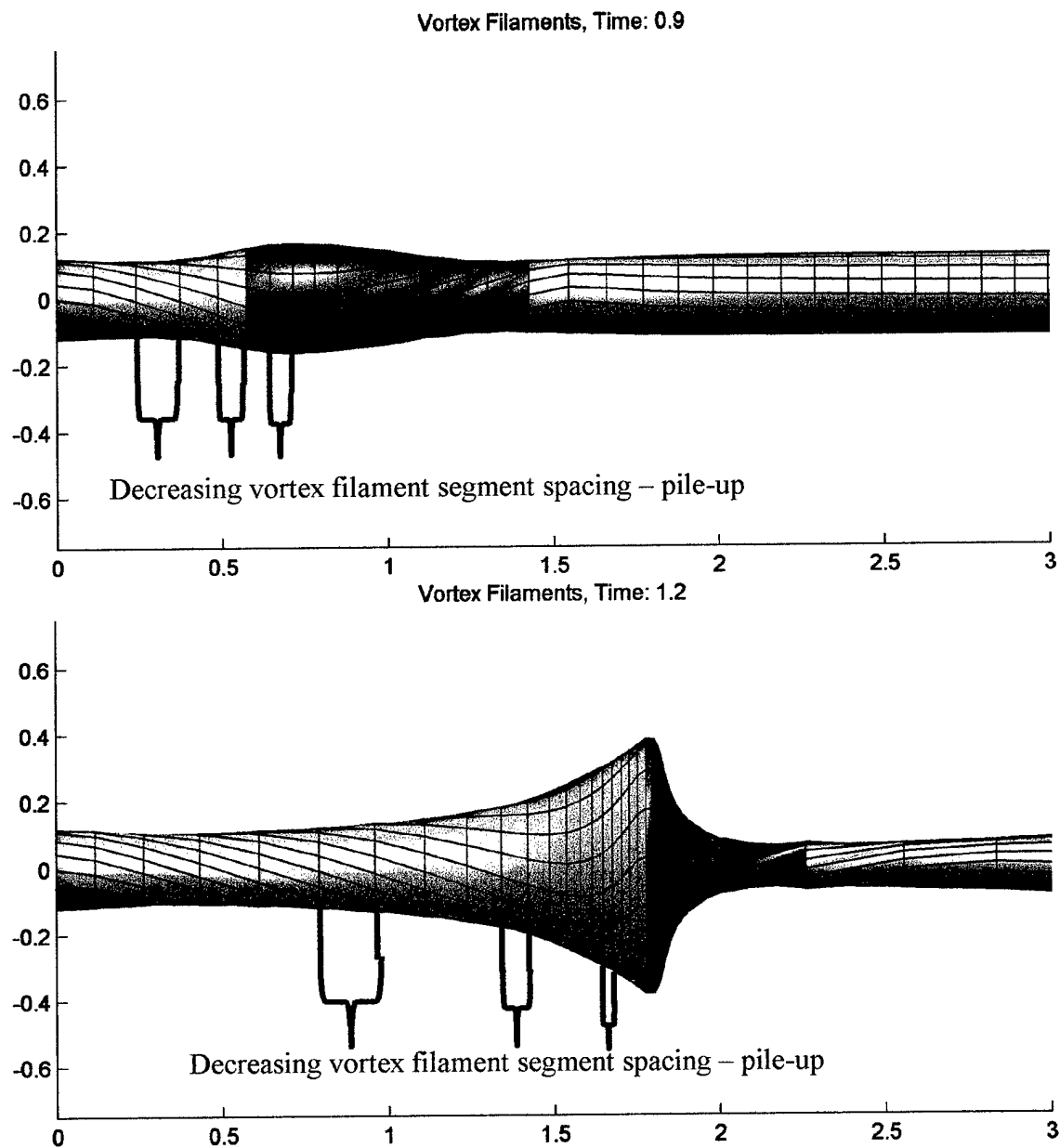


Figure 4-14 Pile-up along vortex tube, rendered $r = 0.12$, (top) $T = 0.9$, (bottom) $T = 1.2$

The effects of pile-up will be clear in the plots of axial velocity along the meridional plane. We should also be able to see the decrease in axial vorticity on this

same meridional plane. Figure 4-15 shows the color contour plot of axial velocity at $T = 0.9$ and $T = 1.2$. Figure 4-16 shows the axial vorticity at this same time.

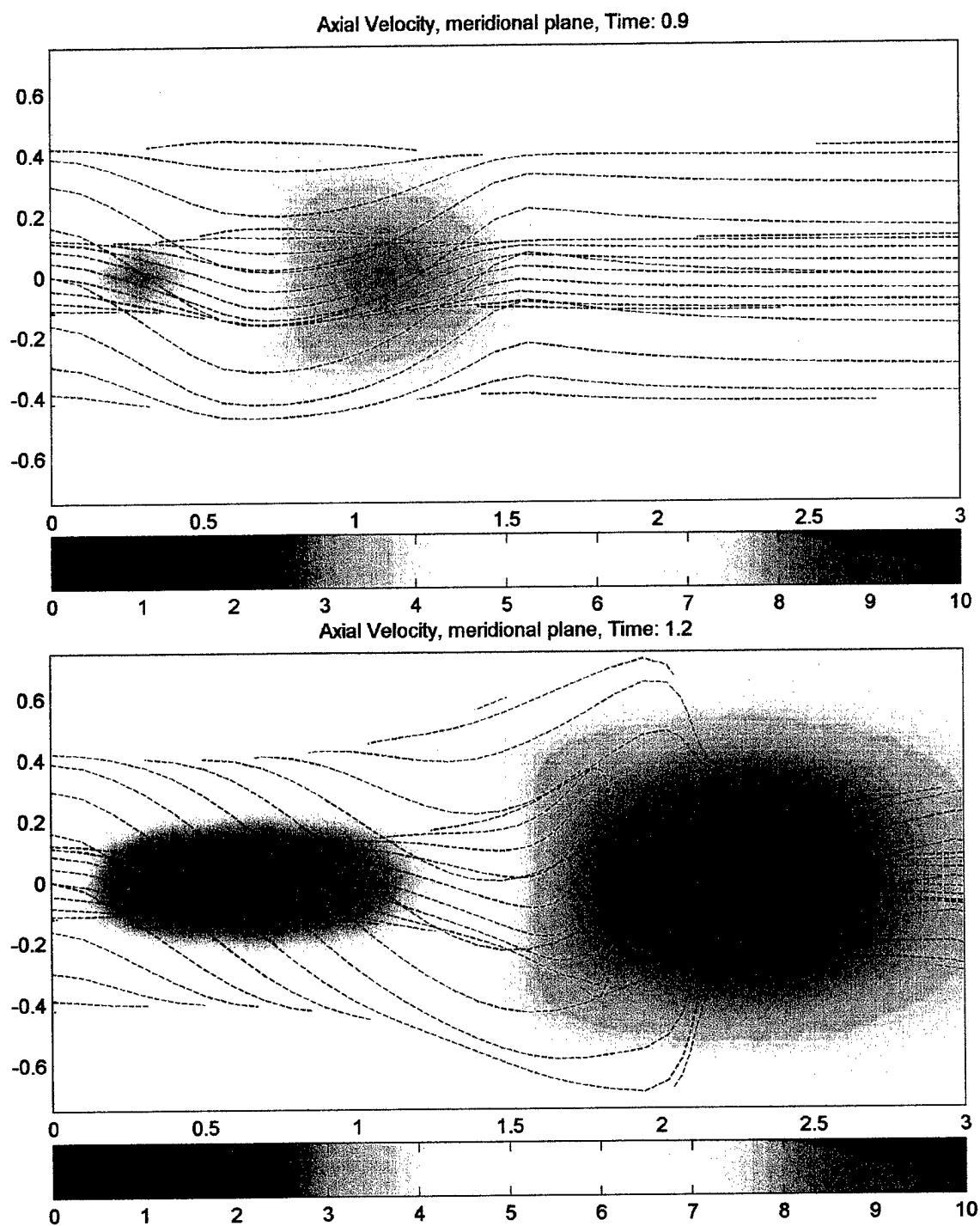


Figure 4-15 Pile-up, axial velocity, , (top) $T = 0.9$, (bottom) $T = 1.2$

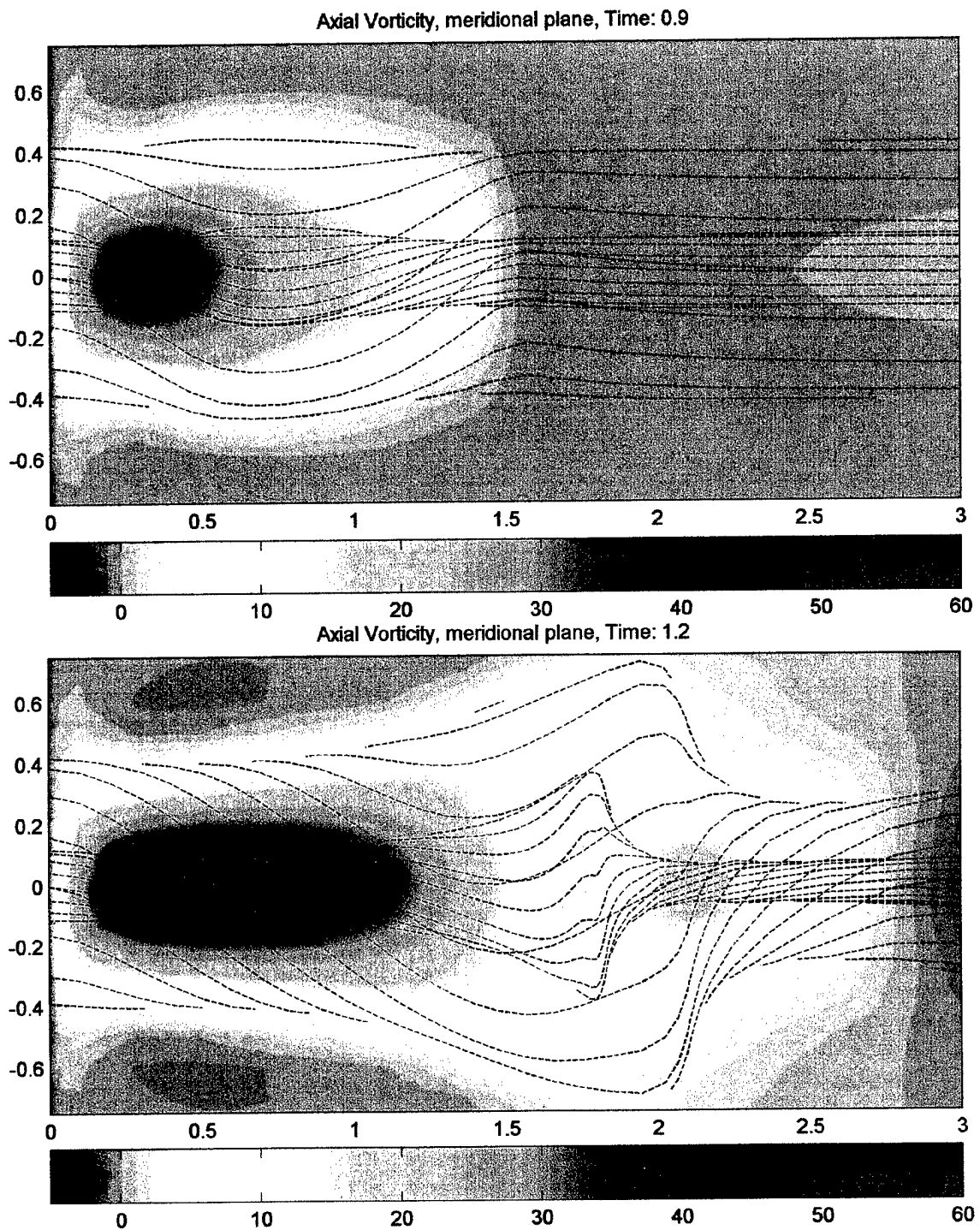


Figure 4-16 Pile-up, axial vorticity, (top) $T = 0.9$, (bottom) $T = 1.2$

Though we have tried to talk about radial expansion and pile-up separately, they are really inseparable. One inevitably leads to the other due to continuity. The continuity

equation for the vortex tube is $\frac{1}{r} \frac{\partial}{\partial r}(ru_r) + \frac{\partial u_z}{\partial z} = 0$. Due to the negative azimuthal

vorticity gradient, there is a negative velocity gradient, and pile-up, so $\frac{\partial u_z}{\partial z} < 0$. Thus,

$\frac{\partial}{\partial r}(ru_r) > 0$ in order for the continuity equation to be satisfied. If we integrate $\frac{\partial}{\partial r}(ru_r)$

from 0 to a where a is the radius of the vortex tube, we find that

$a \cdot u_r(r=a) - a u_r(r=0) > 0$. Of course, $u_r(r=0) = 0$, so $a \cdot u_r(r=a) > 0$ must be

satisfied. The expression $u_r > 0$, implies radial expansion. Thus, through continuity, radial expansion and pile-up are inseparable.

4.4.3 Vorticity sign switch

As a result of pile-up and radial expansion, there is a decrease in axial vorticity in the region of the vorticity gradient. Axial vorticity is associated with azimuthal velocity. Therefore, in the regions of pile-up, radial expansion, and the axial vorticity gradient, the vortex tube will rotate more slowly than the upstream region of the vortex tube. You can also think of this in terms of conservation of angular momentum. If a vortex tube increases in radius, it will have to rotate more slowly in that region to conserve angular momentum. This decrease in azimuthal velocity in the region of radial expansion and pile-up is clearly visible in the color contour plot of this velocity along the meridional plane. It is shown in Figure 4-17.

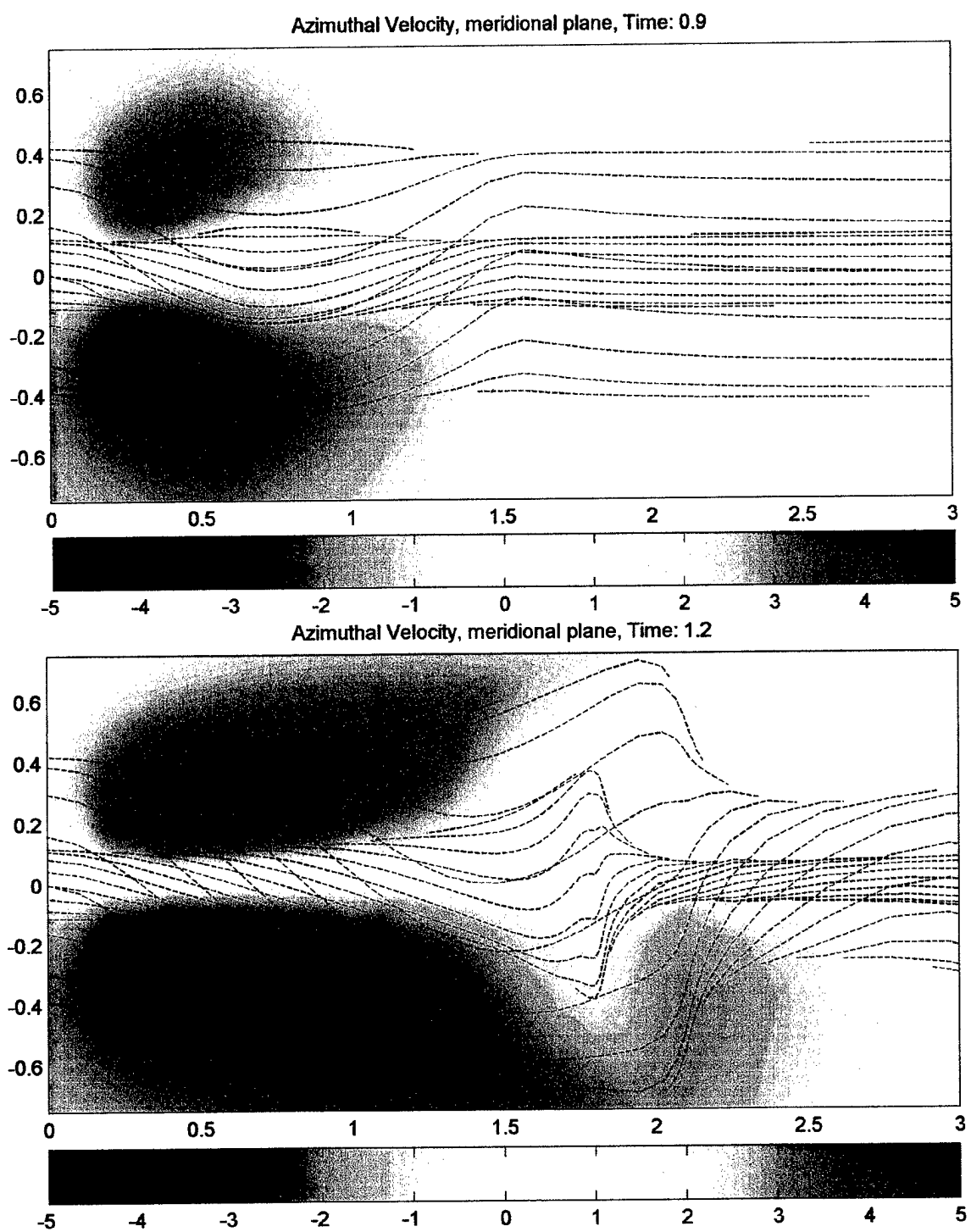


Figure 4-17 Induced azimuthal velocity, (top) $T = 0.9$, (bottom) $T = 1.2$

This azimuthal velocity gradient causes tilting in the vortex filaments in the region of radial expansion and pile-up. The vorticity vector is at all times aligned with the vortex filament. Therefore, due to this tilting, the vector decomposition of the vortex filament will show a sign switch in the azimuthal vorticity. Brown and Lopez were the first to mention this very important result (*ref. 17*). We confirm that result here. To explain this effect, let us look at the diagram in Figure 4-18.

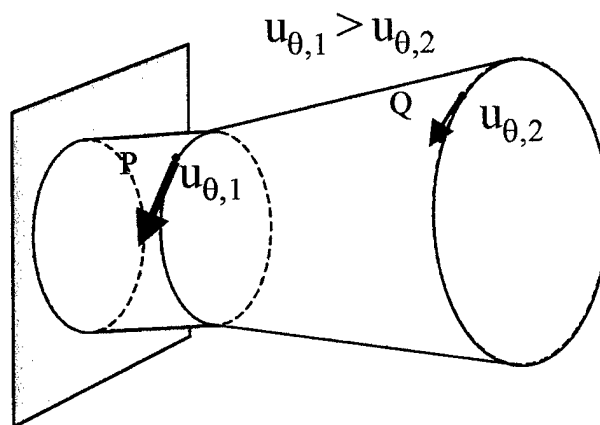


Figure 4-18 Vortex tube, rotating and different velocities

Here, we show the effect of an azimuthal velocity gradient on a portion of a vortex tube. The vortex tube is fixed at its source. At a location, P, downstream of that source, it is rotating at a speed $u_{\theta,1}$. Downstream of P, the vortex tube has undergone pile-up and radial expansion. Thus at Q, it rotates at a slower speed, $u_{\theta,2}$. Now, let us track a vortex filament in this vortex tube. For simplicity, let us say that at one instant, t_0 , the vortex filament is axially aligned with the vortex tube. We will track this the motion of this vortex filament at subsequent times. Figure 4-19 shows how it will move. In this figure, the vortex line is green. Because it is fixed at the source and because it rotates faster, as indicated by $u_{\theta,1}$, we can see that the vortex filament, which moves with the fluid, will develop a “v-shaped” kink.

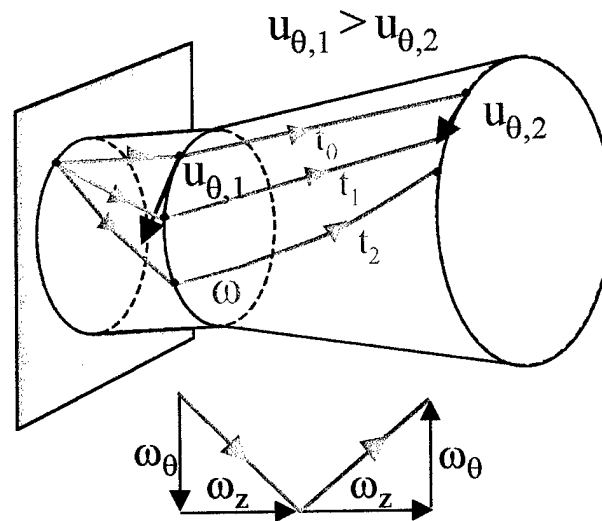


Figure 4-19 Azimuthal vorticity sign switch

The vorticity vector is always aligned with this vortex filament, so if we decompose the vector components of the vortex filament, we can see how the vorticity changes. The axial component of vorticity does not change, but, as the above figure shows, the azimuthal vorticity, ω_{θ} , undergoes a sign switch. This is precisely what happens in the vortex filament simulation. We can see this by looking at a single vortex filament from the vortex filament simulation at $T = 1.2$. Figure 4-20 shows the vortex filaments that were originally at $r = 0.12$.

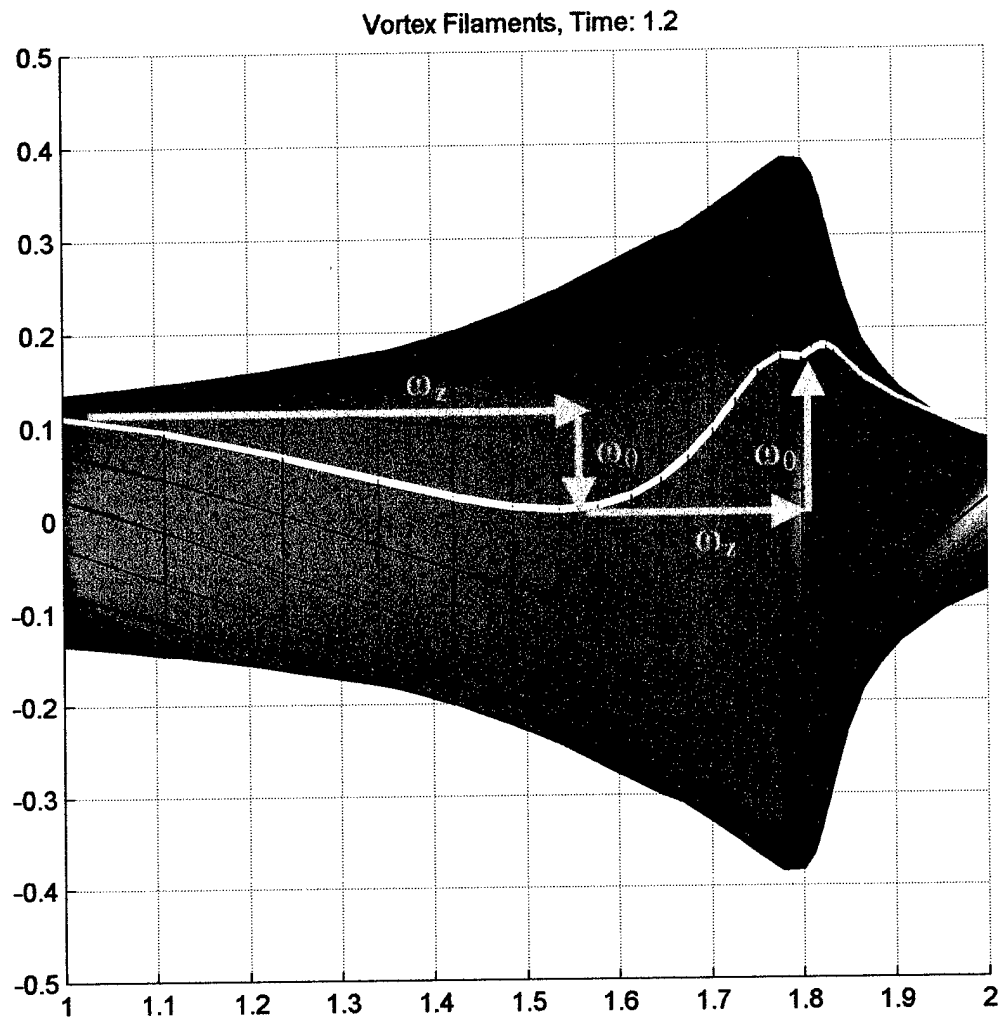


Figure 4-20 Vortex filaments, azimuthal vorticity sign switch

In this view we see the vortex filaments. The yellow line highlights one specific filament. If we decompose that filament into its components, we can see, as was illustrated in Figure 4-19, the azimuthal vorticity sign switch. This vorticity sign switch is especially clear in the vorticity that is calculated along the meridional plane. Figure 4-21 shows the azimuthal vorticity in the meridional plane at $T = 1.2$.

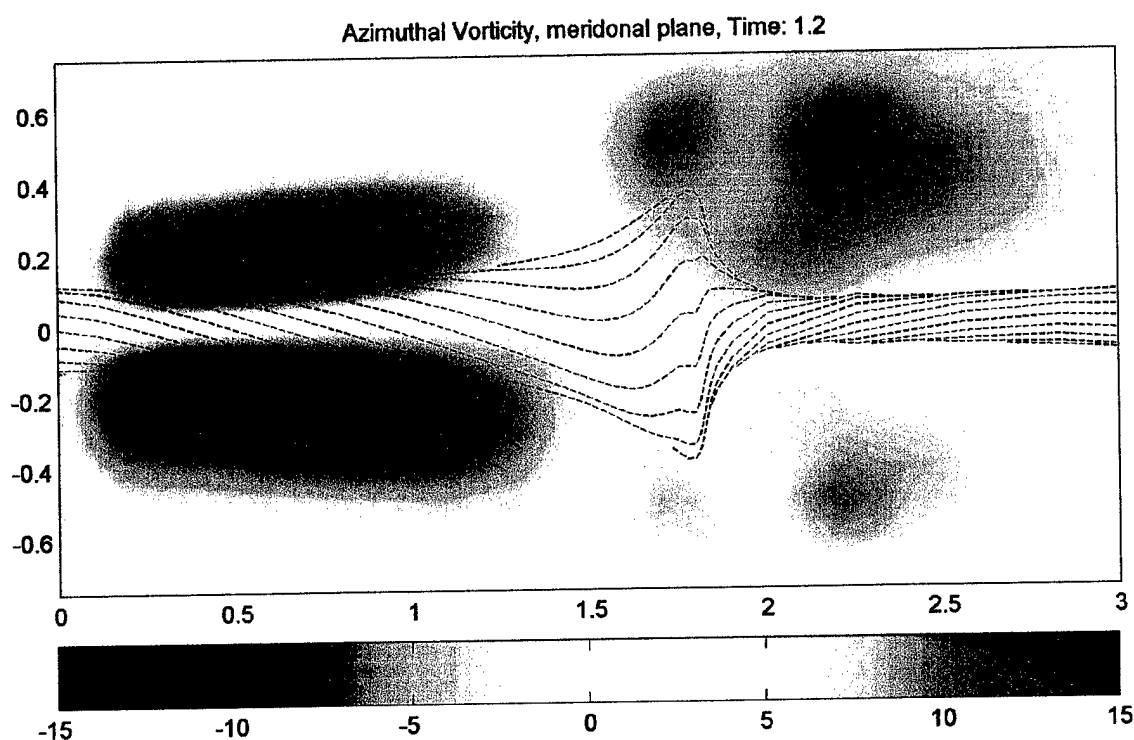


Figure 4-21 Azimuthal vorticity sign switch, meridional plane

This azimuthal vorticity sign switch is important to vortex breakdown because it is the condition that causes backflow within this vortex tube. Without backflow, vortex breakdown would be a transient phenomenon instead of one that can exist at a fixed location relative to an aircraft wing in steady state.

We can understand how the azimuthal vorticity sign switch leads to backflow by looking at the diagram in Figure 4-22. Instead of inducing axial velocities in the direction of the freestream, the region where the azimuthal vorticity has switched its sign induces velocities pointing in the upstream direction. The backflow becomes stronger as the azimuthal vorticity sign switching becomes stronger. When the induced backflow equals the relative freestream velocity, the vortex breakdown region will stop moving downstream.

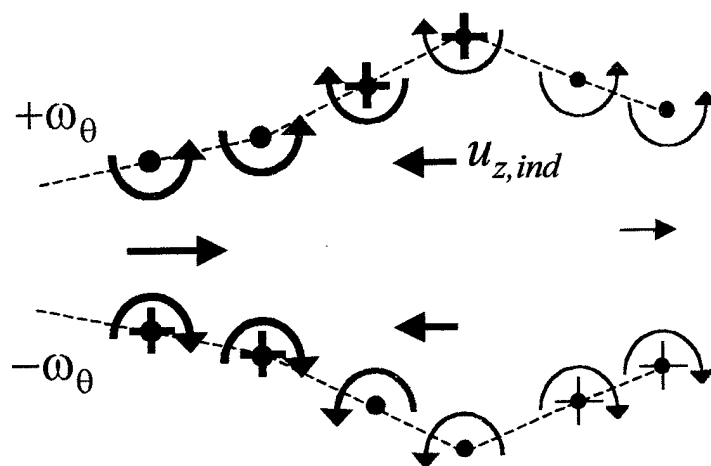
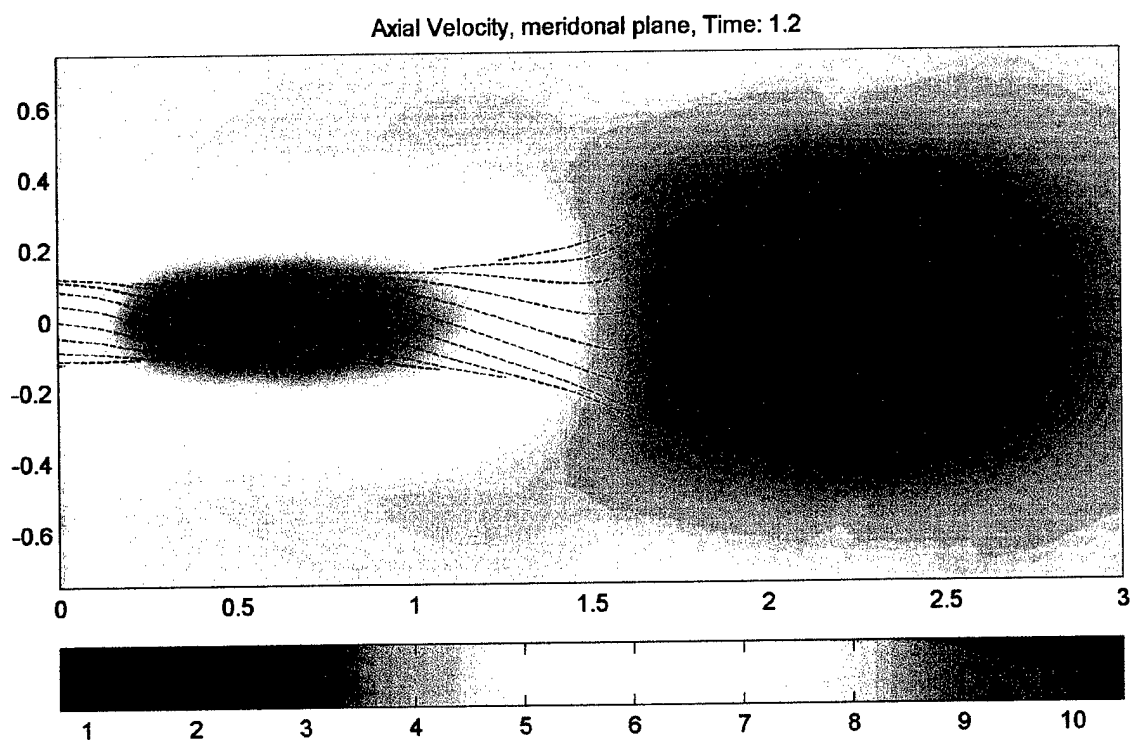


Figure 4-22 Backflow

We can see the start of this backflow in the axial velocity plot along the meridional plane, as in Figure 4-23. We previously looked at this figure in terms of pile-up.

Figure 4-23 Beginning of backflow, axial velocity, $T = 1.2$

We can now see how these mechanisms enhance one another in a feedback loop. As the pile-up continues, the vortex radially expands and the azimuthal vorticity switches

signs to induce backflow. This backflow enhances the pile-up, which enhances the radial expansion, which enhances the vorticity sign switch, which in turn enhances the backflow.

It can also be noted that a radial vorticity sign switch is associated with radial expansion. This is because the vorticity vector is aligned at all times with the vortex filaments. Therefore, in regions of radial expansion, there will be a positive radial component of vorticity just as the radius of the vortex tube increases. Likewise, there will be a negative radial component of where the vortex tube contracts. The position of zero radial vorticity ($\omega_r = 0$) corresponds to the maximum radii of the vortex filaments. Here, the radial expansion ends and radial contraction begins. Beyond this point, the vortex tube starts to close on the downstream end, as compared to the hypothesized open cavity model adopted by Keller et al (see *ref.* 24 and 25 for details on the open cavity model). Figure 4-24 shows the resulting radial vorticity sign switch.

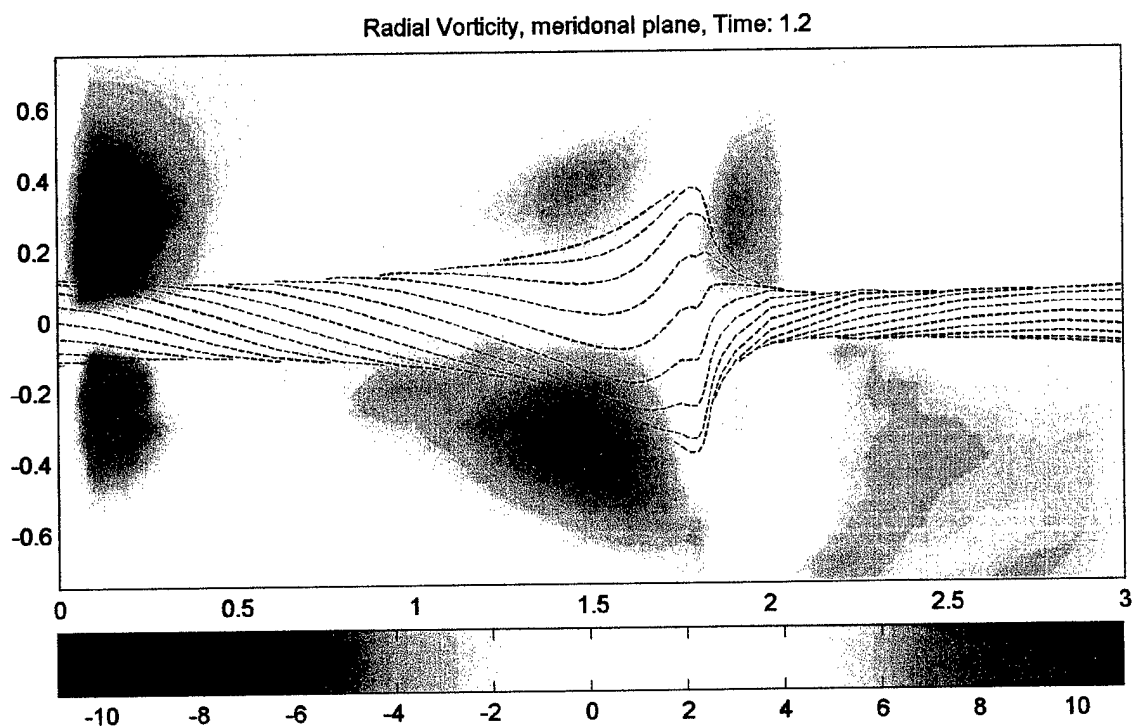


Figure 4-24 Radial vorticity sign switch

4.4.4 Turning point

The azimuthal vorticity sign switch induces velocities that cause backflow inside the vortex tube. However, this backflow also causes vortex filaments to turn inward on themselves. We can see how this happens by looking at the illustration in Figure 4-25. The azimuthal vorticity sign switch induces a turning of the vortex filaments. The filaments turn inward, leading to a radial contraction of the vortex tube as in Figure 4-25 (L). However, they do not stop turning at this point. They continue to turn, being brought upstream, relative to the region of the azimuthal vorticity sign switch, by the induced backflow velocities as in Figure 4-25 (R). This radial contraction is important because, when combined with the backflow, it leads to the culminating point of the inviscid feedback mechanism—the turning point.

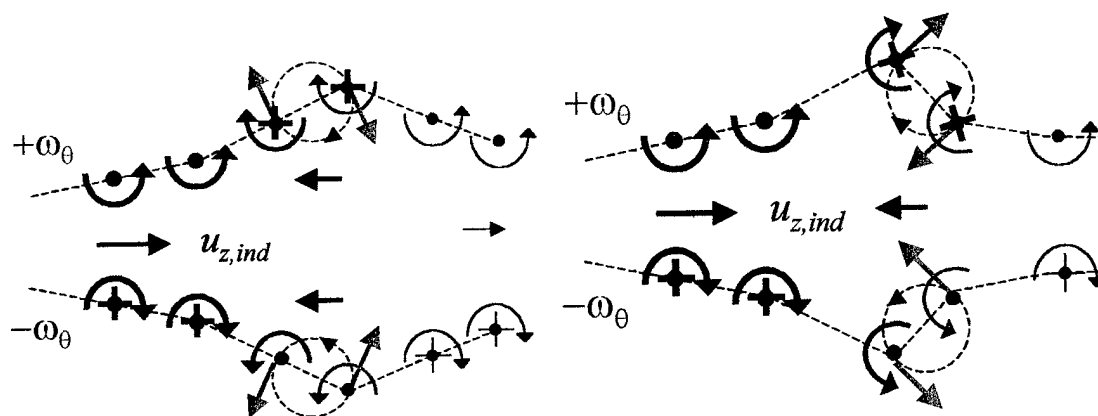


Figure 4-25 Turning point formation

There is a definite location where the vortex filaments have turned inward on themselves, as in Figure 4-26. We call this the turning point. The exact location of the turning point is defined as where the vortex filament is vertical relative to the axial direction.

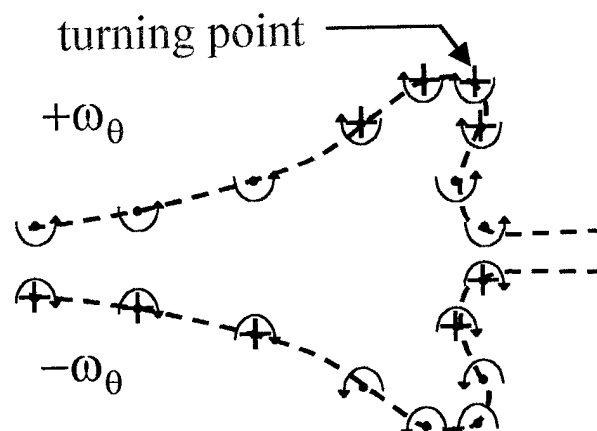
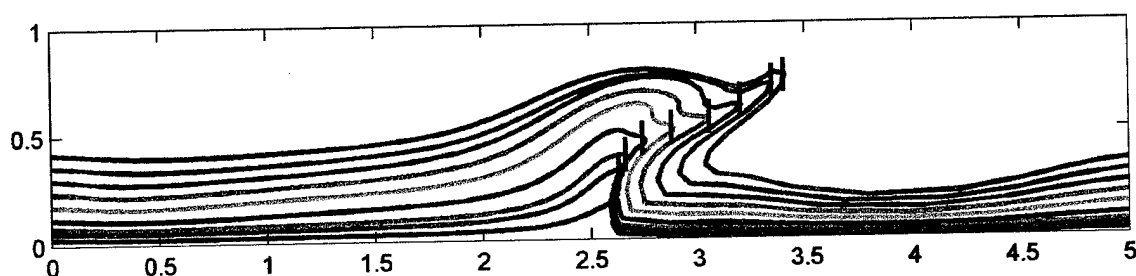


Figure 4-26 Turning point established

At this point, the axial vorticity is zero. Upstream of the turning point, along the vortex filament, the axial vorticity is positive. Downstream of the turning point, along the vortex filament, the axial vorticity is negative. It becomes positive again near the centerline of the vortex tube as the vortex filaments turn back downstream.

We can also see this turning point most clearly in the vortex filament results. If we look at a projection of the vortex filaments onto the meridional half-plane, we can clearly see the location of the turning point at various radii of the vortex tube. Figure 4-27 shows these results. The location of the turning point is marked with a vertical line.

Figure 4-27 Vortex filaments projected on meridional plane, $T = 1.5$

The projection of the vortex filaments onto the meridional half-plane allows us to see the direction of axial and radial vorticity vectors, as they are aligned with the vortex filaments. Thus, we can see the axial vorticity sign switch. Figure 4-28 shows the axial and radial components of the vortex filaments overlaid with the rendered vortex filaments from the $r = 0.12$ initial radius at $T = 1.5$.

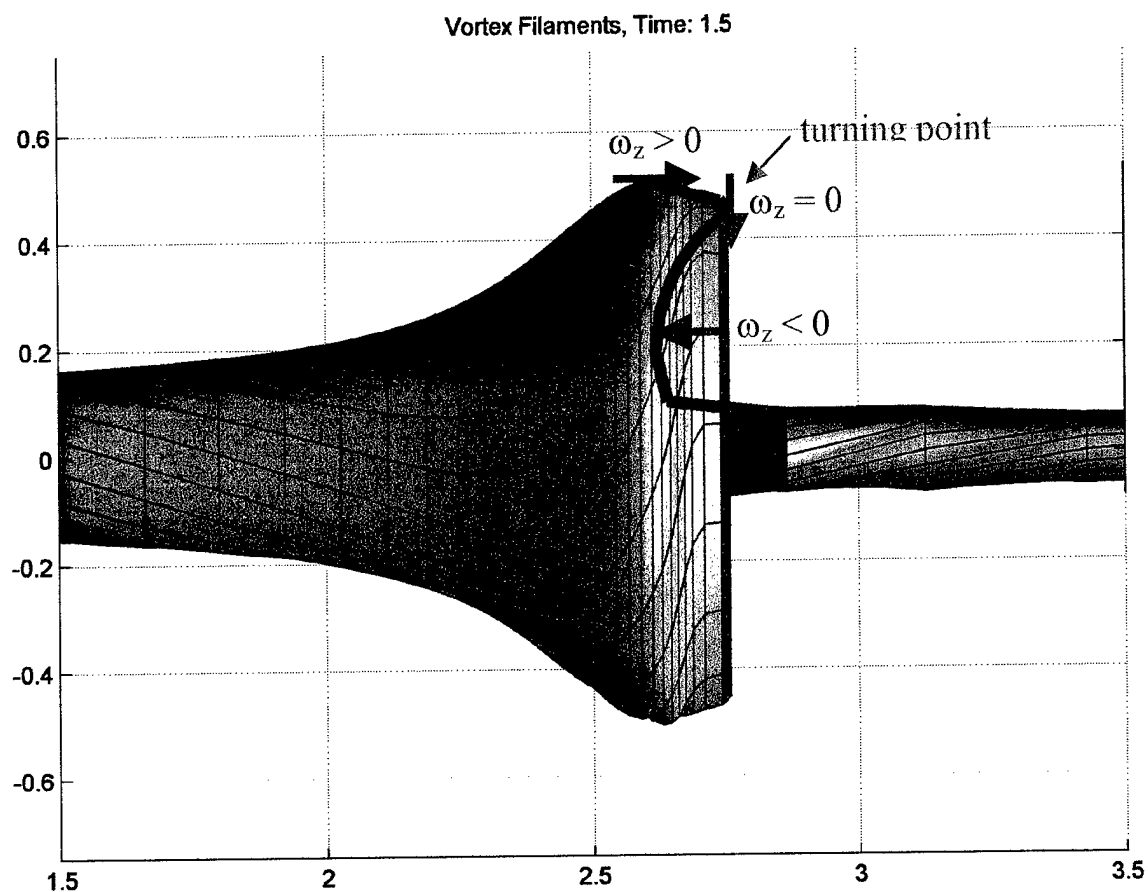


Figure 4-28 Axial vorticity sign switch

We can also see the axial vorticity sign switch in the data along the meridional plane. Figure 4-29 shows this at $T = 1.5$. The axial vorticity sign switch corresponds to the area near the turning point throughout the vortex tube.

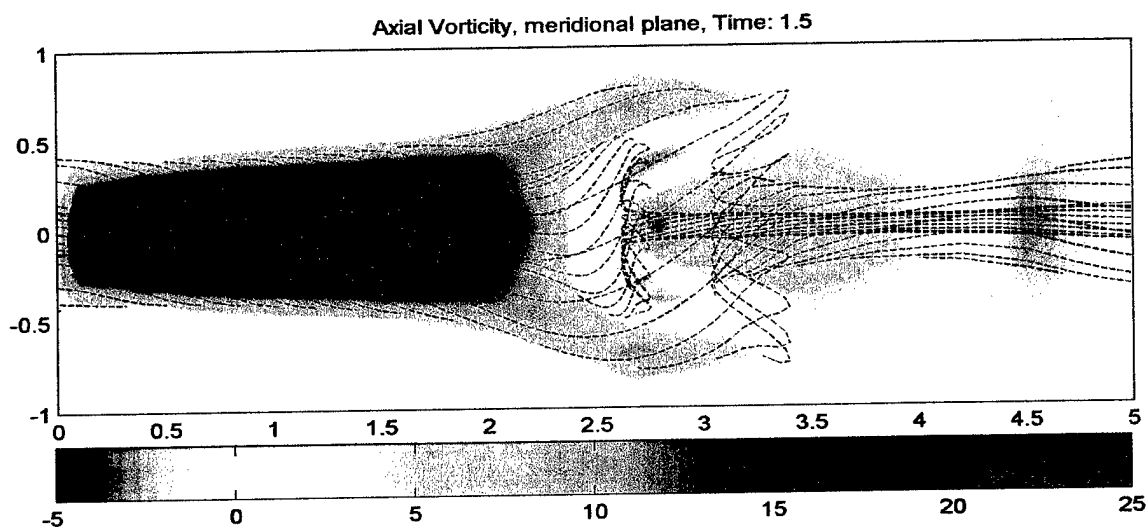


Figure 4-29 Axial vorticity sign switch, meridional plane, $T = 1.5$

This axial vorticity sign switch, interior to the vortex tube, induces counter rotating flows interior to the vortex tube. It is important to note that these counter rotating flows exist only interior to the vortex tube and in the region of the turning point. They do not exist outside of the vortex tube. These counter rotating flows lead to regions where viscosity becomes important with shear layers and the development of small-scale turbulence. As a result, the inviscid model reaches the limits of its assumptions after the turning point forms. However, with the turning point, all features of vortex breakdown, as compared to experimental data, are present. We will compare the numerical results to experimental data in later sections.

In summary, vortex breakdown has been initiated to a recognizable form through an entirely inviscid mechanism of pile-up, radial expansion and contraction, and vorticity sign switching. The vorticity sign switch is present in all forms of vorticity—azimuthal, radial, and axial. These inviscid, self-induced mechanisms work together to form the turning point. Once the turning point forms, the downstream region of the vortex breakdown forms a dissipative, turbulent flow that leads to a steady state vortex breakdown. Thus, vortex breakdown is initiated by a vorticity gradient that manifests itself through an inviscid, self-induced feedback mechanism. This inviscid feedback mechanism continues until it forms the turning point. This turning point and its

associated axial vorticity sign switch cause counter rotating flows interior to the vortex tube, which leads to viscous actions and steady state vortex breakdown. This leads to the conclusion that if we can suppress a portion of the inviscid feedback mechanism, it would seem possible to prevent, weaken, or delay the formation of the turning point, and by doing so, prevent, weaken, or delay the formation of vortex breakdown.

4.5 Implications of self-induction mechanism on vortex breakdown

If we understand that vortex breakdown works through a self-induced, inviscid mechanism, we can better understand why vortex breakdown occurs at specific chordwise locations over a delta wing. If the induced backflow velocity is caused by azimuthal vorticity tilting, it should follow that for a given circulation in a vortex tube, there is a maximum possible induced backflow, depending on the degree of the azimuthal vorticity sign switch. This maximum induced backflow is a function of the circulation of the vortex tube, which itself is a function (in terms of a delta wing) of the delta wing sweep angle, the freestream velocity, the delta wing angle of attack, and yaw angle. The other important factor is the velocity profile along the vortex tube path. As we saw before, that velocity, along the path of the vortex tube, reaches a peak near an airfoil leading edge, and then decreases toward the trailing edge. This velocity profile, itself, is a function of the delta wing sweep angle, the freestream velocity, and the delta wing angle of attack.

Therefore, for a given delta wing sweep angle, freestream velocity, delta wing angle of attack, and yaw angle, there is only one location over the wing where vortex breakdown can remain fixed with reference to the wing. That point is where the relative axial freestream velocity exactly equals the maximum induced backflow velocity as it manifests itself in the vortex tube. The relative axial freestream velocity is the free stream velocity that the region of vortex breakdown experiences. This is relative to the position of the vortex breakdown over the wing since the freestream velocity changes near the vortex along the path of the vortex over the wing. Figure 4-30 illustrates this

idea, where point P corresponds to such a point of balance between the maximum induced backflow and the relative axial freestream velocity.

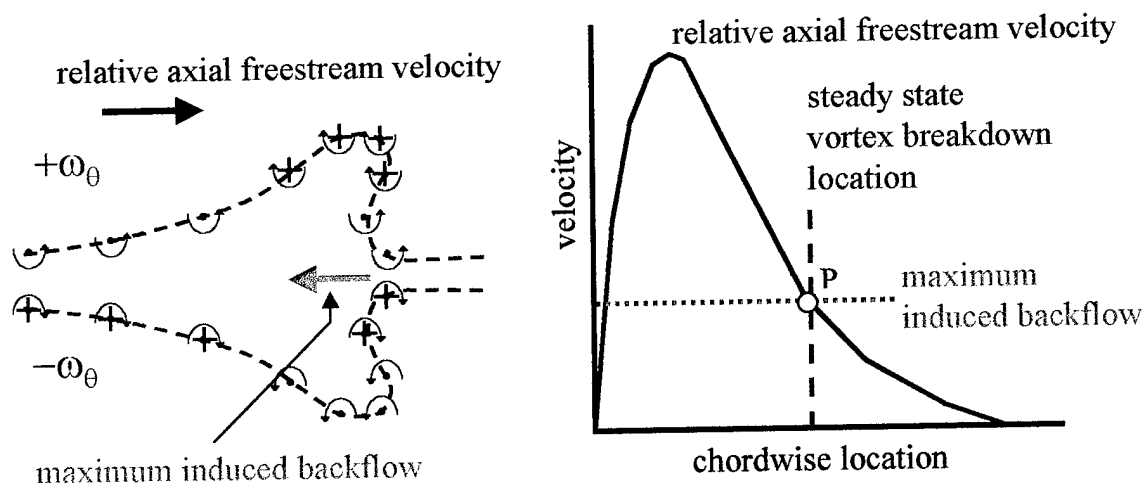


Figure 4-30 Steady state vortex breakdown location

This steady vortex breakdown location would represent a very delicate point, where a slight change in induced backflow velocity or of the relative axial freestream velocity would require the vortex breakdown location to rebalance.

With this idea we can explain how the vortex breakdown location changes as results of an increase in angle of attack. An increase in angle of attack will increase the circulation in the vortex tube and change the relative axial freestream velocity profile by increasing the peak velocity and decreasing the velocities downstream of the peak. As a result of the increase in circulation, the maximum induced backflow velocity will increase. Thus, as we see in Figure 4-31, the steady state vortex breakdown will move forward from P to P'.

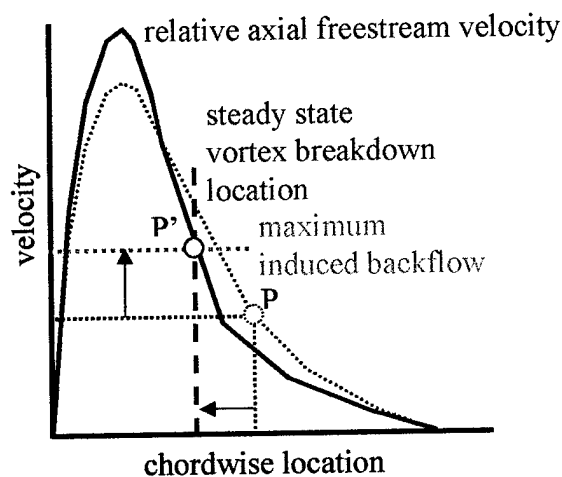


Figure 4-31 Vortex breakdown location change with AOA increase

A decrease in angle of attack does just the opposite. It will cause the vortex breakdown location to move downstream. If the angle of attack is sufficiently small, the maximum induced backflow will not be sufficient to maintain the vortex breakdown over the wing. It will be swept downstream where it will dissipate. The result, at lower angles of attack, is no vortex breakdown over the wing.

A change in freestream velocity, with the angle of attack fixed, results in little change in angle of attack (provided that the Reynolds number is sufficiently low) because the circulation and corresponding maximum induced backflow increases proportionally to the amount that the change in the relative axial freestream velocity profile, as in Figure 4-32.

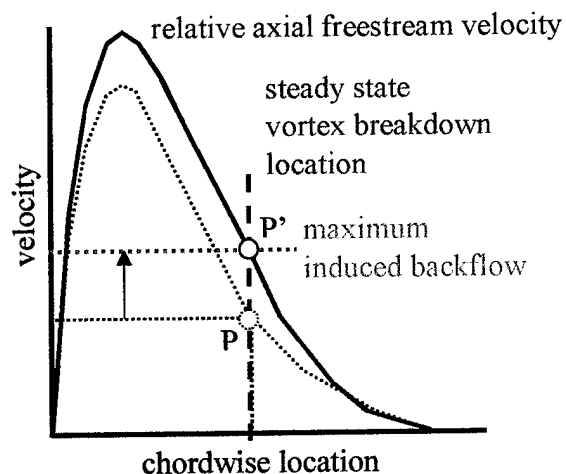


Figure 4-32 Vortex breakdown location change with freestream velocity increase

Typically, the maximum induced backflow and the relative axial freestream velocity are coupled through the freestream velocity, the delta wing angle of attack, yaw angle, and the delta wing sweep angle. However, by understanding how they work together through the self-induction mechanism, we can come up with various schemes to decouple these to effects, and thus provide a way to control the location of vortex breakdown. For example, if we could reduce the circulation in a vortex tube, while keeping the relative axial freestream velocity fixed, we would be able to move the vortex breakdown location downstream. This type of vortex breakdown control mechanism would provide a way to use the location of the vortex breakdown for aircraft control purposes.

5. Experimental and Computational Evidence

While the vortex filament method simulation is a useful tool for understanding vortex breakdown and the self-induction theory of vortex breakdown, it needs to be validated with experimental data. We will validate the vortex filament simulation results qualitatively with several experiments. The first experiment was performed by S. Srigrarom specifically to match the vorticity gradient case. See *ref. 4* for complete details. It involves a delta wing at fixed angle of attack, undergoing a transient increase in freestream velocity. This change in freestream velocity creates a vorticity gradient that leads to vortex breakdown (*ref. 4*). The second experiment illustrates how vorticity gradients in vortex tubes of fixed circulation can lead to vortex breakdown. The third case was a previously published case of vortex breakdown in a cylinder with a rotating end wall by M.P. Escudier (*ref. 27*). This case was chosen because of its similarity to the conditions in the vortex filament simulation. The fourth case is a full Navier-Stokes simulation of the Escudier experiment (*ref. 28*). This allows us to compare qualitatively the velocity and vorticity data of a fully viscous solution of vortex breakdown with the inviscid solution from the vortex filament simulation. Finally, previously published experiments involving vortex breakdown control will be examined in terms of the self-induction theory of vortex breakdown.

5.1 Case 1, vortex breakdown over delta wing with vorticity gradient

To validate the vortex filament simulation, we will compare the vortex filament simulation to the vortex breakdown over a delta wing caused by a vorticity gradient in a water tunnel. This experiment is different than the simulation, because it involves a wing rather than just a vortex tube. This introduces asymmetries that are not present in the simulation. Because of these differences between the experiment and the simulation, we will make qualitative and general comparisons, rather than quantitative comparisons. In the experiment dye flow visualization, laser induced fluorescence (LIF), and particle image velocimetry (PIV) are used to analyze the flow.

5.1.1 Experiment setup

This experiment used a Plexiglas delta wing with a 60 degrees apex angle mounted at 20 degrees angle of attack in a closed circuit water tunnel. A vorticity gradient was generated by quickly increasing the freestream velocity in the water tunnel from 0 to 5 cm/s. This represents a Reynolds number change from 0 to 20,000 based on the delta wing chord. Figure 5-1 shows how this change in freestream velocity creates a negative vorticity gradient.

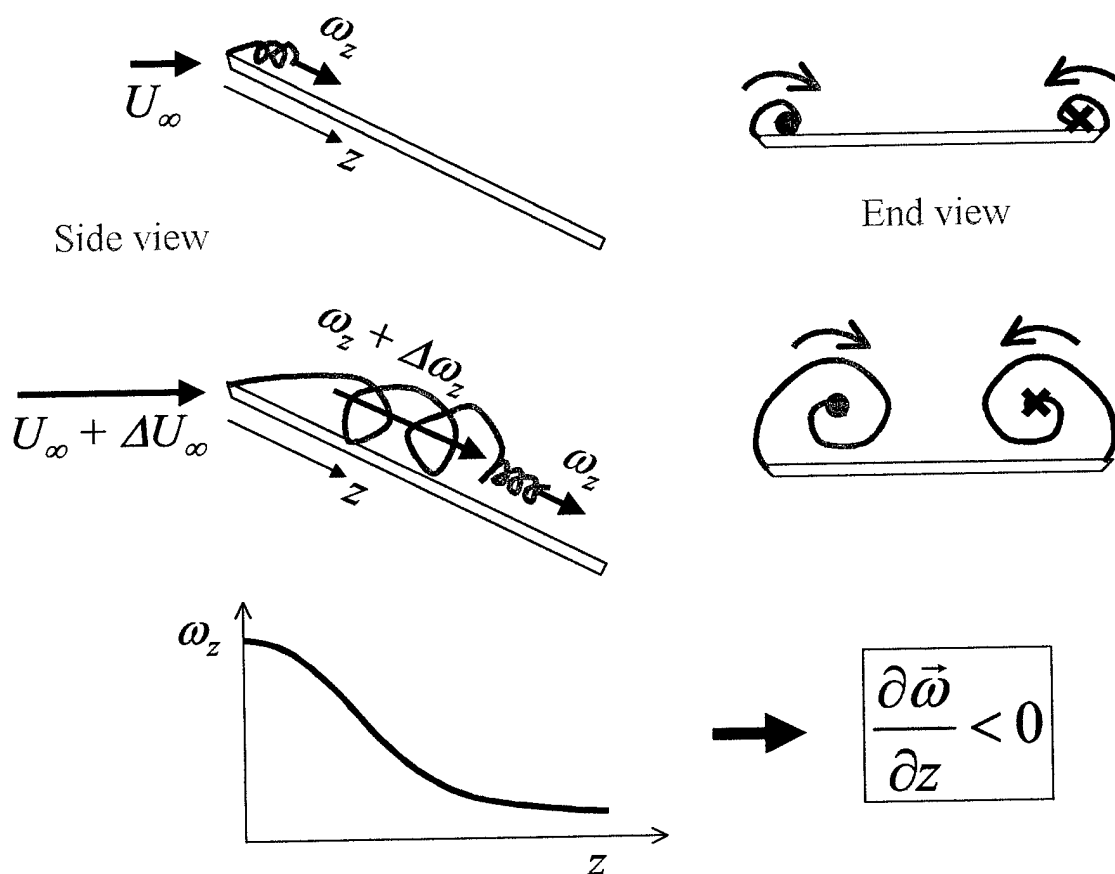


Figure 5-1 Generating a vorticity gradient over a delta wing

This negative vorticity gradient is what leads to vortex breakdown in the vortex filament simulation. If the initial cause of vortex breakdown is a negative vorticity gradient, then the vorticity gradient caused by the freestream velocity increase should

also lead to vortex breakdown in the region of the vorticity gradient. This is precisely what is seen in this delta wing experiment.

5.1.2 Dye flow visualization

Dye was injected at the leading edge of the delta wing just as the freestream velocity is increased. Figure 5-2 shows these results.

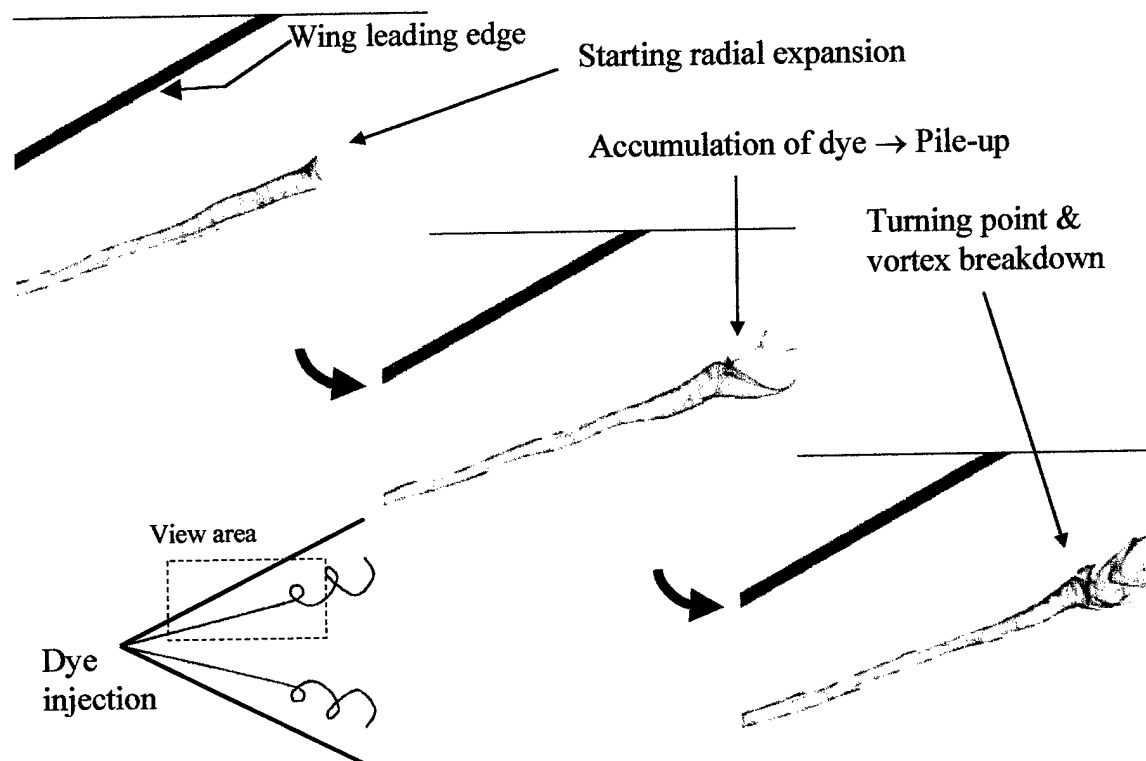


Figure 5-2 Vortex breakdown, dye visualization

The viewing area is from approximately 10% to 60% of the centerline chord. The vortex tube is viewed from the side, as is indicated in the illustration. The dyed particles represent the vortex filaments, since the dyed particles are initially sucked into the low pressure of the cores of the winding vortex filaments and remain always aligned with the vortex filaments by the Helmholtz vortex theorem ($\vec{\omega} = c \cdot \delta \vec{l}$). The thick line is the edge of the delta wing. The three images are taken at successive time intervals. They are chosen to show the process of vortex breakdown in the vorticity gradient region. In the first image, radial expansion begins. In the next image we see continuing radial

expansion and pile-up. The pile-up manifests itself by an increased concentration of dye. This is why the vortex tube looks darker in the radial expansion region in the second image. In the third image, a turning point is visible. Backflow is also present, indicating the presence of the azimuthal vorticity sign switch. Figure 5-3 shows the last image in more detail. All three aspects of vortex breakdown are visible in this image. We see radial expansion of the vortex tube. Pile-up is present, as indicated by the accumulation of dye near the radial expansion region. An azimuthal vorticity sign switch, which will be substantiated later by PIV data, is inducing backflow. This backflow leads to the turning point and soon after, steady state vortex breakdown.

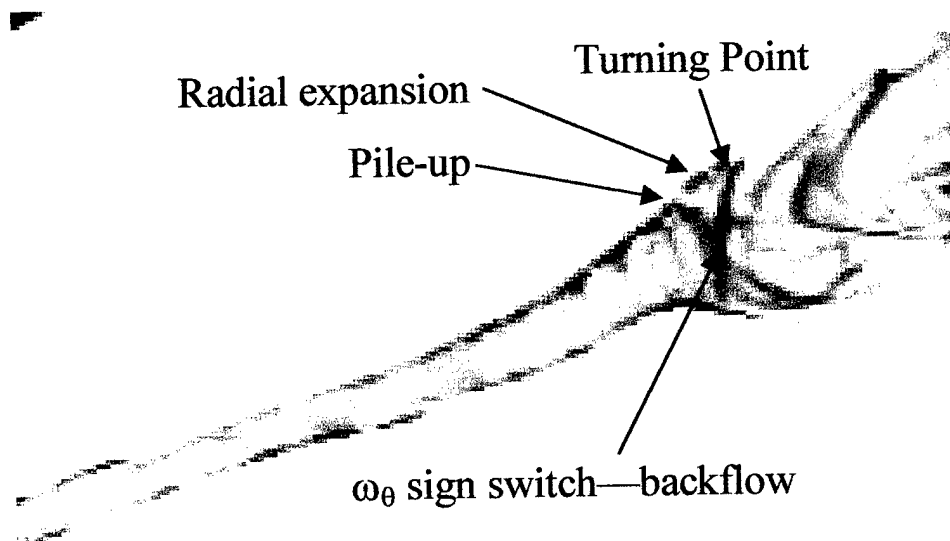


Figure 5-3 Dye flow visualization, turning point

We can compare this image with a rendered image from the vortex filament simulation. Figure 5-4 shows this result. All features of the inviscid self-induction mechanism are present in these images. We see the radial expansion and pile-up along the vortex tube. If we follow the vortex filament, we see the azimuthal vorticity sign switch. We also see where the vortex tube turns inward on itself. This is the turning point. An axial vorticity sign switch characterizes the turning point. The axial vorticity sign switch causes counter-rotation interior to the vortex tube that makes the effects of viscosity important, leading to turbulences downstream of the turning point, as the experiment shows.

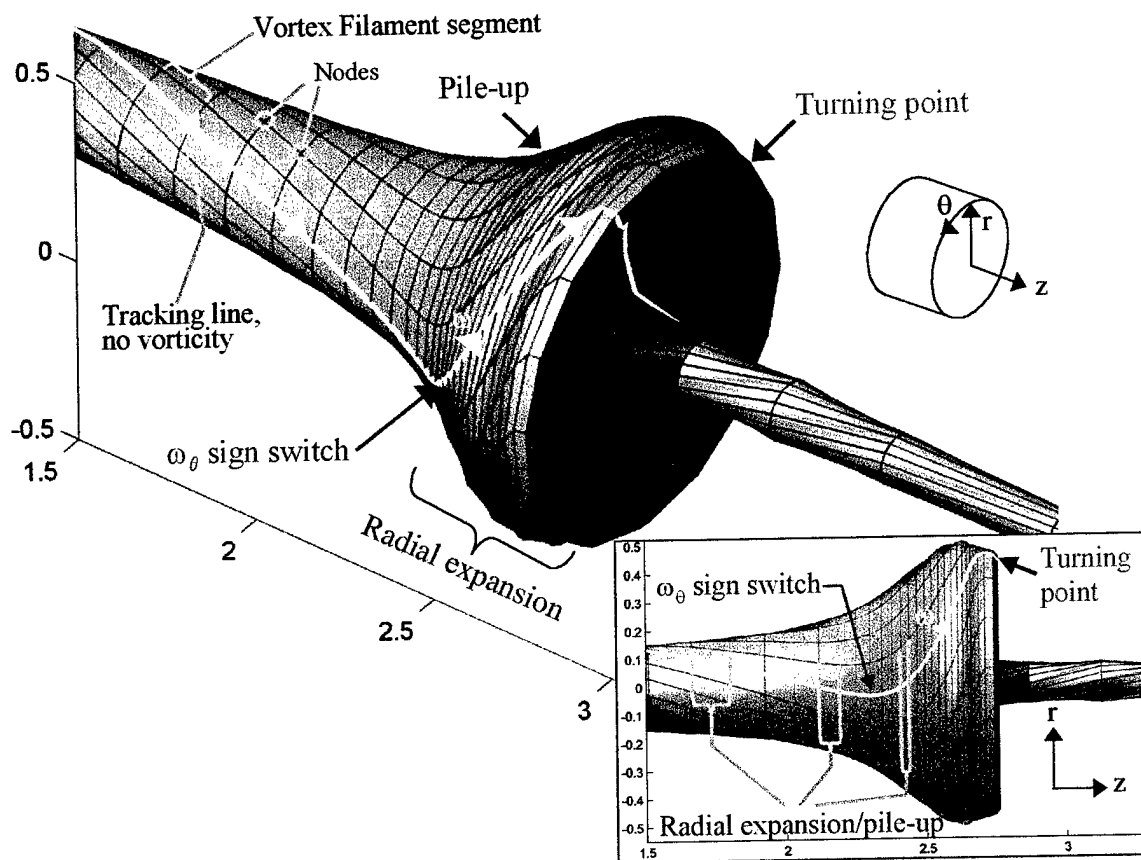


Figure 5-4 Vortex filament simulation, features of self-induction mechanism, $T = 1.5$

Other dye flow visualization experiments also show the turning point. We will present these only briefly for purposes of comparison. These images are from an experiment with vortex breakdown in a pipe (*ref. 8*). This setup allows for a much more symmetric vortex breakdown.

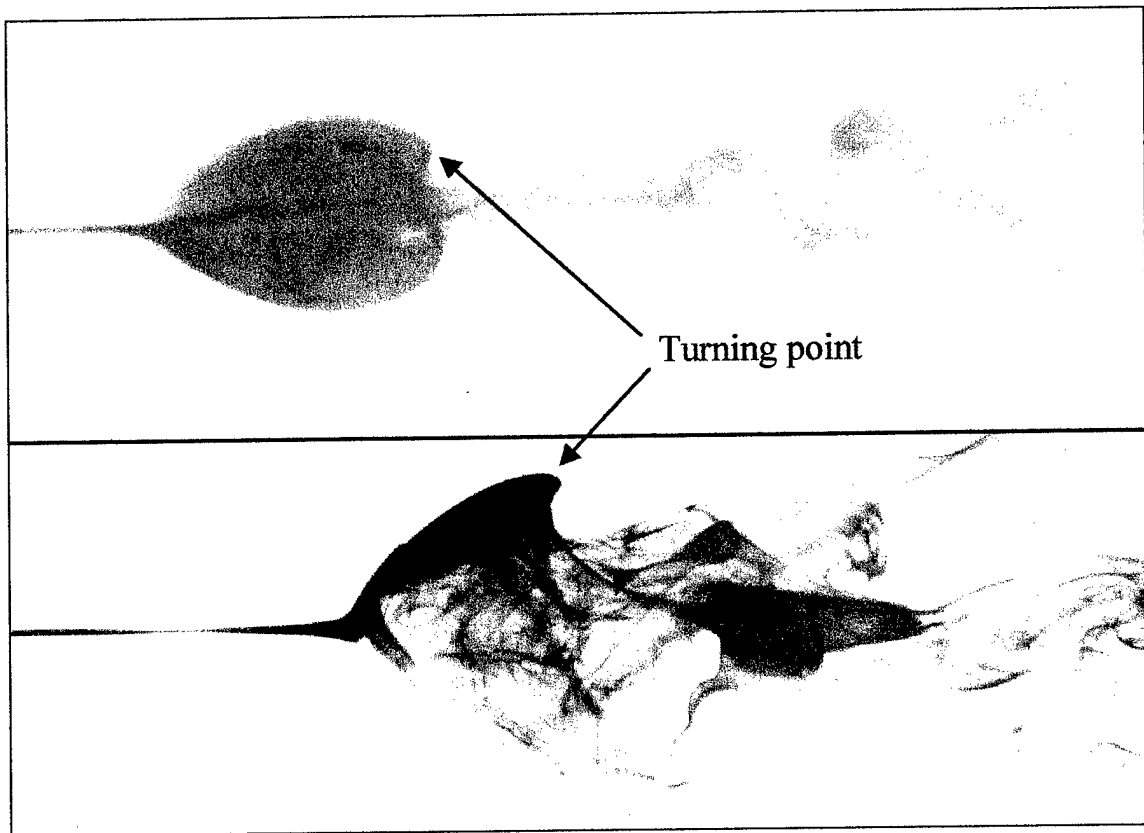


Figure 5-5 Turning in vortex breakdown experiments (*ref. 8*)

5.1.3 Laser induced fluorescence (LIF) flow visualization

A fluorescing dye is injected into the vortex tube at the leading edge of the delta wing. A laser sheet is aligned with the vortex tube along its meridional plane. When the laser sheet illuminates the dye, the dye fluoresces. Figure 5-6 shows the results of the vorticity gradient experiment using LIF. This is a similar perspective to that of the dye flow visualization except the viewing area is smaller. These LIF images show the vortex tube from 40% to 60% of the centerline wing chord. Once again, the manifestations of the vorticity gradient are present. There is radial expansion and pile-up. Pile-up is indicated by the increased intensity of the fluorescence near the radial expansion region. A turning point is visible in the second image. The third image shows the complete vortex breakdown. The results also support the conclusions of the self-induction theory of vortex breakdown.

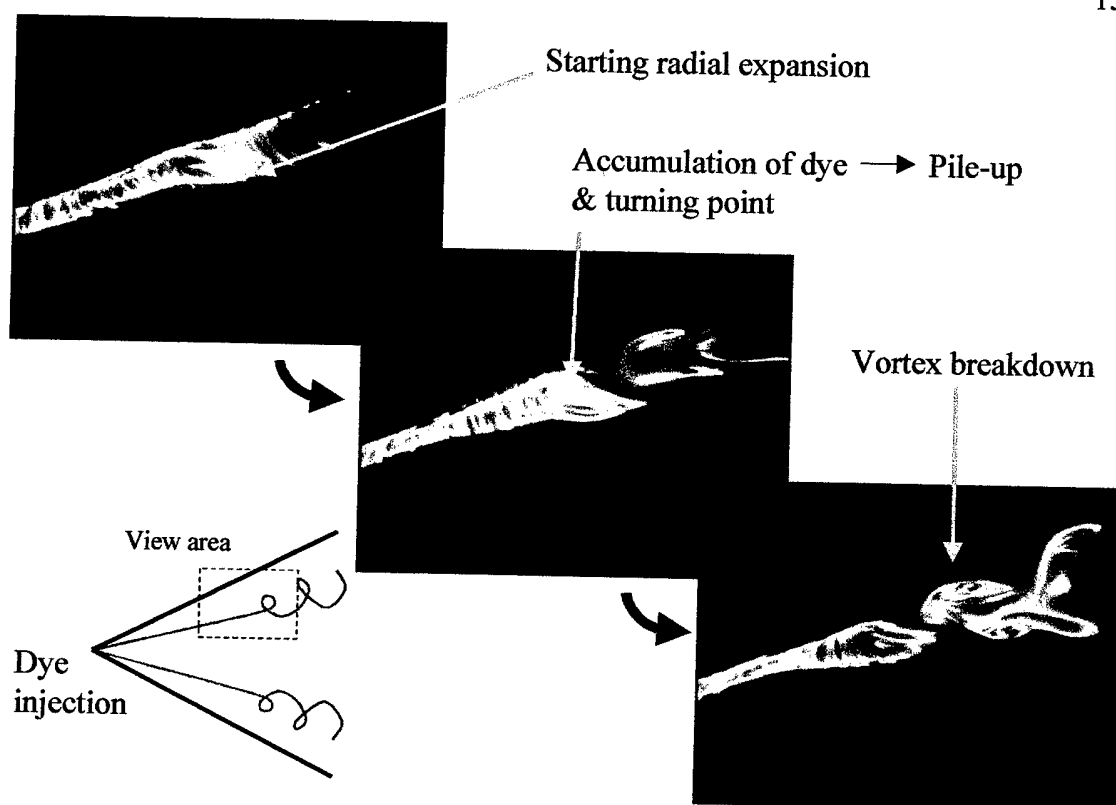


Figure 5-6 Laser induced fluorescence, delta wing vortex breakdown

5.1.4 Particle image velocimetry (PIV)

Dye flow visualization and LIF are useful tools in visualizing vortex breakdown, but they cannot tell us anything about flow velocity. Dye flow visualization and LIF show streaklines, not streamlines, unless the flow is steady. However, we can use another tool, particle image velocimetry (PIV), to find the velocity in a particular plane in the flow. PIV works by seeding the flow with particles and taking the picture of these particles at successive time intervals. Using a statistical correlation scheme, PIV software compares the images from one to the next and determines the direction and how far the particles moved. Since the time between images is known, we can find the velocity vector averaged across the time between images. Since the time between images is usually very short, we can say that the velocity vector is almost an instantaneous picture of the velocity vectors in the flow at that time. Like the LIF, a laser is used

illuminate a plane within the flow. In this case, the meridional plane of the vortex tube is illuminated.

The flow is seeded with small hydrogen bubbles that are lit up by the laser. The hydrogen bubbles are generated by electrolysis with electrodes mounted at the apex of the delta wing. Due to their low density, the hydrogen bubbles are quickly sucked into the center of the vortex tube. To minimize the effects of buoyancy of the hydrogen bubbles, the delta wing is mounted upside down within the water tunnel. Also, because the images were taken at very short time intervals, the effect of buoyancy between these time intervals is negligible. Figure 5-7 shows the setup of this experiment.

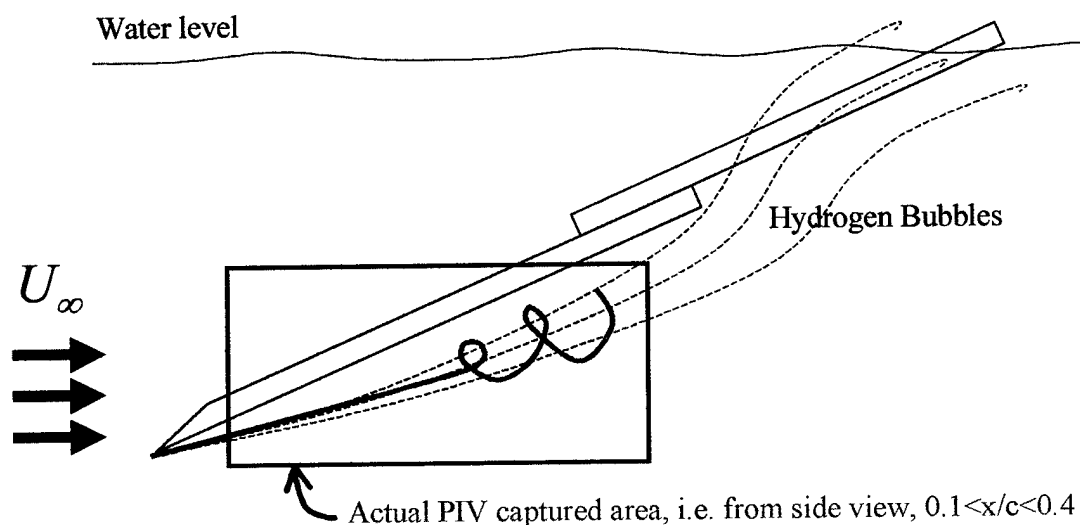


Figure 5-7 PIV experimental setup

With this setup, we can find the velocity vectors along in the meridional plane of the vortex tube. We will have axial and radial velocity data. With that data we can also calculate azimuthal vorticity.

We present the PIV results at three different times. The first image shows the vorticity gradient region as it first enters the PIV capture area. This will be t_0 . After that, images are taken every 5 milliseconds. Three images are then averaged together to make the effective time between images 15 milliseconds. The following results will show the images at t_0 , $t_0 + 45$ ms, and $t_0 + 60$ ms.

Figure 5-8 shows the velocity vectors and vorticity contour plot at t_0 . The vectors in the upper left show the velocity in the meridional plane of the vortex tube. The bottom right color contour plot shows the azimuthal vorticity. Here, the initiating vorticity gradient is clearly visible. The darker red and darker blue upstream show a clear negative azimuthal vorticity gradient $\left(\frac{\partial \omega_\theta}{\partial z} < 0\right)$. We also see radial expansion in the velocity vector plot, as the vortex tube grows radially. Pile-up is also present, since the velocity decelerates in the axial direction along the vortex tube centerline $\left(\frac{\partial u_z}{\partial z} < 0\right)$.

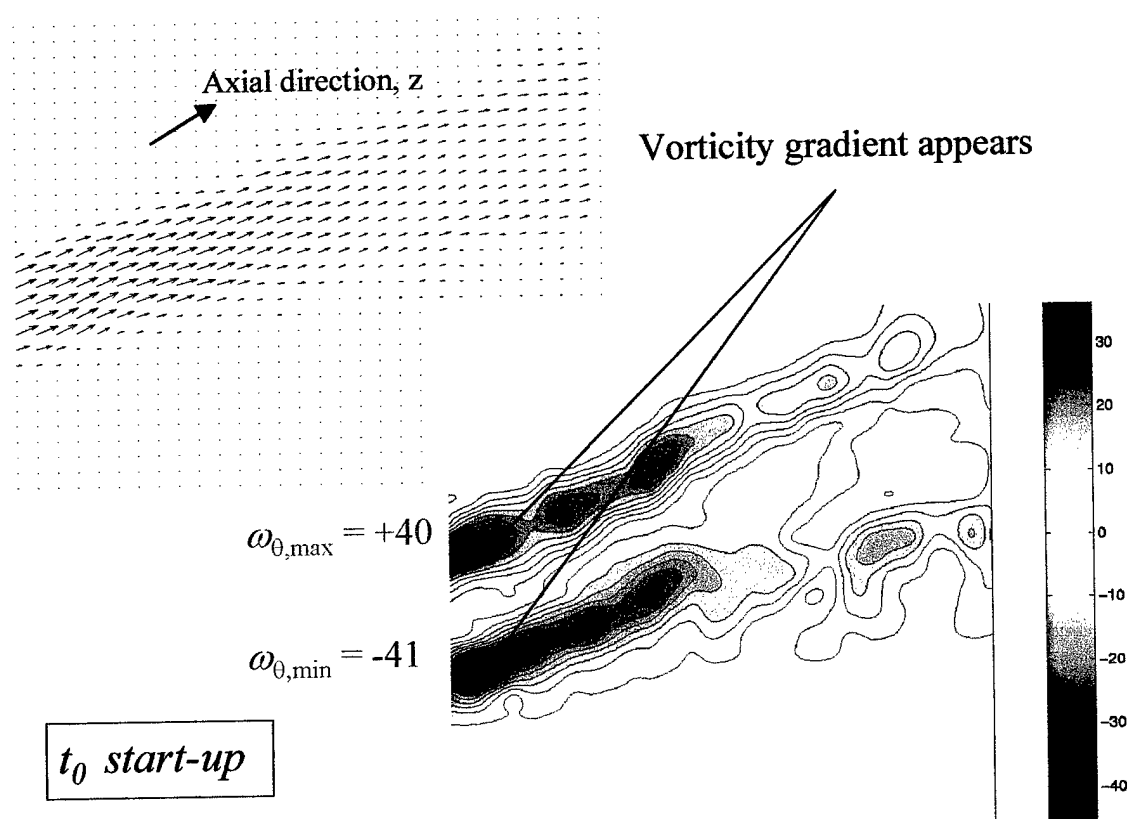


Figure 5-8 PIV results, vorticity gradient enters capture area, $t = t_0$

Figure 5-9 shows the velocity vectors and vorticity color contours at $t = t_0 + 45$ ms. Here the all features of the self-induction mechanism are visible. Radial expansion is clearly indicated in the velocity and vorticity color contour plots. Pile-up is present

and increasing in strength, as the axial velocity gradient becomes more negative in the vorticity gradient region. Now, we can see the azimuthal vorticity sign switch, as indicated in the figure. The effects of this azimuthal vorticity sign switch are evident in the velocity vector plot, as the axial velocity decreases almost to zero in the region associated with the azimuthal vorticity sign switch.

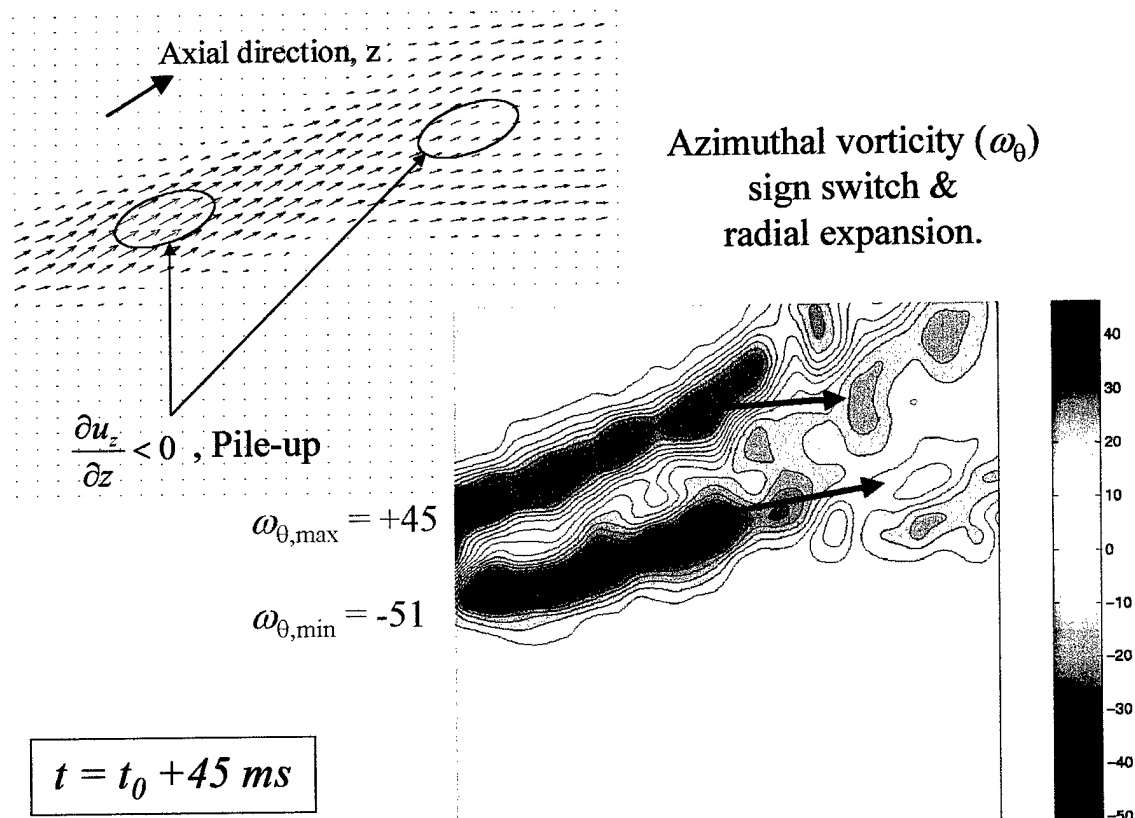


Figure 5-9 PIV results, azimuthal vorticity sign switch, $t = t_0 + 45 \text{ ms}$

Finally, in Figure 5-10, at $t = t_0 + 60 \text{ ms}$ we see the vortex breakdown established and beginning to move upstream. The azimuthal vorticity sign switch is stronger. The maximum induced backflow from this azimuthal vorticity sign switch is seeking to balance itself with the relative freestream velocity. The vortex breakdown will stop moving at the location where the induced backflow equals the relative freestream velocity. In the frame of reference of these images (body-fixed) this point will be when

the total velocity of the particles is zero at and around the vortex breakdown region center.

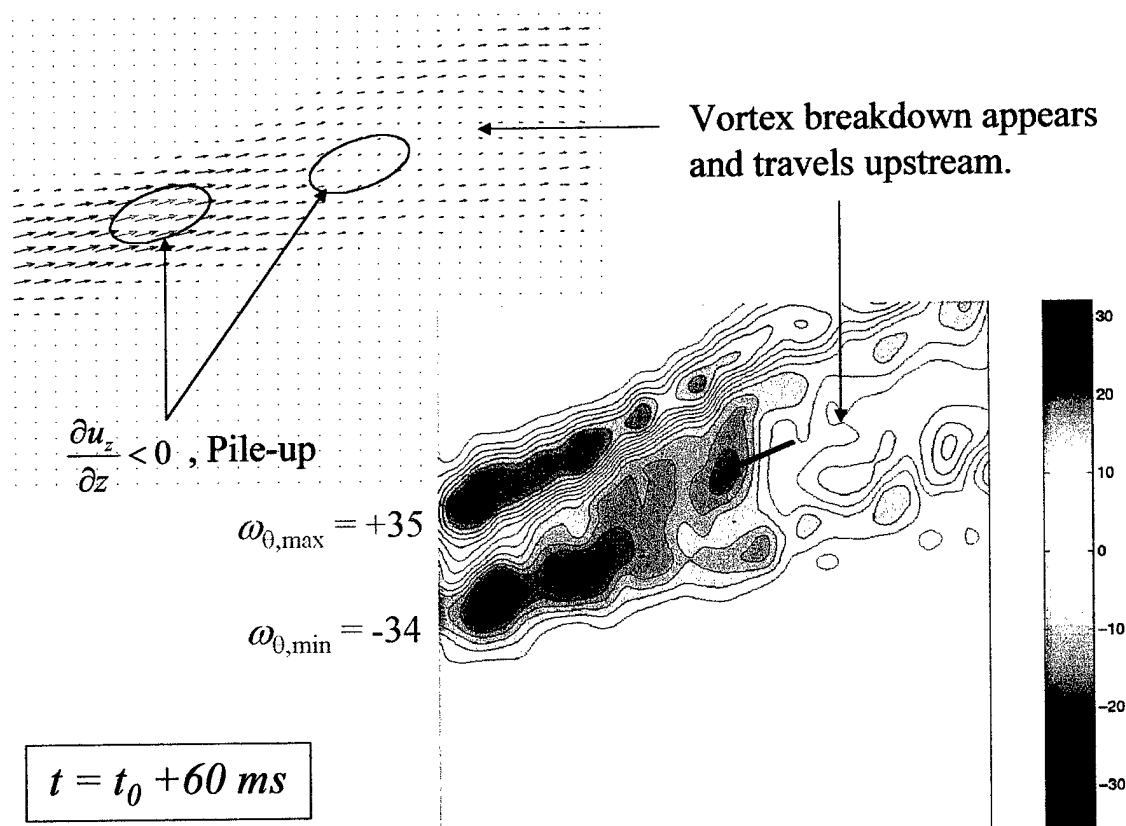


Figure 5-10 PIV results, vortex breakdown established, $t = t_0 + 60 \text{ ms}$

These PIV results capture the transient formation of vortex breakdown, as brought about by a negative vorticity gradient introduced in to the vortex tube by an increase in freestream velocity. Here we see all parts of the self-induction vortex breakdown mechanism—radial expansion, pile-up, and azimuthal vorticity sign switching.

We can compare these results directly with the vortex filament method by looking at the azimuthal vorticity output. Figure 5-11 shows the azimuthal vorticity results from $T = 1.5$ in the vortex filament simulation at $t = t_0 + 45 \text{ ms}$ in the PIV experiment. Many features are similar, though the experiment suffers from the lack of symmetry associated with delta wing vortex breakdown. Still, the vorticity gradient is clear, as is the radial expansion and azimuthal vorticity sign switch.

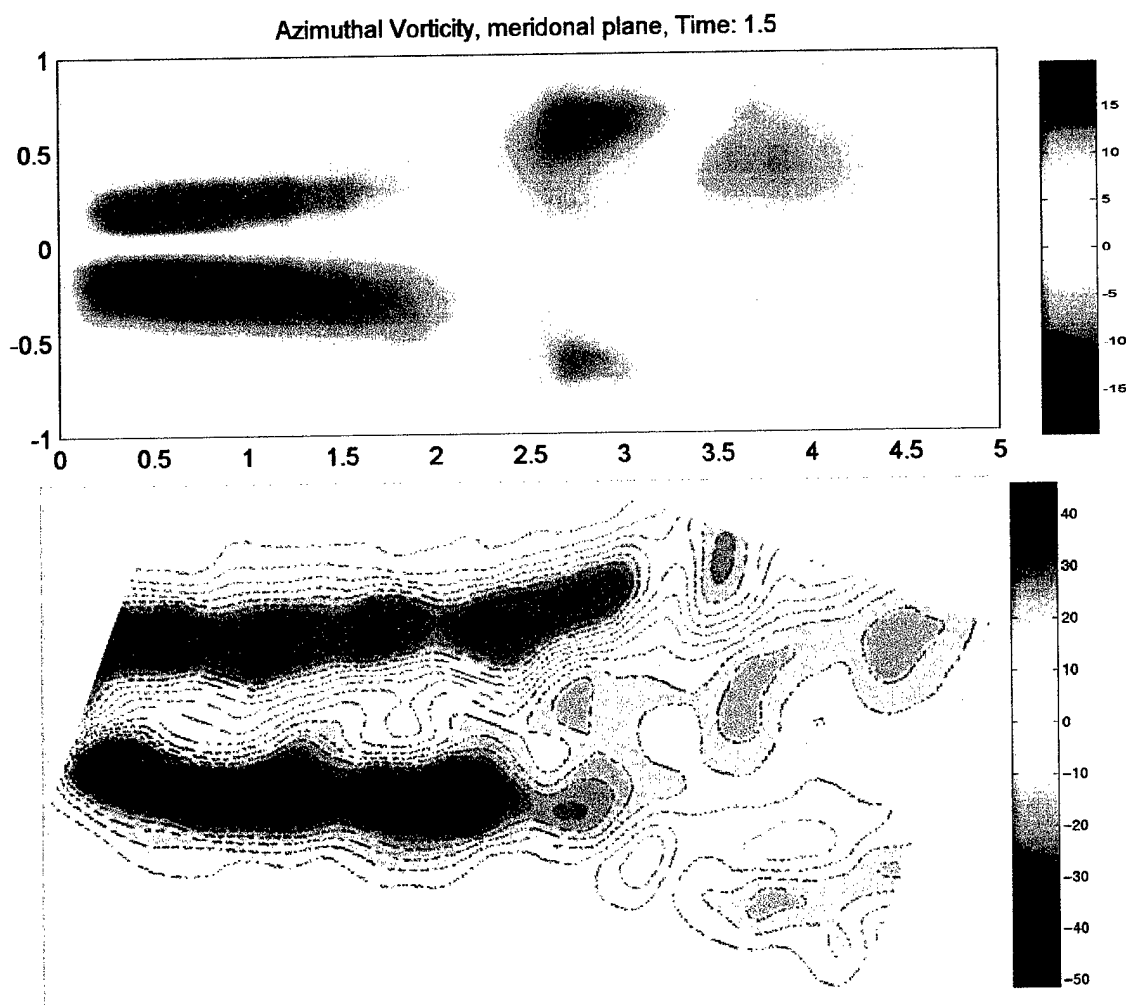


Figure 5-11 Azimuthal vorticity, simulation (top) and experiment (bottom)

We can also compare axial velocity profiles at different axial location. It is well known that the axial velocity profile in a vortex tube is jet-like upstream of the vortex breakdown. However, it changes downstream of the vortex breakdown to a wake-like axial velocity profile. If this same change occurs in the vortex filament simulation, this change in axial velocity from a jet-like to wake-like may be an inviscid mechanism in response to the velocities induced by the azimuthal vorticity in the vortex tube. Figure 5-12 compares the axial velocity at locations upstream and downstream of vortex breakdown with results from the PIV experiment and the vortex filament simulation.

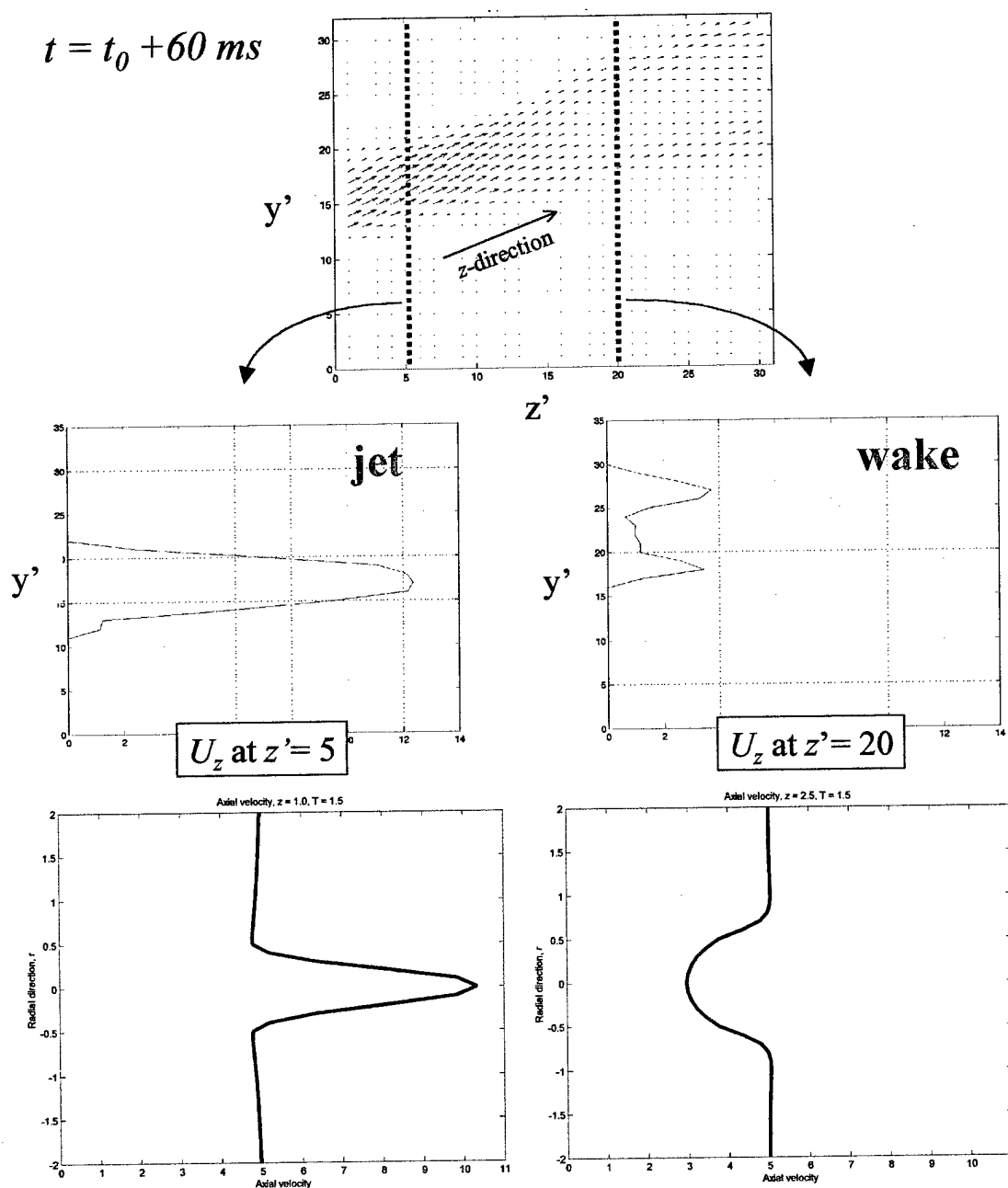


Figure 5-12 Axial velocity profile, experiment (top, middle) and simulation (bottom)

The results are clearly similar. Both the vortex filament simulation and the PIV experiment show jet-like axial velocity profiles upstream of the vortex breakdown, and wake-like axial velocity profiles downstream of the vortex breakdown. However, the simulation only models inviscid self-induction. Thus, we can conclude that these

velocity profiles are caused by induced velocities and not by viscous effects. Figure 5-13 illustrates how this might work.

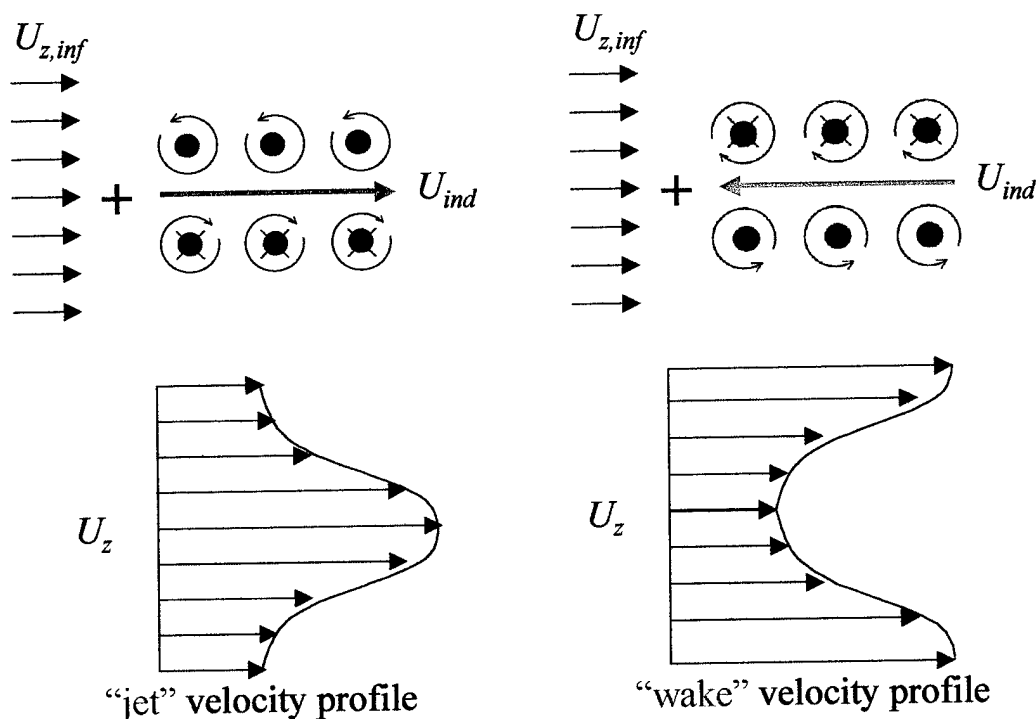


Figure 5-13 Azimuthal vorticity sign switch and velocity profile

If we linearly add the freestream velocity to the velocity induced by azimuthal vorticity components upstream of the vortex breakdown, it will enhance the freestream velocity, leading to the jet-like velocity profile that we see on the left in Figure 5-13. However, with the azimuthal vorticity sign switch downstream of the vortex breakdown, the velocities induced by the azimuthal vorticity will oppose the freestream velocity, leading to the wake-like velocity profile we see on the right.

The dye flow visualization, LIF, and PIV experiments qualitatively confirm the features of the self-induction theory of vortex breakdown. In the experiment, a vorticity gradient causes radial expansion, pile-up and vorticity sign switching, just as in the vortex filament simulation. This provides further evidence that vortex breakdown is initiated by a vorticity gradient that manifests itself in an inviscid self-induction feedback mechanism.

5.2 Case 2, vortex breakdown due to vorticity gradient in vortex tube with fixed circulation

The author performed this experiment for the purposes of investigating how vortex blowing could affect vortex breakdown. The initial goal was to delay vortex breakdown through periodic blowing along the leading edge of the delta wing in order to perturb the vortex core. However, it was observed that this blowing, in fact, caused vortex breakdown. The reason became evident in light of the self-induction theory. If a vortex tube is acted upon by a pulsed blowing that causes a perturbation along its core, a vorticity gradient forms along the axis of the core at the perturbation. Maxwothy, Mory, and Hopfinger in *ref. 26* (among others) recognize that these types of perturbations in the form of waves can lead to vortex breakdown, though they do not comment on the importance of the vorticity gradient and self-induction.

Figure 5-14 illustrates how a perturbation in the vortex tube causes a negative axial vorticity gradient along the main axis of the vortex tube.

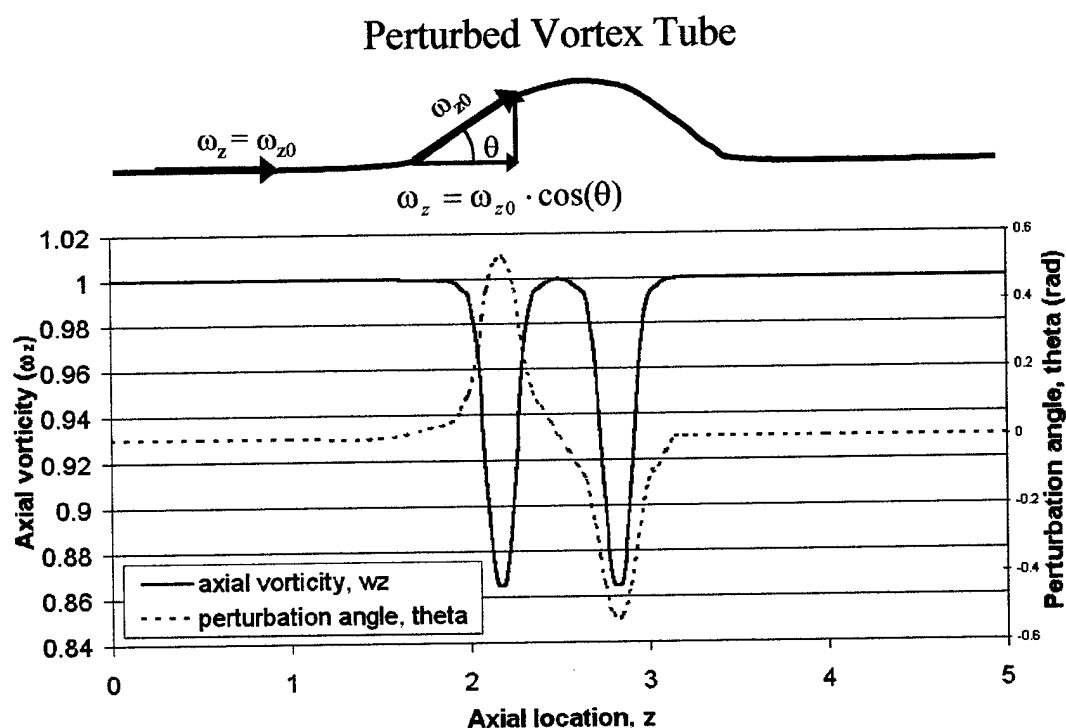


Figure 5-14 Vorticity gradient caused by vortex tube perturbation

In this simplified example, the vorticity along the vortex tube is a constant value, ω_{z0} , and entirely in the axial direction. When the vortex tube is perturbed, the angle between the tube and the main axis of the vortex changes by angle θ , in the region of the perturbation. This causes a local change in the axial vorticity in the region of the perturbation, according to $\omega_z = \omega_{z0} \cdot \cos(\theta)$

This vorticity gradient, if sufficiently strong will lead to vortex breakdown in the region of that vorticity gradient. In this experimental case, a periodic jet on the leading edge of the delta wing momentarily perturbs the vortex on the upper part of the delta wing. Figure 5-15 shows a diagram of this setup. This perturbation leads to an immediate vortex breakdown in the region of the perturbation. A secondary effect (but the main effect we are showing here) is that the lower vortex is also perturbed. This is a weaker perturbation, so the resulting vortex breakdown happens slowly enough that the breakdown process can be captured in the following images. As the perturbation convects downstream, the features described by the self-induction mechanism become visible. Figure 5-16 shows the dye flow visualization over time of this perturbation leading to a localized vortex breakdown.

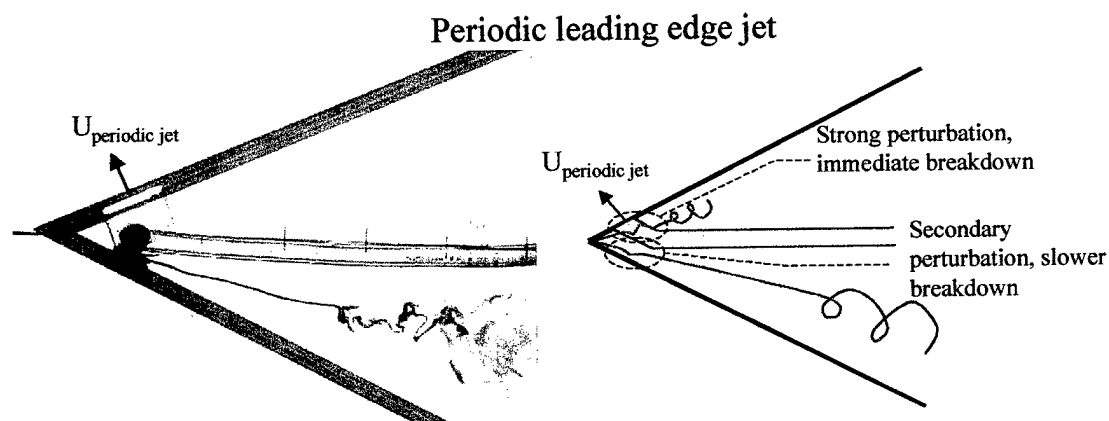


Figure 5-15 Vortex perturbing periodic jet

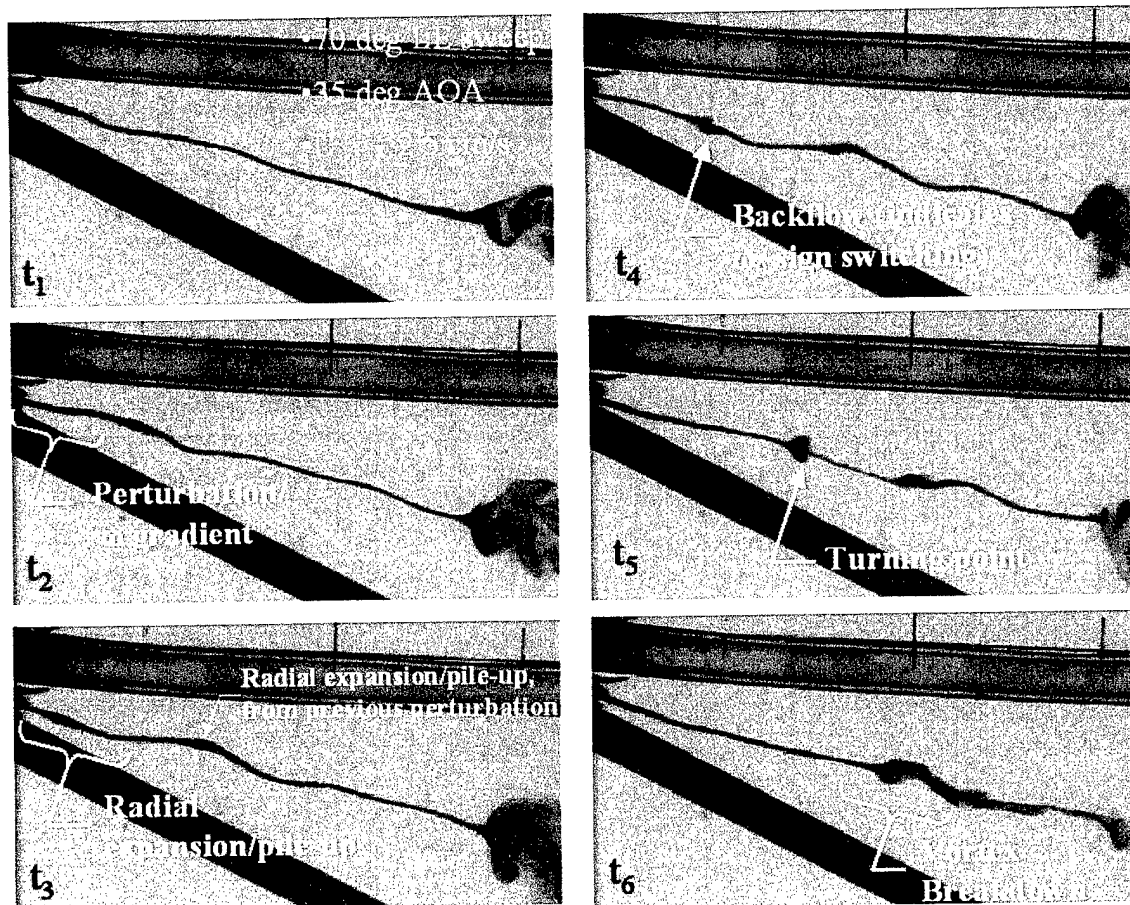


Figure 5-16 Vortex breakdown in perturbed vortex tube

This provides further evidence that vortex breakdown is initiated by a negative vorticity gradient and manifests itself in a feedback mechanism that includes radial expansion and contraction, pile-up, and azimuthal vorticity sign switching (which must be present if there is backflow relative to the freestream velocity). These mechanisms culminate in the turning point where there is a sign switch in the axial vorticity. This axial vorticity sign switch is associated with counter rotating flows that is very quickly disrupted due to the formation of shear layers and the resulting small scale turbulence, which is visible downstream of the main breakdown location.

5.3 Case 3, vortex breakdown in cylinder with rotating end wall

The experiment with the delta wing in the water tunnel was very useful for showing the results of an explicitly specified vorticity gradient. However, the delta wing

disturbs the symmetry of the vortex breakdown, while the vortex filament simulation is inherently symmetric. We will now look at the results from vortex breakdown in a cylinder in order to compare the results with more symmetric cases. This experiment was performed by M.P. Escudier and is published in *ref. 27*. This experiment generates a vortex by rotating the end wall in a cylindrical container filled with water. This rotating end wall causes rotating and recirculation flow due to Ekman layer pumping. At the center of this rotating flow, a vortex forms which can undergo vortex breakdown. Figure 5-17 shows a diagram of the experiment setup.

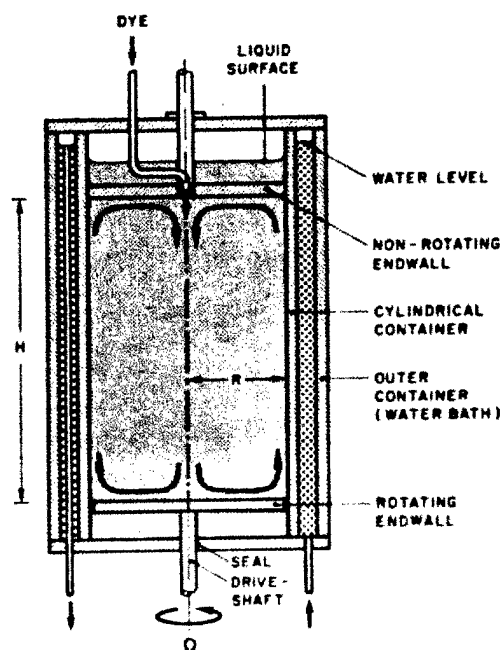
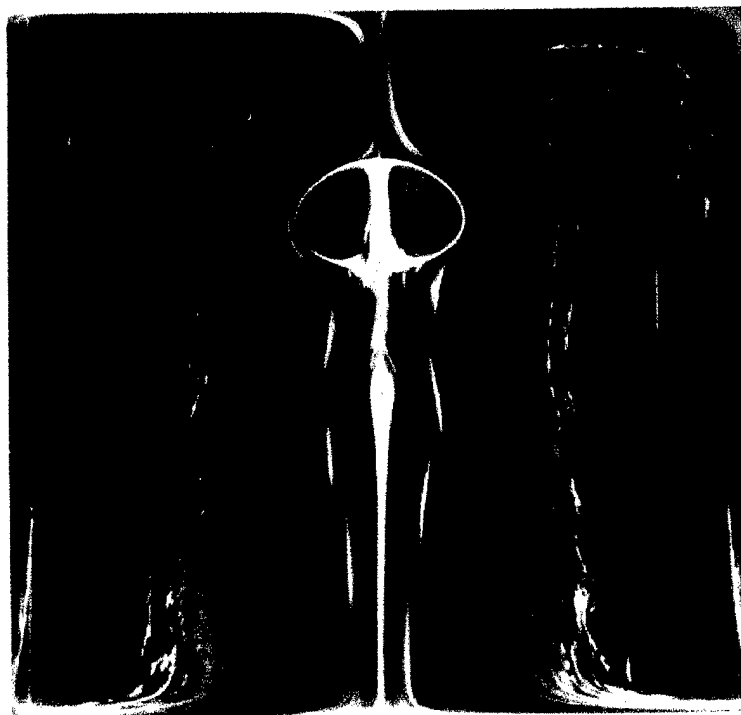


Figure 5-17 Vortex breakdown in cylinder, experiment setup

Using this setup, experiments were performed at various ratios of cylinder height, H , to cylinder radius, R , and at various Reynolds number. In this case, Reynolds number is based on the angular velocity of the rotating end wall, Ω , the radius of the cylinder, R , and the kinematic viscosity of the fluid, ν , giving $Re = \frac{\Omega \cdot R^2}{\nu}$. Flow observations are made using laser-induced fluorescence. The flow presented is steady, so the streaklines from the dye correspond to the streamlines. Figure 5-18 shows the results at $H/R = 2$ and $Re = 1854$.



d 1854

Figure 5-18 Vortex breakdown in cylinder, $H/R = 2$, $Re = 1854$

This compares well with the instantaneous streamline plot from the present vortex filament method, as presented in Figure 5-20. In both results, the radial expansion, pile-up, and backflow near the main vortex breakdown location is evident. Also, what is apparent is a second region of radial expansion downstream of the main breakdown location. This is clear in Escudier's experiment and also in the vortex filament simulation result as Figure 5-20 illustrates. This indicates the formation of a second vortex breakdown downstream of the first. Since the vortex filament simulation captures this result, it too, is likely caused by a vorticity gradient, working through the inviscid feedback mechanism. This can be described by the self-induction theory of vortex breakdown. Due to another ω_θ sign switch associated with the radial contraction of the vortex tube, as seen in Figure 5-19, the sign of ω_θ returns to its initial value, and through the repetitive inviscid mechanism, the secondary vortex breakdown and the secondary ω_θ appears. The capturing of the secondary vortex breakdown by the inviscid simulation

may imply that the inviscid process can persist downstream of the primary vortex breakdown.

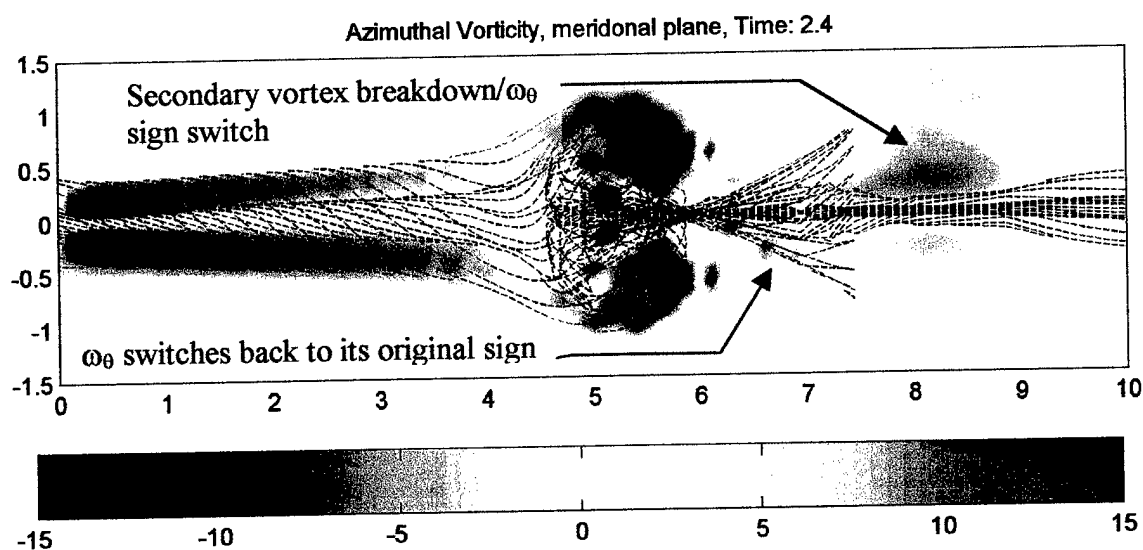


Figure 5-19 Azimuthal vorticity and secondary vortex breakdown, $T = 2.4$

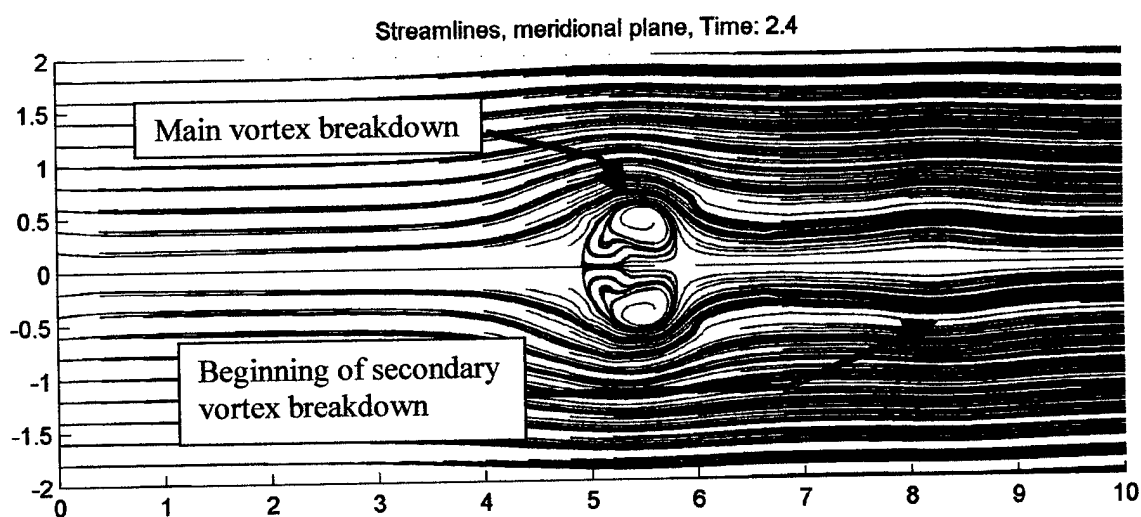


Figure 5-20 Instantaneous streamlines, vortex filament simulation, $T = 2.4$

5.4 Case 4, Navier-Stokes solution to case 2

The Escudier experiment in the cylinder provides only streakline results. Masanori Kikuchi (*ref. 28*) took the conditions of this experiment and calculated a numerical solution using the full Navier-Stokes equation. The benefit of this approach is

that we can get data that the physical experiment cannot provide. Because of the relatively low Reynolds numbers involved, the Navier-Stokes equations can be solved to a very precise degree of accuracy, giving us confidence in the solution. The Navier-Stokes equations capture all possible physics in this problem, including the effects of viscosity. However, if the results from the Navier-Stokes solution compare well with the vortex filament simulation, which does not include the effects of viscosity, it can be concluded that the vortex breakdown process is nearly inviscid.

The results for the numerical Navier-Stokes solution for the Escudier experiment are presented in the following figures. These are for the case of $H/R = 2.5$ and $Re = 2765$. Figure 5-21 shows the streamlines from the numerical solution to the Navier-Stokes Equation (L) and Escudier's experiment (R). The results compare well with each other, as one would expect. Radial expansion and contraction and backflow are clear in both results. The turning point is clearly visible in Escudier's experimental results, though it is not as clear in the simulation results. Still, secondary breakdown exists in both cases. Overall, the Navier-Stokes simulation compares well with the results of the experiment. Thus, we can be confident that the data calculated with the numerical solution will also be accurate.

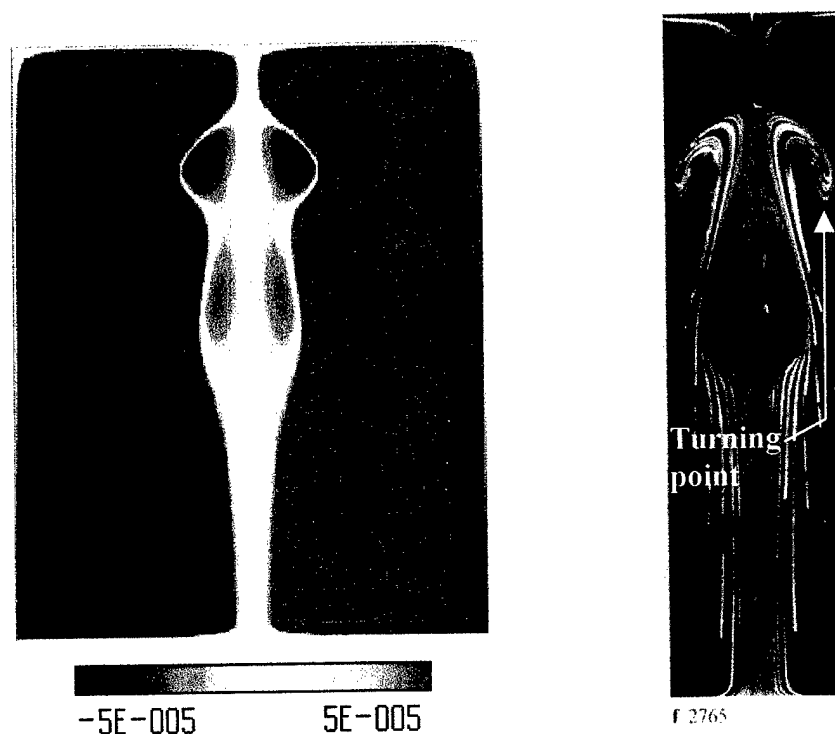


Figure 5-21 Streamlines, Navier-Stokes Simulation (L) and Experiment (R)

Figure 5-22 shows the azimuthal, axial, and radial vorticity data for the Navier-Stokes simulation of the Escudier experiment. These results present the data on the meridional half-plane. Here we see many of the same features as we did in the vortex filament simulations. Namely, vorticity sign switching is clearly present in the azimuthal and radial vorticity. In the axial vorticity, there is no sign switching, though there is a marked decrease in axial vorticity in the vortex breakdown region. This may be due to the weak axial flow rate and the constraints of the cylinder walls in close proximity to the vortex breakdown location. It may also be that, with viscous dissipation possible, any axial vorticity sign switch is quickly worn away by these viscous forces, as was mentioned in the original discussion of the turning point. Even if this is the case, this viscous action does not cause vortex breakdown; it simply wears away some of the indicators of vortex breakdown, after that breakdown has occurred.

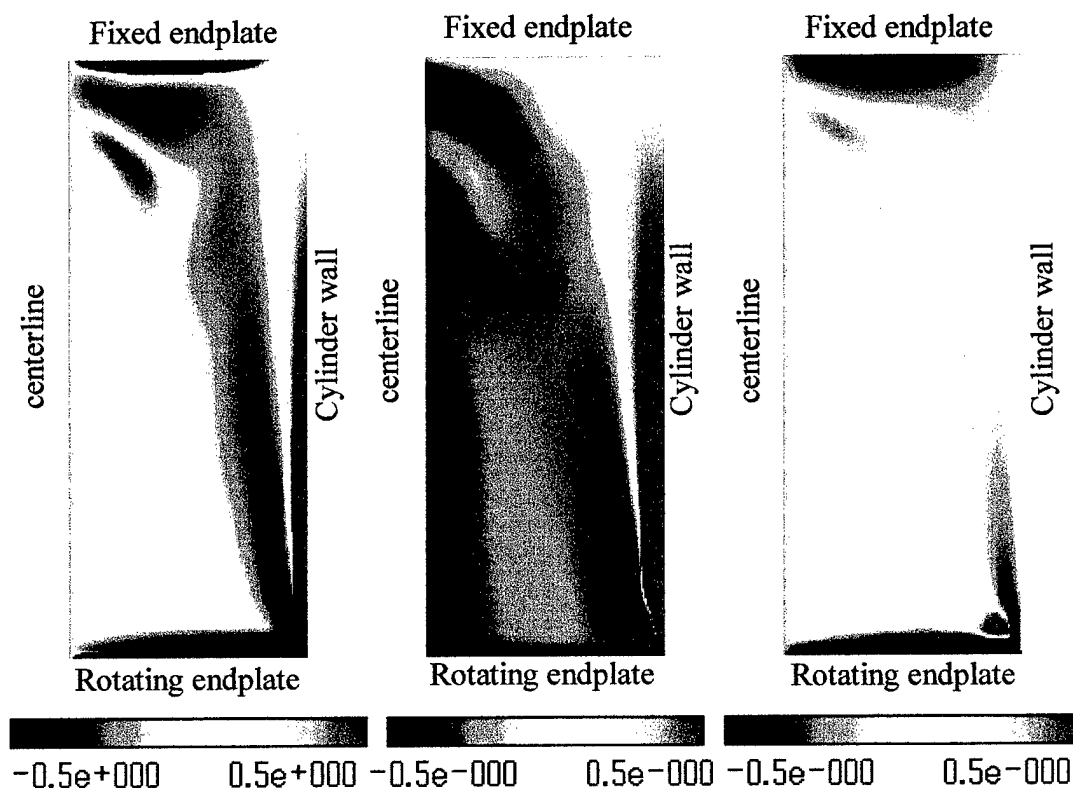


Figure 5-22 Meridional Plane Data, Navier-Stokes Simulation, ω_θ (L), ω_z (C), ω_r (R)

From the Navier-Stokes solution, a three-dimensional plot of vortex lines can be constructed, as shown in Figure 5-23. This is different than the way vortex lines are constructed in the vortex filament simulation, since in the vortex lines are implicit the simulation in the vortex filament method, while in a Navier-Stokes solution they are found through post-processing of the raw data. Still, the results compare well with the vortex filament simulation in terms of the self-induction theory of vortex breakdown. In the Figure 5-23 result, pile-up and radial expansion are clear. Also, the location of the azimuthal vorticity sign switch is visible when you decompose the vortex line into vector components. Compare the result from the Navier Stokes numerical solution to the vortex filament method results at $T = 0.9$, as in Figure 5-24.

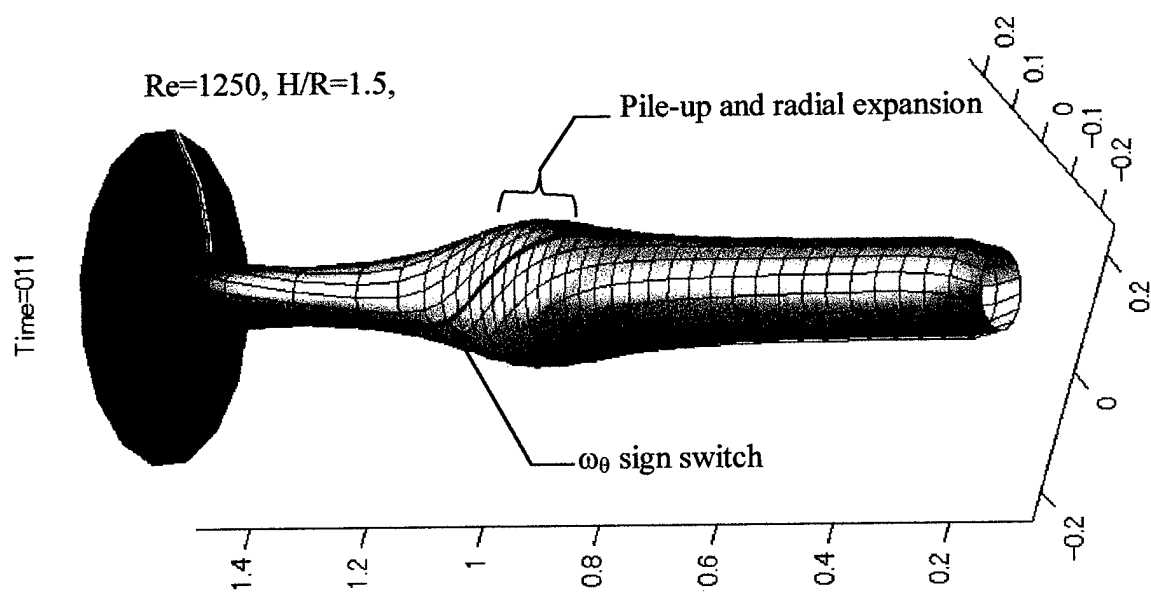


Figure 5-23 Rendered vortex tube, numerical solution to Escudier's experiment

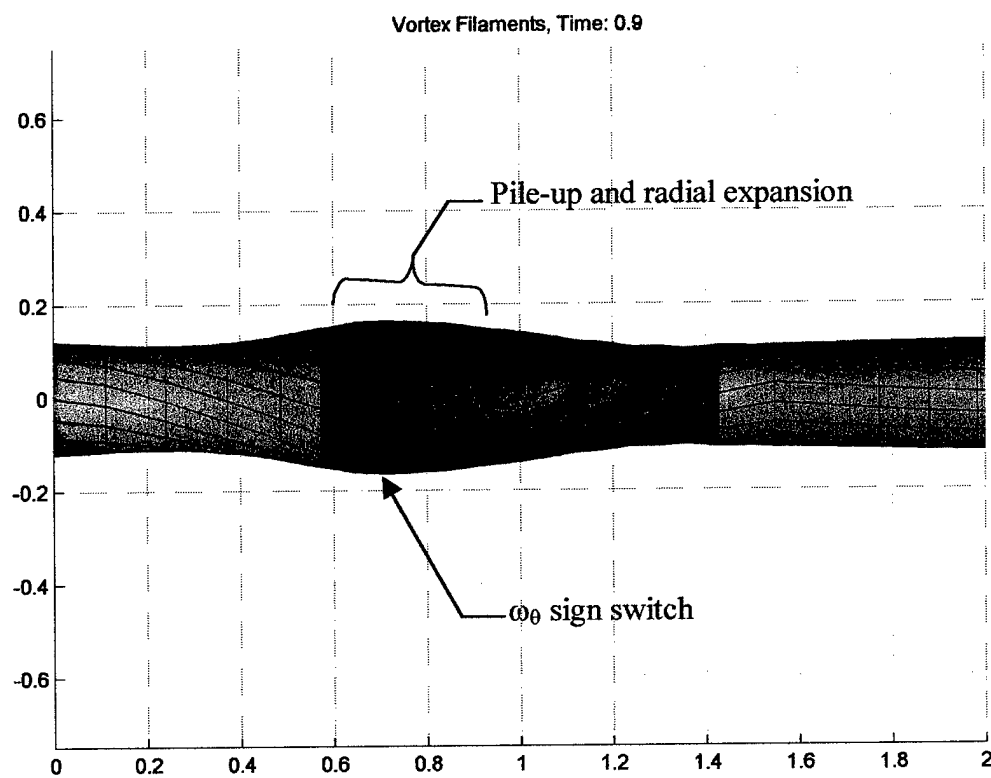


Figure 5-24 Rendered vortex filament simulation results, $T = 0.9$

While there is no axial vorticity sign switch in the Navier-Stokes solution to Escudier's experiment, there are still similarities between the axial vorticity profile in the Navier-Stokes simulation and the vortex filament method simulation. Figure 5-25 presents the axial vorticity along the vortex tube's axis at various radial locations. The trends in axial vorticity are very similar, with the peak axial vorticity occurring along the centerline. That peaks in axial vorticity decreases near the vortex breakdown region before increasing and then returning to zero downstream of the breakdown location. The peaks decrease farther away from the centerline in both simulations. The jaggedness in the vortex filament simulation solution, Figure 5-25 (R), is due to the resolution of the grid that the vorticity data is calculated on. Calculating this data is not implicit to the vortex filament method, though it is for the Navier-Stokes simulation. Still, the trends compare well with each other, with the major difference being the absence of the axial vorticity sign switch, which may be the result of viscosity.

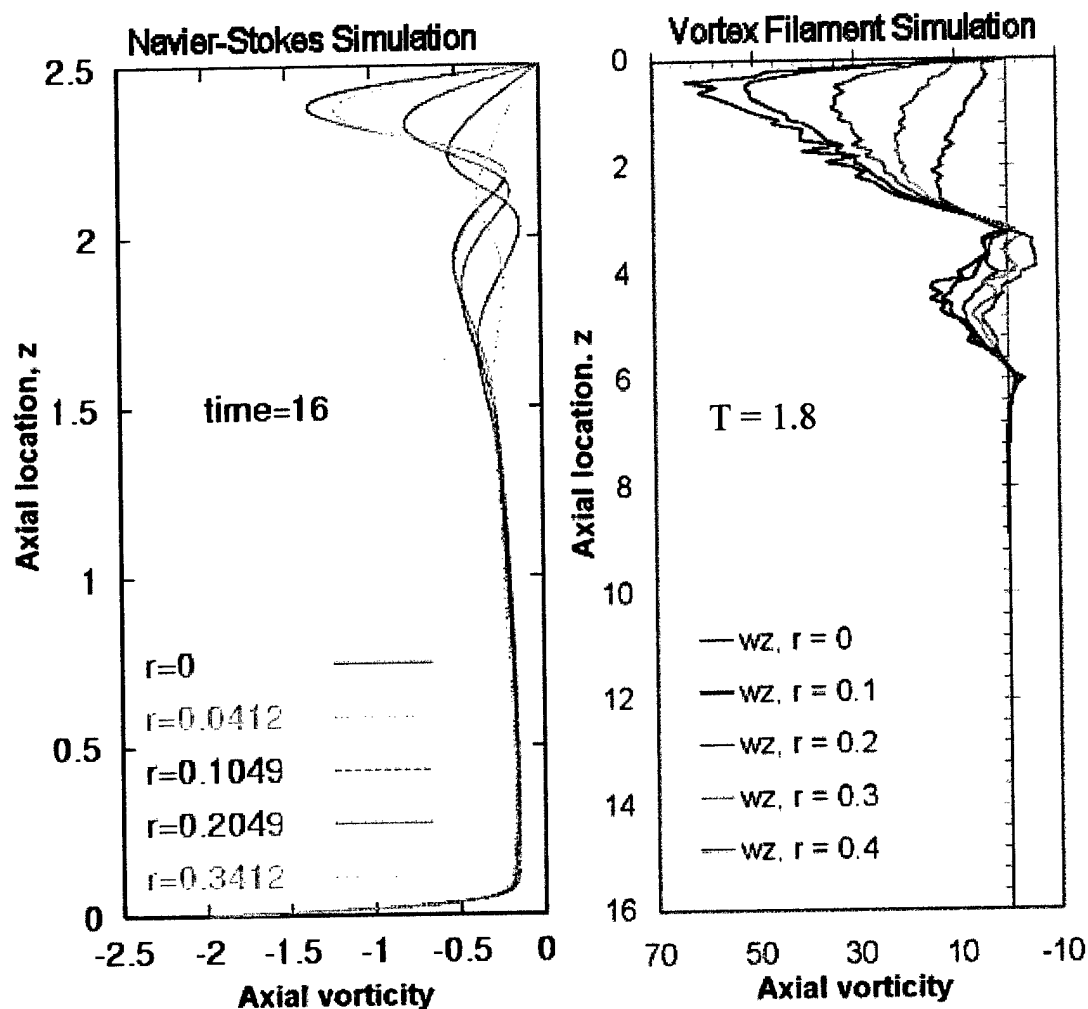


Figure 5-25 Axial vorticity at various radial location along vortex tube, Navier-Stokes Simulation (L) and vortex filament simulation (R)

5.5 Other experimental and computation evidence

Other experiments and computational studies give support to the components of the self-induction theory of vortex breakdown. They provide specific examples of pile-up, radial expansion, and azimuthal and axial vorticity sign switching.

Experiments with vortex flows and shock waves show that vortex breakdown occurs immediately downstream of the location where a vortex crosses a shock wave (see *ref. 29* for details). Figure 5-26 shows a diagram of this. In terms of the self-induction theory of vortex breakdown, the shock causes a strong axial vorticity gradient in the

vortex tube, as a result of the axial velocity decrease downstream of the shock. This also causes pile-up within the vortex tube. All of this begins the inviscid feedback mechanism that leads to steady state vortex breakdown.

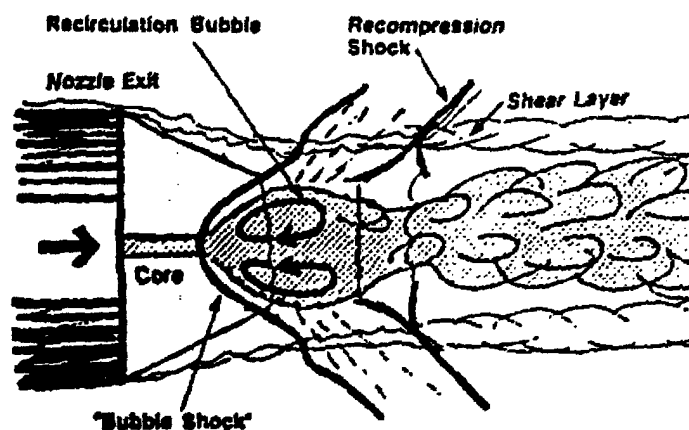


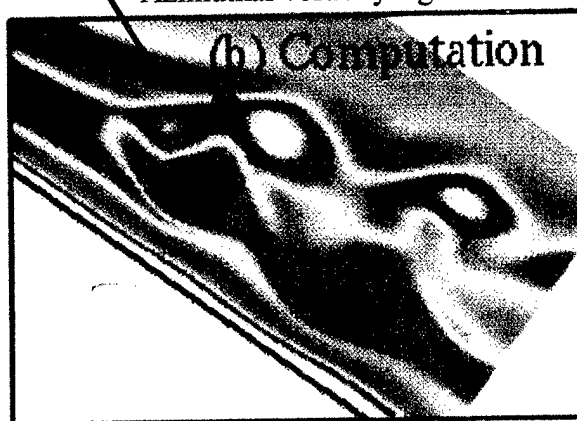
Figure 5-26 Shock wave/vortex interactions (*ref. 29*)

A computational study by M.R. Visbal provides detailed vorticity data for vortex breakdown (see *ref. 30* for details). He compares his computational results to experiments by Shih and Ding. These results show the azimuthal vorticity sign switch in the region of vortex breakdown, confirming the same results in the vorticity gradient experiment of S. Srigarom (*ref. 4*) and the current vortex filament simulation. Figure 5-27 shows these results.

(a) Experiment, Shih and Ding



Azimuthal vorticity sign switch

Figure 5-27 Azimuthal vorticity sign switch (*ref. 30*)

Visbal's computational results also show the axial vorticity sign switch. Figure 5-28 shows these results in both the meridional and cross flow plane. Visbal interprets these results by saying, "... negative axial vorticity concentrations may be the result of the severe upstream tilting of part of the incoming vorticity by the strong reverse flow induced by the spiral" (*ref. 30*). This is exactly what the vortex filament simulation shows.

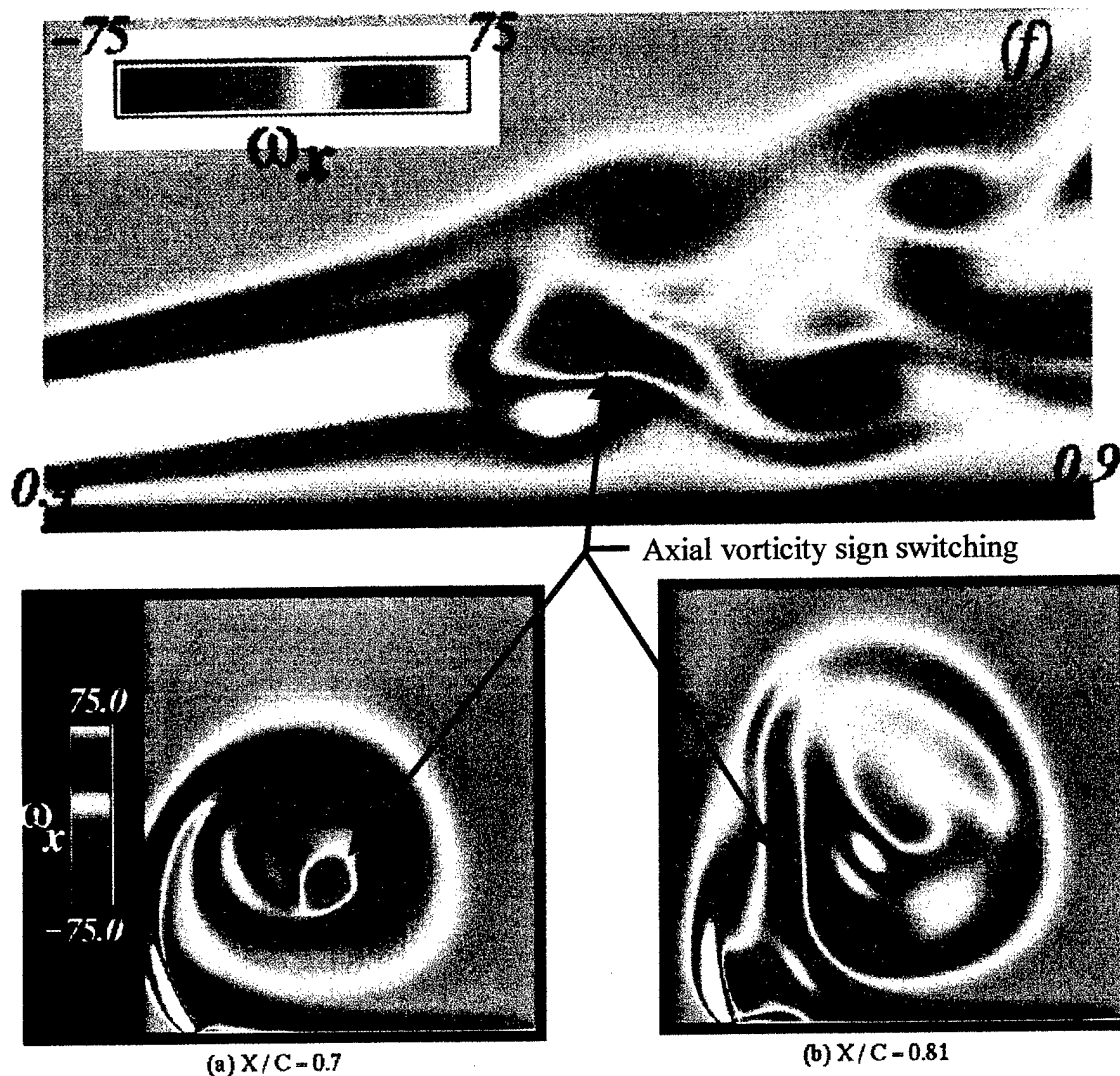


Figure 5-28 Axial vorticity sign switch, meridional (top) and cross flow (bottom) plane (ref. 30)

The experimental data and the results from other computer simulations compare well with the results from the vortex filament method. These results also fit well into the self-induction theory of vortex breakdown. This gives further support to that theory, indicating that vortex breakdown is an inviscid phenomenon, caused by a vorticity gradient, and brought about by an inviscid feedback mechanism consisting of radial expansion and contraction, pile-up, and vorticity sign switching. With this knowledge of the mechanism that may lead to vortex breakdown, one can better formulate ways to

weaken, prevent, or delay vortex breakdown and its corresponding negative effects on aircraft flight.

5.6 Vortex breakdown control experiments and the self-induction theory

The self-induction theory of vortex breakdown provides a clearer picture of the unsteady formation of vortex breakdown. It describes an inviscid feedback mechanism that starts from a negative vorticity gradient and includes radial expansion and contraction, pile-up, and vorticity sign switching. If a negative vorticity gradient and these mechanisms lead to vortex breakdown, then the interruption of one or more of these mechanisms may delay, weaken, or prevent vortex breakdown. Thus we can control vortex breakdown by affecting the vorticity gradient, the radial expansion and contraction, pile-up, or the vorticity sign switching. Various researchers have successfully manipulated the location of vortex breakdown over delta wings and other experimental apparatus. We will look at several of these experiments and discuss them in terms of the self-induction theory of vortex breakdown.

5.6.1 Vorticity gradient

If vortex breakdown is initiated by a vorticity gradient, then anything that would change that vorticity gradient should change the location of the vortex breakdown. As was previously described, a velocity gradient over a wing can lead to a vorticity gradient. Thus, if that velocity gradient (or the associated adverse pressure gradient) is modified, the vorticity gradient will also be modified. A weaker vorticity gradient leads to a more downstream vortex breakdown location, so a weaker velocity gradient should delay vortex breakdown.

This is what happens in the experiments of A. Mitchell et al. See *ref. 31* for details. Through symmetrical and asymmetrical blowing along the trailing edge of a slender delta wing, they were able to delay vortex breakdown. In terms of the self-induction theory, this can be understood in terms of a change in the vorticity gradient. Trailing edge blowing changes the velocity profile over the delta wing and weakens the adverse pressure gradient over the leeward surface of the wing. This corresponds to a

decrease in the velocity gradient and a corresponding decrease in the vorticity gradient. As the self-induction theory predicts, the location of vortex breakdown, at a given angle of attack, should move downstream when the trailing edge blowing is active.

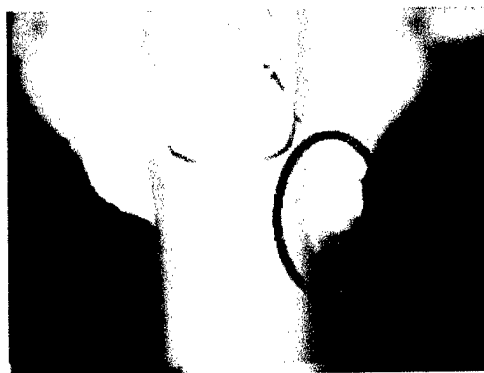
Another way to change the vorticity gradient is to change the shape of the leading edge near the leading edge tip. This is where most circulation in the vortex tube originates, so it will be the most sensitive to small changes in configuration. Adding fillets or rounding off sharp edges will reduce the circulation in the vortex tube, while leaving larger flow properties like the velocity gradient over the wing and the strength of the vortex sheet unchanged. Thus, the total amount of circulation is reduced, and the maximum possible induced backflow velocity is also decreased, resulting in a vortex breakdown location either further downstream over a wing at a fixed angle of attack, or increasing the critical angle of attack where vortex breakdown will first occur at a given location over the wing.

This is what is done by S. Srigrarom in an experiment designed to use the results of the self-induction theory to delay vortex breakdown. See *ref.4* for details about this experiment. The experiment compares the breakdown location over an F/A-18 model (a) with the leading edge of the strake left sharp and (b) with the leading edge rounded using clay. Figure 5-29 shows the modification to the F/A-18 model. This rounded leading edge should reduce the circulation in the vortex tube and therefore delay vortex breakdown.

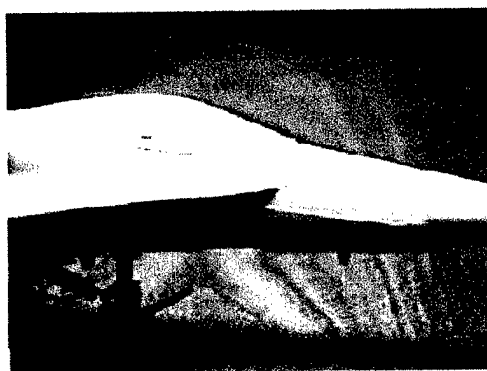
The attachment of clay on F-18 :



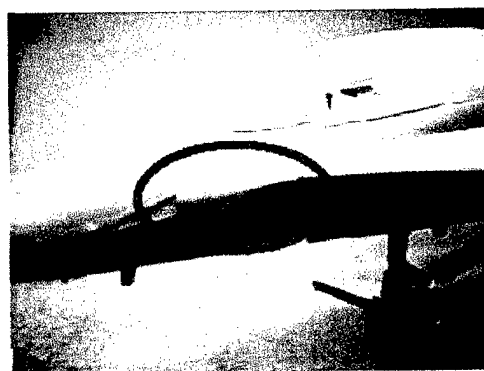
The entire view of F-18.



F-18 Front view, showing clay on right side



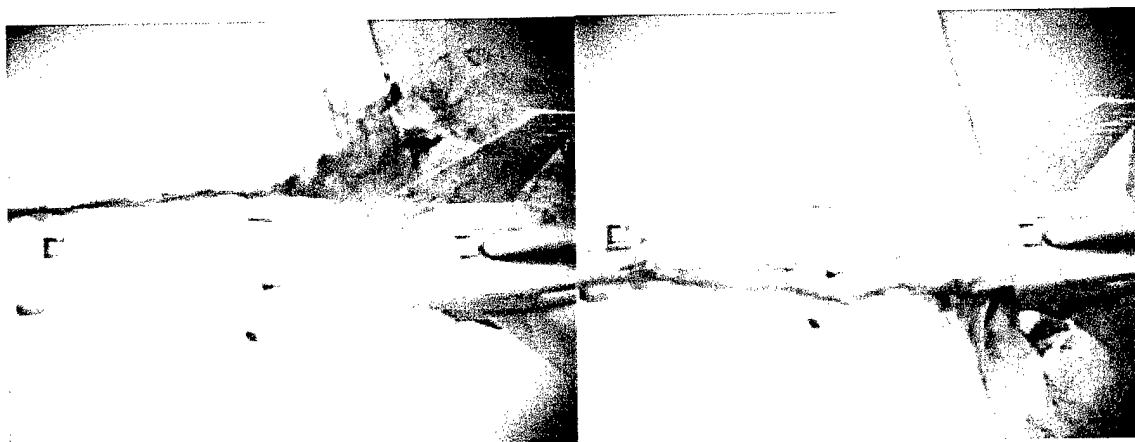
Left side, NO clay attached



Right side, clay attached at the juncture of LEX and the body.

Figure 5-29 F/A-18 Leading edge strake modification (*ref.4*)

The modified F/A-18 is placed in a water tunnel at 25 degrees angle of attack with a tunnel speed of 5 cm/s. The aircraft is aligned such that there is no yaw angle. Dye is used for flow visualization. The vortex breakdown location is noted by rapid radial expansion, backflow, and downstream turbulence. Figure 5-30 shows the results. The image on the left, with the sharp leading edge extension, shows the normal vortex breakdown location for this angle of attack at approximately $0.3c$. However, with the rounded leading edge (right image) there is no visible vortex breakdown. There is only a disruption of the vortex tube when it encounters the vertical tail.



Clean strake LE at root

Rounded strake LE at root

Figure 5-30 Delay in vortex breakdown location with rounded strake LE (*ref. 4*)

Reducing the circulation in the vortex tube may delay vortex breakdown, but it will also reduce the high axial velocities and corresponding low pressures that occur upstream of the vortex breakdown location and provide the increase in lift associated with vortex flows over wings. Still, the vortex will exist intact over a larger area, and the downstream turbulence that leads to high-cycle fatigue will be reduced, so the overall effect may still be positive. The net effect will require further testing.

5.6.2 Radial Expansion

Radial expansion is one of the first manifestations of a vorticity gradient in a vortex flow. If this radial expansion can be limited or delayed, it will delay the formation of vortex breakdown. In a vortex generated in a tube, the walls of the tube constrain the radial expansion. If the radius of the tube is sufficiently small, as compared to the vortex core diameter, radial expansion, and in turn, vortex breakdown can be delayed. Similarly, over a delta wing, a vortex sheet develops that constrains the radial expansion of the vortex core. Figure 5-31 shows this vortex sheet as it separates from the leading edge of a delta wing.

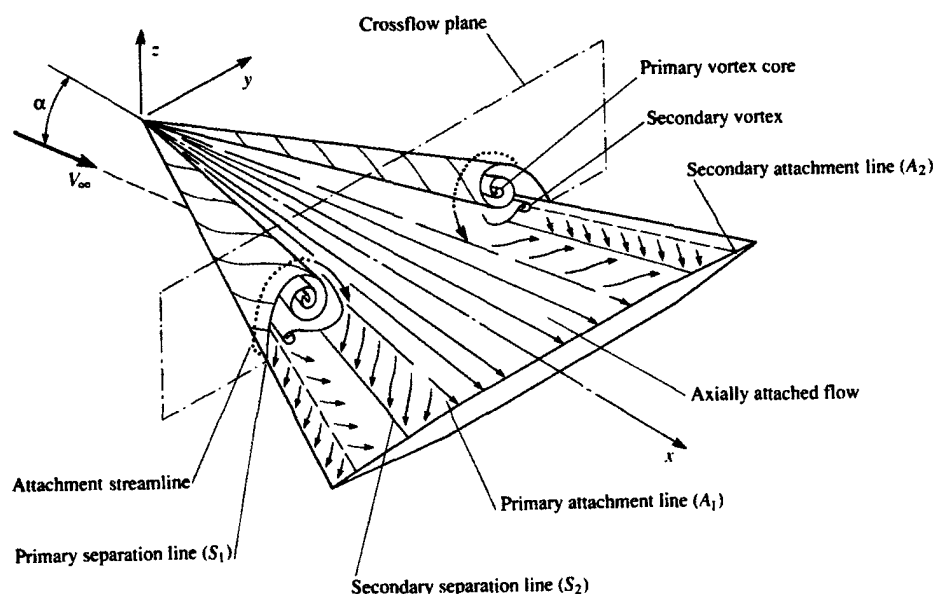


Figure 5-31 Vortex flow over a delta wing (*ref. 9*)

The difference between this vortex sheet and the walls of a pipe is that the vortex sheet is not solid. Thus the strength of the vortex sheet will determine what amount of radial expansion can occur in the vortex core. If a given vortex sheet with a certain strength allows for sufficient radial expansion for vortex breakdown to occur at one location over a delta wing, an increase in strength of that vortex sheet can delay the location of vortex breakdown by reducing the radial expansion mechanism. Reducing this radial expansion reduces pile-up. Together, they reduce the vorticity sign switching, and the maximum possible induced backflow velocity, thereby delaying vortex breakdown.

This seems to be the case in the experiment by Guy, Morrow, and McLaughlin. Through periodic blowing along the leading edge of a delta wing, they delay vortex breakdown by up to $0.2c$ (*ref. 32*). The effect of periodic blowing is mostly jet-like, as the suction stroke tends to draw from low energy flow in the boundary layer near the blowing ports. Therefore, periodic blowing along the leading edge acts to strengthen the vortex sheet. This strengthened vortex sheet constrains radial expansion and delays vortex breakdown.

One might wonder, while increasing angles of attack should also strengthen the vortex sheet and thereby delay vortex breakdown, why breakdown tends to occur further upstream with increased angle of attack. The answer lies in understanding that, as angle of attack increase, circulation in the vortex sheet, and thereby the vortex tube, also increases. However, the adverse pressure gradient and the associated the negative axial velocity gradient along the chord of the wing also increases, thereby increasing the strength of the negative vorticity gradient. Thus, the effects of the increasing the angle of attack is to not only impose a stronger radial constraint, but also to strengthen the negative vorticity gradient and the induced velocities that cause radial expansion. However, this vorticity gradient also causes pile-up and vorticity sign switching. Thus, the overall effect of increasing angle of attack, while tending to delay vortex breakdown in terms of radial expansion, is to move the vortex breakdown location upstream in terms of pile-up and vorticity sign switching. However, when these mechanisms can be decoupled, like when the strength of the radially constraining vortex sheet increases independently of vorticity gradient by means such as leading edge blowing, vortex breakdown can be delayed. Aside from weakening the negative vorticity gradient, decoupling the inviscid feedback mechanism of radial expansion, pile-up, and vorticity sign switching, will be an effective way of weakening, delaying, or preventing vortex breakdown.

5.6.3 *Pile-up*

The effects of pile-up can be delayed by adding an axial velocity component along the axis of the vortex tube. Doing this will implicitly have the effect of delaying vortex breakdown by requiring an increased maximum induced backflow velocity to equal the now increased downstream axial velocity. This may require a more developed (and hence further downstream) vortex, or may not be possible for a given amount of circulation in the vortex tube. Still, axial blowing can be interpreted in terms of suppressing pile-up, thereby weakening radial expansion and vorticity sign switching. The overall result is to move the location of vortex breakdown over a delta wing

downstream or to delay the formation of vortex breakdown for a given chordwise wing location until higher angles of attack. In their experiments with axial blowing over a delta wing A. Mitchell et al showed that they could delay vortex breakdown (*ref. 33*). Increases in blowing along the core further delay vortex breakdown, as the self-induction theory would predict.

5.6.4 *Vorticity sign switching*

The azimuthal vorticity sign switching is a major factor in the development of vortex breakdown because it allows for induced backflow. This backflow leads to feedback with pile-up and radial expansion. Vorticity sign switching occurs when a portion of the vortex tube rotates more slowly than the rest of the vortex tube. This causes the vortex filaments to tilt, with the azimuthal component of the vorticity vector changing sign. This could be delayed or weakened if an addition amount of azimuthal velocity is added to the vortex tube. Conversely, breakdown could be enhanced by somehow slowing down the rotation of the vortex tube in the region of the vorticity gradient. Experiments by H. Husain et al show just this result. See *ref. 34* for details. In their experiments, a vortex is generated in a cylinder in a setup similar to the previously described Escudier experiment. However, a thin rod is added along the centerline of the cylinder where the vortex tube that will develop due to the rotation of the end wall. That rod could be rotated in the same direction as the vortex, or it could be counter-rotated with respect to the main rotating flow. With the rod stationary, vortex breakdown is observed as usual. When the rod is co-rotated at a sufficient rate, vortex breakdown is no longer observed in the flow. However, when the rod is counter-rotated with respect to the main vortex flow, the vortex breakdown was enhanced, with increased radial expansion and strengthened recirculation. This can be interpreted in terms of the azimuthal vorticity sign switch. The co-rotating rod added a rotation velocity to the vortex core large enough to overcome the rotation rate difference initiated by radial expansion. Thus, since this change in rotation rate was decreased, the azimuthal vorticity sign switch could not develop to a sufficient strength to cause vortex breakdown. On the other hand, when the

rod counter-rotated, it enhanced the azimuthal sign switching, leading to increased backflow and radial expansion. Other ways to exploit this effect might include blowing tangential to the vortex tube or wing surface to increase the azimuthal velocity and weaken or remove the possibility of azimuthal vorticity sign switching. Zhi Shi did just this to delay vortex breakdown over a delta wing. See *ref. 35* for details. Figure 5-32 shows the setup of the jets on the surface of a delta wing.

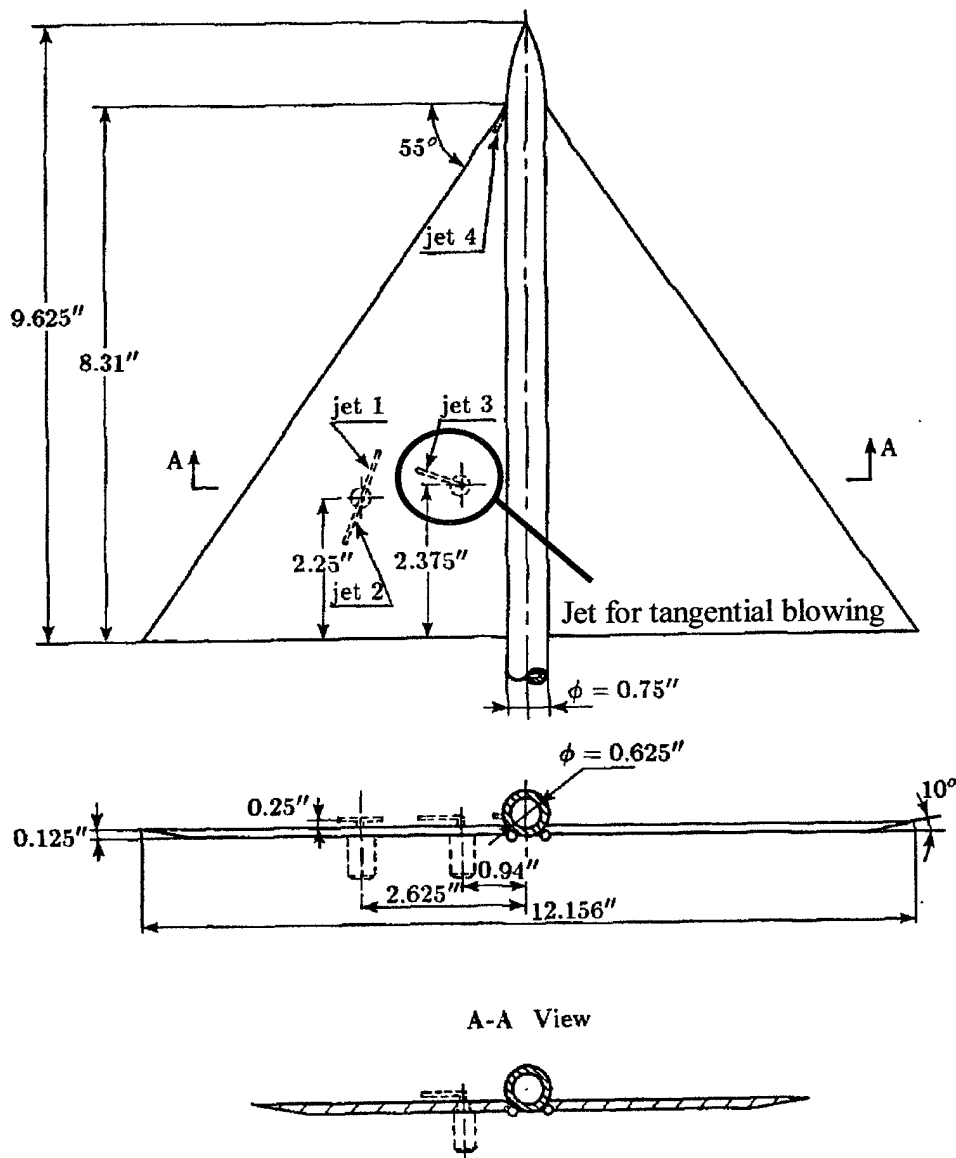
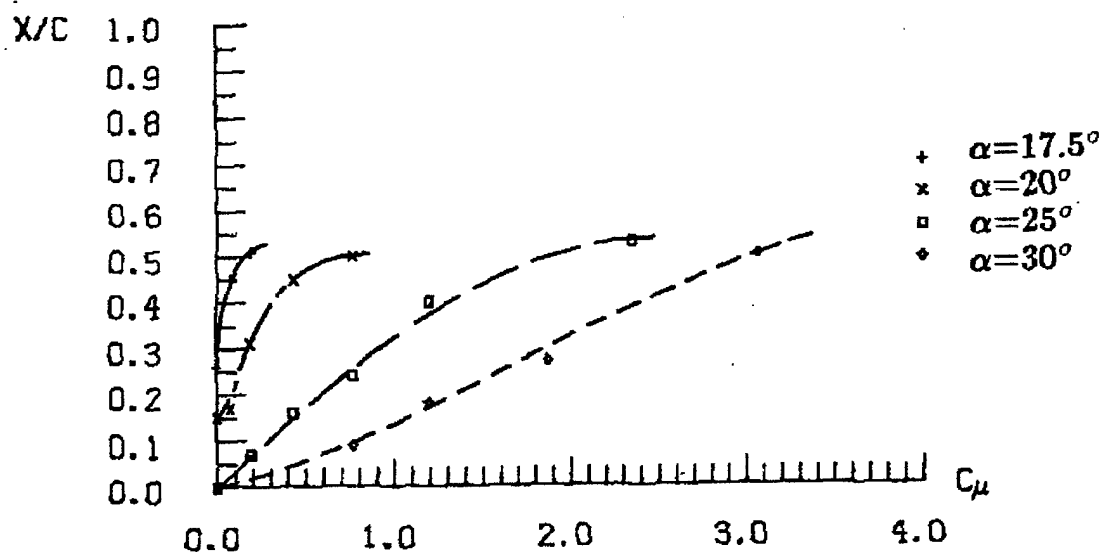


Figure 5-32 Tangential blowing setup (*ref. 35*)

In this setup, jet three blows tangential to the vortex tube in the azimuthal direction. With this blowing turned on, the azimuthal vorticity sign switching, and hence vortex breakdown is delayed. Figure 5-33 shows these results. The variable C_μ is the jet momentum coefficient, X/C is the normalized chordwise breakdown location, and α is angle of attack.



The variation of breakdown position with tangential jet blowing (model II, jet 3, $V_\infty = 2.73$ in/sec).

Figure 5-33 Delaying vortex breakdown with tangential jet (ref. 35)

6. Suggested future work

Much work remains to be done on this subject. Specifically, we need to work to quantify these vortex filament method results and look for the limiting values of vorticity gradient that will lead to vortex breakdown. Furthermore, the case with constant circulation and a velocity gradient needs to be explored. This is likely the most physical way of developing a vorticity gradient. One way to do this would be to treat the freestream velocity as a function of axial distance, z , and time, t . In further research, we need to apply the various possible techniques for delaying vortex breakdown to the vortex filament simulation. To aid in doing this, the simulation program could be written in a generalized, user-friendly interface that would allow it to become a type of vortex filament "lab" where various initial conditions, boundary conditions, and control devices could be setup easily to determining their effect on the resulting vortex motion. Ultimately, it is the hope that this research will lead to better methods for controlling vortex breakdown for the purposes of flow and mixing control.

7. Conclusions

Vortex flows are common in nature and in aircraft flows. The benefit of vortex flows generated by strakes or swept wings on aircraft is their ability to energize the flow, thereby delaying stall and increasing the maximum lift coefficient. However, vortex flows can undergo rapid radial expansion accompanied by backflow and turbulence that has decidedly negative effects on an aircraft, causing instabilities when the vortex breakdown location varies asymmetrically, and structural problems in terms of high cycle fatigue—a problem especially prevalent on twin-tailed aircraft like the F/A-18. While there has been much research aimed at understanding vortex breakdown, a clear, concise, and widely accepted theory is still not available. Furthermore, the theories that are available, while useful in describing flows that experience vortex breakdown, are not very instructive in terms of specifying ways to control vortex breakdown. It is the purpose of this research to provide of framework for understanding the initial cause of vortex breakdown that will lead researchers to effective methods to control that breakdown. The self-induction theory of vortex breakdown provides this framework.

The self-induction theory of vortex breakdown is studied using computer simulations and experiments, as well as examining the results of past experiments. The vortex filament simulation and the vorticity gradient experiments, in additions to the experiments in vortex breakdown control provide strong evidence that vortex breakdown is an inviscid mechanism, initiated by a negative vorticity gradient. Just as in the vortex filament simulation, these experiments show that a vorticity gradient initiates the process of radial expansion, pile-up, and vorticity sign switching that leads to vortex breakdown. This provides further evidence that vortex breakdown is initiated by a vorticity gradient that manifests itself as a radial change in flow through an inviscid self-induction feedback mechanism. This self-induction theory shows how a feedback mechanism works through radial expansion, pile up, and vorticity sign switching, to form a turning point, thereby producing all the features of vortex breakdown.

The primary benefit of the self-induction theory of vortex breakdown is that it allows for a clearer understanding of mechanism that initiates vortex breakdown while also presenting clear ways of preventing, weakening, or delaying that breakdown. Previous theories of vortex breakdown do not illuminate possible control solution as much as they identify the existence of vortex breakdown. With this new paradigm of the self-induction of vortex breakdown, researchers have clear guidelines to supplement their engineering intuition about how to control vortex breakdown. These include changing the vorticity gradient, applying or removing radial constraints, increasing or decreasing pile-up, and preventing or enhancing the azimuthal vorticity sign switching. The experiments that have been presented provide evidence for this way of thinking of vortex breakdown. These past successes in controlling vortex breakdown point to the self-induction theory of vortex breakdown, which in turn provide a clear framework for future successes in manipulation and control of vortex breakdown.

LIST OF REFERENCES

1. NASA-Goddard Space Flight Center, data from NOAA GOES, <http://rsd.gsfc.nasa.gov/pub/goes/960904.fran.persp.jpg>, 2001.
2. NASA Dryden Flight Research Center, <http://www.dfrc.nasa.gov/gallery/photo/F-18HARV/HTML/EC89-0096-206.html>, 1989.
3. Bertin, John J., and Michael L. Smith, *Aerodynamics for Engineers*, Chap 7, Prentice Hall, Upper Saddle River, New Jersey, 1998.
4. Srigrarom, S., "The Transient Formation of Vortex Breakdown" (PhD dissertation in progress).
5. Spall, R.E., "Transition from Spiral- to Bubble-Type Vortex Breakdown", *Physics of Fluids*, Vol. 8, No.5, 1996, pp. 1330-1332.
6. Faler, J.H., and Leibovich, S., "Disrupted States of Vortex Flow and Vortex Breakdown", *Physics of Fluids*, Vol. 20, No.9, 1977, pp. 1385-1400.
7. Snyder, D.O. and Spall, R.E. "Numerical Simulation of Bubble-Type Vortex Breakdown within a Tube-and-Vane Apparatus, *Physics of Fluids*, Vol. 12, 2000, pp. 603-608.
8. Sarpkaya, T., "On stationary and travelling vortex breakdowns", *Journal of Fluid Mechanics*, Vol. 45, part 3, 1971, pp. 545-559.
9. Anderson, John D., *Fundamentals of Aerodynamics, Second Edition* Chap. 5.6, McGraw-Hill, Inc., New York, 1991.
10. Kundu, Pijush K., *Fluid Mechanics*, Chap 3, Academic Press, San Diego, 1990.
11. Jeffrey, Alan, *Handbook of Mathematical Formulas and Integrals*, Academic Press, San Diego, 1995.
12. Serway, Raymond A., *Principle of Physics*, Saunders College Publishing, Fort Worth, Texas, 1994.
13. NASA Dryden Flight Research Center, <http://www.dfrc.nasa.gov/gallery/photo/L-1011/HTML/ECN-7848.html>, 1977.

14. Nakamura, Y., A. Leonard, and P.R. Spalart, "Numerical Simulation of Vortex Breakdown by the Vortex-Filament Method." NASA Ames Research Center, Moffett Field, CA.
15. Saghbini, J.-C. C., and A.F. Ghoniem, "Numerical Simulation of the Dynamics and Mixing in a Swirling Flow." AIAA 97-0507. 35th Aerospace Sciences Meeting and Exhibit.
16. Meiburg, Eckart. "Three-Dimensional Vortex Dynamics Simulations" in S.I. Green (ed) Fluid Vortices, pg. 659.
17. Brown, G.L., and J.M. Lopez, "Axisymmetric vortex breakdown. Part 2. Physical mechanism." Journal of Fluid Mechanics, vol. 224, 1990, pp. 553-576.
18. Kurosaka, M. and P. Sundram, "Illustrative examples of streaklines in unsteady vortices: Interpretational difficulties revisited." Physics of Fluids, 29 (10), pp. 3474-3477, October 1986.
19. M. Raffel, C. Willert and J. Kompenhaus, "Particle Image Velocimetry", Springer-Verlag, New York, 1998, pp. 158-164.
20. Althaus, W. and M. Weimer, "Review of the Aachen work on vortex breakdown,"
21. Kurosaka, M., "Spiralling Shear Layer as a Cause of Vortex Breakdown," Paper No. 152, Proceedings of the 8th International Symposium on Flow Visualization [CD-ROM], National Library of Scotland, Edinburgh, 1998.
22. Srigrarom, S., "Vortex Breakdown Suppression Based on Self-Induction Mechanism Theory," AIAA Paper 00-0017, Jan. 2000;
23. Lighthill, M.J., and G.B. Whitman, Laminar Boundary Layers. Clarendon Press, Oxford, 1963, pp. 53, 122.
24. Keller, J.J., W. Egli, and J. Exley, "Force- and loss-free transitions between flow states." Z. Angew. Math. Phys. Vol 36, pg. 854, 1985.
25. Keller, J.J., W. Egli, and R. Althaus, "Vortex breakdown as a fundamental element of vortex dynamics." Z. Angew. Math. Phys. Vol 39, pg. 404, 1988.
26. Maxworthy, T., M. Mory, E.J. Hopfinger, "Waves on vortex cores and their relationship to vortex breakdown," pp. 29-1—29-13.

27. Escudier, M.P., "Observations of the flow produced in a cylindrical container by a rotating endwall," *Experiments in Fluids*, Vol. 2, pp. 189-196, 1984.
28. Kikuchi, Masanori, "Navier-stokes simulation of flow produced in a cylindrical container by a rotating endwall" (work in progress).
29. Metwally, O., G. Settles, and C. Horstman, "An Experimental Study of Shock Wave/Vortex Interaction." AIAA, Aerospace Sciences Meeting, 27th, Reno, NV, Jan. 9-12, 1989. AIAA Paper 89-0082.
30. Visbal, M.R., "Computed Unsteady Structure of Spiral Vortex Breakdown on Delta Wings." AIAA, Fluid Dynamics Conference, 27th, New Orleans, LA, Jun. 17-20, 1996. AIAA Paper 96-2074.
31. Mitchell, Anthony M., Pascal Molton, Didier Barberis, Jean Delery, "Control of leading-edge vortex breakdown by trailing edge injection." AIAA Applied Aerodynamics Conference, 17th, Norfolk, VA, June 28-July 1, 1999. AIAA Paper 99-3202.
32. Guy, Yair, Julie A. Morrow, Thomas E. McLaughlin, "Control of vortex breakdown on a delta wing by periodic blowing and suction." AIAA, Aerospace Sciences Meeting and Exhibit, 37th, Reno, NV, Jan. 11-14, 1999. AIAA Paper 99-0132.
33. Mitchell, Anthony M., Pascal Molton, Didier Barberis, Jean Delery, "Control of vortex breakdown by along-the-core blowing." Fluids 2000 Conference and Exhibit, Denver, CO, June 19-22, 2000. AIAA Paper 2000-2608.
34. Husain, Hyder, Vladimir Shtern, Fazle Hussain, "Control of vortex breakdown using vortex generators." AIAA, Shear Flow Control Conference, 4th, Snowmass Village, CO, June 29-July 2, 1997. AIAA Paper 97-1879.
35. Shi, Zhi, "An Investigation of Leading-Edge Vortices on Delta Wings," Master of Science Thesis, The University of Tennessee, Knoxville, 1986.

8. APPENDIX A—Vortex Filament Simulation Source Code

8.1 *vlinec.cpp* - Main simulation code

```
//-----
#include <vcl.h>
#include <fstream.h>
#include <istream.h>
#include <iostream.h>
#include <conio.h>
#include <fastmath.h>
#include <time.h>

#pragma hdrstop

//initialize subroutines
int read_data ();
int init ();
void cond_out(char*);
int out(double**, double**, double**, char*, int, int);
void calc_ind ();
void r_calc_ind ();
void init_ind();
void u_update();
void sym_calc();
void r_sym_calc();
void init_incase_rad_spoke(int,double**, double**, double**,double**,double,
int,int*,int,int,double*,double,double,double,double,
double,double,double**,double**,double**,double**,int,int,int);

//-----Declare Global Variables-----
int in_case,velvor_on,blow_on,n_fil,wall_on,wall_ax_node,wall_circ_node;
double t_final,U_inf,beta,r_tube0,r_tube1,r_tube2,r_tube3,r_tube4,r_tube5,
r_tube6,r_tube7,r_tube8,r_tube9,r_tube10,r_tube11,r_tube12;
double sigma_init,C,alpha,U;
double z_on,z_init,x_init,y_init,dz,dt,t_v_out,x_cent,z_start;
int t_index, *on_node, max_node,out_skip,t_out_start,out_count,x_nodes,
z_nodes,end_fix,*r_fil,n_rad,r_fil_in,r_n_fil,r_max_node,r_on_fil;
double t_real,pi,*core_con,*r_tube;
int n_spokes;
char *r_node_out,*r_sigma_out,*gamma_out,*r_gamma_out,*node_out,*sigma_out;
double u_induced_x,u_induced_y,u_induced_z;
double **x_n, **y_n, **z_n, **u_induced_total_x, **u_induced_total_y,
**u_induced_total_z, **sigma;
double **gamma,start_C_inc,stop_C_inc,C_min;
double **r_gamma,**r_x_n, **r_y_n, **r_z_n, **r_u_induced_total_x,
**r_u_induced_total_y, **r_u_induced_total_z, **r_sigma,**r_core_con,
**r_seg_length;

int main(int argc, char **argv)
{
//define output files
node_out = "vlinec.dat";
sigma_out = "sigma_out.dat";
r_node_out = "r_vlinec.dat";
r_sigma_out = "r_sigma_out.dat";
gamma_out = "gamma_out.dat";
r_gamma_out = "r_gamma_out.dat";

int c1 = clock();
read_data(); //read input file
```



```

init();//initialize program variables

//output to screen
cout << "USE FOR CASES THAT ARE ALWAYS SYMMETRIC ONLY!" <<endl;
cout << "T_final: "<<t_final << endl;
cout << "Total iterations: "<<t_final/dt << endl;
cout << "Max nodes: " <<max_node << endl;
cout << "U_inf: "<<U_inf << endl;
cout << "dz: "<<dz << endl;
cout << "Initial condition case: "<<in_case << endl;

//initialize output files, will overwrite previous files!
ofstream outfile(node_out, ios::trunc);
if (!outfile) {
    cout <<"Error opening output file"<<endl;
    outfile.close();

    ofstream sigmafile(sigma_out, ios::trunc);
    if (!sigmafile) {
        cout <<"Error opening output file"<<endl;
        sigmafile.close();

        ofstream r_outfile(r_node_out, ios::trunc);
        if (!r_outfile) {
            cout <<"Error opening output file"<<endl;
            r_outfile.close();

            ofstream r_sigmafile(r_sigma_out, ios::trunc);
            if (!r_sigmafile) {
                cout <<"Error opening output file"<<endl;
                r_sigmafile.close();

                ofstream gammafile(gamma_out, ios::trunc);
                if (!gammafile) {
                    cout <<"Error opening output file"<<endl;
                    gammafile.close();

                    ofstream r_gammafile(r_gamma_out, ios::trunc);
                    if (!r_gammafile) {
                        cout <<"Error opening output file"<<endl;
                        r_gammafile.close();

//output simulation time to screen
cout << "t_index: "<< t_index << " " << "t_real: "<<t_real << endl;

//write program inputs to 1st row of output file
cond_out(node_out);
cond_out(sigma_out);
cond_out(gamma_out);

//write vortex filament node position to file
out(x_n,y_n,z_n,node_out,max_node,n_fil); //main vortex tube
out(r_x_n,r_y_n,r_z_n,r_node_out,r_max_node,r_n_fil); //radial spokes

//write vortex filament core radius to file
out(sigma,sigma,sigma,sigma_out,max_node,n_fil); //main vortex tube
out(r_sigma,r_sigma,r_sigma,r_sigma_out,r_max_node,r_n_fil); //radial spokes

//write vortex filament circulation to file
out(gamma,gamma,gamma,gamma_out,max_node,n_fil); //main vortex tube
out(r_gamma,r_gamma,r_gamma,r_gamma_out,r_max_node,r_n_fil); //radial spokes

//-----Begin main program loop-----
while (t_real < t_final-dt) {

```

```

calc_ind(); //calculate induced velocity on vortex filament nodes

t_index = t_index + 1;
t_real = t_real + dt;

//write current simulation time to screen
int c2 = clock();
cout << "t_index: "<< t_index<<" t_real: "<<t_real << " run time: " <<
double(c2-c1)/CLK_TCK << endl;

//write output to file
if (t_index >= t_out_start && t_index == out_count*out_skip){
    cout <<endl;
    cout<<"Writing node position to file, t_index= "<< t_index<<endl;
    cout <<endl;

    //write vortex filament node position to file
    out(x_n,y_n,z_n,node_out,max_node,n_fil); //main vortex tube
    out(r_x_n,r_y_n,r_z_n,r_node_out,r_max_node,r_n_fil); //radial spokes

    //write vortex filament core radius to file
    out(sigma,sigma,sigma,sigma_out,max_node,n_fil); //main vortex tube
    out(r_sigma,r_sigma,r_sigma,r_sigma_out,r_max_node,r_n_fil); //radial spokes

    //write vortex filament circulation to file
    out(gamma,gamma,gamma,gamma_out,max_node,n_fil); //main vortex tube
    out(r_gamma,r_gamma,r_gamma,r_gamma_out,r_max_node,r_n_fil); //radial spokes

    out_count = out_count + 1; //index for writing output to file
}

int c3 = clock();
cout << endl;
cout <<"Total run time: "<< double(c3-c1)/CLK_TCK << endl;
cout << endl << "Press any key to continue...";
getch();

outfile.close();

return 0;
}
//-----

//-----Function read_data -----
//Read data from vlinec.inp. Input file requires '$' characters and end of line
//-----
int read_data ()
{
    ifstream infile("vlinec_rad_spoke.inp", ios::in);
    if (!infile) return 0;
    infile.ignore(10000, '$');
    infile >> in_case;infile.ignore(1000, '\n');
    infile >> t_final;infile.ignore(1000, '\n');
    infile >> U_inf;infile.ignore(1000, '\n');
    infile >> dz;infile.ignore(1000, '\n');
    infile >> dt;infile.ignore(1000, '\n');
    infile >> max_node;infile.ignore(1000, '\n');
    infile >> r_fil_in;infile.ignore(1000, '\n');
    infile >> n_rad;infile.ignore(1000, '\n');
    infile >> t_out_start;infile.ignore(1000, '\n');
    infile >> out_skip;infile.ignore(1000, '\n');
    infile >> r_tube0;infile.ignore(1000, '\n');
    infile >> r_tube1;infile.ignore(1000, '\n');
    infile >> r_tube2;infile.ignore(1000, '\n');
    infile >> r_tube3;infile.ignore(1000, '\n');
}

```

```

infile >> r_tube4;infile.ignore(1000, '\n');
infile >> r_tube5;infile.ignore(1000, '\n');
infile >> r_tube6;infile.ignore(1000, '\n');
infile >> r_tube7;infile.ignore(1000, '\n');
infile >> r_tube8;infile.ignore(1000, '\n');
infile >> r_tube9;infile.ignore(1000, '\n');
infile >> r_tube10;infile.ignore(1000, '\n');
infile >> r_tube11;infile.ignore(1000, '\n');
infile >> r_tube12;infile.ignore(1000, '\n');
infile >> sigma_init;infile.ignore(1000, '\n');
infile >> C;infile.ignore(1000, '\n');
infile >> start_C_inc;infile.ignore(1000, '\n');
infile >> stop_C_inc;infile.ignore(1000, '\n');
infile >> C_min;infile.ignore(1000, '\n');
infile >> alpha;infile.ignore(1000, '\n');
infile >> z_on;infile.ignore(1000, '\n');
infile >> z_init;infile.ignore(1000, '\n');
infile >> x_init;infile.ignore(1000, '\n');
infile >> y_init;infile.ignore(1000, '\n');
infile.close();
return 0;
}

//-----Function init -----
//Initialize variables
//-----

int init ()
{
    r_fil = new int [n_rad];
    r_tube = new double [n_rad];
    n_fil = 0;

    //initialize number of filaments in a given radius
    r_fil[0] = r_fil_in;
    r_fil[1] = r_fil_in;
    r_fil[2] = r_fil_in;
    r_fil[3] = r_fil_in;
    r_fil[4] = r_fil_in;
    r_fil[5] = r_fil_in;
    r_fil[6] = r_fil_in;
    r_fil[7] = r_fil_in;
    r_fil[8] = r_fil_in;
    //r_fil[9] = r_fil_in;
    //r_fil[10] = r_fil_in;
    //r_fil[11] = r_fil_in;
    //r_fil[12] = r_fil_in;

    //Initiallize vortex filament radii
    r_tube[0]=r_tube0;
    r_tube[1]=r_tube1;
    r_tube[2]=r_tube2;
    r_tube[3]=r_tube3;
    r_tube[4]=r_tube4;
    r_tube[5]=r_tube5;
    r_tube[6]=r_tube6;
    r_tube[7]=r_tube7;
    r_tube[8]=r_tube8;
    //r_tube[9]=r_tube9;
    //r_tube[10]=r_tube10;
    //r_tube[11]=r_tube11;
    //r_tube[12]=r_tube12;

    for (int j = 0; j <= n_rad-1; j++){
        n_fil = r_fil[j]+n_fil;
    }
}

```

```

n_fil = n_fil + 1; //add centerline filament
double **seg_length = new double *[max_node];
for (int i = 0; i < max_node; i++) {seg_length[i] = new double [n_fil];}

//initialize simulation time
t_real = 0.0;
t_index = 0;
out_count = 1;

pi = M_PI; //define pi

z_init = z_init + dz;

//Initiallize dynamic arrays
core_con = new double [n_fil];

on_node = new int [n_fil];

gamma = new double *[max_node];
for (int i = 0; i < max_node; i++) {gamma[i] = new double [n_fil];}

x_n = new double *[max_node];
for (int i = 0; i < max_node; i++) {x_n[i] = new double [n_fil];}

y_n = new double *[max_node];
for (int i = 0; i < max_node; i++) {y_n[i] = new double [n_fil];}

z_n = new double *[max_node];
for (int i = 0; i < max_node; i++) {z_n[i] = new double [n_fil];}

u_induced_total_x = new double *[max_node];
for (int i = 0; i < max_node; i++) {u_induced_total_x[i] =
new double [n_fil];}

u_induced_total_y = new double *[max_node];
for (int i = 0; i < max_node; i++) {u_induced_total_y[i] =
new double [n_fil];}

u_induced_total_z = new double *[max_node];
for (int i = 0; i < max_node; i++) {u_induced_total_z[i] =
new double [n_fil];}

sigma = new double *[max_node];
for (int i = 0; i < max_node; i++) {sigma[i] = new double [n_fil];}

//radial spokes arrays and locations

int m_z = 10;
n_spokes = 16;
r_n_fil = 10*n_spokes;
r_max_node = 5/0.1;

r_gamma = new double *[r_max_node];
for (int i = 0; i < r_max_node; i++) {r_gamma[i] = new double [r_n_fil];}

r_x_n = new double *[r_max_node];
for (int i = 0; i < r_max_node; i++) {r_x_n[i] = new double [r_n_fil];}

r_y_n = new double *[r_max_node];
for (int i = 0; i < r_max_node; i++) {r_y_n[i] = new double [r_n_fil];}

r_z_n = new double *[r_max_node];
for (int i = 0; i < r_max_node; i++) {r_z_n[i] = new double [r_n_fil];}

r_u_induced_total_x = new double *[r_max_node];
for (int i = 0; i < r_max_node; i++) {r_u_induced_total_x[i] =

```

```

new double [r_n_fil]);

r_u_induced_total_y = new double *[r_max_node];
for (int i = 0; i < r_max_node; i++) {r_u_induced_total_y[i] =
new double [r_n_fil];}

r_u_induced_total_z = new double *[max_node];
for (int i = 0; i < r_max_node; i++) {r_u_induced_total_z[i] =
new double [r_n_fil];}

r_sigma = new double *[r_max_node];
for (int i = 0; i < r_max_node; i++) {r_sigma[i] = new double [r_n_fil];}

r_core_con = new double *[r_max_node];
for (int i = 0; i < r_max_node; i++) {r_core_con[i] = new double [r_n_fil];}

r_seg_length = new double *[r_max_node];
for (int i = 0; i < r_max_node; i++) {r_seg_length[i] = new double [r_n_fil];}

//Initialize x_n, y_n, z_n
//Note: z_n is to the right (axial direction), x_n is up,
//y_n is out of page. When plotting, plot z_n to the right, x_n up,
//and y_n out of page.

//subroutine in init_incase_rad_spoke.cpp that initializes vortex filament
//node location
init_incase_rad_spoke(in_case, x_n, y_n, z_n, gamma, C, max_node, r_fil, n_fil, n_rad,
r_tube, x_init, y_init, z_init, dz, start_C_inc, stop_C_inc, C_min,
r_gamma, r_x_n, r_y_n, r_z_n, r_max_node, n_spokes, m_z);

//Initialize sigma, find core constant to maintain constant volume in
//vortex filament segment. This allows simulation to handle vortex
//stretching
for (int n = 0; n <= n_fil-1; n++) {
    for (int m = 0; m <= max_node-2; m++) {

        sigma[m][n] = sigma_init;
        seg_length[m][n] = sqrt((x_n[m+1][n]-x_n[m][n])*
(x_n[m+1][n]-x_n[m][n])+(y_n[m+1][n]-y_n[m][n])*(y_n[m+1][n]-
y_n[m][n])+(z_n[m+1][n]-z_n[m][n])*(z_n[m+1][n]-z_n[m][n]));
    }

    core_con[n] = sigma[1][n]*sigma[1][n]*seg_length[1][n];
}

//initialize sigma for radial spokes
for (int n = 0; n <= r_n_fil-1; n++) {
    for (int m = 0; m <= r_max_node-2; m++) {
        r_sigma[m][n] = sigma_init;

        r_seg_length[m][n] = sqrt((r_x_n[m+1][n]-r_x_n[m][n])*
(r_x_n[m+1][n]-r_x_n[m][n])+(r_y_n[m+1][n]-r_y_n[m][n])*(r_y_n[m+1][n]-
r_y_n[m][n])+(r_z_n[m+1][n]-r_z_n[m][n])*(r_z_n[m+1][n]-r_z_n[m][n]));

        r_core_con[m][n] = r_sigma[m][n]*r_sigma[m][n]*
r_seg_length[m][n];
    }
}

return 0;
}

```

```

//-----Function cond_out-----
// Write inputs to 1st row of output file
//-----
void cond_out(char *out)
{
    ofstream outfile(out, ios::app);
    //need to fill 34 columns
    //output simulation variable to top row of output file
    outfile << in_case << " " << n_fil << " " << max_node << " " << dt << " "
    << dz << " " << U_inf << " " << t_out_start << " " << out_skip << " "
    << r_tube1 << " " << r_tube2 << " " << r_tube3 << " " << r_tube4 << " "
    << r_tube5 << " " << sigma_init << " " << C << " " << alpha << " "
    << z_on << " " << n_rad << " " << r_fil[0] << " " << r_fil[1] << " "
    << r_fil[2] << " " << r_fil[3] << " " << r_fil[4] << " " << r_fil[5] << " "
    << r_fil[6] << " " << r_fil[7] << " " << r_fil[8] << " " << r_fil[9] << " ";
    for (int p=29 ; p<=n_fil+1 ; p++){outfile << 0 << " " ;}
    outfile<< endl;

}
//-----Function out-----
// Write x_n, y_n, z_n to file
//-----
int out(double**a, double**b, double**c, char*out, int m_row, int n_col)
{
    ofstream outfile(out, ios::app);
    if (!outfile) return 0;
    //output x_n
    for (int m = 0; m <= m_row-1; m++){
        for (int n = 0; n <= n_col-1; n++){
            outfile.precision(6);
            outfile << a[m][n] << " ";
        }
        outfile << t_index << endl;
    }
    //output y_n
    for (int m = 0; m <= m_row-1; m++){
        for (int n = 0; n <= n_col-1; n++){
            outfile.precision(6);
            outfile << b[m][n] << " ";
        }
        outfile << t_index << endl;
    }
    //output z_n
    for (int m = 0; m <= m_row-1; m++){
        for (int n = 0; n <= n_col-1; n++){
            outfile.precision(6);
            outfile << c[m][n] << " ";
        }
        outfile << t_index << endl;
    }
    //outfile.close();
    return 0;
}

//-----Function calc_ind-----
// Perform induced velocity calculations
//-----
void calc_ind()
{
    init_ind();

    //calculate induced velocity on each node from every other vortex
    //filament segment
    int n;
    for (int j1 = 0; j1 <= n_rad; j1++){

```

```

    if (j1==0){n = 0;}
    else if (j1==1){n = 1;}
    else if (j1 > 1){n = r_fil[j1-2]+ n;}

    for (int m = 0; m <= on_node[n]-1; m++){
        for (int k = 0; k <= n_fil-1; k++){
            for (int j = 0; j <= on_node[k]-2; j++){

double gam_eq;

double dlx = x_n[j+1][k]-x_n[j][k];
double dly = y_n[j+1][k]-y_n[j][k];
double dlz = z_n[j+1][k]-z_n[j][k];

double rx = x_n[m][n] - (0.5*(x_n[j+1][k] - x_n[j][k]) + x_n[j][k]);
double ry = y_n[m][n] - (0.5*(y_n[j+1][k] - y_n[j][k]) + y_n[j][k]);
double rz = z_n[m][n] - (0.5*(z_n[j+1][k] - z_n[j][k]) + z_n[j][k]);

double r_cross_dr_x = rz*dly - ry*dlz;
double r_cross_dr_y = -(rz*dlx - rx*dlz);
double r_cross_dr_z = ry*dlx - rx*dly;

double abs_rk = sqrt(rx*rx + ry*ry + rz*rz);

double s = 1/(pow(1+(alpha*(sigma[m][n]*sigma[m][n] + sigma[j][k]*sigma[j][k])/
    (2*abs_rk*abs_rk)),1.5));

    if (0.5*(z_n[j+1][k] - z_n[j][k]) + z_n[j][k] <= 0){
        gam_eq = 0.0;
    }
    else {
        gam_eq = gamma[j][k];
    }

double u_ind_dummy_x = (-gam_eq/(4.0*pi))*r_cross_dr_x*s/(pow(abs_rk,3));
double u_ind_dummy_y = (-gam_eq/(4.0*pi))*r_cross_dr_y*s/(pow(abs_rk,3));
double u_ind_dummy_z = (-gam_eq/(4.0*pi))*r_cross_dr_z*s/(pow(abs_rk,3));

    if (j == 0 && k == 0) {

        u_induced_x = u_ind_dummy_x;
        u_induced_y = u_ind_dummy_y;
        u_induced_z = u_ind_dummy_z;
    }

    else {

        u_induced_x = u_induced_x + u_ind_dummy_x;
        u_induced_y = u_induced_y + u_ind_dummy_y;
        u_induced_z = u_induced_z + u_ind_dummy_z;
    }

    }
    }

    if (z_n[m][n] < 0){
        u_induced_total_x[m][n] = 0;
        u_induced_total_y[m][n] = 0;
        u_induced_total_z[m][n] = 0;
    }

    else {
        u_induced_total_x[m][n] = u_induced_total_x[m][n] + u_induced_x;
        u_induced_total_y[m][n] = u_induced_total_y[m][n] + u_induced_y;
        u_induced_total_z[m][n] = u_induced_total_z[m][n] + u_induced_z;
    }
}

```

```

    }
}

//calculate induced velocities on and from radial spoke calculation
r_calc_ind();

//calculate induced velocity for all nodes, based on symmetry
sym_calc();
r_sym_calc();
u_update();
}

void r_calc_ind()
{
    u_induced_x = 0;
    u_induced_y = 0;
    u_induced_z = 0;

    r_on_fil = 0;
    for (int n = 0; n <= r_n_fil-1; n++){
        if (r_z_n[0][n] >= 0) {
            r_on_fil = r_on_fil + 1 ;
        }
    }

    if (r_on_fil >= r_n_fil){
        r_on_fil = r_n_fil;
    }

    //calculate velocity induced on vortex tube filaments by spokes
    int n;
    for (int j1 = 0; j1 <= n_rad; j1++){

        if (j1==0){n = 0;}
        else if (j1==1){n = 1;}
        else if (j1 > 1){n = r_fil[j1-2] + n;}

        for (int m = 0; m <= on_node[n]-1; m++){

            for (int k = 0; k <= r_on_fil-1; k++){
                for (int j = 0; j <= r_max_node-2; j++){

double gam_eq;

double dlx = r_x_n[j+1][k]-r_x_n[j][k];
double dly = r_y_n[j+1][k]-r_y_n[j][k];
double dlz = r_z_n[j+1][k]-r_z_n[j][k];

double rx = x_n[m][n] - (0.5*(r_x_n[j+1][k] - r_x_n[j][k]) + r_x_n[j][k]);
double ry = y_n[m][n] - (0.5*(r_y_n[j+1][k] - r_y_n[j][k]) + r_y_n[j][k]);
double rz = z_n[m][n] - (0.5*(r_z_n[j+1][k] - r_z_n[j][k]) + r_z_n[j][k]);

double r_cross_dr_x = rz*dly - ry*dlz;
double r_cross_dr_y = -(rz*dlx - rx*dlz);
double r_cross_dr_z = ry*dlx - rx*dly;

double abs_rk = sqrt(rx*rx + ry*ry + rz*rz);

double s = 1/(pow(1+(alpha*(sigma[m][n]*sigma[m][n] + r_sigma[j][k]*
    r_sigma[j][k]))/(2*abs_rk*abs_rk)),1.5));

    if (0.5*(r_z_n[j+1][k] - r_z_n[j][k]) + r_z_n[j][k] <= 0){
        gam_eq = 0.0;
    }
    else {
        gam_eq = -r_gamma[j][k];
    }

```



```

    }

double u_ind_dummy_x = (-gam_eq/(4.0*pi))*r_cross_dr_x*s/(pow(abs_rk,3));
double u_ind_dummy_y = (-gam_eq/(4.0*pi))*r_cross_dr_y*s/(pow(abs_rk,3));
double u_ind_dummy_z = (-gam_eq/(4.0*pi))*r_cross_dr_z*s/(pow(abs_rk,3));

    if (j == 0 && k == 0) {

        u_induced_x = u_ind_dummy_x;
        u_induced_y = u_ind_dummy_y;
        u_induced_z = u_ind_dummy_z;
    }

    else {

        u_induced_x = u_induced_x + u_ind_dummy_x;
        u_induced_y = u_induced_y + u_ind_dummy_y;
        u_induced_z = u_induced_z + u_ind_dummy_z;
    }

    }

    }

    if (z_n[m][n] < 0){
        u_induced_total_x[m][n] = 0;
        u_induced_total_y[m][n] = 0;
        u_induced_total_z[m][n] = 0;
    }

    else {
        u_induced_total_x[m][n] = u_induced_total_x[m][n] + u_induced_x;
        u_induced_total_y[m][n] = u_induced_total_y[m][n] + u_induced_y;
        u_induced_total_z[m][n] = u_induced_total_z[m][n] + u_induced_z;
    }
}

}

//calculate velocity induced on spokes by vortex tube filaments

for (int n = 0; n <= r_n_fil-1; n++){
    for (int m = 0; m <= r_max_node-1; m++){
        r_u_induced_total_x[m][n] = 0;
        r_u_induced_total_y[m][n] = 0;
        r_u_induced_total_z[m][n] = 0;
    }
}

u_induced_x = 0;
u_induced_y = 0;
u_induced_z = 0;

for (int j1 = 0; j1 <= r_on_fil/n_spokes-1; j1++){
    n = n_spokes*j1;

    for (int m = 0; m <= r_max_node-1; m++){

        for (int k = 0; k <= n_fil-1; k++){
            for (int j = 0; j <= on_node[k]-2; j++){

double gam_eq;

double dlx = x_n[j+1][k]-x_n[j][k];
double dly = y_n[j+1][k]-y_n[j][k];
double dlz = z_n[j+1][k]-z_n[j][k];

double rx = r_x_n[m][n] - (0.5*(x_n[j+1][k] - x_n[j][k]) + x_n[j][k]);

```

```

double ry = r_y_n[m][n] - (0.5*(y_n[j+1][k] - y_n[j][k]) + y_n[j][k]);
double rz = r_z_n[m][n] - (0.5*(z_n[j+1][k] - z_n[j][k]) + z_n[j][k]);

double r_cross_dr_x = rz*dly - ry*dlz;
double r_cross_dr_y = -(rz*dlx - rx*dlz);
double r_cross_dr_z = ry*dlx - rx*dly;

double abs_rk = sqrt(rx*rx + ry*ry + rz*rz);

double s = 1/(pow(1+(alpha*(r_sigma[m][n]*r_sigma[m][n] +
sigma[j][k]*sigma[j][k]))/(2*abs_rk*abs_rk)),1.5));

if (0.5*(z_n[j+1][k] - z_n[j][k]) + z_n[j][k] <= 0){
    gam_eq = 0.0;
}
else {
    gam_eq = gamma[j][k];
}

double u_ind_dummy_x = (-gam_eq/(4.0*pi))*r_cross_dr_x*s/(pow(abs_rk,3));
double u_ind_dummy_y = (-gam_eq/(4.0*pi))*r_cross_dr_y*s/(pow(abs_rk,3));
double u_ind_dummy_z = (-gam_eq/(4.0*pi))*r_cross_dr_z*s/(pow(abs_rk,3));

if (j == 0 && k == 0) {
    u_induced_x = u_ind_dummy_x;
    u_induced_y = u_ind_dummy_y;
    u_induced_z = u_ind_dummy_z;
}

else {
    u_induced_x = u_induced_x + u_ind_dummy_x;
    u_induced_y = u_induced_y + u_ind_dummy_y;
    u_induced_z = u_induced_z + u_ind_dummy_z;
}

}

if (r_z_n[m][n] < 0){
    r_u_induced_total_x[m][n] = 0;
    r_u_induced_total_y[m][n] = 0;
    r_u_induced_total_z[m][n] = 0;
}

else {
    r_u_induced_total_x[m][n] = r_u_induced_total_x[m][n]+u_induced_x;
    r_u_induced_total_y[m][n] = r_u_induced_total_y[m][n]+u_induced_y;
    r_u_induced_total_z[m][n] = r_u_induced_total_z[m][n]+u_induced_z;
}
}

}

//-----Function init_ind-----
// Initialize induced velocity calculations
//-----
void init_ind()
{
    for (int n = 0; n <= n_fil-1; n++){
        on_node[n] = 0;
        for (int m = 0; m <= max_node-1; m++){

            u_induced_total_x[m][n] = 0;
            u_induced_total_y[m][n] = 0;

```

```

u_induced_total_z[m][n] = 0;

    if (z_n[m][n] >= 0) {
        on_node[n] = on_node[n] + 1;
    }
}

if (on_node[n] >= max_node){
    on_node[n] = max_node;
}
}

}

//-----Function init_ind-----
// Update node positions and filament parameters
//-----
void u_update(){

    double **seg_length = new double *[max_node];
    for (int i = 0; i < max_node; i++) {seg_length[i] = new double [n_fil];}

    for (int n = 0; n <= n_fil-1; n++){
        for (int m = 0; m <= max_node-1; m++){
            x_n[m][n] = x_n[m][n] + u_induced_total_x[m][n]*dt;
            y_n[m][n] = y_n[m][n] + u_induced_total_y[m][n]*dt;
            z_n[m][n] = z_n[m][n] + (u_induced_total_z[m][n] + U_inf)*dt;
        }
    }
    for (int n = 0; n <= n_fil-1; n++){
        for (int m = 0; m <= max_node-2; m++){
            seg_length[m][n] = sqrt((x_n[m+1][n]-x_n[m][n])*
            (x_n[m+1][n]-x_n[m][n])+(y_n[m+1][n]-y_n[m][n])*(y_n[m+1][n]-
            y_n[m][n])+(z_n[m+1][n]-z_n[m][n])*(z_n[m+1][n]-z_n[m][n]));

            sigma[m][n] = sqrt((core_con[n]/seg_length[m][n]));
        }
    }

    //update radial spokes

    r_seg_length = new double *[r_max_node];
    for (int i = 0; i < r_max_node; i++) {r_seg_length[i] = new double [r_n_fil];}

    for (int n = 0; n <= r_n_fil-1; n++){
        for (int m = 0; m <= r_max_node-1; m++){

            r_x_n[m][n] = r_x_n[m][n] + r_u_induced_total_x[m][n]*dt;
            r_y_n[m][n] = r_y_n[m][n] + r_u_induced_total_y[m][n]*dt;
            r_z_n[m][n] = r_z_n[m][n] + (r_u_induced_total_z[m][n] + U_inf)*dt;
        }
    }

    for (int n = 0; n <= r_n_fil-1; n++){
        for (int m = 0; m <= r_max_node-2; m++){
            r_seg_length[m][n] = sqrt((r_x_n[m+1][n]-r_x_n[m][n])*
            (r_x_n[m+1][n]-r_x_n[m][n])+(r_y_n[m+1][n]-r_y_n[m][n])*(r_y_n[m+1][n]-
            r_y_n[m][n])+(r_z_n[m+1][n]-r_z_n[m][n])*(r_z_n[m+1][n]-r_z_n[m][n]));

            r_sigma[m][n] = sqrt((r_core_con[m][n]/r_seg_length[m][n]));
        }
    }

    //cout <<"Umax: "<<Umax<<" Umin: "<<Umin<<endl;
    delete[] seg_length;

```

```

}

void sym_calc(){
    int n;
    for (int j1 = 1; j1 <= n_rad; j1++){
        if (j1==1){n = 1;}
        else if (j1 > 1){n = r_fil[j1-2] + n;}

        for (int k = n; k <= n+r_fil[j1-1]-1; k++){
            for (int m = 0; m <= on_node[k]-1; m++){

                double u_rad = (x_n[m][n]/sqrt(x_n[m][n]*x_n[m][n]+y_n[m][n]*
                    y_n[m][n]))*u_induced_total_x[m][n]+(y_n[m][n]/sqrt(x_n[m][n]*
                    x_n[m][n]+y_n[m][n]*y_n[m][n]))*u_induced_total_y[m][n];
                double u_theta = -(y_n[m][n]/sqrt(x_n[m][n]*x_n[m][n]+y_n[m][n]*
                    y_n[m][n]))*u_induced_total_x[m][n]+(x_n[m][n]/sqrt(x_n[m][n]*
                    x_n[m][n]+y_n[m][n]*y_n[m][n]))*u_induced_total_y[m][n];
                double u_ax = u_induced_total_z[m][n];

                u_induced_total_x[m][k] = (x_n[m][k]/sqrt(x_n[m][k]*x_n[m][k]+
                    y_n[m][k]*y_n[m][k]))*(u_rad) - (y_n[m][k]/sqrt(x_n[m][k]*
                    x_n[m][k]+y_n[m][k]*y_n[m][k]))*(u_theta);
                u_induced_total_y[m][k] = (y_n[m][k]/sqrt(x_n[m][k]*x_n[m][k]+
                    y_n[m][k]*y_n[m][k]))*(u_rad) + (x_n[m][k]/sqrt(x_n[m][k]*
                    x_n[m][k]+y_n[m][k]*y_n[m][k]))*(u_theta);
                u_induced_total_z[m][k] = u_ax;
            }
        }
    }

    void r_sym_calc(){
        int n;
        for (int j1 = 0; j1 <= r_on_fil/n_spokes-1; j1++){
            n = n_spokes*j1;

            for (int k = n; k <= n+n_spokes-1; k++){
                for (int m = 0; m <= r_max_node-1; m++){

                    double u_rad = (r_x_n[m][n]/sqrt(r_x_n[m][n]*r_x_n[m][n]+r_y_n[m][n]*
                        r_y_n[m][n]))*r_u_induced_total_x[m][n]+(r_y_n[m][n]/
                        sqrt(r_x_n[m][n]*r_x_n[m][n]+r_y_n[m][n]*r_y_n[m][n]))*
                        r_u_induced_total_y[m][n];
                    double u_theta = -(r_y_n[m][n]/sqrt(r_x_n[m][n]*r_x_n[m][n]+
                        r_y_n[m][n]*r_y_n[m][n]))*r_u_induced_total_x[m][n]+(r_x_n[m][n]/
                        sqrt(r_x_n[m][n]*r_x_n[m][n]+r_y_n[m][n]*r_y_n[m][n]))*
                        r_u_induced_total_y[m][n];
                    double u_ax = r_u_induced_total_z[m][n];

                    r_u_induced_total_x[m][k] = (r_x_n[m][k]/sqrt(r_x_n[m][k]*
                        r_x_n[m][k]+r_y_n[m][k]*r_y_n[m][k]))*(u_rad) - (r_y_n[m][k]/
                        sqrt(r_x_n[m][k]*r_x_n[m][k]+r_y_n[m][k]*r_y_n[m][k]))*(u_theta);
                    r_u_induced_total_y[m][k] = (r_y_n[m][k]/sqrt(r_x_n[m][k]*
                        r_x_n[m][k]+r_y_n[m][k]*r_y_n[m][k]))*(u_rad) + (r_x_n[m][k]/
                        sqrt(r_x_n[m][k]*r_x_n[m][k]+r_y_n[m][k]*r_y_n[m][k]))*(u_theta);
                    r_u_induced_total_z[m][k] = u_ax;
                }
            }
        }
    }
}

```

8.2 *init_incase.cpp - Vortex filament initialization code*

```

#include <vcl.h>
#include <fstream.h>
#include <istream.h>
#include <iostream.h>
#include <conio.h>
#include <fastmath.h>

#pragma hdrstop

void init_incase_rad_spoke(int in_case, double** x_n, double** y_n,
double** z_n, double** gamma, double C, int max_node, int* r_fil, int n_fil,
int n_rad, double* r_tube, double x_init, double y_init,
double z_init, double dz, double start_C_inc, double stop_C_inc, double C_min,
double** r_gamma, double** r_x_n, double** r_y_n, double** r_z_n,
int r_max_node, int n_spokes, int m_z)
{
    double pi = M_PI;
    double C1;
    double C_up;
    double C_down;
    double z_up;
    double z_down;
    double z_up1;
    double z_down1;

    double ampl;
    double per;
    double phase;
    double slope;
    double inter;
    double gamsum;
    double r_tubel;
    int incr = 0;

    //r_tube_sum = r_tube_sum - r_tube[0];

    //Switch cases for C distribution
    switch (in_case) {
case 1:
//Initialize vortex filament node positions
for (int m = 0; m <= max_node-1; m++){
    x_n[m][0]=x_init;
    y_n[m][0]=y_init;
    z_n[m][0]=z_init - dz*(m);
    for (int j = 0; j <= n_rad-1; j++){
        for (int n = 0; n <= r_fil[j]-1; n++){
            x_n[m][n+incr] = r_tube[j]*cos((n)*pi*2/r_fil[j]) + x_init;
            y_n[m][n+incr] = r_tube[j]*sin((n)*pi*2/r_fil[j]) + y_init;
            z_n[m][n+incr] = z_init-dz*(m);
        }
        incr = incr + r_fil[j];
    }
    incr = 0;
}

//Initialize circulation in vortex tube, must be done in conjunction
//with radial spoke circulation
z_up = stop_C_inc;
z_down = start_C_inc;
z_up1 = z_init-1;
z_down1 = z_init;
C_up = C;

```

```

C_down = C_min;

incr = 0;
for (int m = 0; m <= max_node-1; m++){

    if (z_n[m][0]>=z_up1 && z_n[m][0]<=z_down1){
        C1 = ((C_down-0)/(z_down1-z_up1))* (z_down1-z_n[m][0]) + 0;
    }
    else if (z_n[m][0]>=z_down && z_n[m][0]<z_up1){
        C1 = C_down;
    }
    else if (z_n[m][0]>=z_up && z_n[m][0]<z_down ){
        C1 = ((C_up-C_down)/(z_down-z_up))* (z_down-z_n[m][0]) + C_down;
    }
    else if (z_n[m][0]<z_up){
        C1 = C_up;
    }
    else{
        C1 = 0;
    }
    cout <<C1<< " ";

    //Gaussian vorticity distribution, calculated explicitly based on the
    //method of the Lagrange multiplier
    gamma[m][0] = 0;
    int j = 0;
    for (int i = 0; i <= r_fil[j]-1; i++){
        gamma[m][i+0*r_fil[j]] = .008114549976*C1; //r_0
        gamma[m][i+1*r_fil[j]] = .004780605093*C1; //r_1
        gamma[m][i+2*r_fil[j]] = .01061059381*C1; //r_2
        gamma[m][i+3*r_fil[j]] = .01097097189*C1; //r_3
        gamma[m][i+4*r_fil[j]] = .01223904142*C1; //r_4
        gamma[m][i+5*r_fil[j]] = .009090954102*C1; //r_5
        gamma[m][i+6*r_fil[j]] = .002429657471*C1; //r_6
        gamma[m][i+7*r_fil[j]] = .002628594294*C1; //r_7
        gamma[m][i+8*r_fil[j]] = .001640452531*C1; //r_8
    }
    cout <<endl;

    //calculate total circulation
    gamsum = 0;
    for (int n = 0; n <= n_fil; n++){
        gamsum = gamma[max_node-1][n] + gamsum;
    }

    //initialize radial spokes

    //radial spoke node location interior to vortex tube
    incr = 0;
    for (int j = 0; j <= m_z -1; j++){
        for (int n = 0; n <= n_spokes-1; n++){
            for (int m = 0; m <= n_rad-1; m++){
                r_x_n[m][n+incr] = r_tube[n_rad-1-m]*cos((n)*pi*2/n_spokes)
                + x_init;
                r_y_n[m][n+incr] = r_tube[n_rad-1-m]*sin((n)*pi*2/n_spokes)
                + y_init;
                r_z_n[m][n+incr] = start_C_inc-dz*(j);
            }
        }
        incr = incr + n_spokes;
    }
    //radial spoke node location exterior to vortex tube
    incr = 0;
    for (int j = 0; j <= m_z -1; j++){
        for (int n = 0; n <= n_spokes-1; n++){

```

```

        for (int m = 9; m <= r_max_node-1; m++){
            r_x_n[m][n+incr] = 0.1*(m-4)*cos((n)*pi*2/n_spokes) + x_init;
            r_y_n[m][n+incr] = 0.1*(m-4)*sin((n)*pi*2/n_spokes) + y_init;
            r_z_n[m][n+incr] = start_C_inc-dz*(j);
        }
    }
    incr = incr + n_spokes;
}
//radial spoke circulation interior to vortex tube
incr = 0;
for (int j = 0; j <= m_z -1; j++){
    for (int n = 0; n <= n_spokes-1; n++){
        r_gamma[0][n+incr] = (C-C_min)/10*.001640452531;
        r_gamma[1][n+incr] = (C-C_min)/10*.002628594294+r_gamma[0][n+incr];
        r_gamma[2][n+incr] = (C-C_min)/10*.002429657471+r_gamma[1][n+incr];
        r_gamma[3][n+incr] = (C-C_min)/10*.009090954102+r_gamma[2][n+incr];
        r_gamma[4][n+incr] = (C-C_min)/10*.012239041420+r_gamma[3][n+incr];
        r_gamma[5][n+incr] = (C-C_min)/10*.010970971890+r_gamma[4][n+incr];
        r_gamma[6][n+incr] = (C-C_min)/10*.010610593810+r_gamma[5][n+incr];
        r_gamma[7][n+incr] = (C-C_min)/10*.004780605093+r_gamma[6][n+incr];
        r_gamma[8][n+incr] = (C-C_min)/10*.008114549976+r_gamma[7][n+incr];
    }
    incr = incr + n_spokes;
}

//radial spoke circulation exterior to vortex tube
incr = 0;
for (int j = 0; j <= m_z -1; j++){
    for (int n = 0; n <= n_spokes-1; n++){
        for (int m = 9; m <= r_max_node-1; m++){
            r_gamma[m][n+incr] = r_gamma[8][n+incr];
        }
    }
    incr = incr + n_spokes;
}
break;

case 2:
//Initialize vortex filament node positions
for (int m = 0; m <= max_node-1; m++){
    x_n[m][0]=x_init;
    y_n[m][0]=y_init;
    z_n[m][0]=z_init - dz*(m);
    for (int j = 0; j <= n_rad-1; j++){
        for (int n = 0; n <= r_fil[j]-1; n++){
            x_n[m][n+incr] = r_tube[j]*cos((n)*pi*2/r_fil[j]) + x_init;
            y_n[m][n+incr] = r_tube[j]*sin((n)*pi*2/r_fil[j]) + y_init;
            z_n[m][n+incr] = z_init-dz*(m);
        }
        incr = incr + r_fil[j];
    }
    incr = 0;
}

//Initialize gamma
z_up = stop_C_inc;
z_down = start_C_inc;
z_up1 = z_init-1;
z_down1 = z_init;
C_up = C;
C_down = C_min;

incr = 0;
for (int m = 0; m <= max_node-1; m++){
    if (z_n[m][0]>=z_up1 && z_n[m][0]<=z_down1){

```

```

C1 = ((C_down-0)/(z_down1-z_up1))* (z_down1-z_n[m][0]) + 0;
}
else if (z_n[m][0]>=z_down && z_n[m][0]<z_up1){
C1 = C_down;
}
else if (z_n[m][0]>=z_up && z_n[m][0]<z_down ){
C1 = ((C_up-C_down)/(z_down-z_up))* (z_down-z_n[m][0]) + C_down;
}
else if (z_n[m][0]<z_up){
C1 = C_up;
}
else{
C1 = 0;
}
cout <<C1<< " ";

//Gaussian vorticity distribution, calculated explicitly.
gamma[m][0] = 0;
int j = 0;
        for (int i = 0; i <= r_fil[j]-1; i++){
gamma[m][i+1+0*r_fil[j]] = .008114549976*C1; //r_0
gamma[m][i+1+1*r_fil[j]] = .004780605093*C1; //r_1
gamma[m][i+1+2*r_fil[j]] = .01061059381*C1; //r_2
gamma[m][i+1+3*r_fil[j]] = .01097097189*C1; //r_3
gamma[m][i+1+4*r_fil[j]] = .01223904142*C1; //r_4
gamma[m][i+1+5*r_fil[j]] = .009090954102*C1; //r_5
gamma[m][i+1+6*r_fil[j]] = .002429657471*C1; //r_6
gamma[m][i+1+7*r_fil[j]] = .002628594294*C1; //r_7
gamma[m][i+1+8*r_fil[j]] = .001640452531*C1; //r_8
        }

cout <<endl;
//cout <<endl<<"r_tube[0] = "<<r_tube[0] <<endl;
//cout <<endl<<"r_fil[0] = "<<r_fil[0] <<endl;
gamsum = 0;
for (int n = 0; n <= n_fil; n++){
gamsum = gamma[max_node-1][n] + gamsum;
}
//cout <<endl<<"n_fil = "<<n_fil <<endl;
cout <<endl<<"sum of gamma = "<<gamsum <<endl;

//initialize radial spokes

//radial spoke node location interior to vortex tube
incr = 0;
for (int j = 0; j <= m_z -1; j++){
    for (int n = 0; n <= n_spokes-1; n++){
        for (int m = 0; m <= n_rad-1; m++){
            r_x_n[m][n+incr] = r_tube[n_rad-1-m]*cos((n)*pi*2/n_spokes)
            + x_init;
            r_y_n[m][n+incr] = r_tube[n_rad-1-m]*sin((n)*pi*2/n_spokes)
            + y_init;
            r_z_n[m][n+incr] = start_C_inc-dz*(j);
        }
    }
    incr = incr + n_spokes;
}

//radial spoke node location exterior to vortex tube
incr = 0;
for (int j = 0; j <= m_z -1; j++){
    for (int n = 0; n <= n_spokes-1; n++){
        for (int m = 9; m <= r_max_node-1; m++){
            r_x_n[m][n+incr] = 0.1*(m-4)*cos((n)*pi*2/n_spokes) + x_init;
            r_y_n[m][n+incr] = 0.1*(m-4)*sin((n)*pi*2/n_spokes) + y_init;
        }
    }
}

```



```

        r_z_n[m][n+incr] = start_C_inc-dz*(j);
    }
    incr = incr + n_spokes;
}
//radial spoke circulation interior to vortex tube
incr = 0;
for (int j = 0; j <= m_z -1; j++){
    for (int n = 0; n <= n_spokes-1; n++){
        r_gamma[0][n+incr] = (C-C_min)/10*.001640452531;
        r_gamma[1][n+incr] = (C-C_min)/10*.002628594294+r_gamma[0][n+incr];
        r_gamma[2][n+incr] = (C-C_min)/10*.002429657471+r_gamma[1][n+incr];
        r_gamma[3][n+incr] = (C-C_min)/10*.009090954102+r_gamma[2][n+incr];
        r_gamma[4][n+incr] = (C-C_min)/10*.012239041420+r_gamma[3][n+incr];
        r_gamma[5][n+incr] = (C-C_min)/10*.010970971890+r_gamma[4][n+incr];
        r_gamma[6][n+incr] = (C-C_min)/10*.010610593810+r_gamma[5][n+incr];
        r_gamma[7][n+incr] = (C-C_min)/10*.004780605093+r_gamma[6][n+incr];
        r_gamma[8][n+incr] = (C-C_min)/10*.008114549976+r_gamma[7][n+incr];
    }
    incr = incr + n_spokes;
}

//radial spoke circulation exterior to vortex tube
incr = 0;
for (int j = 0; j <= m_z -1; j++){
    for (int n = 0; n <= n_spokes-1; n++){
        for (int m = 9; m <= r_max_node-1; m++){
            r_gamma[m][n+incr] = r_gamma[8][n+incr];
        }
    }
    incr = incr + n_spokes;
}
    break;
}
}

```

8.3 *init_incase.cpp* - Vortex filament input file

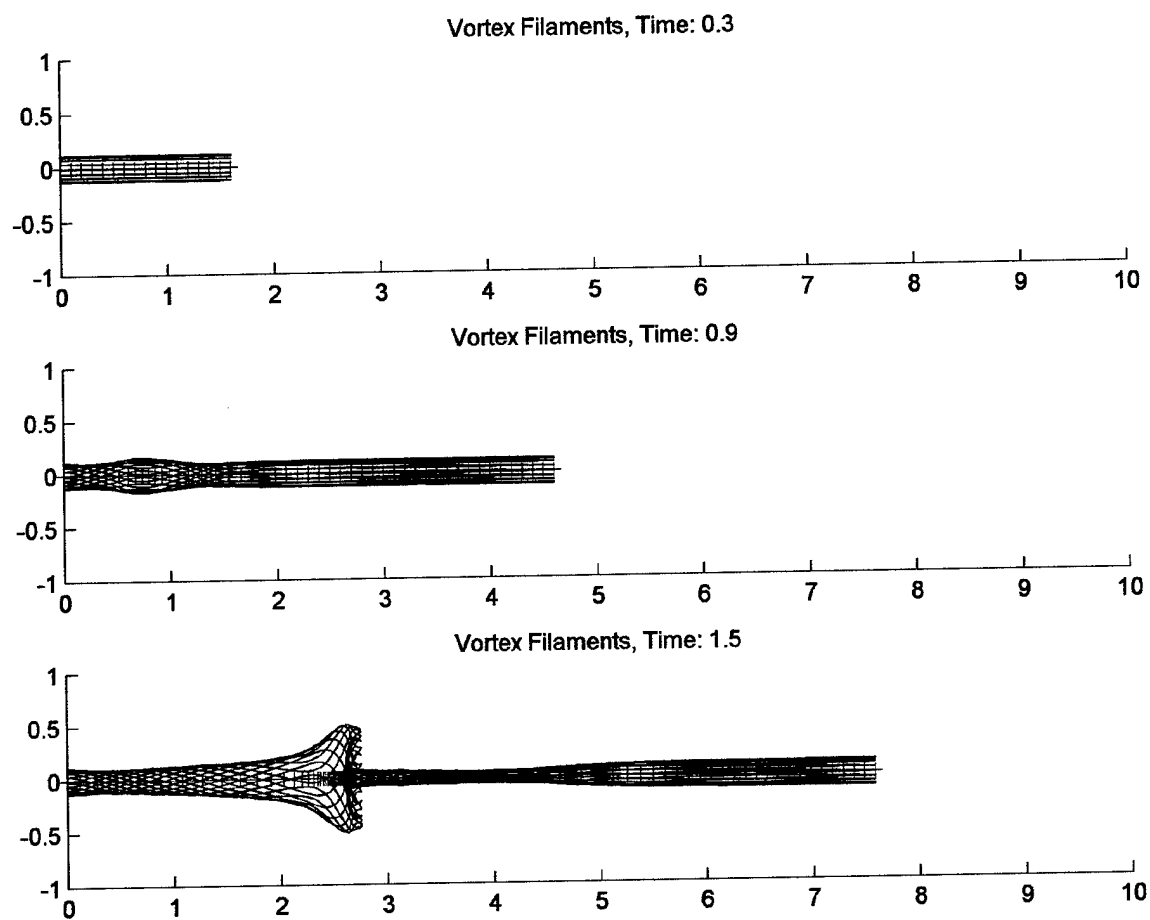
```

//-----
// This is the input file for vlinec.exe Do not modify the structure.
// To change an input value, just replace the existing value
// Do not delete the dollar sign symbols below
//-----
$
1      //Simulation initial condition case, see init_incase.cpp
2.7    //t_final. . . final simulation time
5      //U_inf. . . freestream velocity
0.1    //dz. . . initial axial separation between vortex filament nodes
0.01   //dt. . . simulation time step
251    //max_node. . . maxnumber of nodes in a filament (excluding radial spokes)
16     //number of filaments at a given radius
9      //number of radii (excluding centerline)
0      //t_out_start. . . t_index output starts
30     //out_skip. . . number of iterations before writing data to file
0.42   //r_tube0. . . initial radial location of an axial vortex filament
0.36   //r_tube1
0.3    //r_tube2
0.24   //r_tube3
0.18   //r_tube4
0.12   //r_tube5
0.08   //r_tube6
0.06   //r_tube7
0.03   //r_tube8
0.0    //r_tube9
0.0    //r_tube10
0.0    //r_tube11
0.0    //r_tube12
0.12   //sigma_init. . . initial vortex filament radius
15.0   //Cmax. . . final value of total circulation in vortex tube
-3     //start_C_inc. . . axial location where linear C increase starts
-4     //stop_C_inc. . . axial location where linear C increase ends
0.1    //C_min. . . intial value of total circulation in vortex tube
0.413  //alpha. . . parameter defining velocity near filament center
0.0    //z_on. . . axial location where self induction starts
0.0    //z_init. . . sets overvall initial location of vortex tube
0.0    //x_init. . . sets overvall initial location of vortex tube
0.0    //y_init. . . sets overvall initial location of vortex tube

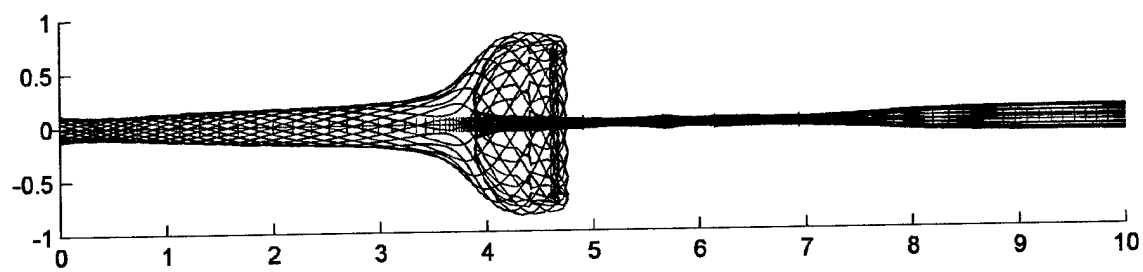
```

9. Appendix B—Additional Vortex filament simulation results

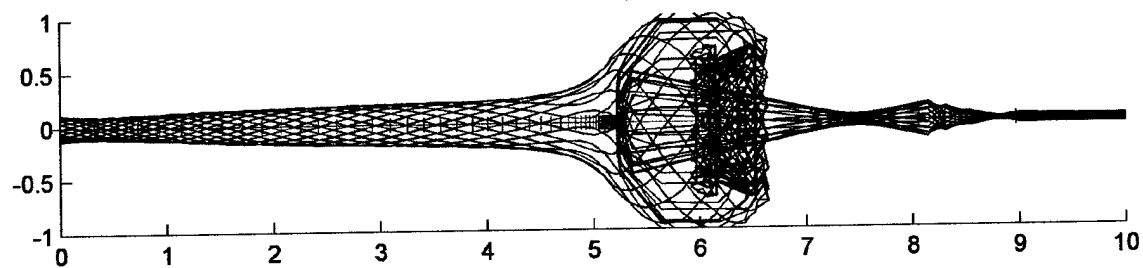
9.1 Vortex filament, $r = 0.12$, side view



Vortex Filaments, Time: 2.1

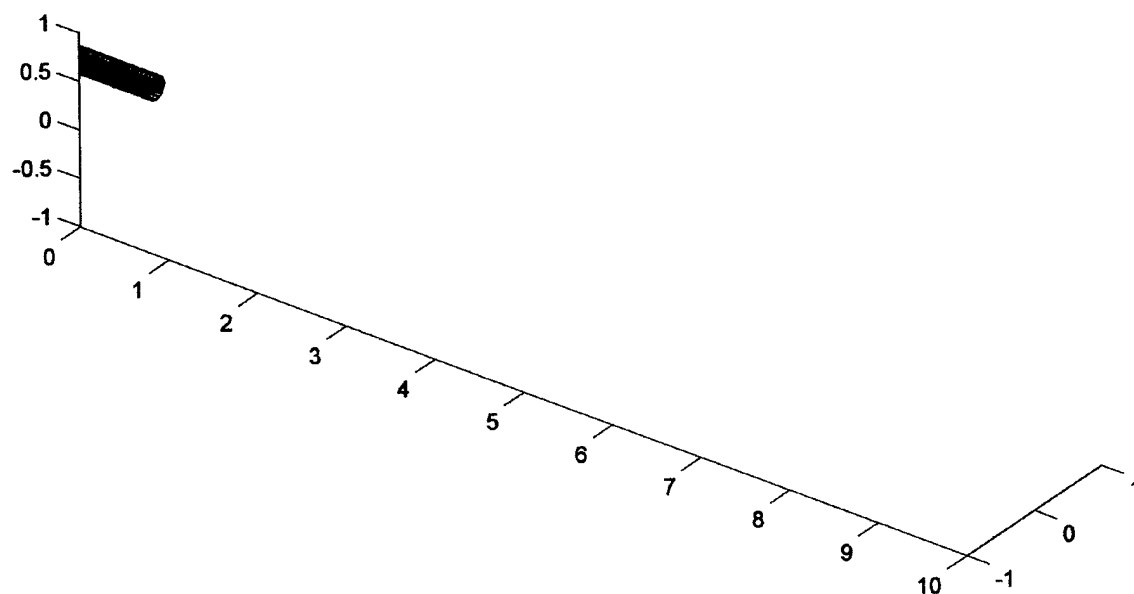


Vortex Filaments, Time: 2.7

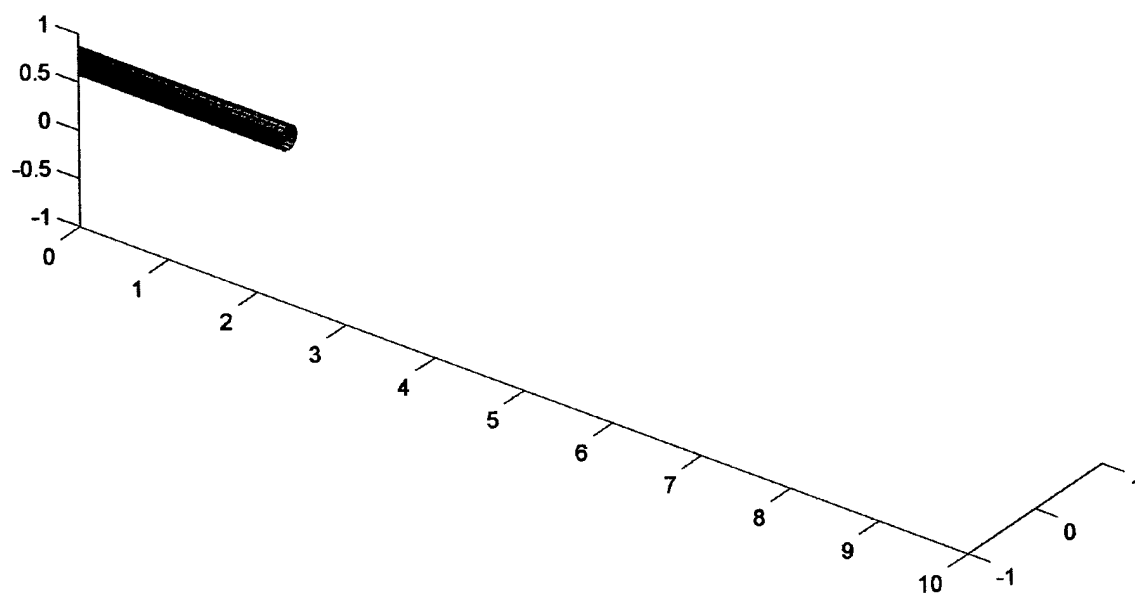


9.2 Vortex filament, $r = 0.12$, rendered perspective view

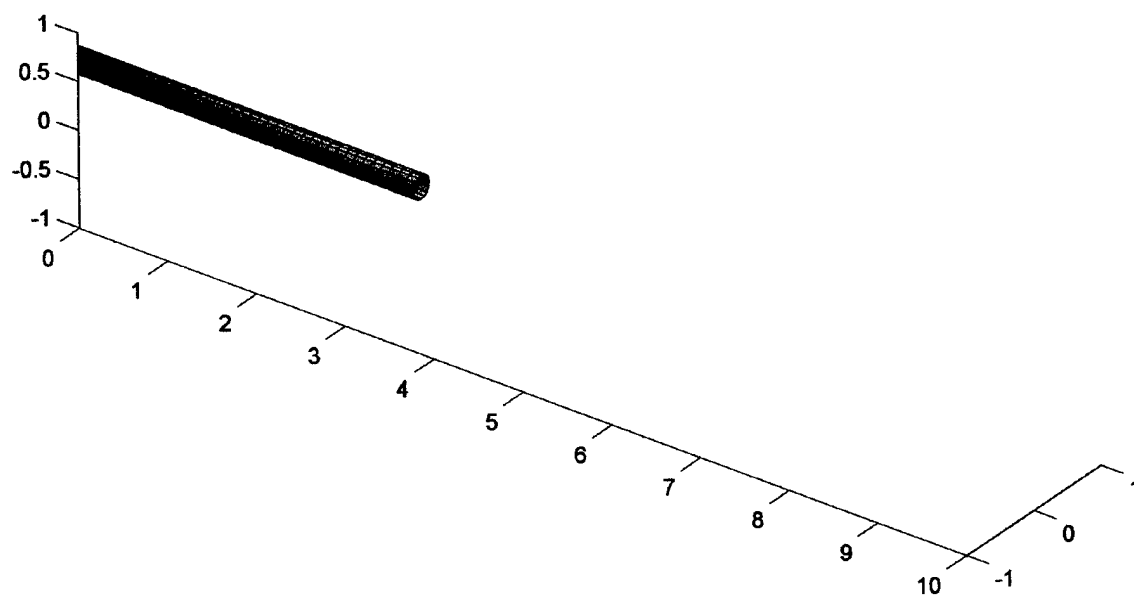
Vortex Filaments, Time: 0



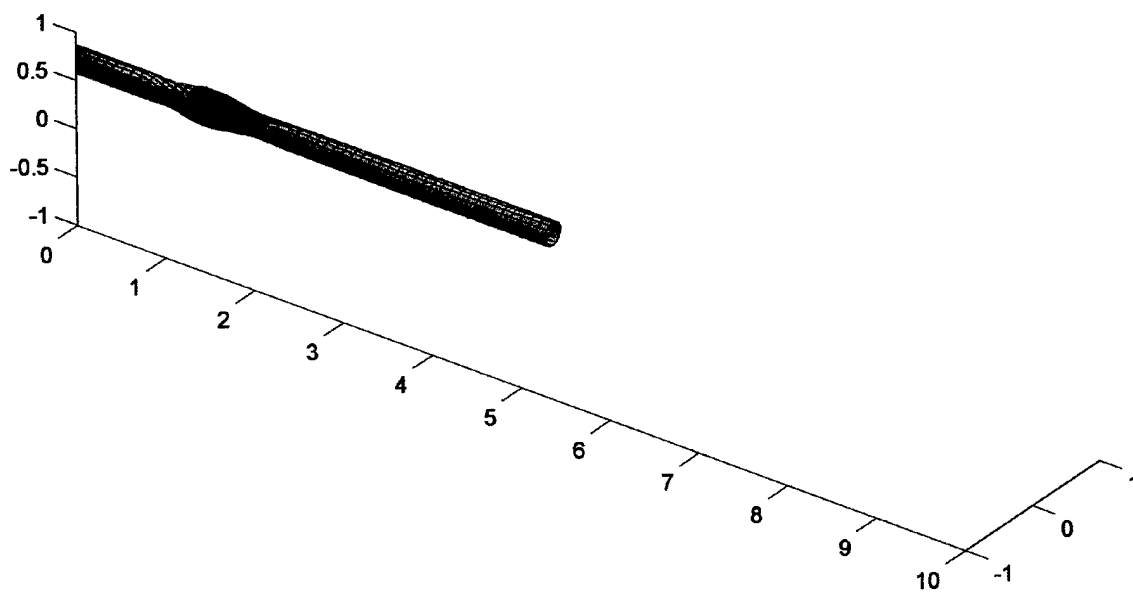
Vortex Filaments, Time: 0.3



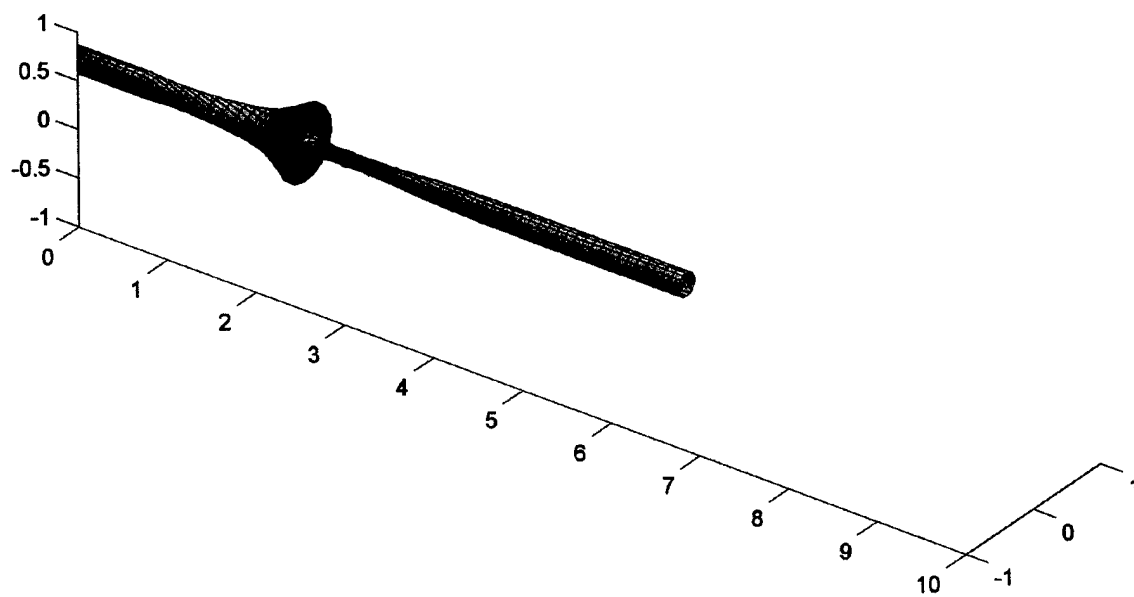
Vortex Filaments, Time: 0.6



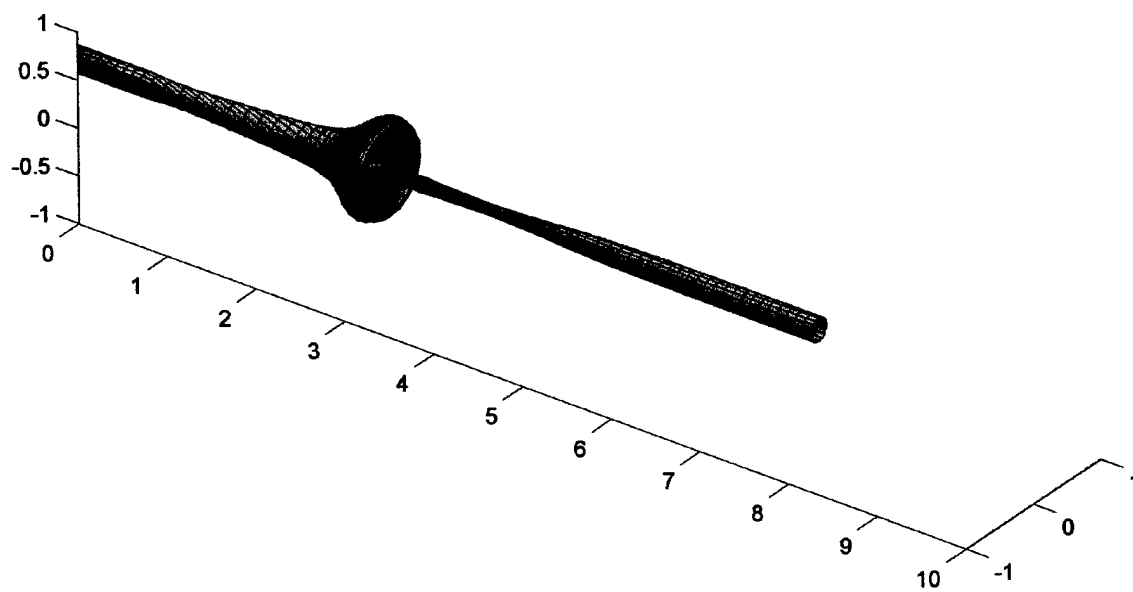
Vortex Filaments, Time: 0.9



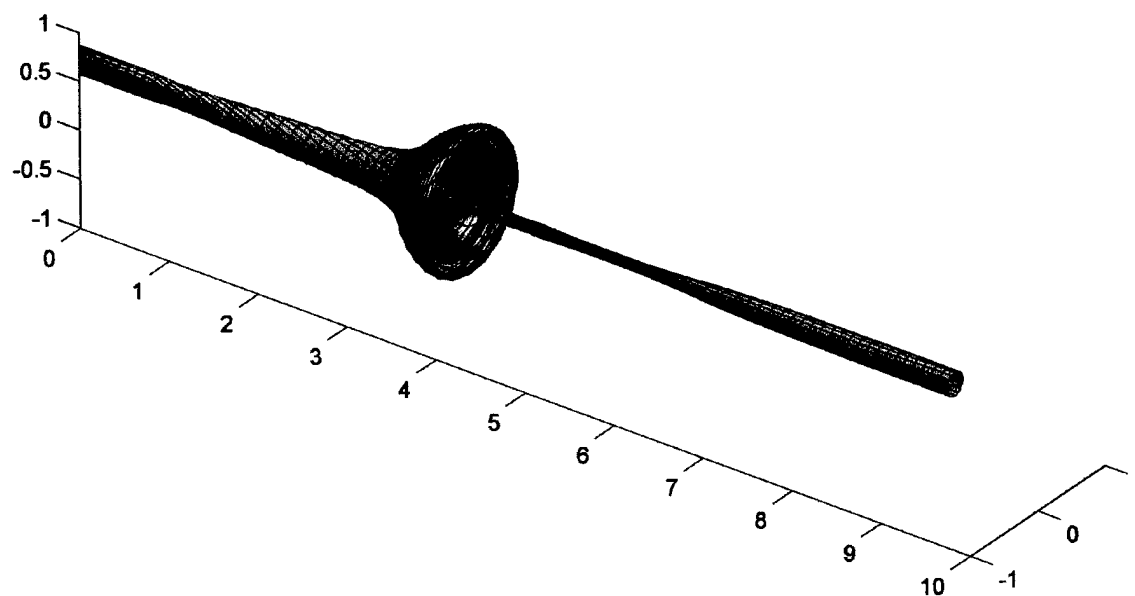
Vortex Filaments, Time: 1.2



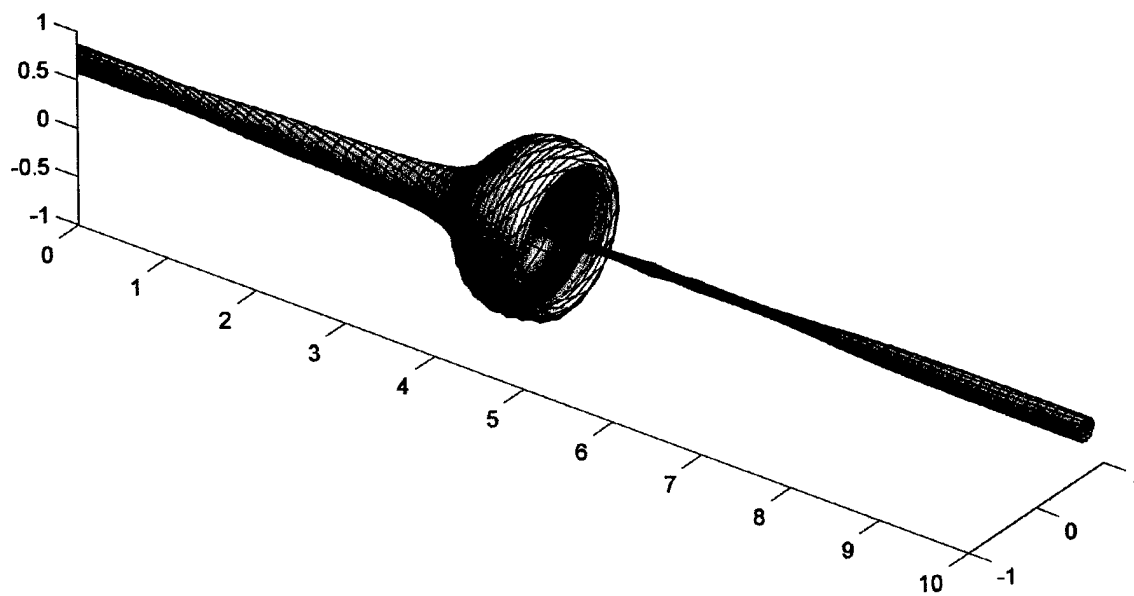
Vortex Filaments, Time: 1.5



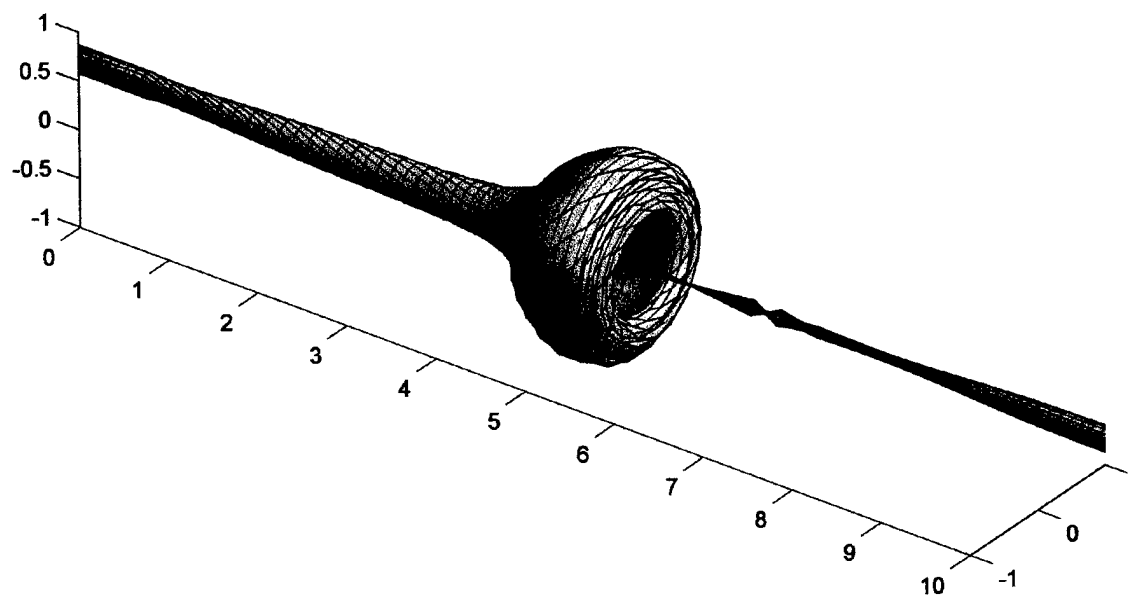
Vortex Filaments, Time: 1.8



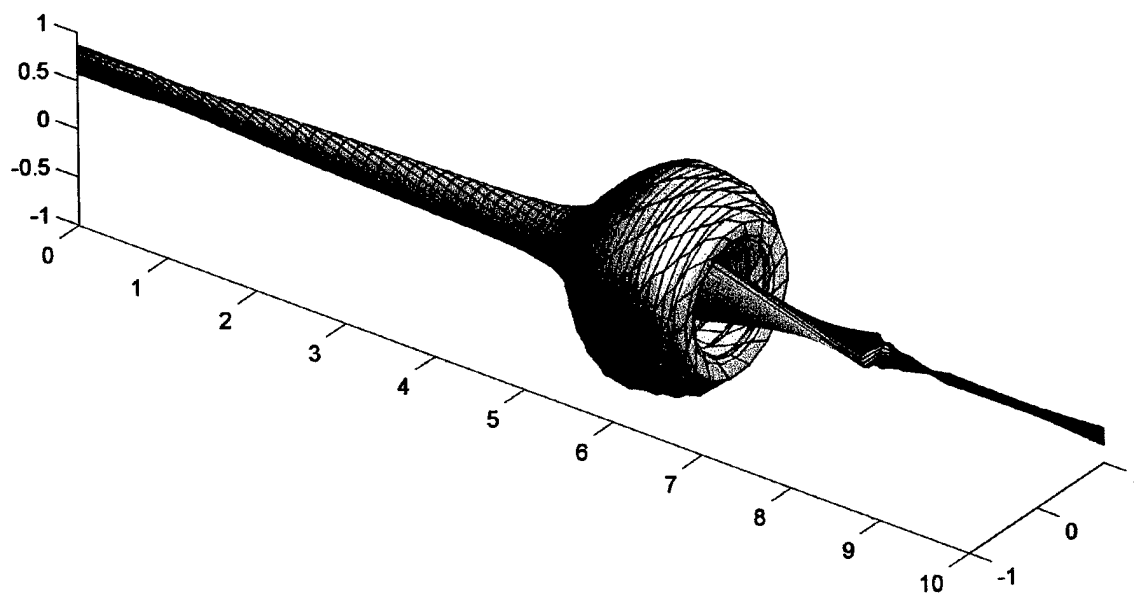
Vortex Filaments, Time: 2.1



Vortex Filaments, Time: 2.4

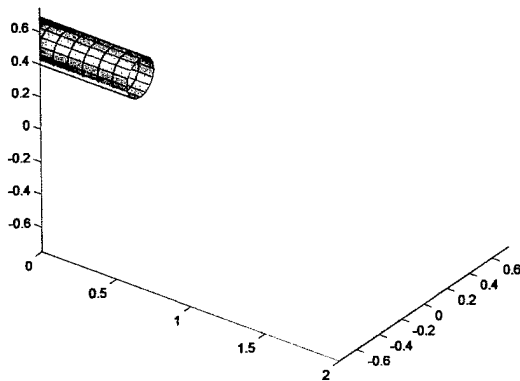


Vortex Filaments, Time: 2.7

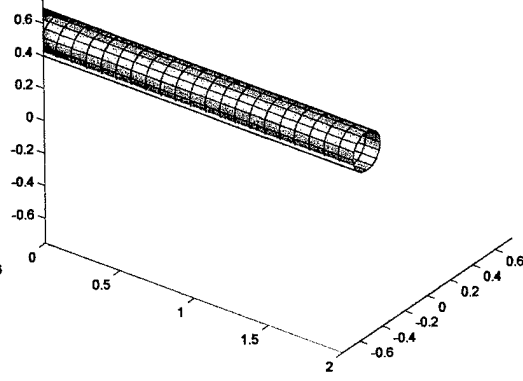


9.3 Vortex filament, $r = 0.12$, closer rendered perspective view

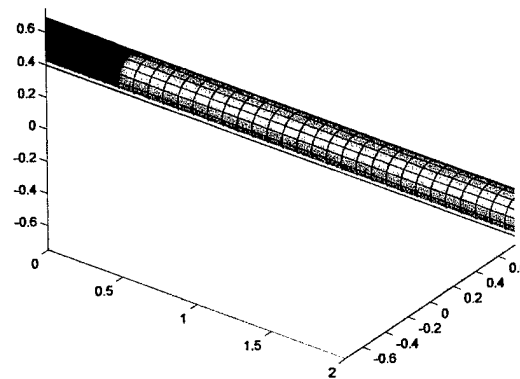
Vortex Filaments, Time: 0, rinit: 0.12



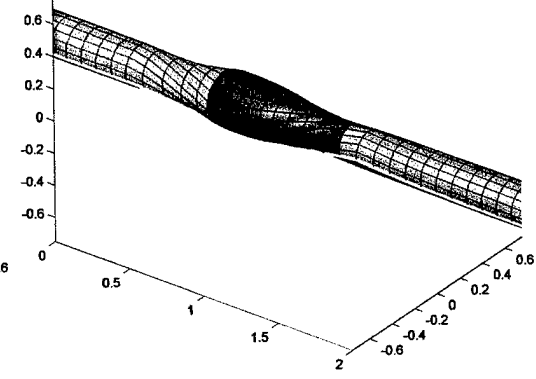
Vortex Filaments, Time: 0.3, rinit: 0.12



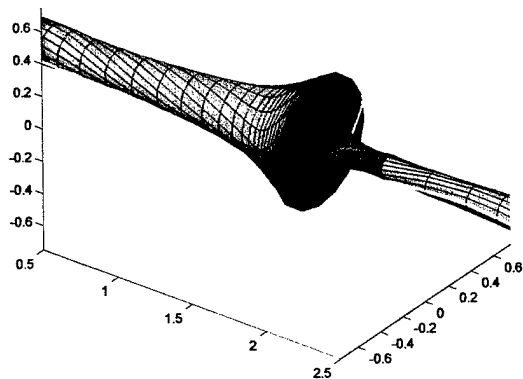
Vortex Filaments, Time: 0.6, rinit: 0.12



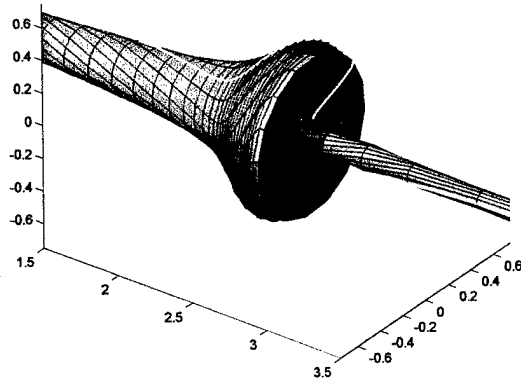
Vortex Filaments, Time: 0.9, rinit: 0.12



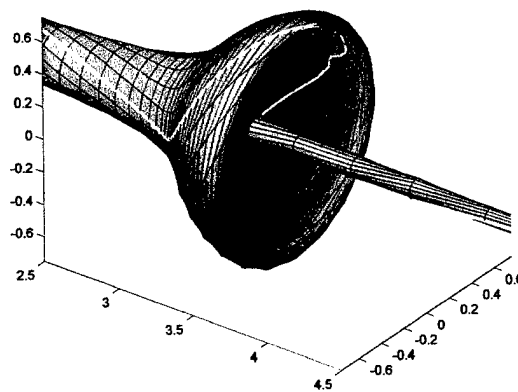
Vortex Filaments, Time: 1.2, rini: 0.12



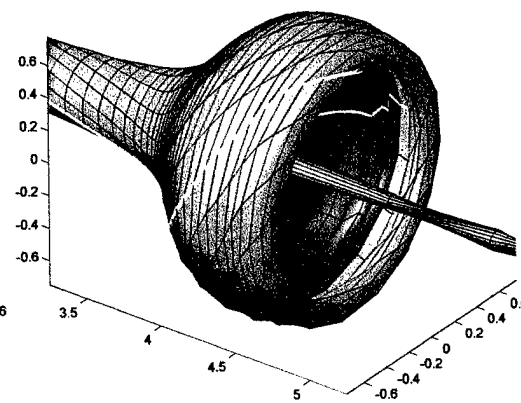
Vortex Filaments, Time: 1.5, rini: 0.12



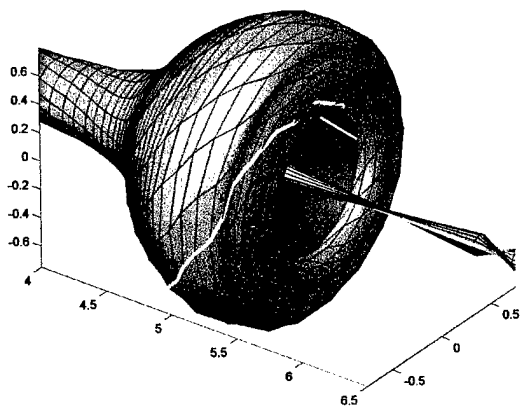
Vortex Filaments, Time: 1.8, rini: 0.12



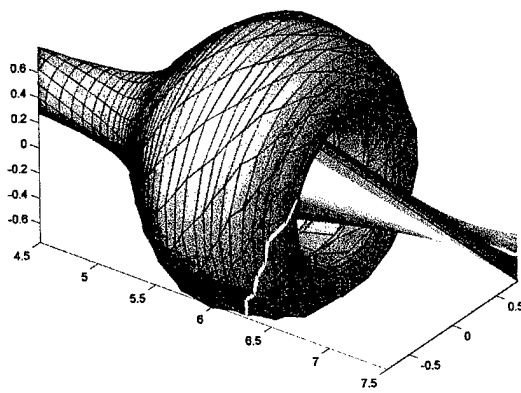
Vortex Filaments, Time: 2.1, rini: 0.12



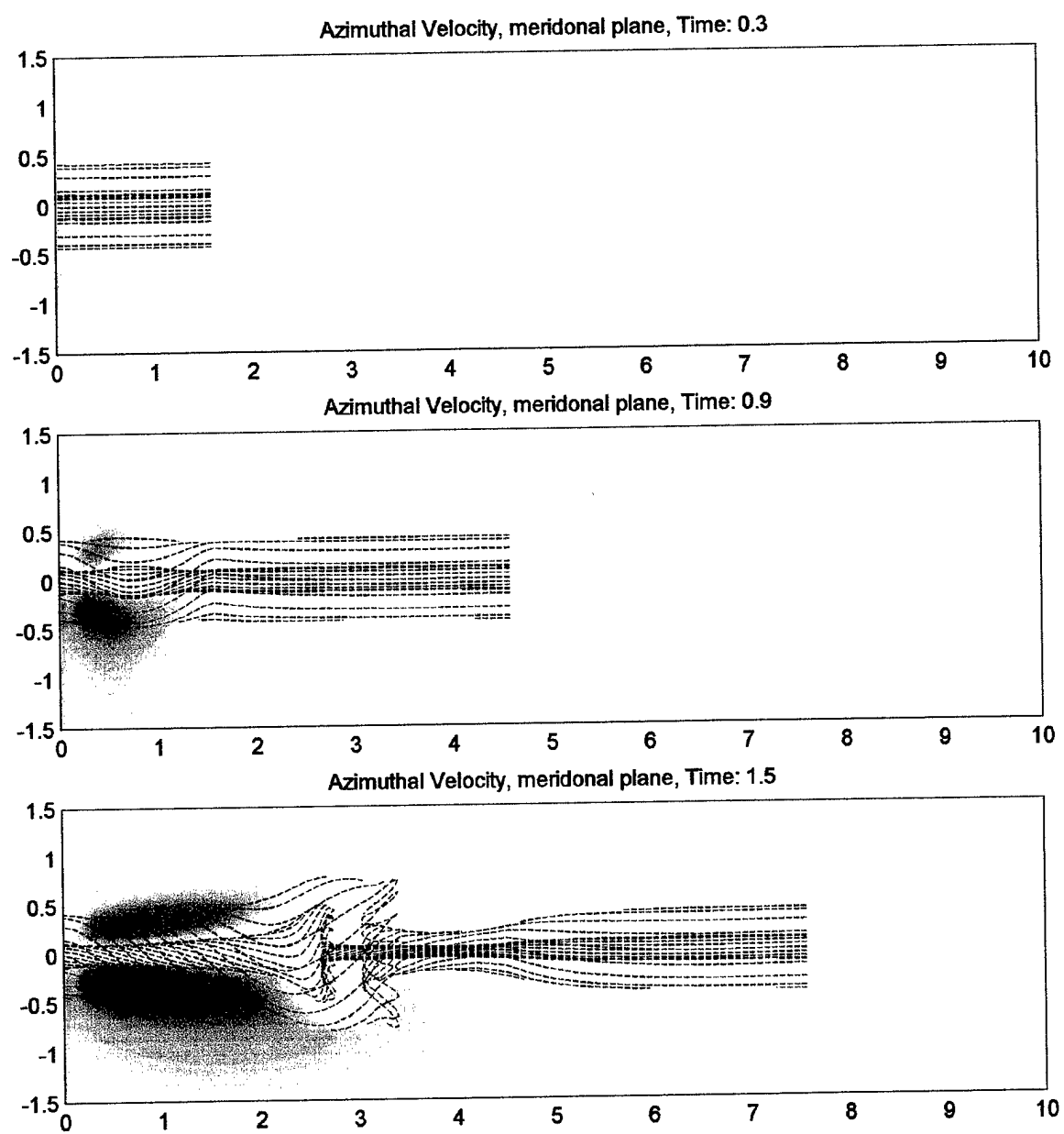
Vortex Filaments, Time: 2.4, rini: 0.12



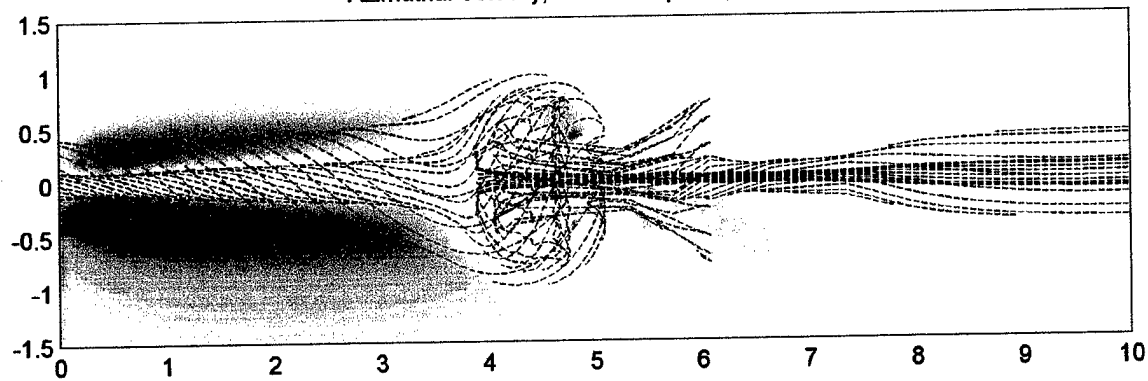
Vortex Filaments, Time: 2.7, rini: 0.12



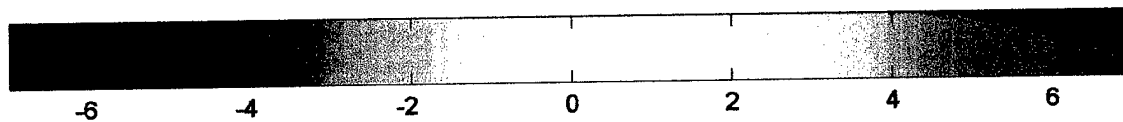
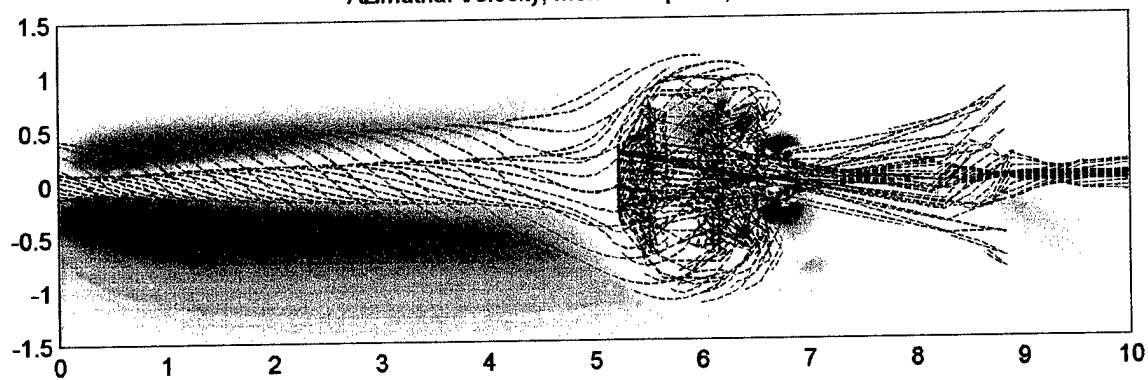
9.4 Color contour azimuthal velocity plots



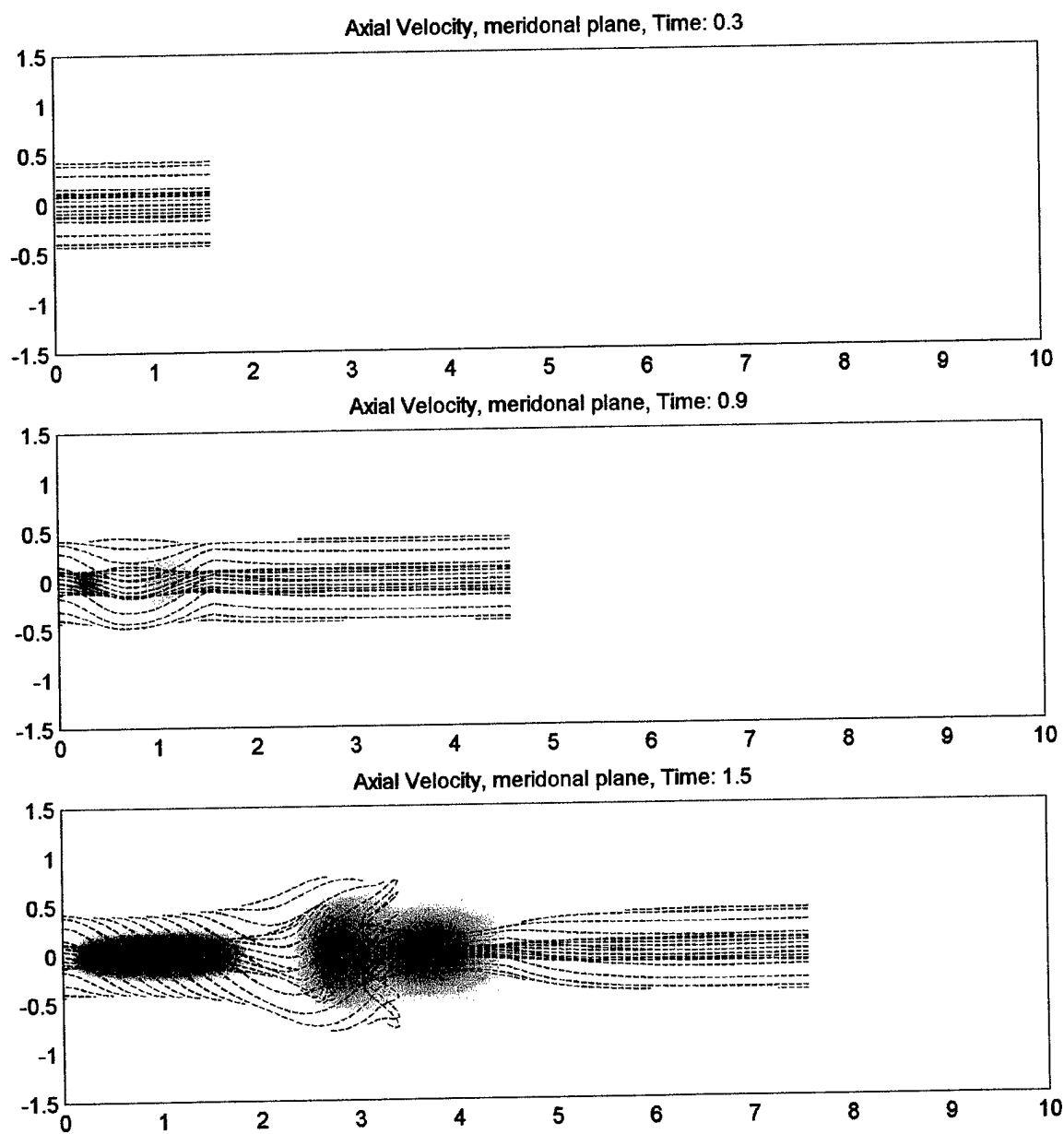
Azimuthal Velocity, meridional plane, Time: 2.1



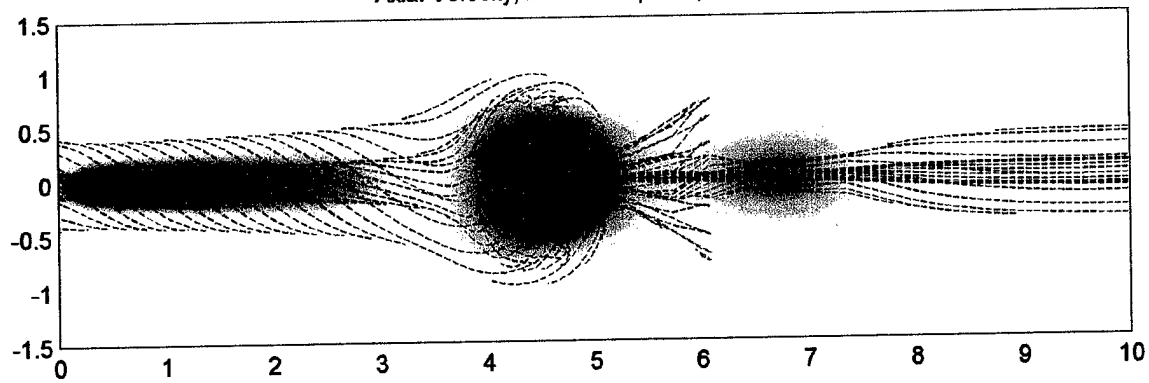
Azimuthal Velocity, meridional plane, Time: 2.7



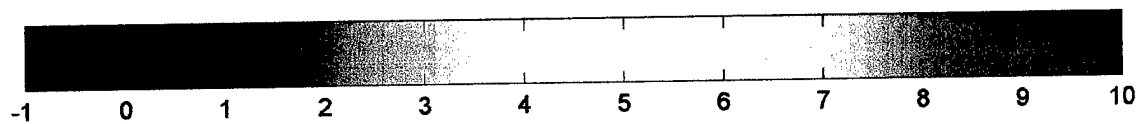
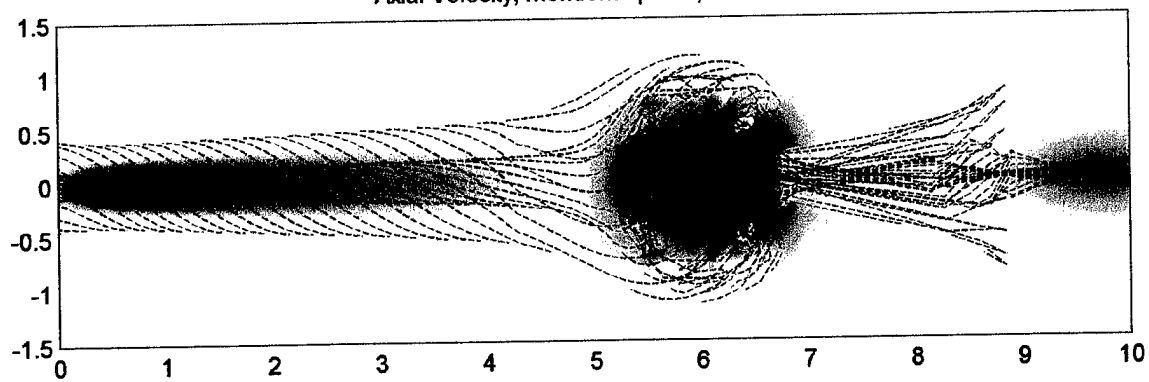
9.5 Color contour axial velocity plots



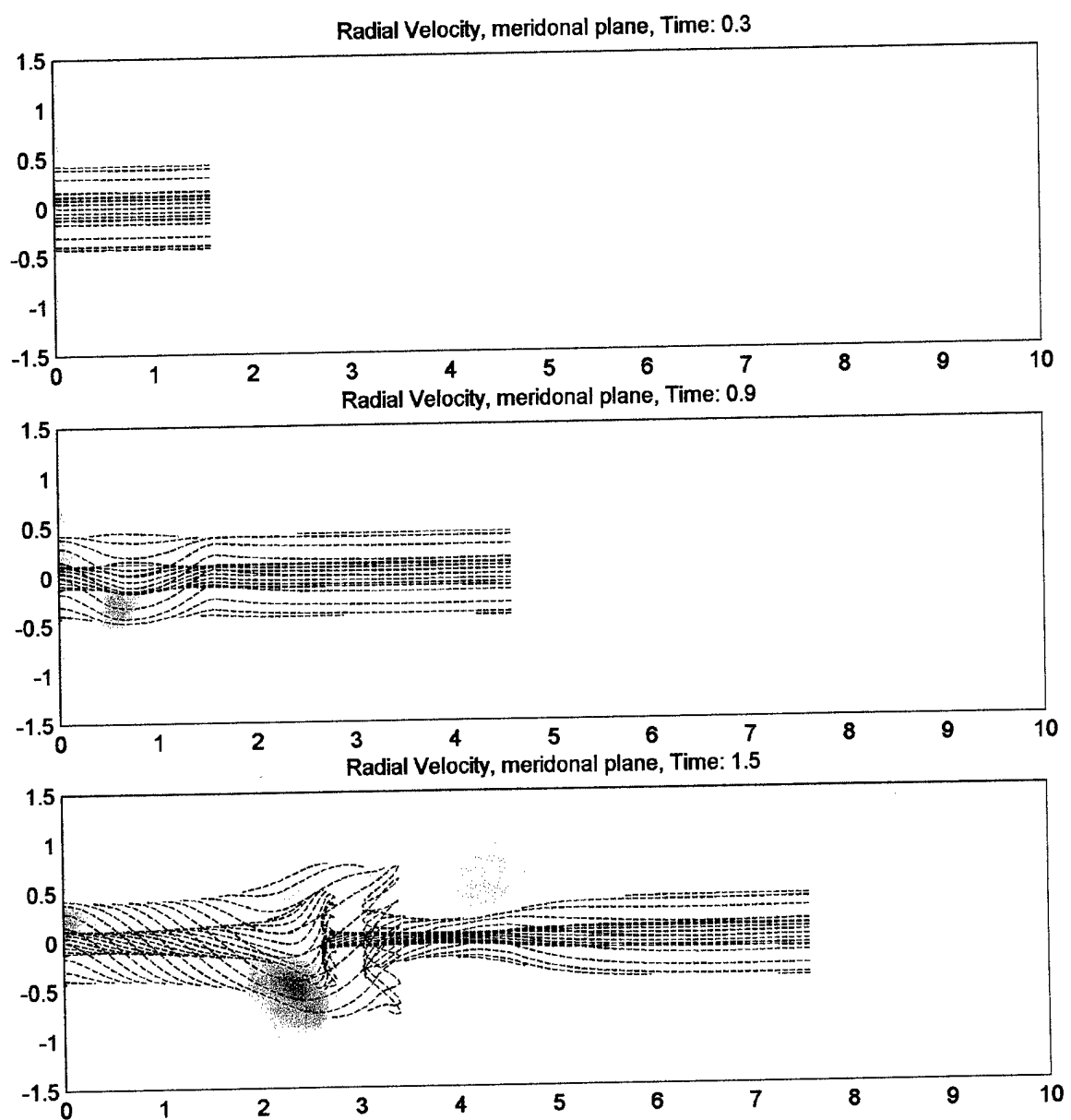
Axial Velocity, meridonal plane, Time: 2.1

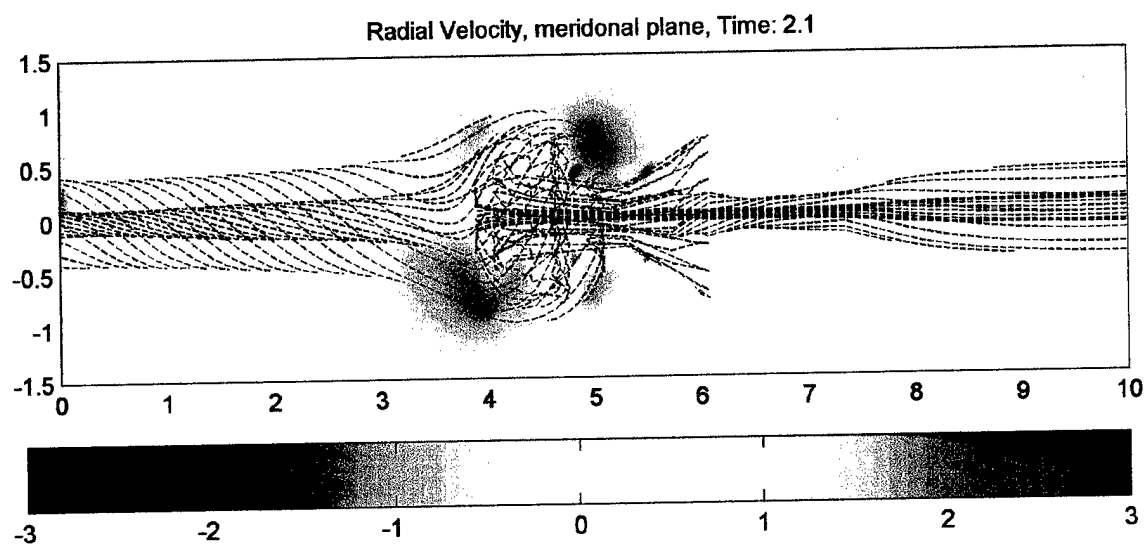


Axial Velocity, meridonal plane, Time: 2.7

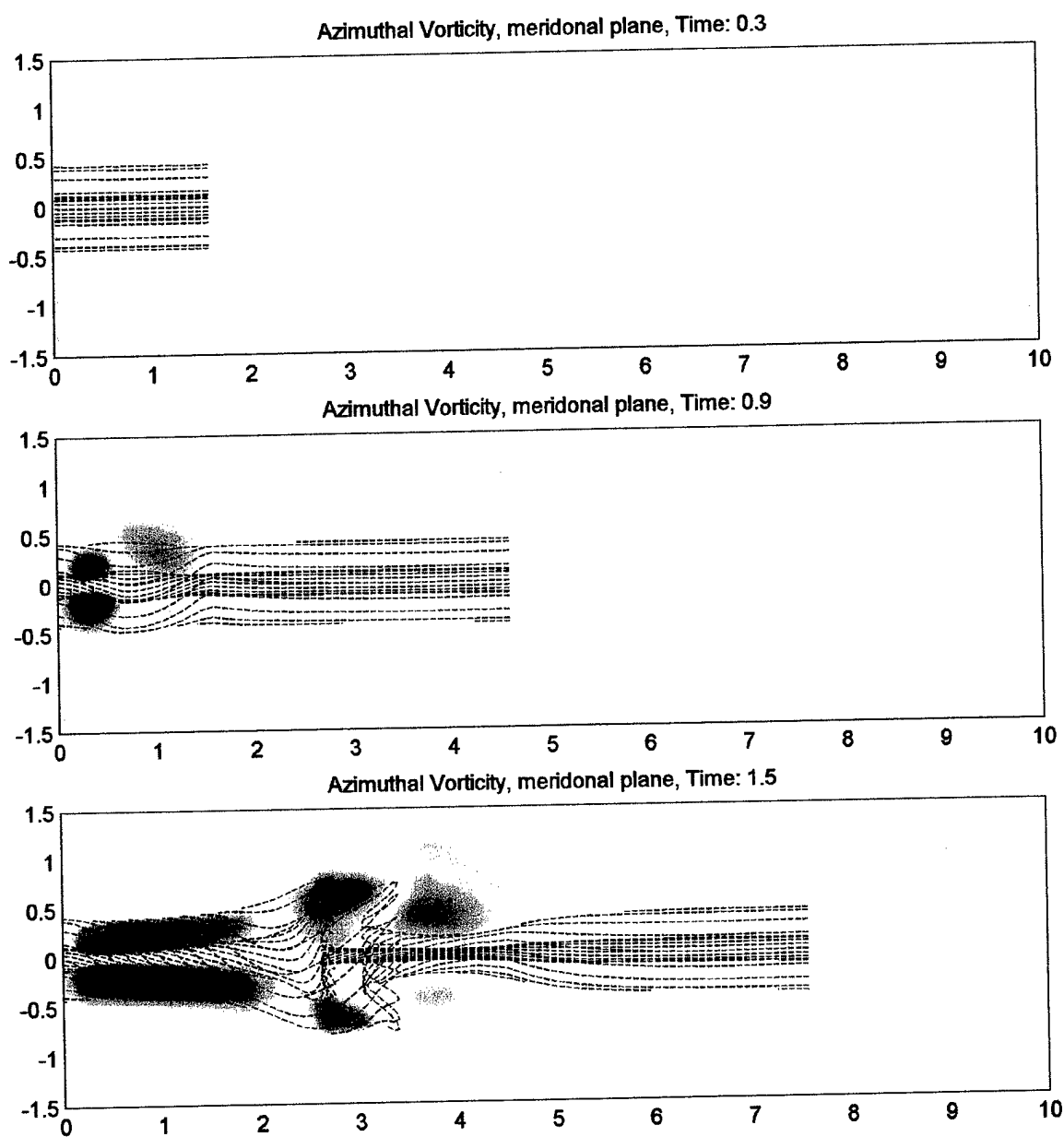


9.6 Color contour radial velocity plots

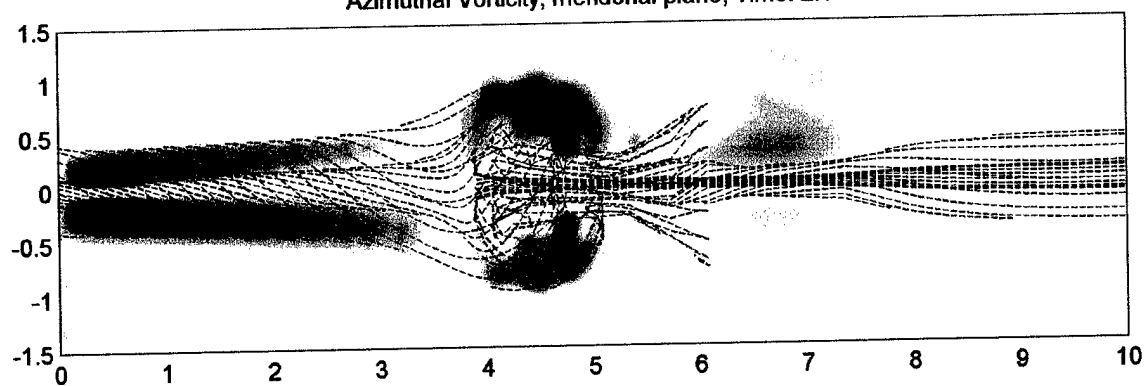




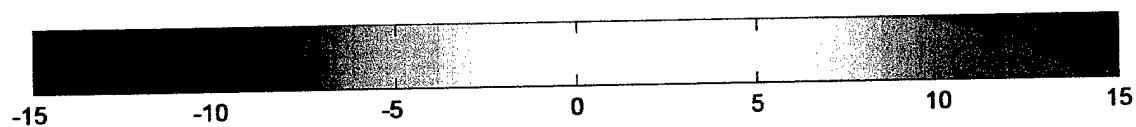
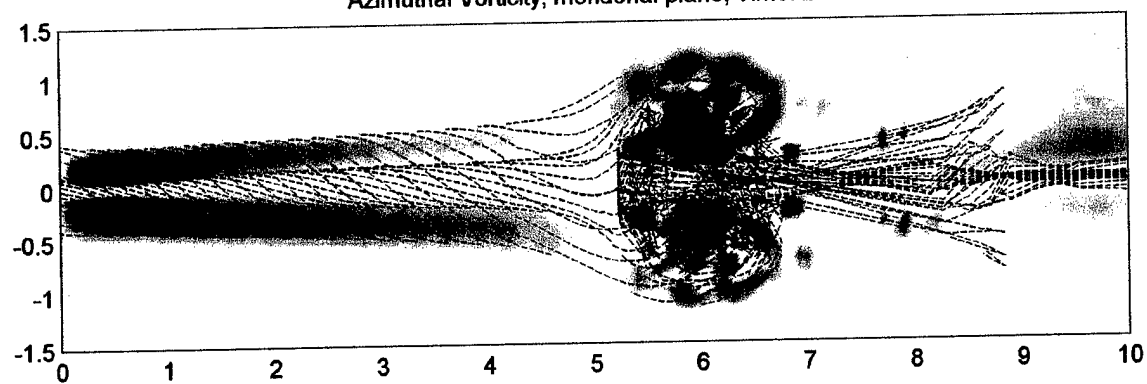
9.7 Color contour azimuthal vorticity plots



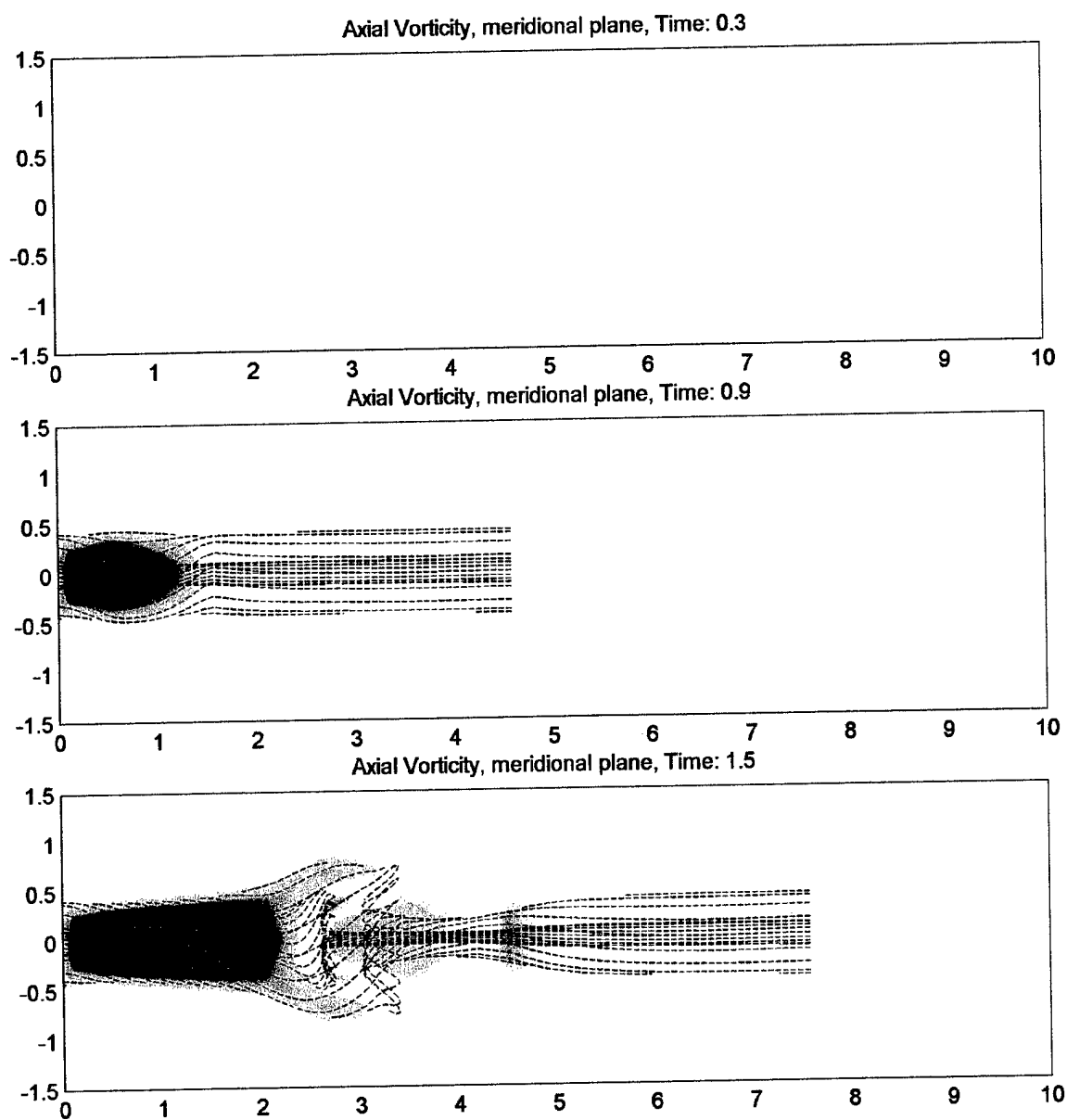
Azimuthal Vorticity, meridional plane, Time: 2.1

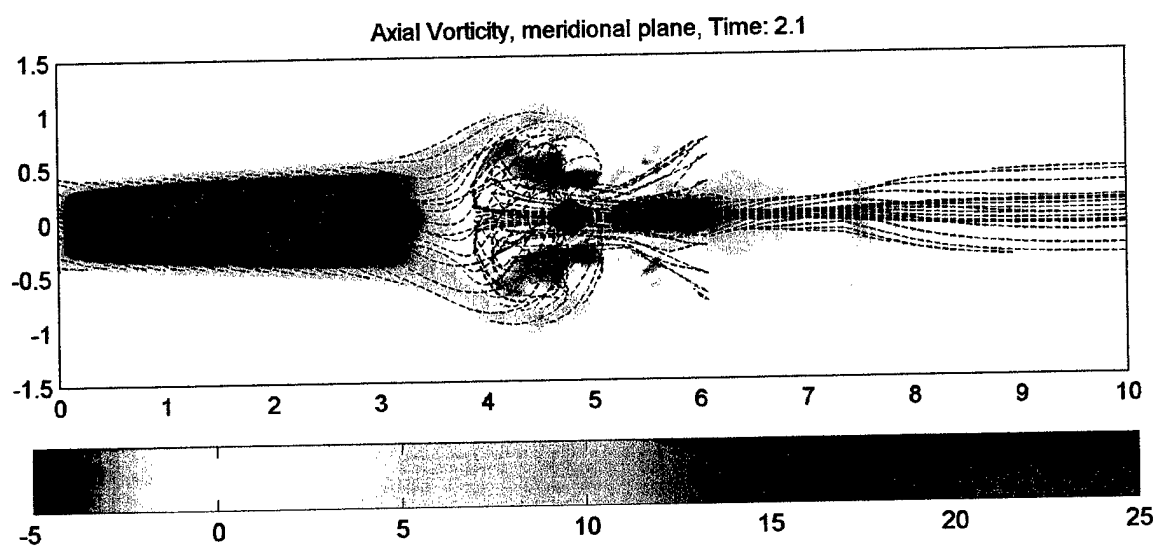


Azimuthal Vorticity, meridional plane, Time: 2.7



9.8 Color contour axial vorticity plots





9.9 Color contour radial vorticity plots

